frontiers | Research Topics

Model organisms in plant science: Maize

Edited by
Ana Butron, Rogelio Santiago Carabelos and Manje S. Gowda

Published in
Frontiers in Plant Science

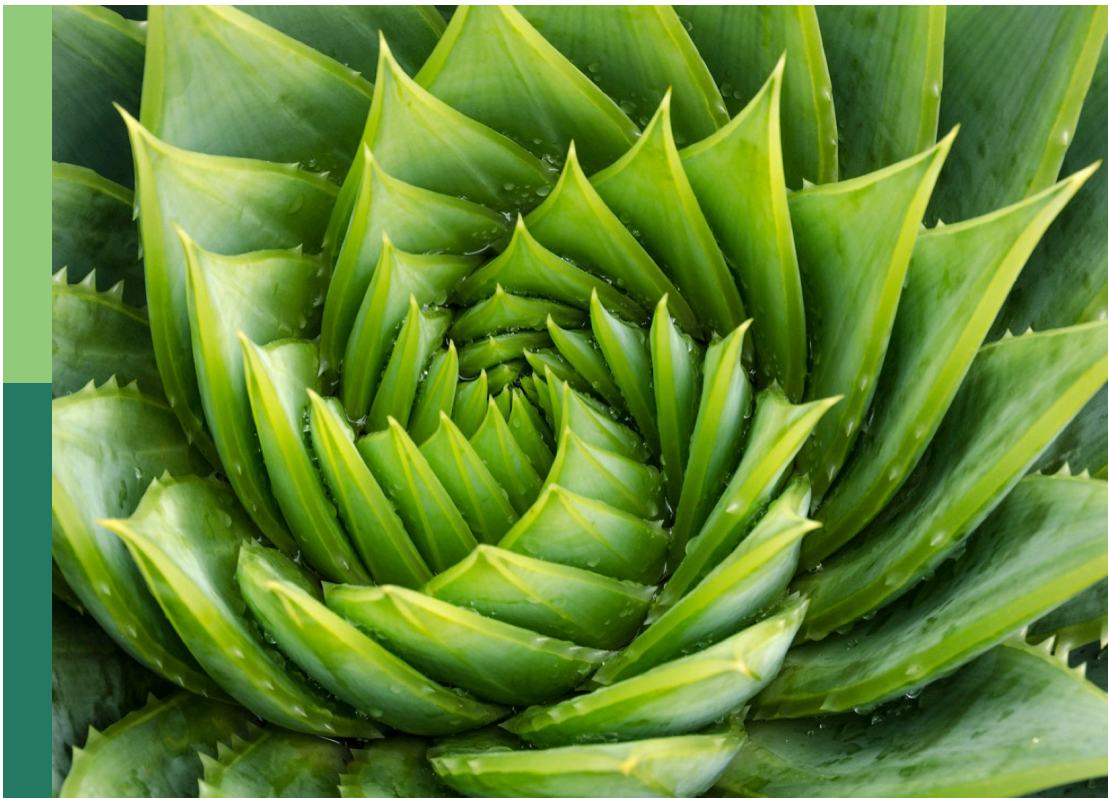

ISSN 1664-8714
ISBN 978-2-83251-746-8
DOI 10.3389/978-2-83251-746-8

About Frontiers

Frontiers is more than just an open access publisher of scholarly articles: it is a pioneering approach to the world of academia, radically improving the way scholarly research is managed. The grand vision of Frontiers is a world where all people have an equal opportunity to seek, share and generate knowledge. Frontiers provides immediate and permanent online open access to all its publications, but this alone is not enough to realize our grand goals.

Frontiers journal series

The Frontiers journal series is a multi-tier and interdisciplinary set of open-access, online journals, promising a paradigm shift from the current review, selection and dissemination processes in academic publishing. All Frontiers journals are driven by researchers for researchers; therefore, they constitute a service to the scholarly community. At the same time, the *Frontiers journal series* operates on a revolutionary invention, the tiered publishing system, initially addressing specific communities of scholars, and gradually climbing up to broader public understanding, thus serving the interests of the lay society, too.

Dedication to quality

Each Frontiers article is a landmark of the highest quality, thanks to genuinely collaborative interactions between authors and review editors, who include some of the world's best academicians. Research must be certified by peers before entering a stream of knowledge that may eventually reach the public - and shape society; therefore, Frontiers only applies the most rigorous and unbiased reviews. Frontiers revolutionizes research publishing by freely delivering the most outstanding research, evaluated with no bias from both the academic and social point of view. By applying the most advanced information technologies, Frontiers is catapulting scholarly publishing into a new generation.

What are Frontiers Research Topics?

Frontiers Research Topics are very popular trademarks of the *Frontiers journals series*: they are collections of at least ten articles, all centered on a particular subject. With their unique mix of varied contributions from Original Research to Review Articles, Frontiers Research Topics unify the most influential researchers, the latest key findings and historical advances in a hot research area.

Find out more on how to host your own Frontiers Research Topic or contribute to one as an author by contacting the Frontiers editorial office: frontiersin.org/about/contact

Model organisms in plant science: Maize

Topic editors

Ana Butron — Misión Biológica de Galicia, Spanish Council for Scientific Research (MBG-CSIC), Spain

Rogelio Santiago Carabelos — Biological Mission of Galicia, Spanish National Research Council (CSIC), Spain

Manje S. Gowda — The International Maize and Wheat Improvement Center (CIMMYT), Kenya

Citation

Butron, A., Carabelos, R. S., Gowda, M. S., eds. (2023). *Model organisms in plant science: Maize*. Lausanne: Frontiers Media SA. doi: 10.3389/978-2-83251-746-8

Table of contents

frontiers | Frontiers in Plant Science

TYPE Editorial
PUBLISHED 08 February 2023
DOI 10.3389/fpls.2023.1147857

OPEN ACCESS

EDITED AND REVIEWED BY
Diego Rubiales,
Institute for Sustainable Agriculture (CSIC), Spain

*CORRESPONDENCE
Ana Butrón
abutron@mbg.csic.es

SPECIALTY SECTION
This article was submitted to Plant Breeding, a section of the journal Frontiers in Plant Science

RECEIVED 19 January 2023
ACCEPTED 31 January 2023
PUBLISHED 08 February 2023

CITATION
Butrón A, Santiago R and Gowda M (2023) Editorial: Model organisms in plant science: Maize.
Front. Plant Sci. 14:1147857.
doi: 10.3389/fpls.2023.1147857

Editorial: Model organisms in plant science: Maize

Ana Butrón[1]*, Rogelio Santiago[1,2] and Manje Gowda[3]

[1]Misión Biológica de Galicia, Spanish Council for Scientific Research (MBG-CSIC), Pontevedra, Spain, [2]Agrobiología Ambiental, Calidad de Suelos y Plantas University of Vigo (UVIGO), Unidad Asociada a la MBG (CSIC), Vigo, Spain, [3]Global Maize Program, International Maize and Wheat Improvement Center (CIMMYT), Nairobi, Kenya

KEYWORDS

***Zea mays* L., maize, model organism, plant physiology, plant breeding, heterosis, genomic selection**

Editorial on the Research Topic
Model organisms in plant science: Maize

Maize has been an organism of historical importance to all biologists as eminent researchers such as Beadle, Emerson, McClintock, Stadler and Rhoades made ground-breaking genetic discoveries in maize that hold true for all living organisms (Andorf et al., 2016). Nowadays, plant lignocellulose represents the world's greatest repository of renewable energy amenable to conversion into liquid, and maize has become one of the preferred choices due to their high biomass yields, broad geographic adaptation, carbon sequestration potential and nutrient utilization (Courtial et al., 2013; van der Weijde et al.). Therefore, this Research Topic aimed (1) to put forward the importance of research focuses in maize as a model organism, presenting recent developments and important accomplishments in moving forward the study of plants, and (2) to shed light on the progress made in the past decade working with maize as an important crop used worldwide.

Today, plant genome editing using clustered regularly interspaced short palindromic repeats (CRISPR)/CRISPR-associated protein 9 (Cas9)) technology has rapidly become the preferred tool to generate mutants for functional genomics in plants. Despite their rapid success, plant genome editing is still a labour-intensive process. Fierlej et al. presented an optimized maize protoplast system and a specifically developed bioinformatics pipeline to evaluate rapidly the efficiency of CRISPR/Cas9 constructs or of novel Cas9 variants before engaging in time- and resource-consuming stable transformation. This protocol is useful in improving maize genome editing processes which ultimately improve its success rate. This knowledge can be meaningful for breeding programs.

Another paper that makes a direct contribution to plant breeding practice has been written by Ni et al. These authors show that the use of correlated traits and sparse phenotyping can yield high prediction accuracies while reducing the cost of extensively phenotyping for difficult to measure traits like kernel water content at black layer formation. Recommended methodological approaches although applied to a relevant trait for maize breeding could be useful for performing genomic selection for traits that are difficult to measure/record in any other plant organism.

In the same way, five other research papers and one corrigendum that deal with fundamental aspects of plant breeding were accepted. Paper by Sang et al. contributed to a better comprehension of heterosis; this phenomena along with transgressive segregation being the reasons that plant breeding works (Mackay et al., 2021). Sang et al. show that epistasis contribution to heterosis is not

negligible because the interaction of many minor-effect genes in the hybrids could activate the transcription activators of epistatic genes, resulting in a cascade of amplified yield heterosis. Authors also provide recommendations to accelerate hybrid maize breeding by activating epistatic effects.

Zhang et al. in a research paper and a corrigendum provide important findings allowing further elucidation of the molecular mechanism of regulation of leaf angle. Leaf angle is closely associated with canopy structure and photosynthetic efficiency under high planting density and have become crucial for improving yield. The leaf angle regulation functions of bHLH TF have been studied in rice, but important questions remain unsolved. Authors compare the transcriptome of a *Zmbhlh112* mutant, which displays a relatively small leaf angle, and the wild-type B73, and found that ribosomal subunits may play an important role in leaf development.

Li et al. also focuses in the genetic control of traits related to grain yield as ear fascination and tillering. Although most of the modern maize hybrid cultivars cultivated in the high-dense stands in temperate environment develop only one ear, the potential presence of multiple ears per plant has physiological and breeding implications. The fasciation effects and the correlated effect on kernel row number were confirmed across genetic backgrounds, making the QTL identified an interesting source of yield-positive alleles. Unexpectedly, authors did not find correlation or QTL overlaps between ear prolificacy and tillering, although these traits share a developmental basis.

On the other hand, due to climate change, plants need to adapt more quickly under unpredictable climate change scenarios. Low temperature effect on germination of maize seedlings is critical to have good germination. For eight low-temperature resistance related traits Zhou et al. identified twenty QTL, of which seven QTL overlapped in single region on chromosome 1 at 197-202 Mb named as cQTL1-2. QTL identified on this region explained 5 to 26% of total phenotypic variation and were consistent with previous studies on low temperature resistance QTL. Two candidate genes identified in this region, GRMZM2G082630 and GRMZM2G115730, were upregulated in low-temperature tolerant lines. The authors proposed these candidate genes can be exploited through breeding to improve the low-temperature tolerance during seedlings germination.

Maize shows significant variation for salinity tolerance which encourages the researchers to identify and understand the genetic architecture of salinity tolerance. Root system plays an important role in salinity tolerance and lateral roots are important for water and nutrient acquisition. Zhang et al. planned experiment to identify the genetic basis of natural variation in lateral root length which is of great agronomic relevance to improve salt tolerance. Through GWAS, authors identified the causative gene *ZmSULTR3;4*, which encodes a plasma membrane-localized sulfate transporter and is associated with natural variation in maize lateral root length under salt stress. Overall, authors conclude the *ZmSULTR3;4* gene has regulatory role in lateral root growth which can be used to improve maize root traits and salinity tolerance by molecular breeding.

As previously mentioned, drought and heat stresses are major limiting factors for crop growth and productivity (Fahad et al.), and they cause the greatest annual loss of crops (Ray et al., 2015). Plants have developed multiple responses at the developmental, physiological, and molecular levels that enable them to escape, avoid, and/or tolerate unfavorable environmental conditions (Chávez-Arias et al.). From a physiological point of view, an interesting mini review paper by Serna explores how maize yield may persevere through climate change by focusing on the stomatal regulation of gas exchange. The paper reviews the maize stomatal response to drought and heat stresses and the possible molecular mechanisms of maize stomatal development in response to climate change. Under drought stress, maize respond by increasing abscisic acid levels and thereby reducing stomatal opening (Zhao et al., 2015), whereas author put forward that in order to avoid plant heat damage, maize could increase the number of stomatal files and, consequently, the stomatal density, by expanding the expression domain of *ZmSHR1*.

The accepted articles demonstrate how cutting-edge approaches in maize genetics and breeding are useful in crop improvement. The contributions of authors are of highest quality and illuminate the strong international interest in this Research Topic. These results would help maize researchers, geneticists, and breeders in order to improve the understanding on maize genetics and contribute to increase maize yield under diverse agroclimatic conditions.

Author contributions

AB, RS, and MG contributed to the writing of this editorial. All authors revised and improved the final version of the editorial.

Funding

AB and RS work was financed by Spanish National Research Council (CSIC), MG was supported by the Bill and Melinda Gates Foundation (B&MGF), and the United States Agency for International Development (USAID) through the AGGMW (Accelerating Genetic Gains in Maize and Wheat for Improved Livelihoods, B&MGF Investment ID INV-003439) project.

Acknowledgments

The Guest Editors would like to thank all the authors who contributed to this Research Topic.

Conflict of interest

The authors declare that the research was conducted in the absence of any commercial or financial relationships that could be construed as a potential conflict of interest.

The handling editor DR declared a shared parent affiliation with the authors AB and RS at the time of review.

Publisher's note

References

Andorf, C. M., Cannon, E. K., Portwood, J. L., Gardiner, J. M., Harper, L. C., Schaeffer, M. L., et al. (2016). MaizeGDB update: New tools, data and interface for the maize model organism database. *Nucleic Acids Res.* 44 (D1), D1195–D1201. doi: 10.1093/nar/gkv1007

Courtial, A., Soler, M., Chateigner-Boutin, A. L., Reymond, M., Méchin, V., Wang, H., et al. (2013). Breeding grasses for capacity to biofuel production or silage feeding value: An updated list of genes involved in maize secondary cell wall biosynthesis and assembly. *Maydica* 58, 67–102. Available at: https://typeset.io/papers/breeding-grasses-for-capacity-to-biofuel-production-or-33u9aubwcf.

Mackay, I. J., Cockram, J., Howell, P., and Powell, W. (2021). Understanding the classics: the unifying concepts of transgressive segregation, inbreeding depression and heterosis and their central relevance for crop breeding. *Plant Biotechnol. J.* 19 (1), 26–34. doi: 10.1111/pbi.13481

Ray, D. K., Gerber, J. S., Macdonald, G. K., and West, P. C. (2015). Climate variation explains a third of global crop yield variability. *Nat. Commun.* 6, 5989. doi: 10.1038/ncomms6989

Zhao, W., Sun, Y., Kjelgren, R., and Liu, X. (2015). Response of stomatal density and bound gas exchange in leaves of maize to soil water deficit. *Acta Physiol. Plant* 37, 1704. doi: 10.1007/s11738-014-1704-8

frontiers | Frontiers in Plant Science

ORIGINAL RESEARCH
published: 30 June 2022
doi: 10.3389/fpls.2022.930429

Genomic Prediction Strategies for Dry-Down-Related Traits in Maize

Pengzun Ni[1,2,3], Mahlet Teka Anche[2], Yanye Ruan[1], Dongdong Dang[1], Nicolas Morales[2], Lingyue Li[1], Meiling Liu[1], Shu Wang[3] and Kelly R. Robbins[2]**

[1] Shenyang Key Laboratory of Maize Genomic Selection Breeding, Liaoning Province Research Center of Plant Genetic Engineering Technology, College of Biological Science and Technology, Shenyang Agricultural University, Shenyang, China, [2] Section of Plant Breeding and Genetics, School of Integrative Plant Sciences, Cornell University, Ithaca, NY, United States, [3] College of Agronomy, Shenyang Agricultural University, Shenyang, China

For efficient mechanical harvesting, low grain moisture content at harvest time is essential. Dry-down rate (DR), which refers to the reduction in grain moisture content after the plants enter physiological maturity, is one of the main factors affecting the amount of moisture in the kernels. Dry-down rate is estimated using kernel moisture content at physiological maturity and at harvest time; however, measuring kernel water content at physiological maturity, which is sometimes referred as kernel water content at black layer formation (BWC), is time-consuming and resource-demanding. Therefore, inferring BWC from other correlated and easier to measure traits could improve the efficiency of breeding efforts for dry-down-related traits. In this study, multi-trait genomic prediction models were used to estimate genetic correlations between BWC and water content at harvest time (HWC) and flowering time (FT). The results show there is moderate-to-high genetic correlation between the traits (0.24–0.66), which supports the use of multi-trait genomic prediction models. To investigate genomic prediction strategies, several cross-validation scenarios representing possible implementations of genomic prediction were evaluated. The results indicate that, in most scenarios, the use of multi-trait genomic prediction models substantially increases prediction accuracy. Furthermore, the inclusion of historical records for correlated traits can improve prediction accuracy, even when the target trait is not measured on all the plots in the training set.

Keywords: kernel water content, dry-down rate, genomic prediction, MT-GBLUP, correlated traits

OPEN ACCESS

Edited by:
Ana Butron, Misión Biológica de Galicia, Spanish Council for Scientific Research (MBG-CSIC), Spain

Reviewed by:
Anna Rogers, Bayer Crop Science, United States
Zhiwu Zhang, Washington State University, United States

***Correspondence:**
Shu Wang
swang123@syau.edu.cn
Kelly R. Robbins
krr73@cornell.edu

Specialty section:
This article was submitted to Plant Breeding, a section of the journal Frontiers in Plant Science

Received: *27 April 2022*
Accepted: *23 May 2022*
Published: *30 June 2022*

Citation:
Ni P, Anche MT, Ruan Y, Dang D, Morales N, Li L, Liu M, Wang S and Robbins KR (2022) Genomic Prediction Strategies for Dry-Down-Related Traits in Maize. Front. Plant Sci. 13:930429. doi: 10.3389/fpls.2022.930429

KEY MESSAGE

- When data are limited on difficult to measure traits in historical datasets or in sparse phenotyping approaches, the use of correlated traits in multi-trait predictions models significantly increases prediction accuracy.

INTRODUCTION

Maize (*Zea mays* L.) is one of the most widely grown food crop across the world (Lawrence et al., 2008; Shiferaw et al., 2011). With efforts to increase maize grain yield/production to meet the growing global food demand (Ray et al., 2013), mechanization of grain harvesting has become a common practice in many countries (Pari et al., 2020). In maize, low grain moisture content

at harvest is essential for efficient mechanical harvesting (Brooking, 1990; Singh et al., 1998; Liu et al., 2020). When the moisture content is low, mechanical harvesting becomes more efficient due to easier grain shelling (Chowdhury and Buchele, 1978), and low grain moisture content at harvest time is highly desirable by farmers as it allows long-term grain storage (Weinberg et al., 2008). Many developed countries have fully implemented mechanical harvesting in maize (Du Plessis, 2003); however, due to differences in technological advancements and climatic conditions, implementation is still limited in many countries (Du Plessis, 2003). In northern China, for example, efficient mechanical harvesting requires grain moisture content of maize hybrids to be between 25 and 40% (Nielsen, 2011), making the reduction in grain moisture at harvest a main objective of maize breeders in China.

Grain moisture content, at harvest time, depends on the dry-down rate at maturity (Liu et al., 2020). Dry-down rate, which refers to the reduction in grain moisture content after physiological maturity, is an important trait for reaching the desired level of grain moisture content at harvest time (Cross, 1985; Cross and Kabir, 1989; Martinez-Feria et al., 2019). Varieties with a fast dry-down rate can stay-green late into the season to provide nutrients to the grain (Arriola et al., 2012) while ensuring lower grain moisture content at harvest. Dry-down rate is a polygenic quantitative trait (Li et al., 2021) and is usually inferred from grain moisture content at physiological maturity and grain moisture content at harvest time (Cross and Kabir, 1989; Kebebe et al., 2015). To determine the physiological maturity of maize, time of black layer formation on the grain, an indication of physiological maturity of the grain (Rench and Shaw, 1971; Daynard, 1972; Carter and Poneleit, 1973), needs to be recorded. Grain moisture content at physiological maturity or at black layer formation is very difficult and time-consuming to measure since it requires diligent monitoring of the grain for black layer formation (Knittle and Burris, 1976; Tekrony and Hunter, 1995). Therefore, predicting grain moisture content at black layer formation from genomic information and readily available correlated trait(s), such as grain moisture content at harvest time (HWC) and flowering time (FT), is desirable and beneficial to drive genetic improvement using multi-trait genome prediction methods (Schulthess et al., 2016).

Genomic selection (GS) is a popular method that implements and improves upon marker-assisted selection (MAS). Genomic selection (GS) is especially beneficial when dealing with complex traits that are affected by many quantitative loci each with very small effects (Goddard and Hayes, 2007; Hayes et al., 2009; Heffner et al., 2009; Jannink et al., 2010; Crossa et al., 2017). Genomic selection (GS) takes advantage of genome-wide molecular markers, single-nucleotide polymorphisms (SNPs), and has been successfully implemented in both animal and plant breeding to predict genomic breeding values (GEBVs) (Ceballos et al., 2015; Hickey et al., 2017; Zenger et al., 2019). Multi-trait genome prediction (MTGP) models have emerged as a promising approach for joint analyses of multiple traits (Guo et al., 2014; Lyra et al., 2017; Lado et al., 2018; Runcie and Cheng, 2019). MTGP benefits from the information of genetically correlated traits in order to improve genomic prediction accuracies for traits that are difficult to measure/record and can be otherwise inferred from readily available correlated traits (Schulthess et al., 2016).

In this study, multi-trait genomic best linear unbiased prediction (MT-GBLUP) models were used to estimate genetic correlations between BWC and HWC and FT. MT-GBLUP was performed using different model training approaches to investigate optimal prediction strategies and investigate prediction accuracy for BWC when using HWC and FT as secondary traits.

MATERIALS AND METHODS

Materials

The population used in this study contained 397 diverse maize inbred lines with a wide genetic background. These lines were sourced from China (281 lines), United States (105 lines), and CIMMYT (11 lines). Most of the inbred lines from the United States and China are from a temperate environment background, whereas the inbred lines from CIMMYT are from tropical backgrounds.

All 397 inbred lines were planted in three locations in China: Shenyang City in 2019 (19SN) located in northeastern China (N40°82', E123°56'), Shenfu City in 2017 (17SF) located in northeastern China (N41°51', E123°54'), and Hainan Province in 2017 (17HN) located in southern China (N18°45', E109°10'). **Figure 1** shows the location of the three field trials in the experiment, where the blue, red, and green circles represent SN, SY, and HN, respectively. All lines were planted using a randomized complete block design with two replicates per line. The lines were planted in a single row plot of 2-m long, 0.6-m wide, with a 0.4-m aisle between rows.

Since grain moisture at physiological maturity is a component of dry-down rate calculations (Cross and Kabir, 1989; Yang et al., 2010), it was important to determine when the inbred lines entered maturity. Using black layer as a mark for maturity (Daynard and Duncan, 1969; Daynard, 1972; Carter and Poneleit, 1973), all maize inbred lines were phenotyped for time to black layer formation. This was done by observing all plants after pollination until the starch layer of maize grains gradually decreased and the black layer formed. When the black layer appeared, the water content of the kernels was measured for six plants that were randomly selected from each inbred line and showed uniform growth. The water content of the kernels was measured with a moisture meter to a depth of 3 mm at two time points, first when the black layer appeared, and then either 15 or 7 days, for temperate or tropical, respectively. Hainan province is located in the tropical zone with little rainfall and high temperatures, so the dry-down rate of kernels is faster than in temperate zones. A preliminary experiment was done and found that approximately 90% of the lines were ready for harvest after 15 and 7 days after physiological maturity in temperate or tropical zones, respectively. Therefore, a modification to dry-down rate was made to ensure correct comparisons between tropical and temperate zones, after the black layer formation as the moisture content at harvest. Days to flowering was defined as the time taken from planting for 50% of the plants in a

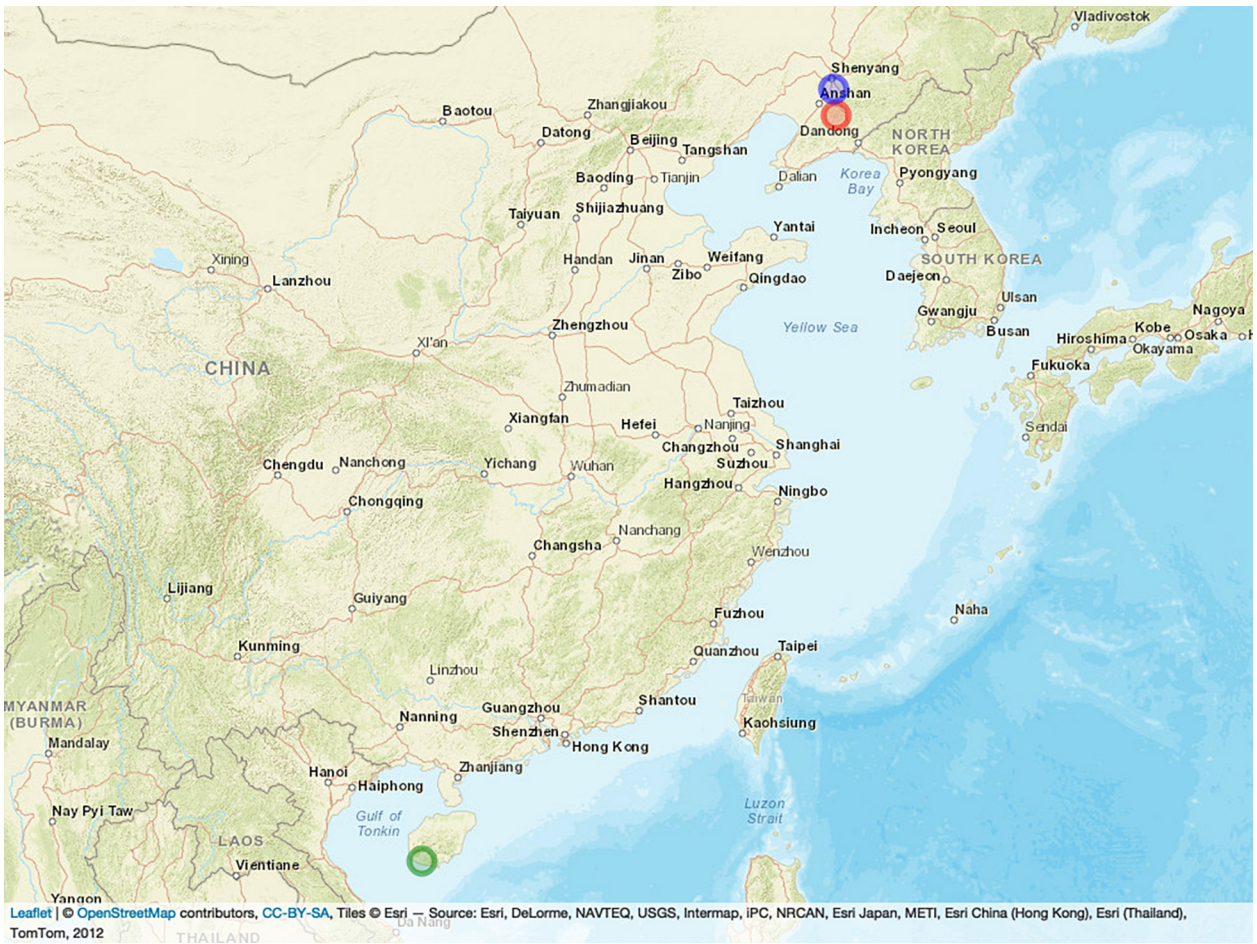

FIGURE 1 | Locations of the three field trials. The blue, red, and green circles represent SN, SY, and HN, respectively.

plot to commence flowering. The experiment was conducted in two ecological zones, the temperate and tropical. The temperate ecological zone had two locations (SN and SF), while the tropical ecological zone had only one location (HN). All phenotypes were collected on the 397 inbred lines.

Genotyping-by-sequencing data with 600 K single-nucleotide polymorphism (SNP) markers were available for the 397 inbred lines. After quality control for missing rate ($< 10\%$), minor allele frequency (MAF > 0.05), and LD pruning (at 0.9), missing genotypes were imputed using TASSEL 5.0 (Bradbury et al., 2007).[1] A total of 56,563 SNP markers were used.

Methods

Dry-down rate was calculated for the temperate and tropical regions as follows in Equations 1 and 2.

$$DR_{TRO} = \frac{(BWC - HWC)}{7} \quad (1)$$

$$DR_{TEM} = \frac{(BWC - HWC)}{15} \quad (2)$$

[1]https://tassel.bitbucket.io/

where DR_{TRO} and DR_{TEM} are dry-down rate (DR) for the tropical and temperate climate zone, respectively. BWC is grain moisture content when black layer appeared, and HWC is grain moisture content at harvest time.

Single-trait genomic best linear unbiased predictions (ST-GBLUP) were used to estimate genetic and residual variances in each location using the following model for each trait (BWC, HWC, and FT):

$$\mathbf{y} = \boldsymbol{\mu} + \mathbf{Xb} + \mathbf{Zu} + \mathbf{e} \quad (3)$$

where $\mathbf{y}$ is the vector of raw phenotypes, $\boldsymbol{\mu}$ is the overall mean, $\mathbf{b}$ is the fixed effect of replication, $\mathbf{u}$ is the vector of random additive genetic effects for inbred lines, $\mathbf{X}$ is a design matrix for the fixed effect of replicate, $\mathbf{Z}$ is the design matrix for additive genetic effects, and $\mathbf{e}$ is the vector of residuals. The distribution of the random effect $\mathbf{u}$ was assumed to be $\mathbf{u} \sim \mathbf{N}\left(0, \sigma^2_{\mathbf{u}} \bigotimes \mathbf{G}\right)$, where σ^2_u is the additive genetic variance and the $\mathbf{G}$ is the additive genomic relationship matrix between the inbred lines (Vanraden, 2008) calculated as follows:

$$\mathbf{G} = \frac{\mathbf{WW}'}{2\sum p_j(1-p_j)} \quad (4)$$

Elements of matrix **W** are w_{ij} where w_{ij} is the genotype represented as the number of copies of the major allele of line i at marker j, denoted as 0 or 2 for the minor and major homozygous genotypes, respectively, and p_j is the allele frequency at marker j. Each column of **W** is mean centered prior to calculation of **G**.

Narrow sense heritability (h^2) explains the proportion of phenotypic variation due to additive genetic variance. Heritability was calculated as follows:

$$h^2 = \frac{\sigma_u^2}{\sigma_u^2+\sigma_e^2} \quad (5)$$

Where σ_u^2 is the additive genetic variance, and σ_e^2 is the residual error. Variance components were estimated by fitting a ST-GBLUP model with the genomic relationship matrix (GRM).

A MT-GBLUP model was fit to estimate the genetic and residual covariance between three traits: black layer water content (BWC), harvest time water content (HWC), and flowering time (FT). The general MT-GBLUP model within each ecological zone was as follows:

$$\begin{bmatrix} \mathbf{y_1} \\ \mathbf{y_2} \\ \mathbf{y_3} \end{bmatrix} = \begin{matrix} \boldsymbol{\mu}_1 \\ \boldsymbol{\mu}_2 \\ \boldsymbol{\mu}_3 \end{matrix} + \begin{bmatrix} \mathbf{X}_1 & \mathbf{0} & \mathbf{0} \\ \mathbf{0} & \mathbf{X}_2 & \mathbf{0} \\ \mathbf{0} & \mathbf{0} & \mathbf{X}_3 \end{bmatrix} \begin{bmatrix} \mathbf{b_1} \\ \mathbf{b_2} \\ \mathbf{b_3} \end{bmatrix} + \begin{bmatrix} \mathbf{Z}_1 & \mathbf{0} & \mathbf{0} \\ \mathbf{0} & \mathbf{Z}_2 & \mathbf{0} \\ \mathbf{0} & \mathbf{0} & \mathbf{Z}_3 \end{bmatrix} \begin{bmatrix} \mathbf{u_1} \\ \mathbf{u_2} \\ \mathbf{u_3} \end{bmatrix} + \begin{matrix} \mathbf{e_1} \\ \mathbf{e_2} \\ \mathbf{e_3} \end{matrix} \quad (6)$$

where $\mathbf{y_1}$, $\mathbf{y_2}$, and $\mathbf{y_3}$ are the vectors of phenotypes for BWC, HWC, and FT, respectively, $\boldsymbol{\mu}_1$, $\boldsymbol{\mu}_2$, and $\boldsymbol{\mu}_3$ are the overall mean for each trait, $\mathbf{b_1}$, $\mathbf{b_2}$, and $\mathbf{b_3}$ are the fixed effects of location and replication nested within location, $\mathbf{u_1}$,$\mathbf{u_2}$, and $\mathbf{u_3}$ are vectors of the random additive genetic effects for each trait, $\mathbf{X_1}$, $\mathbf{X_2}$, and $\mathbf{X_3}$ are the design matrices for the fixed effect of replication, $\mathbf{Z_1}$, $\mathbf{Z_2}$, and $\mathbf{Z_3}$ are the design matrices for the random genetic effect, and $\mathbf{e_1}$, $\mathbf{e_2}$, and $\mathbf{e_3}$ are the vectors of residuals. It was assumed that $[\mathbf{u_1}, \mathbf{u_2}, \mathbf{u_3}] \sim \mathbf{N}\left(0, \mathbf{G_o} \bigotimes \mathbf{G}\right)$, where $\mathbf{G}_o$ is the variance–covariance matrix of the genetic effect of the traits as follows:

$$\mathbf{G_0} = \begin{bmatrix} \sigma_{g1}^2 & \sigma_{g12} & \sigma_{g13} \\ \sigma_{g21} & \sigma_{g2}^2 & \sigma_{g23} \\ \sigma_{g31} & \sigma_{g32} & \sigma_{g3}^2 \end{bmatrix} \quad (7)$$

where $\mathbf{G_0}$ represents a symmetrical 3 × 3 variance–covariance matrix of the genomic effect of genotypes in the environments. The diagonal of the $\mathbf{G_0}$ matrix is the additive genetic variance for three traits, while the off-diagonal elements represent the genetic covariance between the traits.

G is the same as Eq. 3, and residual errors were assumed to be distributed as $[\mathbf{e_1}, \mathbf{e_2}, \mathbf{e_3}] \sim \mathbf{N}(0, \mathbf{I} \bigotimes \mathbf{R})$, where **I** is the identity matrix and **R** is a symmetrical unstructured matrix of the residual (co) variances:

$$\mathbf{R} = \begin{bmatrix} \sigma_1^2 & \sigma_{12} & \sigma_{13} \\ \sigma_{21} & \sigma_2^2 & \sigma_{23} \\ \sigma_{31} & \sigma_{32} & \sigma_3^2 \end{bmatrix} \quad (8)$$

ST-GBLUP and MT-GBLUP models were fit separately for each ecological region. For the temperate zone where there were two locations, both Eqs 3 and 6 were modified to account for the random location effect and the effect of replicate was nested within location. However, since there is only one location in the tropical ecological zone, the location effect in both Eqs 3 and 6 was ignored.

Multi-Trait Genomic Prediction and Cross-Validations

Genomic predictions were performed using MT-GBLUP and ST-GBLUP using Eqs 6 and 3 for different cross-validation scenarios. This was done to assess prediction accuracy for BWC using information on correlated traits, HWC and FT, in each ecological zone. For that purpose, three cross-validation scenarios were considered.

Figure 2 shows an example of the first cross-validation scenario (CV1). In CV1, a standard 5-fold cross-validation scenario was used; however, the phenotypic value for BWC was set to missing for an additional randomly selected 20, 40, or 60% of the training set. The phenotypic information for HWC and FT was either kept as complete (**Figure 2A**) or set to missing (**Figure 2B**) when BWC was missing. The purpose of this scenario was to examine a genomic selection approach in which historical data are used to predict performance of untested lines and to determine the value of including historical records for correlated traits, even when the target trait (BWC) was missing. This represents a likely scenario as the cost of phenotyping BWC on all tested lines at all test locations will likely be cost prohibitive.

Figure 3 shows an example of the second cross-validation scenario (CV2). CV2 tested prediction accuracy using 10-, 5-, 3-, and 2-fold cross-validation. In each case, the entire dataset was subdivided to groups, with one of the groups used as a validation set (BWC set to missing), with the rest of the group used as a training set. **Figure 3B** shows an additional scenario (CV_90), in which the validation set was constructed by setting the BWC phenotype of 90% of the maize inbred lines to missing. In this scenario, 90% of the population were randomly selected and BWC was set to missing and fit using MT-GBLUP model. This process was replicated 10 times. In all CV2 scenarios, the phenotypic value for BWC was set to missing in the validation set, while keeping the phenotypic information for HWC and FT. This scenario was used to compare the prediction accuracy in a sparse phenotyping scenario where only a subset of lines are phenotyped for the difficult to measure BWC trait. To examine the impact of using genomic information on prediction accuracy, as opposed to only using correlated trait information, the MT-BLUP model was also fit with an identity matrix in place of the GRM.

In the third scenario (CV3), the validation and training sets were constructed in such a way that one replication or one location was selected and used as a validation set, with the remaining locations and replications used as a training set. In the validation set, the phenotypic value for BWC was set to missing while keeping phenotypic information for HWC and FT. The purpose of this scenario was to simulate a breeding program where BWC is measured only in one replicate or in one location while HWC and FT are recorded in all replicates and locations.

The prediction models were run 10 times, and the Pearson correlation between phenotypic values for BWC (corrected for fixed effects) and predicted values was calculated in each run. The

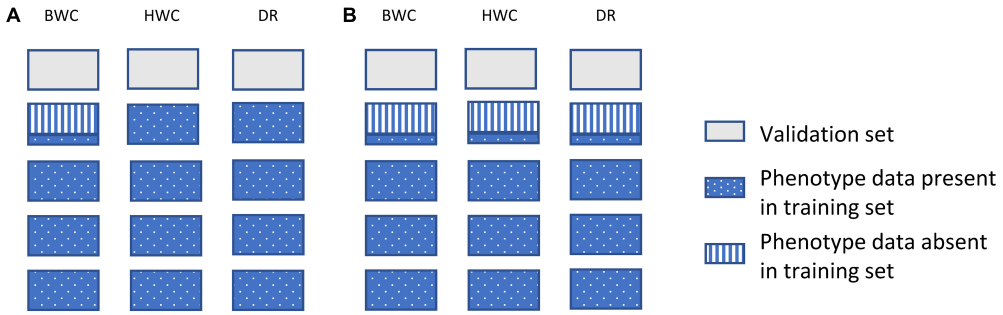

FIGURE 2 | Data used for ST-GBLUP and MT-GBLUP prediction in CV1. Each box indicates the presence or absence of phenotypic data for a particular trait in either the training or validation set. The presence and absence of phenotypic data are indicated by blue dotted (phenotypic data present in the training set), gray (phenotypic data absent in the validation set), and blue vertical stripes (phenotypic data absent in the training set). The phenotypic information for HWC and FT was either kept as complete in the training set **(A)** or set to missing when BWC was missing **(B)**.

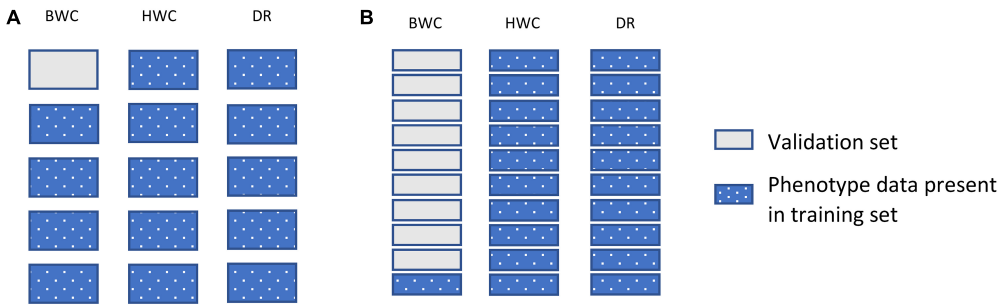

FIGURE 3 | Data used for ST-GBLUP and MT_GBLUP prediction modeling in CV2 **(A)** and the CV_90 scenario where 90% of the inbred lines were randomly selected and had BWC phenotypes set to missing **(B)**. Each box indicates the presence or absence of the phenotypic data for a particular trait on either the training or validation set. The presence and absence of phenotypic data are indicated by dotted blue and gray filled, respectively.

result presented here is the average of the 10 runs. All single- and multi-trait analyses were done using ASReml 4 (Gilmour, 1997)[2].

RESULTS

Heritability and Genetic Correlations

Heritability estimates for BWC, HWC, and DR were obtained using the ST-GBLUP model. As shown in **Table 1**, small (0.22)-to-moderate (0.69) heritability estimates were obtained for BWC across the different locations and ecological zones. Heritability estimates for HWC ranged from small (0.27) to moderate (0.51) across locations and ecological zones, and heritability estimates for DR ranged from 0.15 to 0.26. **Table 2** shows MT-GBLUP genetic correlations, genetic variance, and genetic covariance between BWC, HWC, and FT in temperate ecological zone. Genetic correlations between the BWC, HWC, and FT ranged from 0.24 to 0.66, with the highest genetic correlation between BWC and HWC and the lowest between BWC and FT. Low-to-moderate heritability estimates for BWC and HWC indicate that effective selection pressure can be placed on these traits, and high genetic correlations between BWC, HWC, and FT suggest that multi-trait genomic selection may represent the best approach for genomic prediction for these traits.

Prediction Accuracies

Figure 4 shows prediction accuracy for BWC in the temperate ecological zone from CV1. Only results from the temperate zone (2 locations) are illustrated, as inconsistent model convergence was observed for the tropical environment, likely due to the limited phenotypic data collected in tropical zone. The box plots on the left side of the dotted line are prediction accuracies where all individuals in the training set have phenotypes for the three traits (BWC, HWC, and FT) and when 5-fold cross-validation

TABLE 1 | ST-GBLUP heritability estimates for BWC, HWC, and DR within each agro-ecological zone and location.

Ecological zone	Location	Traits		
		BWC	HWC	DR
Temperate	Shenfu	0.45	0.47	0.22
	Shenyang	0.25	0.27	0.15
	Combined locations	0.22	0.28	0.18
Tropical	Hainan	0.69	0.51	0.26

[2]https://www.vsni.co.uk/software/asreml

TABLE 2 | MT-GBLUP genetic correlation, genetic variance, and genetic covariance between BWC, HWC, and FT in the temperate ecological zone.

	BWC	HWC	FT
BWC	11.59	0.66	0.24
HWC	4.36	3.78	0.42
FT	4.42	4.29	28.16

Genetic variance of the traits is presented on the diagonal; the upper diagonal shows the genetic correlation between the traits, and the lower diagonal is the genetic covariance between the traits.

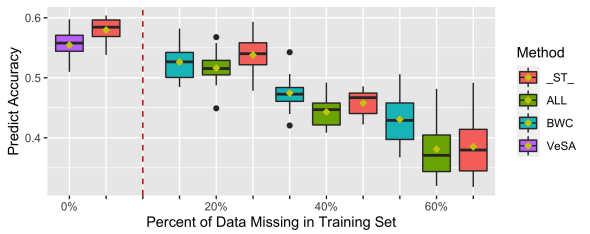

FIGURE 4 | Prediction accuracy from ST-GBLUP and MT-GBLUP models from the first cross-validation (CV1) scenario in temperate zone. Method "_ST_" is the ST-GBLUP model; Method "ALL" is a multi-trait model with all the three dry-down-related traits set to missing for an additional 20, 40, and 60% of the training set; Method "BWC" is a multi-trait model where only the phenotype for BWC is missing for an additional 20, 40, and 60% of the training set; Method "VeSA" is a multi-trait model with complete phenotypic data for all traits in the training set. The results to the left of the dashed lined had no missing data for any trait in the training set.

without additional missing data in training set was used (purple bars). As shown in the **Figure 4**, when all the three dry-down-related traits were set to missing for additional 20, 40, and 60% of the training set (green bars), lower prediction accuracies were observed compared to the case where only the phenotype for BWC was set to missing (blue bars). ST-GBLUP model gave the highest accuracy (red bars) in the cases where the phenotype for BWC was set to missing for additional 20% of validation set, but the MT-GBLUP model performed best when all correlated phenotypes were included in the training set and BWC was set to 40 and 60% missing.

Figures 5A,B shows prediction accuracies for BWC from CV2 in the temperate and tropical ecological zones, respectively. Red and blue box plots represent prediction accuracies from the MT-GBLUP model with genomic relationship matrix (GRM) or identity matrix (IDM), respectively. The box plots on left side of the dotted line are the prediction accuracies from 10-, 5-, 3-, and 2-fold cross-validation scenario. The box plots on right side of the dotted line are the prediction accuracies when 90% of the lines in the population were used as the validation set (CV_90). As shown in **Figure 5A**, prediction accuracies in temperate ecological zone range from 0.45 to 0.79 when the GRM was fit in the MT-GBLUP model, as compared to accuracies ranging from 0.4 to 0.65 when the identity matrix was used. **Figure 5B** shows prediction accuracies for BWC in the tropical ecological zone following the CV2 and CV_90 scenarios. When the GRM was fit in the MT-GBLUP model, prediction accuracies ranged from 0.5 to 0.87 as compared to accuracies ranging from 0.8 to 0.82 when the identity matrix was used. In general, the results from CV2 indicate that higher prediction accuracies are obtained when the GRM is used instead of an identity matrix in the MT-BLUP model.

Table 3 shows prediction accuracies in the temperate ecological zone following the CV3 scenario. As shown in **Table 3**, high prediction accuracies ranging from 0.79 to 0.96 were obtained for BWC in the temperate ecological zone from the MT-GBLUP model. This result indicates that unreplicated designs for BWC data collection can produce accurate results, with potentially large savings in labor and logistical costs.

DISCUSSION

Development of maize varieties with low HWC is an ideal situation that ensures efficient mechanical harvesting can be applied. To achieve this goal, a good breeding strategy which can reduce the consumption of resources while achieving desired rates of genetic gain for the target traits is essential. In this study, we consider the genetic architecture of dry-down-related traits and effective prediction strategies for genomic-enabled breeding, leveraging correlated traits (HWC and FT) that are relatively easy to phenotype (Tsuruta et al., 2011; Jia and Jannink, 2012; Guo et al., 2014; Okeke et al., 2017; Lozada and Carter, 2019). Compared with single-trait genomic prediction model (ST-GBLUP), when a target trait has lower heritability and phenotypic data on highly correlated traits are available, multi-trait genomic prediction model (MT-GBLUP) has a great advantage (Guo et al., 2014). In MT-GBLUP, secondary traits are used to predict a target trait, which is often difficult to phenotype or measure (Lozada and Carter, 2019). The use of MT-GBLUP in US Holstein breeding efforts has improved prediction accuracy of several traits to varying degrees when compared to ST-GBLUP, (Tsuruta et al., 2011). Analogously, when multi-trait and multi-environment mixed models were used to predict agronomic traits, 40% improvement were obtain in prediction ability in cassava (Okeke et al., 2017).

The advantage of MT-GBLUP model, however, depends on the genetic correlation between the target and the secondary traits (Jia and Jannink, 2012). Estimates of (co) variance components for maturity and dry-down traits indicate that moderate-to-strong genetic correlations exist between routinely measured maturity and harvest moisture traits and the more difficult to measure traits like BWC and DR (**Table 2**). These results, combined with the moderate-to-low heritability found for DR (**Table 1**), suggest that genomic-enabled breeding strategies for selection on DR related traits should consider the use of correlated traits. The moderate-to-high correlations between HWC and BWC also indicate that strategies focused primarily on selection for HWC and yield could be used effectively to apply indirect selection pressure on DR. In this study, both hold (CV1 and CV2) and instant (CV_90) prediction accuracy calculations were used. It should be noted that the use of hold prediction accuracies can create negative bias in the correlations used to estimate prediction accuracy, this bias increases as the number of folds increases (Zhou et al., 2016).

The first cross-validation scenario (CV1) focused on breeding strategies that rely on generating predictions for lines that

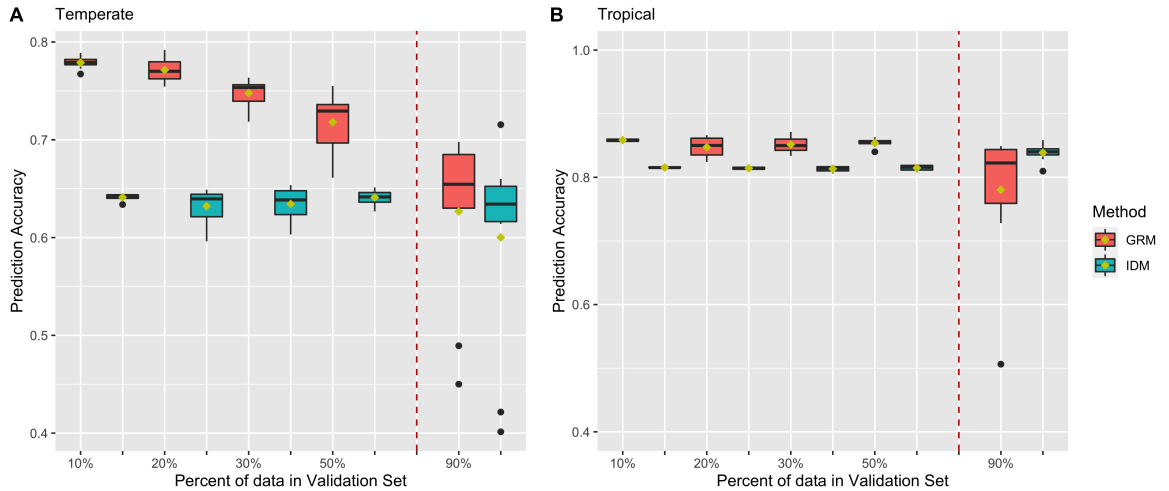

FIGURE 5 | Prediction accuracy for black layer water content (BWC) in temperate **(A)** and tropical **(B)** ecological zones from the CV2) scenario (left of the dashed line) and an CV_90 scenario where 90% of the inbred lines were selected and had BWC phenotypes set to missing (right of the dashed line). Methods "GRM" and "IDM" refer to multi-trait models using a genomic relation matrix or identity matrix for the genetic effect, respectively.

have yet to be tested in the field. As such, no phenotypic information on correlated traits is available on lines in the validation or prediction set. As seen in **Figure 4**, in situations where no correlated traits have been measured, MT-GBLUP model has no comparative advantage over ST-GBLUP when the training dataset has complete records for BWC. In fact, the results suggest that in this scenario, the use of ST-GBLUP may be a more parsimonious model leading to results that are as good or slightly better than MT-GBLUP. These results agree with previous findings that the advantage of MT-GBLUP is largest when the correlated traits were measured on prediction candidates and included in the model (Maier et al., 2015; Mehrban et al., 2019).

In the first cross-validation scenario (CV1), we further investigated the impact of including records in the training set that have no BWC phenotypic information but do have phenotypic records for correlated traits like FT and HWC. Many maize breeding programs record HWC and FT as agronomic traits for many generations (Abadassi, 2015), while BWC is rarely phenotyped. As a result, it is likely that historical data will have far more phenotypic data points for HWC and FT than for BWC. Historical HWC and FT provide breeders a considerable amount of historical data on correlated traits that can be used to predict BWC. The impact of including historical records without the target trait measured varies depending on how unbalanced the historical data are, but as the number of BWC records in the training set decreases, the advantage of MT-GBLUP increases when all correlated trait records are included for model training. These results suggest that including correlated traits in the training set can improve prediction accuracy substantially when there is sparse information on the target trait in historical datasets.

In CV2, the phenotype for BWC was set to missing for a subset of the population in order to mimic a breeding program that collects data on a trait that is expensive and difficult to measure on a subset of the population and predicts the phenotype for the rest of the population using routinely collected data on correlated traits. This is not an uncommon scenario as in most breeding programs, resource and time efficiency are important factors to consider (Morris and Bellon, 2004; Ceccarelli, 2015). The results in **Figure 5** indicate that by using MT-GBLUP, BWC can be predicted with high accuracy for the majority of the population, thus reducing the cost and time that is required to record BWC for all lines being tested in the program.

As shown in **Figure 5**, the inclusion of correlated traits in the validation set resulted in significantly higher prediction accuracies (0.77 compare to 0.55) when compared to results from CV1, as the model exploits genetic correlation with the traits for which phenotypic data is available (Calus and Veerkamp, 2011; Lyra et al., 2017; Lado et al., 2018; Lozada and Carter, 2019; Runcie and Cheng, 2019). Prediction accuracies decreased as the number of lines with missing BWC data increased. Comparison of MT-GBLUP using a GRM with MT-GBLUP using the identity matrix shows that the GRM contributes significantly to prediction accuracy when there is more training data available for BWC. As the number of BWC phenotypic records decreases, the relative advantage of using the GRM decreases, indicating

TABLE 3 | Prediction accuracy from the CV3 scenario for the temperate zone.

	Set-to missing	Accuracy
Replicate	Replicate 1	0.91
	Replicate 2	0.79
Location	Shenfu	0.86
	Shenyang	0.79
Replicate-location	Replicate 1—Shenfu	0.96
	Replicate 1—Shenyang	0.96
	Replicate 2—Shenfu	0.94
	Replicate 2–Shenyang	0.92

that the prediction accuracy is derived largely from correlated traits measured on the lines with missing BWC phenotypes when there are few BWC phenotypic records available to train the model. This trend is more pronounced in the temperate environments as compared to the tropical environment. The presence of several low prediction accuracy outliers for CV_90 is not unexpected given only 10% of the records have BWC information. The composition of the training set for these outliers was examined, and no obvious cause (i.e., population structure) of the lower accuracies was detected.

Multi-location and multi-replication trails play an important role in agronomic research and plant breeding programs (Crossa, 1990). In such cases, phenotyping a trait that is difficult or expensive to measure, such as BWC, in one location or one replication and predicting the phenotype for the other locations/replicates using correlated traits represents a cost-effective testing strategy. The CV3 scenario examines a sparse phenotyping approach in which only one replicate is phenotyped for BWC, while FT and HWC are phenotyped on all plots. The results show high accuracies for BWC predictions (>0.79), indicating that sparse phenotyping approaches can be effectively used to reduce the cost of BWC phenotyping without making large sacrifices in BWC predictions. This approach could be applied in combination with CV2, in which a sparse phenotyping approach is used for field trails after an initial line selection is made based on predictions from a MT-GBLUP model trained using historical BWC records as well data on correlated traits.

CONCLUSION

In this study, multi-trait genomic prediction was tested using different cross-validation scenarios to investigate prediction strategies for genomic-enabled breeding for dry-down-related traits in maize. The results clearly show that the use of correlated traits, like HWC and FT, and sparse phenotyping can yield high prediction accuracies while reducing the cost of extensively phenotyping for difficult to measure traits like BWC. While the sparse phenotyping approaches consistently yielded very high prediction accuracies, the need to phenotype selection candidates on correlated traits places limitations on gains that can be made by increasing selection intensity and reducing generation intervals. Examining strategies for predicting untested lines, the accuracy of model prediction drops substantially when compared to sparse phenotyping; however, this strategy does enable gains in response to selection through increased selection intensity and reductions in the generation interval. Regardless of the breeding strategy, the results of this study show clear advantages to using correlated traits when information on the target trait is sparse in historical datasets.

DATA AVAILABILITY STATEMENT

The phenotype data presented in the study are included in the article/**Supplementary Material**; The genotype data reported in this paper have been deposited in the Genome Variation Map (GVM) in Big Data Center, Beijing Institute of Genomics (BIG), Chinese Academy of Science, under accession numbers GVM000350 at http://bigd.big.ac.cn/gvm/getProjectDetail?project=GVM000350; Further inquiries can be directed to the corresponding author.

AUTHOR CONTRIBUTIONS

PN was involved in manuscript preparation, phenotypic data collection, statistical analysis, development of analysis code, visualization, revision, and check. KR and MA were involved in manuscript preparation, statistical analysis, visualization, revision, and check. SW and YR were involved in conceptualization, research design, revision, and check. DD and LL were involved in phenotypic data collection, revision, and check. NM and ML were involved in revision and check. All authors contributed to the article and approved the submitted version.

FUNDING

This work was supported by the Science and Technology Plan Project of Shenyang City (21-110-3-06), Cornell University (Robbins lab startup funds), and China Scholarship Council (CSC).

ACKNOWLEDGMENTS

PN was grateful to all members in Robbins laboratory for providing help during this study.

SUPPLEMENTARY MATERIAL

The Supplementary Material for this article can be found online at: https://www.frontiersin.org/articles/10.3389/fpls.2022.930429/full#supplementary-material

Supplementary Figure 1 | Example scatter plot for phenotype value against predict value for **(A)** CV1 (20% BWC set to missing), **(B)** CV2 (5-fold CV in the temperate ecological zone), and **(C)** the scenario in which 90% of the inbred lines were random selected and had BWC phenotypes set to missing (CV_90).

Supplementary Table 1 | Information on the phenotype data of dry-down-related traits.

REFERENCES

Abadassi, J. (2015). Maize agronomic traits needed in tropical zone. *Int. J. Sci. Environ. Technol.* 4, 371–392.

Arriola, K., Kim, S., Huisden, C., and Adesogan, A. (2012). Stay-green ranking and maturity of corn hybrids: 1. Effects on dry matter yield, nutritional value, fermentation characteristics, and aerobic stability of silage hybrids in Florida. *J. Dairy Sci.* 95, 964–974. doi: 10.3168/jds.2011-4524

Bradbury, P. J., Zhang, Z., Kroon, D. E., Casstevens, T. M., Ramdoss, Y., and Buckler, E. S. (2007). TASSEL: software for association mapping of complex traits in diverse samples. *Bioinformatics* 23, 2633–2635. doi: 10.1093/bioinformatics/btm308

Brooking, I. R. (1990). Maize ear moisture during grain-filling, and its relation to physiological maturity and grain-drying. *Field Crops Res.* 23, 55–68.

Calus, M. P., and Veerkamp, R. F. (2011). Accuracy of multi-trait genomic selection using different methods. *Genet. Select. Evol.* 43, 1–14. doi: 10.1186/1297-9686-43-26

Carter, M., and Poneleit, C. (1973). Black layer maturity and filling period variation among inbred lines of corn (*Zea mays* L.) 1. *Crop Sci.* 13, 436–439.

Ceballos, H., Kawuki, R. S., Gracen, V. E., Yencho, G. C., and Hershey, C. H. (2015). Conventional breeding, marker-assisted selection, genomic selection and inbreeding in clonally propagated crops: a case study for cassava. *Theor. Appl. Genet.* 128, 1647–1667. doi: 10.1007/s00122-015-2555-4

Ceccarelli, S. (2015). Efficiency of plant breeding. *Crop Sci.* 55, 87–97.

Chowdhury, M. H., and Buchele, W. F. (1978). The nature of corn kernel damage inflicted in the shelling crescent of grain combines. *Transactions ASAE* 21, 610–0614.

Cross, H. (1985). A selection procedure for ear drying-rates in maize. *Euphytica* 34, 409–418.

Cross, H., and Kabir, K. (1989). Evaluation of field dry-down rates in early maize. *Crop Sci.* 29, 54–58.

Crossa, J. (1990). Statistical analyses of multilocation trials. *Adv. Agron.* 44, 55–85.

Crossa, J., Pérez-Rodríguez, P., Cuevas, J., Montesinos-López, O., Jarquín, D., De Los Campos, G., et al. (2017). Genomic selection in plant breeding: methods, models, and perspectives. *Trends Plant Sci.* 22, 961–975. doi: 10.1016/j.tplants.2017.08.011

Daynard, T. (1972). Relationships among black layer formation, grain moisture percentage, and heat unit accumulation in corn 1. *Agron. J.* 64, 716–719.

Daynard, T., and Duncan, W. G. (1969). The black layer and grain maturity in corn 1. *Crop Sci.* 9, 473–476.

Du Plessis, J. (2003). *Maize Production*. Pretoria: Department of Agriculture, Directorate Agricultural Information Services Private Bag X144.

Gilmour, A. (1997). Asreml for testing fixed effects and estimating multiple trait variance components. *Proc. Assoc. Adv. Anim. Breed. Genet.* 12, 386–390. doi: 10.3168/jds.2011-4148

Goddard, M., and Hayes, B. (2007). Genomic selection. *J. Anim. Breed. Genet.* 124, 323–330.

Guo, G., Zhao, F., Wang, Y., Zhang, Y., Du, L., and Su, G. (2014). Comparison of single-trait and multiple-trait genomic prediction models. *BMC Genet.* 15:30. doi: 10.1186/1471-2156-15-30

Hayes, B. J., Bowman, P. J., Chamberlain, A. J., and Goddard, M. E. (2009). Invited review: genomic selection in dairy cattle: progress and challenges. *J. Dairy Sci.* 92, 433–443. doi: 10.3168/jds.2008-1646

Heffner, E. L., Sorrells, M. E., and Jannink, J.-L. (2009). Genomic selection for crop improvement. *Crop Sci.* 49, 1–12.

Hickey, J. M., Chiurugwi, T., Mackay, I., and Powell, W. (2017). Genomic prediction unifies animal and plant breeding programs to form platforms for biological discovery. *Nat. Genet.* 49, 1297–1303. doi: 10.1038/ng.3920

Jannink, J.-L., Lorenz, A. J., and Iwata, H. (2010). Genomic selection in plant breeding: from theory to practice. *Brief. Funct. Genom.* 9, 166–177. doi: 10.1093/bfgp/elq001

Jia, Y., and Jannink, J.-L. (2012). Multiple-trait genomic selection methods increase genetic value prediction accuracy. *Genetics* 192, 1513–1522.

Kebebe, A., Reid, L., Zhu, X., Wu, J., Woldemariam, T., Voloaca, C., et al. (2015). Relationship between kernel drydown rate and resistance to *Gibberella* ear rot in maize. *Euphytica* 201, 79–88.

Knittle, K., and Burris, J. (1976). Effect of kernel maturation on subsequent seedling vigor in maize 1. *Crop Sci.* 16, 851–855.

Lado, B., Vázquez, D., Quincke, M., Silva, P., Aguilar, I., and Gutiérrez, L. (2018). Resource allocation optimization with multi-trait genomic prediction for bread wheat (*Triticum aestivum* L.) baking quality. *Theor. Appl. Genet.* 131, 2719–2731.

Lawrence, C. J., Harper, L. C., Schaeffer, M. L., Sen, T. Z., Seigfried, T. E., and Campbell, D. A. (2008). MaizeGDB: the maize model organism database for basic, translational, and applied research. *Int. J. Plant Genom.* 2008:496957. doi: 10.1155/2008/496957

Li, W., Yu, Y., Wang, L., Luo, Y., Peng, Y., Xu, Y., et al. (2021). The genetic architecture of the dynamic changes in grain moisture in maize. *Plant Biotechnol. J.* 19, 1195–1205. doi: 10.1111/pbi.13541

Liu, J., Yu, H., Liu, Y., Deng, S., Liu, Q., Liu, B., et al. (2020). Genetic dissection of grain water content and dehydration rate related to mechanical harvest in maize. *BMC Plant Biol.* 20:118. doi: 10.1186/s12870-020-2302-0

Lozada, D. N., and Carter, A. H. (2019). Accuracy of single and multi-trait genomic prediction models for grain yield in US Pacific Northwest winter wheat. *Crop Breed. Genet. Genom.* 1:23. doi: 10.3390/genes11070779

Lyra, D. H., De Freitas Mendonça, L., Galli, G., Alves, F. C., Granato, ÍS. C., and Fritsche-Neto, R. (2017). Multi-trait genomic prediction for nitrogen response indices in tropical maize hybrids. *Mol. Breed.* 37, 1–14.

Maier, R., Moser, G., Chen, G.-B., Ripke, S., Absher, D., Agartz, I., et al. (2015). Joint analysis of psychiatric disorders increases accuracy of risk prediction for schizophrenia, bipolar disorder, and major depressive disorder. *Am. J. Hum. Genet.* 96, 283–294. doi: 10.1016/j.ajhg.2014.12.006

Martinez-Feria, R. A., Licht, M. A., Ordóñez, R. A., Hatfield, J. L., Coulter, J. A., and Archontoulis, S. V. (2019). Evaluating maize and soybean grain dry-down in the field with predictive algorithms and genotype-by-environment analysis. *Sci. Rep.* 9, 1–13. doi: 10.1038/s41598-019-43653-1

Mehrban, H., Lee, D. H., Naserkheil, M., Moradi, M. H., and Ibáñez-Escriche, N. (2019). Comparison of conventional BLUP and single-step genomic BLUP evaluations for yearling weight and carcass traits in Hanwoo beef cattle using single trait and multi-trait models. *PLoS One* 14:e0223352. doi: 10.1371/journal.pone.0223352

Morris, M. L., and Bellon, M. R. (2004). Participatory plant breeding research: opportunities and challenges for the international crop improvement system. *Euphytica* 136, 21–35. doi: 10.1111/tpj.15472

Nielsen, R. (2011). *Field Drydown of Mature Corn Grain*. West Lafayette: Purdue University.

Okeke, U. G., Akdemir, D., Rabbi, I., Kulakow, P., and Jannink, J.-L. (2017). Accuracies of univariate and multivariate genomic prediction models in African cassava. *Genet. Select. Evol.* 49, 1–10. doi: 10.1186/s12711-017-0361-y

Pari, L., Latterini, F., and Stefanoni, W. (2020). Herbaceous oil crops, a review on mechanical harvesting state of the art. *Agriculture* 10:309.

Ray, D. K., Mueller, N. D., West, P. C., and Foley, J. A. (2013). Yield trends are insufficient to double global crop production by 2050. *PLoS One* 8:e66428. doi: 10.1371/journal.pone.0066428

Rench, W. E., and Shaw, R. H. (1971). Black layer development in corn. *Agron. J.* 63, 303–305.

Runcie, D., and Cheng, H. (2019). Pitfalls and remedies for cross validation with multi-trait genomic prediction methods. *G3 Genes Genomes Genet.* 9, 3727–3741. doi: 10.1534/g3.119.400598

Schulthess, A. W., Wang, Y., Miedaner, T., Wilde, P., Reif, J. C., and Zhao, Y. (2016). Multiple-trait- and selection indices-genomic predictions for grain yield and protein content in rye for feeding purposes. *Theor. Appl. Genet.* 129, 273–287. doi: 10.1007/s00122-015-2626-6

Shiferaw, B., Prasanna, B. M., Hellin, J., and Bänziger, M. (2011). Crops that feed the world 6. Past successes and future challenges to the role played by maize in global food security. *Food Secur.* 3, 307–327.

Singh, V., Haken, A. E., Paulsen, M. R., and Eckhoff, S. R. (1998). Starch yield sensitivity of maize hybrids to drying temperature and harvest moisture content. *Starch Stärke* 50, 181–183.

Tekrony, D., and Hunter, J. (1995). Effect of seed maturation and genotype on seed vigor in maize. *Crop Sci.* 35, 857–862.

Tsuruta, S., Misztal, I., Aguilar, I., and Lawlor, T. (2011). Multiple-trait genomic evaluation of linear type traits using genomic and phenotypic data in US Holsteins. *J. Dairy Sci.* 94, 4198–4204. doi: 10.3168/jds.2011-4256

Vanraden, P. M. (2008). Efficient methods to compute genomic predictions. *J. Dairy Sci.* 91, 4414–4423. doi: 10.3168/jds.2007-0980

Weinberg, Z., Yan, Y., Chen, Y., Finkelman, S., Ashbell, G., and Navarro, S. (2008). The effect of moisture level on high-moisture maize (*Zea mays* L.) under hermetic storage conditions—*in vitro* studies. *J. Stored Prod. Res.* 44, 136–144.

Yang, J., Carena, M., and Uphaus, J. (2010). Area under the dry down curve (AUDDC): a method to evaluate rate of dry down in maize. *Crop Sci.* 50, 2347–2354. doi: 10.1111/ppl.13048

Zenger, K. R., Khatkar, M. S., Jones, D. B., Khalilisamani, N., Jerry, D. R., and Raadsma, H. W. (2019). Genomic selection in aquaculture: application, limitations and opportunities with special reference to marine shrimp and pearl oysters. *Front. Genet.* 9:693. doi: 10.3389/fgene.2018.00693

Zhou, Y., Vales, M. I., Wang, A., and Zhang, Z. (2016). Systematic bias of correlation coefficient may explain negative accuracy of genomic prediction. *Brief. Bioinformatics* 18, 744–753.

Conflict of Interest: The authors declare that the research was conducted in the absence of any commercial or financial relationships that could be construed as a potential conflict of interest.

Publisher's Note: All claims expressed in this article are solely those of the authors and do not necessarily represent those of their affiliated organizations, or those of the publisher, the editors and the reviewers. Any product that may be evaluated in this article, or claim that may be made by its manufacturer, is not guaranteed or endorsed by the publisher.

frontiers | Frontiers in Plant Science

ORIGINAL RESEARCH
published: 11 July 2022
doi: 10.3389/fpls.2022.921608

Epistasis Activation Contributes Substantially to Heterosis in Temperate by Tropical Maize Hybrids

Zhiqin Sang[1,2], Hui Wang[1,3,4], Yuxin Yang[1], Zhanqin Zhang[2], Xiaogang Liu[1], Zhiwei Li[1] and Yunbi Xu[1,5]**

[1] Institute of Crop Sciences, Chinese Academy of Agricultural Sciences, Beijing, China, [2] Xinjiang Academy of Agricultural and Reclamation Science, Shihezi, China, [3] Crop Research Institute, Shandong Academy of Agricultural Sciences, Jinan, China, [4] National Engineering Research Center of Wheat and Maize, Shandong Technology Innovation Center of Wheat, Shandong Academy of Agricultural Sciences, Jinan, China, [5] International Maize and Wheat Improvement Center, Texcoco, Mexico

OPEN ACCESS

Edited by:
Ana Butron,
Misión Biológica de Galicia, Spanish Council for Scientific Research (MBG-CSIC), Spain

Reviewed by:
Wentao Zhang,
National Research Council Canada, Canada
Kailiang Bo,
Insititute of Vegetables and Flowers (CAAS), China

***Correspondence:**
Zhiqin Sang
sangzhiqin@126.com
Yunbi Xu
y.xu@cgiar.org

Specialty section:
This article was submitted to Plant Breeding, a section of the journal Frontiers in Plant Science

Received: 16 April 2022
Accepted: 16 June 2022
Published: 11 July 2022

Citation:
Sang Z, Wang H, Yang Y, Zhang Z, Liu X, Li Z and Xu Y (2022) Epistasis Activation Contributes Substantially to Heterosis in Temperate by Tropical Maize Hybrids. Front. Plant Sci. 13:921608. doi: 10.3389/fpls.2022.921608

Epistasis strongly affects the performance of superior maize hybrids. In this study, a multiple-hybrid population, consisting of three hybrid maize sets with varied interparental divergence, was generated by crossing 28 temperate and 23 tropical inbred lines with diverse genetic backgrounds. We obtained 1,154 tested hybrids. Among these tested hybrids, heterosis increased steadily as the heterotic genetic distance increased. Mid-parent heterosis was significantly higher in the temperate by tropical hybrids than in the temperate by temperate hybrids. Genome-wide prediction and association mapping was performed for grain weight per plant (GWPP) and days to silking (DTS) using 20K high-quality SNPs, showing that epistatic effects played a more prominent role than dominance effects in temperate by tropical maize hybrids. A total of 33 and 420 epistatic QTL were identified for GWPP and DTS, respectively, in the temperate by tropical hybrids. Protein–protein interaction network and gene-set enrichment analyses showed that epistatic genes were involved in protein interactions, which play an important role in photosynthesis, biological transcription pathways, and protein synthesis. We showed that the interaction of many minor-effect genes in the hybrids could activate the transcription activators of epistatic genes, resulting in a cascade of amplified yield heterosis. The multiple-hybrid population design enhanced our understanding of heterosis in maize, providing an insight into the acceleration of hybrid maize breeding by activating epistatic effects.

Keywords: maize, heterosis, GWAS, epistatic effects, protein–protein interaction, multiple-hybrid population

INTRODUCTION

Hybrid vigor or heterosis refers to the phenotypic superiority of F_1 hybrid plants over their parents. The mechanism of heterosis can be determined according to three primary hypotheses based on classical genetics. The dominance hypothesis explains heterosis by the action of superior dominant alleles from both parents at multiple loci, which complement corresponding unfavorable alleles leading to the enhancement of hybrid vigor. Such complementation might allow hybrids to be similar to or better than the superior parent (Jones, 1917; Birchler, 2015). According to

the single locus overdominance hypothesis, various alleles interact to perform a function better than that performed by homozygous alleles. Therefore, the increase in vigor is proportional to the degree of heterozygosity (East, 1936; Lamkey and Edwards, 1999). Dominance and overdominance hypotheses are based on the action of a single gene, but most heterosis-related traits are quantitatively inherited and involve multiple genes with different effects. The epistasis hypothesis emphasizes the role of inter-allele interactions among genetic loci and associated pathways, which might include all possible forms of molecular interactions (Powers, 1944; Jinks and Jones, 1958; Jiang et al., 2017). Many researchers suggested that partial or complete dominance, rather than super dominance, account for the inheritance of heterosis in maize (Hallauer et al., 2010). Although some researchers have focused on single-gene models, several studies have suggested that heterosis is generally the result of the action of multiple loci, which affect heterosis of different traits and hybrids (Bauman, 1959; Doebley et al., 1995; Ma et al., 2007; Hallauer et al., 2010).

As East (1936) stated, "the problem of heterosis is the problem of the inheritance of quantitative characters," and quantitative traits are typically affected by multiple genes (Flint-Garcia et al., 2009). The genotype of a population has a "net-like" structure; hence, different loci might affect the variation in several characters (Wright, 1984). Additionally, substituting one gene might affect several characters (Yu et al., 1997; Xiao et al., 2021). Based on this perspective, epistasis is one of the most important genetic components in the inheritance of quantitative characters. Epistasis might also contribute to the genetic basis of heterosis (Hua et al., 2003; Hochholdinger and Baldauf, 2018). Epistasis not only shapes which loci can express heterosis but can also mimic overdominance (Fiévet et al., 2010). Several studies have investigated the epistatic effects using quantitative and biparental population genetic approaches (Doebley et al., 1995; Culverhouse et al., 2004). Biparental populations have a narrow genetic basis, which further restricts the effective detection of epistasis (Jiang et al., 2017; Xiao et al., 2021). Due to the lack of tailored quantitative genetic approaches to determine the function of epistasis in hybrid breeding populations, epistatic effects in the populations developed by crossing a panel of diverse breeding materials could not be assessed (Boeven et al., 2020). A quantitative genetic framework was developed to determine the relative contributions of dominance and epistatic effects to heterosis (Jiang et al., 2017), allowing the integration of epistasis in hybrid populations to derive from different parents.

In line with the quantitative genetic hypothesis, hybrid vigor is determined by the interparental genetic distance (Wei and Zhang, 2018). Assuming that all quantitative trait loci (QTL) contribute to heterosis, the genetic distance can be estimated by the squared difference of the interparental allele frequency (Frankham, 1996; Boeven et al., 2020). When heterosis mainly results from dominance and overdominance effects, it is positively correlated with genetic distance (Lamkey and Edwards, 1998). The genetic distance between parents in maize was found to be moderately or highly correlated with middle parent heterosis (Laude and Carena, 2015), which was contrary to several other reports from the tropical region (Badu-Apraku et al., 2013; Oyekunle et al., 2015). Most artificial selection techniques involved reshaping gene networks rather than single genes (Doust et al., 2014). Thus, due to thousands of years of artificial and natural selection, temperate germplasm exhibits significantly lower genetic diversity compared to tropical germplasm, as shown by the diversity of haplotypes and SNP markers (Lu et al., 2009, 2011). Therefore, the genetic distance between temperate and tropical maize is greater than that within temperate maize. Ignoring the genetic architecture of heterosis within and between alleles might show incorrect relationships between heterosis and genetic distance, especially for the temperate by tropical hybrids with significant genetic differentiation (Boeven et al., 2020).

To understand the genetic mechanism of heterosis in different types of maize, three different hybrid maize panels were developed in this study. The temperate by temperate panel comprised 377 temperate maize hybrids, the temperate by tropical panel comprised 641 temperate and tropical hybrids, and the tropical by tropical panel comprised 136 tropical hybrids. In this study, we found that the heterosis of grain yield and flowering stage increased with heterotic genetic distance. Genome-wide association studies on the heterosis of grain yield and days to silking revealed changes in the genetic architecture of the hybrids from the temperate by temperate to temperate by tropical panels, indicating novel epistatic effects underlying the heterosis in the temperate by tropical panel. The results of the protein–protein interaction (PPI) network analysis and gene-set enrichment analysis (GSEA) demonstrated that many minor loci interacting with the gene networks might improve the performance of the hybrids.

MATERIALS AND METHODS

Plant Materials and Phenotyping

The multiple-hybrid population used in this study was derived from the cross between 23 tropical and 28 temperate inbred lines, representing high diversity in temperate and tropical regions. These lines were grouped into seven heterotic pools according to their pedigrees, original regions, and genetic population structure inferred from molecular markers (Wang et al., 2017). The temperate diallel contained 377 hybrids derived from Griffing IV (temperate by temperate) with 28 temperate maize inbred lines (13 U.S. and 15 Chinese lines), representing different heterotic groups. The NC II (temperate by tropical) hybrid panel contained 641 hybrids generated from 23 tropical and 28 temperate inbred lines. The tropical diallel contained 136 hybrids derived from Griffing IV (tropical by tropical) with 17 tropical inbred lines as parents, many of which were developed at the International Maize and Wheat Improvement Center (CIMMYT) (**Supplementary Figure 1**). For 325 temperate diallel crosses and 263 NC II crosses, enough hybrid seeds were generated to conduct field trials for phenotyping in 2013, 2014, and 2015 at Xinxiang, Henan (35.1°N, 113.8°E) and Shunyi, Beijing (40.2°N, 116.6°E) using randomized block design with two duplicates for each experiment (Wang et al., 2017; Yu et al., 2020). Tropical diallel hybrids were phenotyped in

Jinghong, Yunnan (22.0°N, 100.8°E) in 2014 and Sanya, Hainan (18.4°N, 109.2°E) in 2015 using the same experimental design (Wang et al., 2017). For 377 temperate diallel crosses and 641 NC II crosses, enough hybrid seeds were generated to conduct field trials for 2 years (2017–2018) in Shihezi, Xinjiang (45.2°N, 84.68°E), using alpha designs with two replicates (**Supplementary Table 1**). For each replicate, during field trials, all the hybrids and their 51 parents were split into two adjacent trials. Herbicides, insecticides, and fertilizers were applied following the farmer's practices in intensive maize production.

Days to silking (DTS) and days to anthesis (DTA) were recorded as the number of days from planting to when 50% of the plants in a plot had shed pollen and extruded silks, respectively; anthesis–silking interval (ASI) was defined as the time interval between DTS and DTA. After female flowering, the PH values were recorded as the averaged value of the five plants from the center of the plot. The grain yield per plant (GWPP) was estimated based on the mean value of 10 plants. The grain number per row (GNPR), the row number (RN), and the ear barren tips (TIP) were measured as the averaged value of 10 ears from each plot. Harvesting was performed manually, and the harvest was adjusted to a moisture content of 140 g H_2O kg^{-1}.

Phenotypic Data Analysis

A two-stage method was adopted for phenotypic data analysis (Möhring and Piepho, 2009), where effects were modeled and estimated for each environment first, and then the means of genotypes across environments were calculated. In the first step, we used a mixed model approach for analyzing the modeling effects of individual environments for genotypes, replications, and the blocks within replications, based on the statistical model

$$y_{ijkl} = g_{ij} + r_k + b_{lk} + e_{ijkl} \quad (1)$$

where y_{ijk} represents the phenotypic performance of the ijth genotype (hybrid $j \neq i$ or parental line $i = j$) within the lth incomplete block for the kth replication, g_{ij} represents the genetic effect of the ijth genotype, r_k represents the effect of the kth replication, b_{lk} represents the effect of the lth incomplete block within the kth replication, and e_{ijkl} represents the residual. Except for the effect of g_{ij} , the remaining effects were random.

In the second step, to analyze the phenotypes in various environments, we used a linear mixed model based on the adjusted best linear unbiased estimates (BLUEs) of individual environments:

$$y_{ijn} = g_{ij} + l_n + \left(g_{ij}l\right) + e_{ijn} \quad (2)$$

where g_{ij} and l_n denote the genotypes and individual environments, respectively. Except for the effect of g_{ij} , all other effects were random.

The fixed genotypic effects were used to obtain the BLUEs for parental and hybrid genotypic values. Next, we used the BLUEs for calculating mid-parent heterosis ($_{MPH}$) of all hybrids by $MPH = F_1 - MP$, where, F_1 represents the hybrid performance, and MP represents the mid-parent value for two parents, P_1 and P_2 . Then, we determined the relative $MPH(\%)$ for all hybrids using the formula $MPH(\%) = (\frac{MPH}{MP}) \times 100$. Next, we determined better-parent heterosis ($_{BPH}$) using the formula $BPH = F_1 - P_{\text{Better}}$, where P_{Better} represents the performance of the better-performing parental line. We measured relative BPH using the formula $BPH\,(\%) = (\frac{BPH}{P_{\text{Better}}}) \times 100$. Pearson's product–moment correlation coefficients were calculated to test the BLUEs-based correlations. Student's t-tests were performed to compare the BLUEs among diverse genotypes.

The mixed linear model approach was used to estimate variance components, and except for the group effect, the remaining effects were random. Then, we decomposed the total variance of the temperate by temperate and temperate by tropical set to the variances resulting from the effects of the general combining ability (GCA) of female and male subjects, as well as the variance resulting from the specific combining ability (SCA) of the hybrids (Zhao et al., 2015):

$$\begin{aligned} y_{ijkl} = a + l_n + lr_{nk} + g_i + g_j + g_{ij} \\ + g_i : l_n + g_j : l_n + g_{ij} : l_n + e_{ijn} \end{aligned} \quad (3)$$

where y_{ijkl} represents the phenotypic performance of the ijth entry (hybrid $i \neq j$, or line $i = j$) in the nth environment, a represents hybrid and line group effects, l_n indicates the effect of the nth environment, g_i and g_j indicate the genetic effects of the parental lines, g_{ij} represents the SCA effect of the crosses between i and j lines, $g_i : l_n$ and $g_j : l_n$ represents the interplay effect between the i/jth parental lines and the nth environment, $g_{ij} : l_n$ represents the interplay effect between the SCA and the environment, whereas, e_{ijn} represents the residual. Heritability was estimated by the genotypic-to-phenotypic variance ratio, $H^2 = \frac{\delta_G^2}{\delta_G^2 + \delta_G^2/E + \delta_\varepsilon^2/(E \times R)}$, where, E represents environment number, R represents the mean replication number in each entry in one location, and δ_e^2 represents the combined error variance. The MPH was estimated according to the block-corrected values of the hybrids in each environment and their parental BLUEs obtained across all environments. These MPH values calculated for each environment were used to construct the linear mixed model (Equation 3) and estimate heritability. The ASReml-R 4.0 software package was used for performing statistical analysis in the R environment (Butler et al., 2009).

Genotypic Data Analysis

In a previous study, we genotyped the 51 parental lines with the Maize55K chip (Wang et al., 2017; Xu et al., 2017). From this SNP dataset, quality control of minor allele frequency (MAF > 5%), missing data (<5%), and SNP were filtered based on linkage disequilibrium (LD) (eliminating one in each SNP pair when LD was greater than 0.5 among 50 SNPs). We retained 22,510 high-quality SNP markers for further analyses. For some SNPs with less than 5% MAF in the temperate hybrids, 20,555 high-quality SNPs were finally selected and used for genome-wide prediction and association mapping in the temperate by temperate set. The marker profiles for each hybrid were deduced from the corresponding parental lines. In the genome-wide prediction and association mapping of the additive model, the minor homozygote was coded as "2," the major homozygote was coded as "0," and the heterozygote was coded as "1,"

The F_{st} statistic and SNP nucleotide divergence (π) between the temperate and tropical inbred lines were calculated using VCFtools (Danecek et al., 2011) and visualized in R (R Core Team, 2018). For each 1,000-kb window, we calculated the F_{st} statistics and sequence diversity statistics (π) with 100-kb steps in the maize genome. We also determined π values for temperate and tropical inbred lines, and the ratio of π ($\pi_{temperate}/\pi_{tropical}$) was used to detect the genetic-improvement sweeps. For parental lines and hybrids, the LD decomposition, based on the genetic map distance, was evaluated by fitting the natural smoothing splines to r^2 values using the software package PLINK (Purcell et al., 2007). Principal component analysis (PCA) was performed to analyze the population structures of the hybrids and parental lines using the software TASSEL (Bradbury et al., 2007), and MEGA version 7.0.26 was used for clustering based on modified Nei's genetic distance (Tamura et al., 2013). Rogers' distance (RD) was used to measure the genetic distance (Boggs and Rogers, 1990). We conducted genome-wide prediction for the hybrid phenotype to obtain dominance effects for GWPP and DTS (Zhao et al., 2013; Alves et al., 2019); then, we used them to weigh the marker loci. Furthermore, we determined the heterotic genetic distance developed by Boeven et al. (2020), which was expressed depending on Rogers' distance by including the predicted dominance effects for SNP, as shown in Equation 4:

$$\int_{RD}(X, Y) = \frac{1}{L}\sum_{u=1}^{L} w_u \sqrt{\frac{\sum_{j=1}^{n_u}(X_{uj} - Y_{uj})^2}{2}} \quad (4)$$

where X and Y represent two genotypes, X_{uj} and Y_{uj} represent the frequency of the jth allele at the uth locus, n_u represents the allele number in the uth locus, L represents the locus number, and w_u indicates the dominance weight at the $_u$th locus. Bayes method was used to predict the dominance effects of SNPs (Zhao et al., 2013; Alves et al., 2019). Additionally, five-fold cross-validation was conducted with 100 iterations for predicting dominance effects and assessing the relationship of heterosis with $\int_{RD}$. Locally weighted linear regression was performed to determine the relationship between heterosis and genetic distance.

Partitioning of Genetic Variance Components for Mid-Parent Heterosis

We fitted the extended genomic BLUE model that included the digenic epistatic and dominance effects to estimate the genetic variance components of MPH (Zhou et al., 2012; Jiang et al., 2017; Boeven et al., 2020). The model is shown below:

$$y = g_d + g_{aa} + g_{ad} + g_{dd} + e \quad (5)$$

Here, y represents the MPH vector of every hybrid, g_d, g_{dd}, g_{ad}, and g_{aa} indicate genetic values of the vectors related to dominance, dominance-by-dominance, additive-by-dominance, and additive-by-additive effects, and e represents the residual. It is assumed that $g_d \sim N(0, K_d\delta_d^2)$, $g_{aa} \sim N(0, K_{aa}\delta_{aa}^2)$, $g_{ad} \sim N(0, K_{ad}\delta a_d^2)$, $g_{dd} \sim N(0, K_{dd}\delta_{dd}^2)$, and $e \sim N(0, TT'\delta_e^2)$ in the formula, where K_d ,K_{aa} , K_{ad} , and K_{dd} indicate the kinship matrices derived from the markers of different genetic effects, T indicates the linear transformation $r \times (r + s)$ matrix from the original trait vectors to the MPH vector, r indicates the hybrid number, and s represents the parental line number. Next, the F metric was used for calculating kinship matrices derived from the markers, resulting in model non-orthogonal parametrization (Jiang et al., 2017). The multi-kernel approach was adopted to estimate the variance components δ_d^2 , δ_{aa}^2 , δ_{ad}^2 , and δ_{dd}^2 using the R package BGLR (Pérez and De Los Campos, 2014), following previously published settings (Jiang et al., 2017).

Estimation of Heterotic Effects

For a locus, its heterotic effect represents its genetic contribution to MPH and also the combination of the self-dominance effect and epistatic interaction effect with the entire genetic background (Jiang et al., 2017). Specifically, Q was assumed to be the entire QTL set for each phenotypic trait. QTL was assigned a value of 0, 1, or 2, based on the selected allele number at each locus. For each hybrid, $R_{kl}\,(k,\ l = 0 \text{ or } 2)$ was denoted as the locus subset, where the male and female parents had the genotypes l and k, respectively. For $i, j \in Q$ and i $\neq$ j, d_i is assumed as the dominance effect of the ith QTL, while aa_{ij} , ad_{ij} , and dd_{ij} represent the additive-by-additive, additive-by-dominance, and dominance-by-dominance epistatic effects between ith and jth QTL. For the ith locus, its heterotic effect is shown below:

$$h_i = \begin{cases} d_i - \frac{1}{2}\sum_{j\in R_{20}} aa_{ij} + \frac{1}{2}\sum_{j\in R_{02}} aa_{ij} + \frac{1}{2}\sum_{j\in R_{22}} ad_{ij} \\ \quad -\frac{1}{2}\sum_{j\in R_{00}} aad_{ij} + \frac{1}{2}\sum_{j\in R_{20}\cup R_{02}} dd_{ij} \text{ if } i \in R_{20} \\ d_i - \frac{1}{2}\sum_{j\in R_{02}} aa_{ij} + \frac{1}{2}\sum_{j\in R_{20}} aa_{ij} + \frac{1}{2}\sum_{j\in R_{22}} ad_{ij} \\ \quad -\frac{1}{2}\sum_{j\in R_{00}} aad_{ij} + \frac{1}{2}\sum_{j\in R_{20}\cup R_{02}} dd_{ij} \text{ if } i \in R_{02} \\ \quad \frac{1}{2}\sum_{j\in R_{20}\cup R_{02}} ad_{ij} \text{ if } i \in R_{22} \\ \quad \frac{1}{2}\sum_{j\in R_{20}\cup R_{02}} dd_{ij} \text{ if } i \in R_{00} \end{cases} \quad (6)$$

According to the definition, the MPH value of the hybrid represents the summation of all heterotic effects among polymorphic loci.

Genome-Wide Scanning for Significant Heterotic Effects

A three-step process proposed by Jiang et al. (2017) was used to detect significant heterotic effects. First, we conducted genome-wide association mapping to identify significant component effects. Additionally, a standard linear mixed model was constructed along with the kinship matrix derived from the markers to control the structure of various polygenic background effects and relatedness levels (Yu et al., 2005). Assuming the presence of epistasis, a model that controls polygenic background effects, including epistatic and main effects, needs to be constructed (Xu, 2013; Jiang et al., 2017). This model is shown below:

$$y = m\alpha + g_d + g_{aa} + g_{ad} + g_{dd} + e \quad (7)$$

Here, y, g_d , g_{aa} , g_{ad} , g_{dd} , and e represent the same parameters as those presented in Equation 5. Particularly, α represents the dominance effect of a marker or the epistatic interaction effect of a pair of markers, and m represents the relevant coefficient. We assumed α to be an unknown fixed parameter, while the rest were assumed to be the same as those in Equation 5. We

converted this model into a standard linear regression model for calculating efficiency, where only the residual terms were random. The converted model was similar to the original one as long as the effect of different parameters on the estimation of the variance components was negligible (Lippert et al., 2011; Xu, 2013). Next, we performed the *F* test to assess the significance of the effect of α (Jiang et al., 2017).

Second, we integrated the significant component effects into the heterotic effects based on Equation 6. We set each non-significant effect as zero.

Third, for all loci, we analyzed their heterotic effect h_i using the permutation test. Specifically, we predicted the hybrid absolute MPH values through their respective heterotic effects. Then, we determined Pearson's correlation coefficient between the actual and estimated MPH values and conducted permutation tests for the correlation coefficients.

In steps one and three, we examined the genome-wide threshold for the *p*. For the temperate by tropical panel, heterotic and dominance effects were tested by Bonferroni corrected threshold at $p = 0.001/n$. In contrast, the additive-by-additive, additive-by-dominance, and dominance-by-dominance epistatic effects were tested at $p < 0.001/[n(n-1)]$, where *n* denotes the tested number of SNPs (Holm, 1979; Jiang et al., 2017). The small population size restricted the power to detect significant effects for the temperate by temperate panel. Thus, the threshold for the heterotic and dominance effects in GWPP was set at $p < 0.05/n$, whereas the epistatic effects were tested at $p < 0.05/[n(n-1)]$.

Omics Network Analysis and Gene-Set Enrichment

To further interpret the genetic structure and identify the important candidate epistatic genes for the two tested traits, the genes adjacent to the significant SNPs less than 55 kb were considered to be the candidate genes, while the length of linkage disequilibrium (LD) decay was 245 kb at $r^2 = 0.1$ (Jung et al., 2004). In this study, the MaizeGDB database[1] was used to convert candidate gene names from AGPv3 to AGPv4, and the candidate genes were annotated based on the data from the MaizeGDB database (Harper et al., 2016). A seed indicated the input gene used to query protein–protein interactions (PPI), and the interactome comprised its direct interactor genes. The first layer network comprised the seeds; the second layer network comprised all interactors that interacted with the seeds; the specific network was composed of the first + second layer interactomes. The candidate genes were assigned to PPI using the Maize Interactome Platform (MIP) developed in another study (Han et al., 2020), and the first layer network was constructed based on the interaction of the candidate genes with each other. Each gene in the first layer network acted as seeds, which were used to query the direct interactor genes in the MIP Network Creation tool. Then, all of their genes were selected with the MIP Slim-interactive Omics Network tool to classify them into corresponding modules. The direct interactor genes were used to compose the second layer network. The gene network obtained from MIP was imported into Cytoscape version 3.7.2 for further analysis and displayed. The genes in the different modules were then assigned to perform Gene Ontology under the categories of biological process (GO-BP) to identify biological functions with a false discovery rate (FDR) less than 0.05, based on the online AgriGO Singular Enrichment Analysis tool[2] (Tian et al., 2017).

RESULTS

Broad Breeding Germplasm From Temperate and Tropical Regions to Determine Heterosis

We produced a multiple-hybrid population of maize with 1,154 hybrids from three subpopulations. The largest genetic distance was identified between the temperate and tropical lines ($p < 0.001$; 0.38), followed by the groups of the tropical (0.36) and temperate lines (0.35). The genetic diversity in the intergroup was also determined, and a faster LD decay was found in the temperate by tropical hybrid set than in the other two hybrid sets. The PCA confirmed the differences among the three hybrid sets, with three final patterns being distributed in different spaces. Using an NJ phylogenetic tree, cluster analysis based on GD estimates identified 49 groups, and the hybrids derived from a parent were mostly clustered into the same group (**Figure 1**). The F_{ST} and θπ for the entire maize genome were observed from the volcano plot. We discovered 125 candidate selective-sweep areas, which covered 0.61% of the maize genome.

Higher Level of Heterosis Identified in Temperate by Tropical Hybrids

We evaluated the heterosis of DTS and GWPP for the temperate by temperate and temperate by tropical hybrids from eight agro-ecological sites and the tropical by tropical hybrids in two agro-ecological sites. The heterosis for both GWPP and DTS were normally distributed (**Supplementary Figures 2, 3**). A moderate-to-high heritability was found, with a value of 0.79 for the temperate by temperate set and a value of 0.84 for the temperate by tropical set for GWPP (**Supplementary Figure 4**). The broad-sense heritability for GWPP was 0.63 for the temperate by tropical hybrids and 0.77 for the temperate by temperate hybrids. The broad-sense heritability for MPH of DTS was 0.88 for the temperate by temperate hybrids and 0.93 for the temperate by tropical hybrids. The MPH heritability estimates for both traits were higher for the temperate by tropical hybrids (**Supplementary Figure 4**).

For GWPP, the mean relative MPH for the temperate by temperate, temperate by tropical, and tropical by tropical hybrids were 128.92, 166.24, and 185.88%, respectively (**Supplementary Figure 2**; **Table 1**). The average absolute MPH decreased gradually from the temperate by tropical hybrids to the tropical by tropical hybrids, and finally, to the temperate by temperate hybrids. Hybrids in the temperate by tropical panel had significantly higher absolute MPH than in the temperate by the temperate panel ($p < 0.01$; 84.15 g plant^{-1} vs. 78.48 g plant^{-1};

[1] http://www.maizegdb.org

[2] http://systemsbiology.cau.edu.cn/agriGOv2

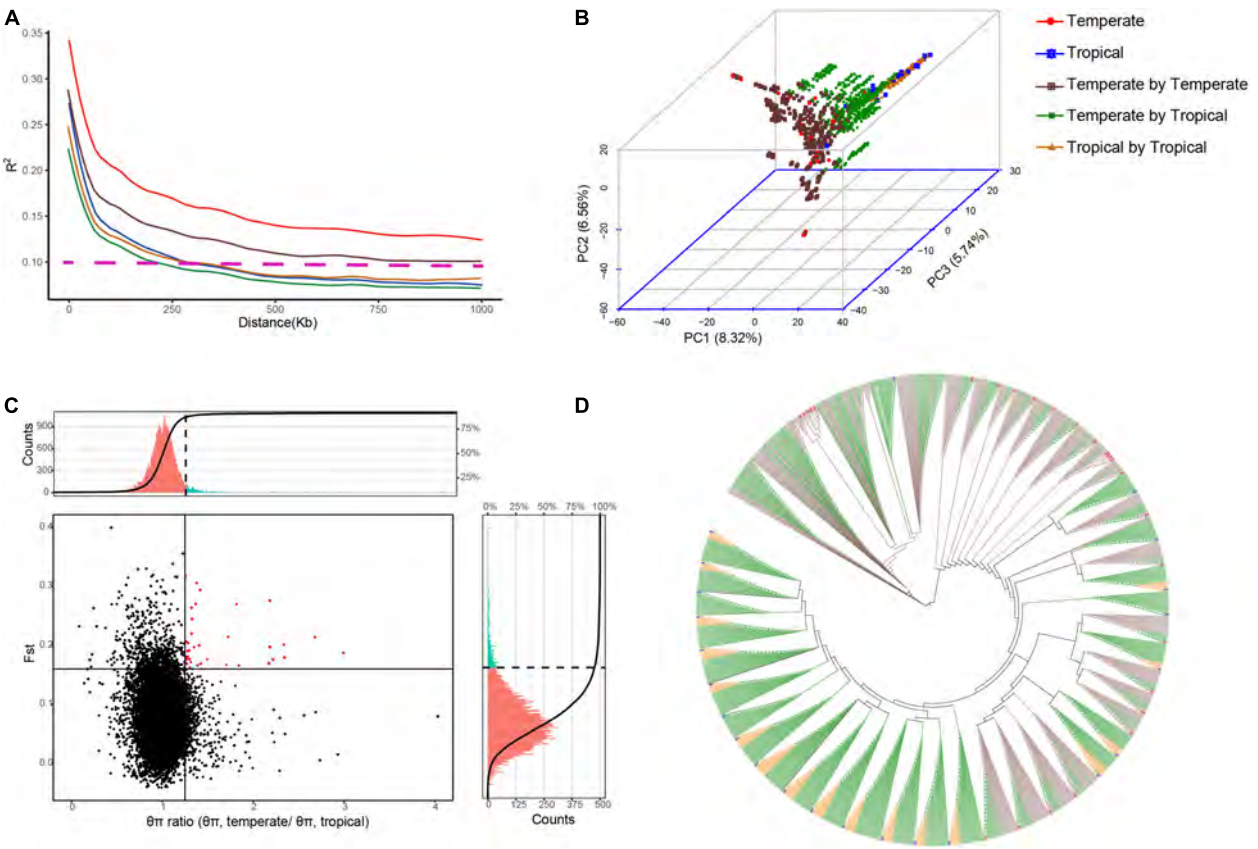

FIGURE 1 | Genetic diversity identified among the hybrids in multiple hybrid populations. Population structure and LD were analyzed for 28 temperate parents, 23 tropical parents, and 1,154 hybrids from the multiple hybrid populations. **(A)** LD decay (R^2) is plotted as a function of the genetic map distance based on pairwise correlations of the LD phase. Horizontal dotted lines represent LD decay lower than 0.1. **(B)** Principal component analysis (PCA) based on the maximum likelihood method. The numbers in the parentheses are genotypic variance proportions explained with the PC1, PC2, and PC3. **(C)** Genome-wide selective sweep analysis on tropical and temperate maize groups. Vertical and horizontal solid lines represent threshold lines for the top 5% of θπ ratios and F_{ST} values, respectively. Red dots in the right upper sector indicate selective signatures for temperate maize lines. The portions of histograms in red and blue colors indicate the θπ ratio (upper) and the F_{ST} (right) values above the thresholds. **(D)** Neighbor-joining tree based on genetic distances.

Figures 2A,B). Lower yield in tropical parents might lead to a higher level mid-parent heterosis in the temperate by tropical hybrids, considering that the temperate parents had 46.49% higher GWPP than tropical parents. However, the temperate by tropical hybrids had 4.7% higher absolute BPH than the temperate by temperate hybrids. The average absolute MPH for DTS decreased significantly from the temperate by tropical hybrids (−4.46 days) to the temperate by temperate hybrids (−5.07 days), and finally, to the tropical by tropical hybrids (−7.00 days) (**Figures 2C,D**). The extent of heterosis showed high specificity for every hybrid set, which could be interpreted either by different interparental genetic distances or the genetic mechanisms for the heterosis between hybrid panels.

Linear Relationship Between Heterosis and Heterotic Genetic Distance

Based on the dominance model, heterosis for GWPP showed a monotonic increase as the interparental heterotic genetic distance increased, explaining 70.78% of the variation (**Figure 3A**; **Supplementary Figures 5, 6**). The unknown part of the variation probably resulted from epistatic effects or the noise. The former was obtained from heterosis variance partitioning with various components, and the results should be interpreted with caution (Huang and Mackay, 2016). For GWPP and DTS, epistasis accounted for 62 and 79% of the total genetic variation in the temperate by tropical hybrids and 57 and 60% in the temperate by temperate hybrids, respectively (**Figure 4**). The contribution of the dominant effect to the total genetic variance of heterosis was relatively low, and the close relationship between heterotic genetic distance and heterosis was not contradictory. On the contrary, the estimated dominant effect also captured different types of epistatic interactions, as shown by the correlation between the marker-derived dominant kinship matrix and the three types of digenic epistatic effects (**Supplementary Tables 2, 3**). The correlation between genetic distances and heterosis was weak when the dominant effects were ignored while estimating the genetic distances (**Figures 3B,D**; **Supplementary Figures 5, 6**).

TABLE 1 | Summary statistics for tested traits (GWPP and DTS) and their heterosis.

Source	DTS (days)	GWPP (g plant^{-1})
Temperate line (Min; Max)	61.75 (56.03; 68.61)	62.45 (36.91; 94.32)
Tropical line (Min; Max)	68.23 (59.76; 77.30)	42.63 (29.07; 63.08)
Temperate by temperate hybrids (*n* = 377)		
Average (Min; Max)	56.67 (51.67; 65.48)	140.99 (57.26; 217.01)
Average MPH (Min; Max)	−5.07 (−10.06; 2.23)	78.48 (8.36; 166.97)
Average MPH% (Min; Max)	−8.20 (−15.89; 3.53)	128.92 (16.5; 333.64)
Average BPH (Min; Max)	−6.90 (−15.88; 1.83)	70.15 (2.83; 161.59)
Average BPH% (Min; Max)	−10.79 (2.87; −23.15)	103.09 (5.20; 291.53)
Temperate by tropical hybrids (*n* = 641)		
Average (Min; Max)	63.48 (52.48; 81.7)	136.73 (35.47; 205.06)
Average MPH (Min; Max)	−4.46 (−11.84; 12.09)	84.15 (−29.69; 157.24)
Average MPH% (Min; Max)	−6.61 (−17.02; 17.46)	166.24 (−45.56; 422.31)
Average BPH (Min; Max)	−10.68 (−22.02; 6.95)	73.45 (−46.86; 149.99)
Average BPH% (Min; Max)	−14.28 (−27.81; 9.58)	125.21 (−56.92; 355.62)
Tropical by tropical hybrids (*n* = 136)		
Average (Min; Max)	67.56 (60.77; 76.27)	126.93 (87.26; 165.67)
Average MPH (Min; Max)	−7.00 (−13.05; −2.09)	79.71 (28.7; 124.25)
Average MPH% (Min; Max)	−9.37 (−16.87; −2.78)	185.88 (38.62; 377.9)
Average BPH (Min; Max)	−9.85 (−17.35; −2.88)	70.70 (−15.59; 123.08)
Average BPH% (Min; Max)	−12.67 (−21.65; −3.64)	152.75 (−13.15; 375.15)

DTS, days to silking; GWPP, grain weight per plant; BPH%, better parent heterosis percentage; BPH, absolute better-parent heterosis; MPH%, mid-parent heterosis percentage; MPH, absolute mid-parent heterosis.

Heterosis continuously increased with heterotic genetic distance, and the mean heterosis increased considerably in the temperate by tropical hybrids than in the temperate by temperate hybrids. The regression line of heterosis with heterotic genetic distance for the temperate by tropical hybrids was lower than that for the temperate by temperate hybrids at the beginning, and then the regression line of the temperate by tropical hybrids exceeded that of the temperate by temperate hybrids, increasing almost in parallel with the increase in the heterotic genetic distance (**Figure 3A**). However, for a given heterotic genetic distance, heterosis performance for GWPP was lower in the temperate by temperate hybrids compared to the temperate by tropical hybrids, but for DTS, it showed an opposite trend (**Figure 3C**), which might be due to the violation of the assumption that genetic effects should be similar among different hybrid sets when heterotic genetic distances are estimated.

Epistatic Effects Make Greater Contributions to Heterosis in the Temperate by Tropical Hybrids

Based on the framework proposed by Jiang et al. (2017), we conducted whole-genome prediction of heterosis for GWPP using 644 temperate by tropical hybrids and 377 temperate by temperate hybrids by modeling digenic epistatic and dominance effects. As revealed by five-fold cross-validation with 100 runs, the model predicted 68.43 and 78.56% of heterosis-related genetic variances for GWPP, and 65.93 and 80.76% for DTS, in the temperate by tropical and the temperate by temperate hybrid sets, respectively (**Supplementary Table 4**). The additive-by-additive model performed better than the dominance effects, with an increase in the genome-wide prediction accuracy by 6.5 and 4.5% in the temperate by tropical hybrids for GWPP and DTS, respectively. However, the combination of the effects in the two models of digenic epistatic and dominance did not affect prediction accuracy, which was probably caused by the high correlation between epistasis and dominance kinship matrices derived from the markers (**Supplementary Table 2** and **Supplementary Figure 7**). Additionally, whole-genome prediction accuracies for GWPP based on the dominance effects outperformed the additive-by-additive effects by 1.46% in the temperate by temperate hybrids, and combining both types of effects did not improve the prediction accuracy, mainly because the dominance model explained the major portion of genetic variance (**Figure 4**; **Supplementary Figure 7**). Partitioning the total genetic variance of heterosis into its components described a particularly important role in epistasis (**Figure 4**), and the additive-by-dominance and additive-by-additive epistasis largely contributed to heterosis in the temperate by tropical hybrids.

Genome-wide association mapping for GWPP discovered four SNP loci with significant dominance effects in the temperate by temperate hybrids and 33 pairs of markers with significant epistatic effects (**Figures 5A–F** and **Supplementary Data Sheets 2, 3**) in the temperate by tropical hybrids, including 11 additive-by-additive, 13 additive-by-dominance, and nine dominance-by-dominance interactions (**Figures 5A,C**). The absence of significant dominance effects in the temperate by tropical hybrids could be partly interpreted by the low contribution (38%) of the dominance effects to the grain-yield heterosis-related genetic variance. The dominance effects in the temperate by temperate hybrids were positive, while 31 of the 33 (93.9%) epistatic effects in the temperate by tropical hybrids were negative. Whether there were significant heterotic QTL effects was determined by the association of the detected heterosis with the estimated contribution of single heterosis QTL, with 14 and 3 heterotic QTL identified in the temperate by tropical and the temperate by temperate hybrid sets, explaining 32.67 and 31.16% of the mean phenotypic variance, respectively (**Figures 5Ac,Dc**).

Genome-wide association mapping for DTS detected 81 pairs of markers with significant epistatic effects in the temperate by temperate hybrids (**Supplementary Data Sheets 4, 5**), including 34 additive-by-additive and 46 additive-by-dominance interactions (**Figures 6Da,E,F**), and 420 marker pairs with significant epistatic effects in the temperate by tropical hybrids, including 93 additive-by-additive, 145 additive-by-dominance, and 182 dominance-by-dominance interactions (**Figures 6A–C**). The absence of significant dominance effects could partly be interpreted by the low contribution of the dominance effects (21 and 40%) to the DTS heterosis-related genetic variance. Of the 420 epistatic effects identified in the temperate by tropical hybrids, 68 (16.43%) were negative (**Supplementary Data Sheet 4**), while 33 of the 238 (13.87%) epistatic effects in the temperate by temperate hybrids were negative. A total of 139 and 37 heterotic QTL were identified in the temperate by tropical and the temperate by temperate hybrid sets (**Figure 8A**; **Supplementary Data Sheet 4**), respectively, which explained

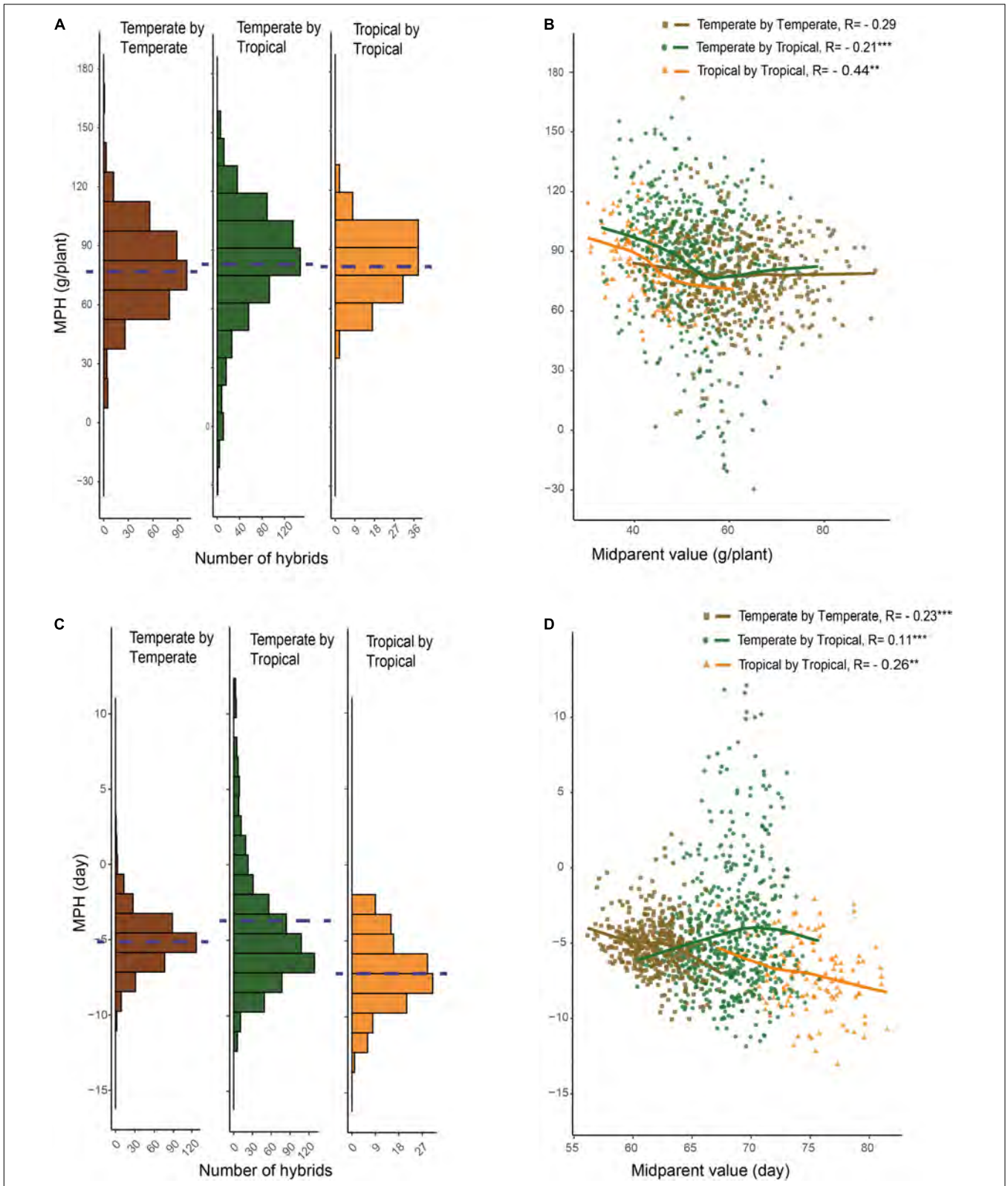

FIGURE 2 | Relationship between hybrid heterosis and mid-parent performance. **(A)** Mid-parent heterosis (MPH) of GWPP for temperate by temperate, temperate by tropical, and tropical by tropical hybrids. **(B)** Relationship between MPH and mid-parent (MP) performance for GWPP. **(C)** Distribution of MPH for days to silking for temperate by temperate, temperate by tropical, and tropical by tropical hybrids. **(D)** Relationship between MPH and MP performance for days to silking. The dashed lines in the histograms indicate the averages.

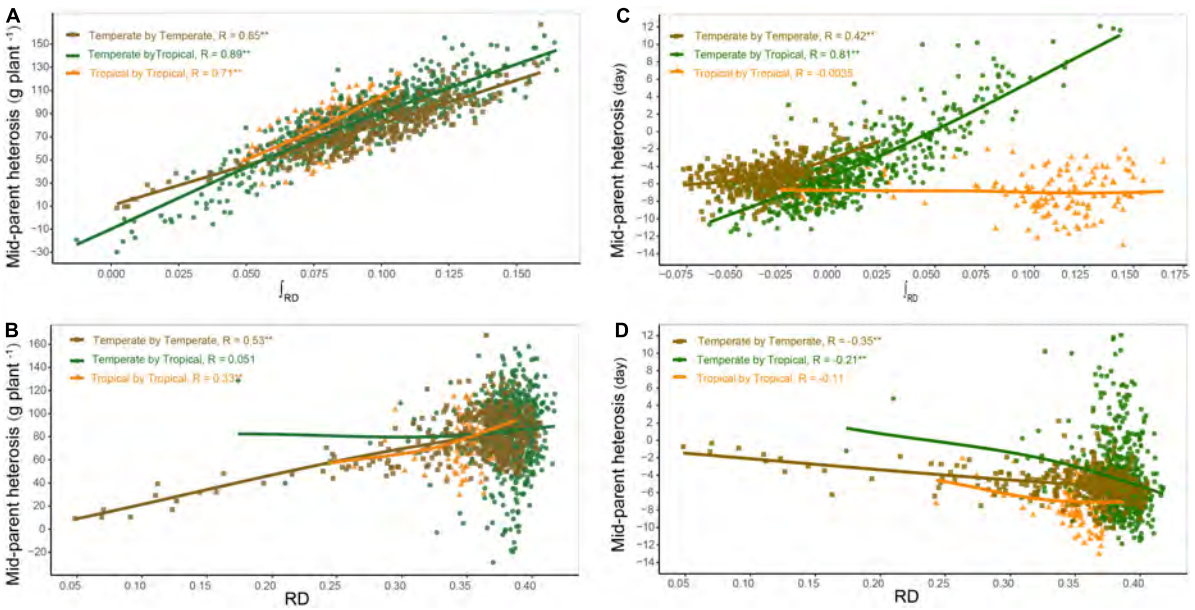

FIGURE 3 | Relationship between genetic distance and heterosis. Panels **(A,B)** show the relationship of mid-parent heterosis (MPH) with heterotic genetic distance ($\int_{RD}$) and Rogers' distance (RD) for grain yield per plant (GWPP), respectively. Panels **(C,D)** show the relationship of MPH with $\int_{RD}$ and RD for days to silking (DTS), respectively. The regression lines in different colors represent the locally weighted regressions for temperate by temperate (golden), temperate by tropical (green), and tropical by tropical (orange) hybrid sets.

31.9 and 50.71% of the phenotypic variance on average (**Figures 6Ac,Dc**).

Candidate Genes and Epistasis Identified in the Temperate by Tropical Hybrids

The interactomes associated with digenic epistasis showed that gene interactions were involved in various biological processes. A total of nine million interactions spanning all levels of genetic information flow across the entire maize lifecycle have been elucidated using the Maize Interactome platform (Han et al., 2020). For GWPP in the temperate by tropical hybrids, a significant locus (Chr2.47114632) was analyzed, along with the other five epistatic loci. A total of 16 candidate genes within 55 kb widows of the epistatic loci were identified using the online Maize Interactome platform PPI Network tool, and five core genes were found with interactions (**Figure 7A**). The five genes were used to build a protein network using the Network Creation instrument, with 90 interacted genes identified. The 90 genes were then analyzed using the online Maize Interactome platform Slim-interactive Omics Network tool, which could be classified into two modules. The first module included 25 genes enriched with GO-BP terms, which could be classified into three functional categories, photosynthesis system (photosystem II assembly, photosynthesis, light reaction, and photosynthesis), positive regulation of transcription (nucleic acid templated transcription modulation, transcription modulation, and RNA biosynthetic process modulation), and protein synthesis (protein complex assembly, protein complex biosynthesis, ribonucleoprotein complex biogenesis, protein complex subunit organization, and ribosome biogenesis) (**Figure 7B**).

For DTS in the temperate by tropical hybrids, a significant locus (Chr6.47114632) with the other nine epistatic interaction loci were analyzed. A total of 40 candidate genes within 55 kb widows of their epistatic loci were analyzed; 12 core genes showed interactions (**Figure 7C**). The 12 core genes were used to build a protein network, with 296 interacted genes and four modules identified. The first module with 64 genes was enriched with GO-BP terms, which were involved in various growth and development processes, such as "cell differentiation," "single-organism development process," "multicellular organism development," "cell development process," "cell response to stress," "reproductive process," and "cell response to stimulus" (**Figure 7D**). The third module with 31 genes was enriched with GO-BP terms, which supported various biosynthesis processes, including the "cellular carbohydrate biosynthesis process," "glucan metabolic process," and " beta-glucan biosynthesis process," and the abiotic stress responses, including the "salt stress response" and "osmotic stress response" (**Figure 7E**).

Epistasis Activation Contributes to Greater Heterosis in the Temperate by Tropical Hybrids

In the parental population, the homozygous background was assumed to suppress the expression of Gene 1 (**Figure 8A**). In the F_1 hybrids, however, such suppression was relieved due to the complementation of heterozygosity, which resulted in the activation of epistasis between Gene 1 and Gene 2. Thus, Gene 1 and Gene 2 might be considered to be epistatically controlled QTL (**Figure 8A**). Using the half-sib hybrids generated between

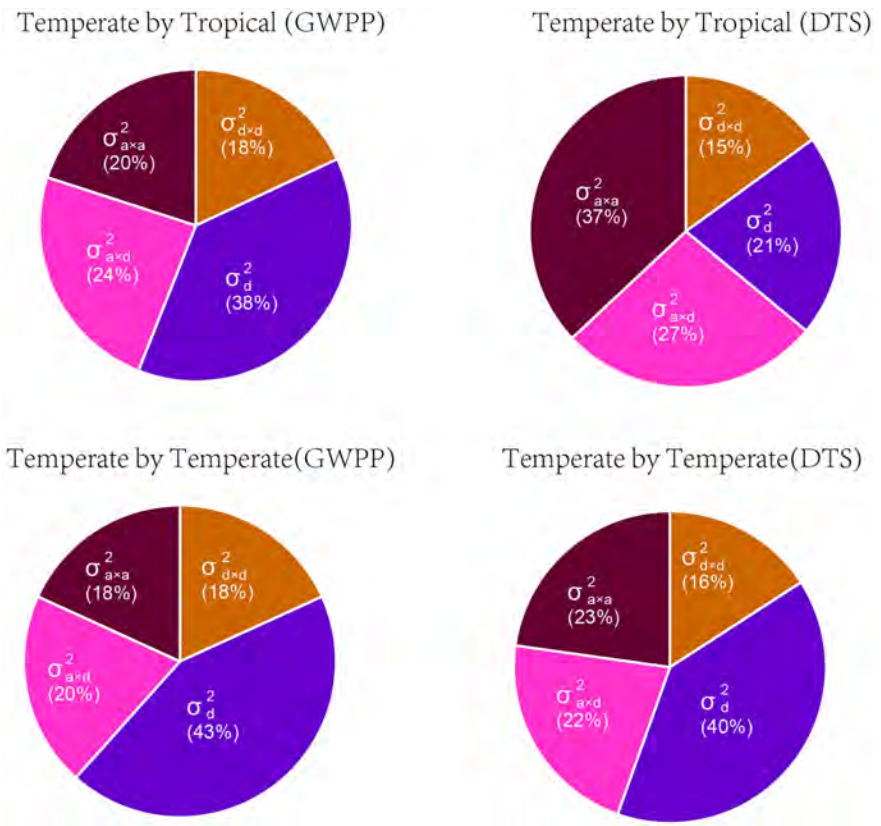

FIGURE 4 | The relative contributions of genetic variance components for mid-parent heterosis for grain yield per plant (GWPP) and days to silking (DTS). Variance components predicted by Bayesian generalized linear regression: σ^2_d, dominance variance; $\sigma^2_{d\times d}$, dominance-by-dominance variance; $\sigma^2_{a\times d}$, additive-by-dominance variance; and $\sigma^2_{a\times a}$, additive-by-additive variance.

the temperate and tropical maize, the genetic mechanisms of heterosis for single-crosses might be explained. The alleles at Gene 1 had additive or dominant effects, but they were undetectable by GWAS in the temperate population due to the absence of the weak activating allele and no phenotypic difference. However, a phenotypic difference was found in the temperate by tropical hybrids, as shown by GWPP. One possible mechanism for the difference identified using the two sets of hybrids might involve transcriptional regulation and PPI, that is, the upstream PPI network in the hybrids released the inhibition of background Gene 1, and the product of Gene 1 further activated the expression of Gene 2 (**Figure 8B**).

The molecular interpretation of the above-mentioned epistasis can be exemplified by the QTL chr2.47114632 and the epistatic QTL chr6.119876370. We hypothesized that this epistatic interaction agreed with the scenario illustrated in **Figure 8B**, because the genotype chr2.47114632-AA was detected in only three tropical parents. Genetic analysis of the two loci, chr2.47114632 and chr6.119876370, indicated that the homozygous genotype at chr2.47114632 was probably inhibited by the background genotype in the parent lines. In the F_1 hybrids, however, a specific of PPI occurred when two parental genomes combined, as the proteome of each parent might provide novel interacting partners (Li et al., 2020). As a result, the repression at chr2.47114632 was removed, which allowed the expression of the chr2.47114632 allele. The full expression of the genotype chr2.47114632-TT activated the chr6.119876370 allele to fully express GWPP, and the genotype chr2.47114632-AT activated the chr6.119876370 allele to weakly express GWPP (**Figure 9A**). The three tropical lines carrying the AA genotypes at chr2.47114632 exhibited lower GWPP in the parent lines, and in the F_1 hybrids, the genotype chr2.47114632-AT also had a relatively low GWPP, indicating that the genotype chr2.47114632-AA was unfavorable to GWPP. Similar interaction occurred between chr2.47114632 and three other loci (**Figures 9B–D**), indicating that chr2.47114632 might host an important regulatory gene involved in multiple biological processes in the formation of GWPP.

DISCUSSION

The hybrids generated from inbred lines in the earlier generation showed higher levels of fitness and heterosis (Rhode and Cruzan, 2005). Various models have been proposed to explain heterosis, including dominance, overdominance, and epistasis with complex allelic, intragenomic, and intergenomic interactions (Birchler et al., 2010; Kaeppler, 2012). According

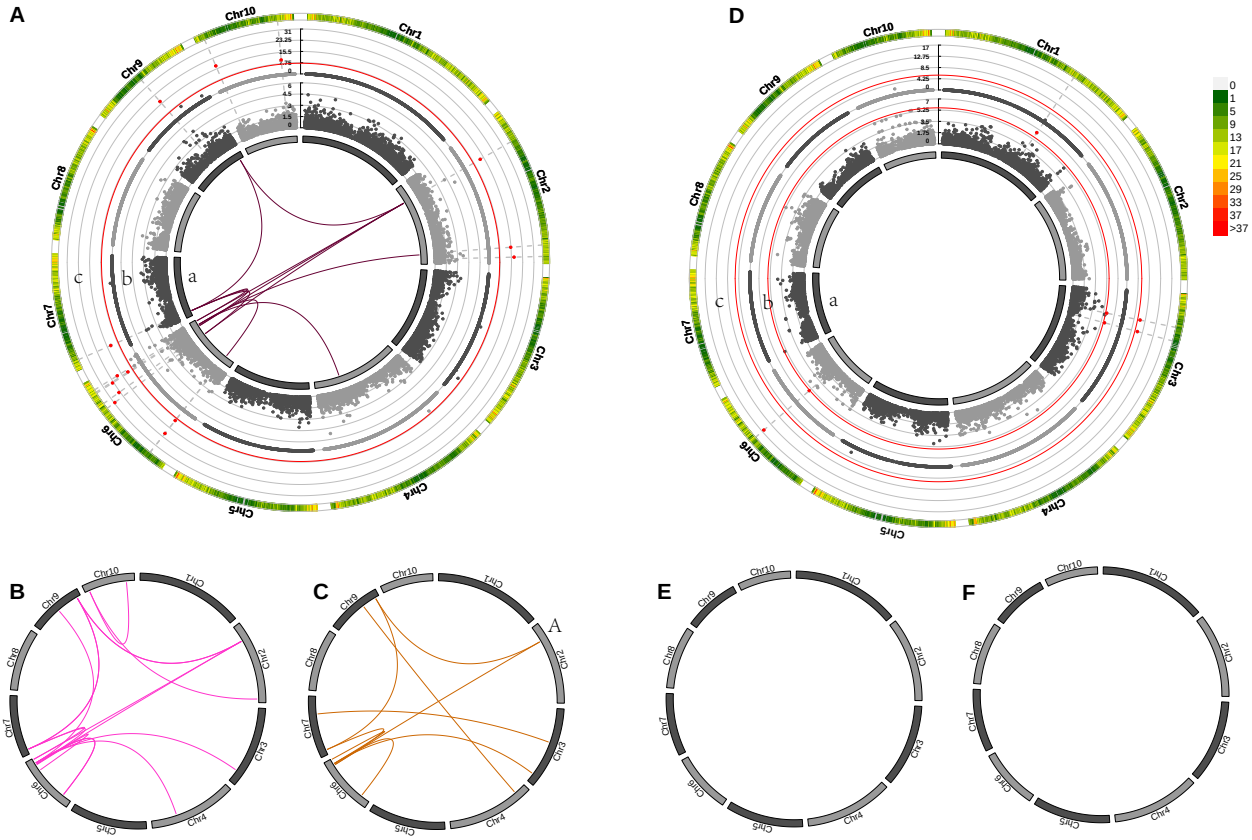

FIGURE 5 | Genetic effects of mid-parent heterosis for maize GWPP in temperate by tropical **(A–C)** and temperate by temperate **(D–F)** hybrids. **(A–F)** In the inner circle, 10 chromosomes are indicated by bars. Gray lines indicate the genetic map locations of SNPs. Color links within the circle indicate significant digenic epistatic interactions, including additive-by-additive [**(A)**a, **(D)**a], additive-by-dominance **(B,E)**, and dominance-by-dominance **(C,F)** interactions. Manhattan plots for the heterotic effects [**(A)**c, **(D)**c] and the dominance effects [**(A)**b, **(D)**b] from genome wide association mapping are presented using Manhattan plots from GWAS. Red lines indicate the threshold of significance. Bar colors denote marker density, with one bar representing a window size of 1 Mb.

to recent studies on rice and maize (Huang et al., 2015; Yang et al., 2017), most heterotic genes exhibit incomplete or partial dominance. However, the relationship between multiple-locus epistasis and heterosis has been under-studied due to the complexity and difficulty in profiling a bonafide and comprehensive interactome in F_1 hybrids (Li et al., 2020). Additionally, the overall contribution of individual small-scale mutations to heterosis was mostly weaker than the effects arising from genetic variations in major alleles, but the cumulative effects from dozens to hundreds of small-scale mutations might contribute to the undiscovered component of heterosis. The unique design of multi-hybrid populations derived from the temperate and tropical lines provides a chance to understand the genetic mechanism of heterosis. Furthermore, tropical maize with favorable alleles for abiotic and biotic stress resistance should be used to increase genetic diversity and accumulate favorable QTL with minor effects. With such a design, the alleles in the tropical lines with minor positive or negative effects on fitness might have been retained, resulting in the accumulation of many minor favorable or deleterious mutations. Therefore, the founder lines used in our study can be used to detect such rare mutations to increase the understanding of the contribution of minor gene interactions to heterosis.

Hybrid breeding largely depends on heterosis, which can be determined by the genetic distance between parental lines (Tian et al., 2016). The level of heterosis is generally related to parental genetic diversity (Tian et al., 2019). However, some studies have found a weak or no relationship between marker diversity and yield (Oyekunle et al., 2015; Boeven et al., 2020). Therefore, genetic diversity is important but is not enough to give rise to desirable heterosis performance (Fu et al., 2014). Heterosis in the temperate by tropical and temperate by temperate hybrid sets increased with the heterotic genetic distance, and the temperate by tropical hybrids showed a relatively higher level of heterosis for grain yield. This indicated that intensive selection by breeding, possible genetic drift, or both had created a divergence between the two maize groups, resulting in an increase in heterosis associated with a non-dominant effect. This is supported by the fact that GWPP showed a weak correlation with plant height (r = 0.07), grain number per row (0.25), ASI (r = 0.17), and hundred-grain weight (0.34) for tropical parents, due to the negative correlation between mid-parent performance and

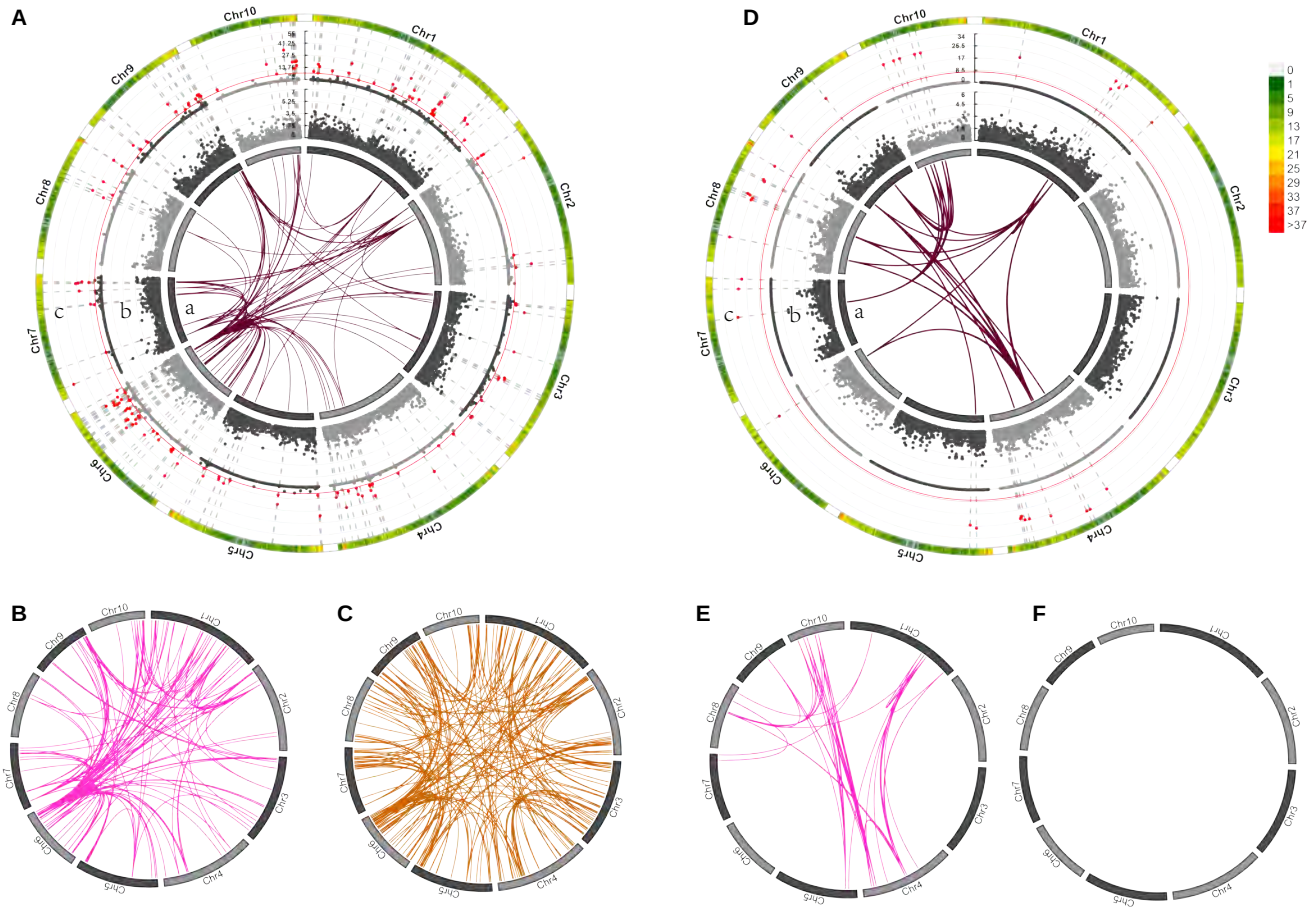

FIGURE 6 | The different mid-parent heterosis genetic effects for days to silking (DTS) in temperate by tropical **(A–C)** and temperate by temperate **(D–F)** hybrids. **(A–F)** In the inner circle, 10 chromosomes are expressed in the form of bars. Gray connector lines indicate the genetic map locations of the SNPs. The colored links within the circle indicate obvious digenic epistatic effects, including additive-by-additive effects [**(A)**a, **(D)**a], additive-by-dominance effects **(B,E)**, as well as dominance-by-dominance effects **(C,F)**. Manhattan plots for the heterotic effects [**(A)**c, **(D)**c] and the dominance effects [**(A)**b, **(D)**b] from genome wide association mapping. Red lines indicate the threshold of significance. The different bar colors denote marker density, with one bar representing a window size of 1 Mb.

heterosis (**Supplementary Figure 8**). Genetic divergence occurs in isolated populations, which decreases the hybrid fitness, but there are many instances where hybrids show a higher degree of fitness than their parents (Dagilis et al., 2019). Thus, in this study, we adopted the quantitative genetic framework proposed by Jiang et al. (2017) to understand possible genetic causes for heterosis and identified epistatic effects that contributed to stronger heterosis in the temperate by tropical hybrids. Additionally, our results indicated that the most prevalent heterosis was controlled by epistatic genes in the tropical by temperate hybrids, and the prevalence of multiple-locus epistatic interactions might explain the genetic control of hybrid vigor in general. This is analogous to Fisher's geometric model where heterosis is involved in the crosses between distantly related inbred lines, and the fitness values of the hybrids include epistatic effects among many loci (Simon et al., 2018; Dagilis et al., 2019).

The complexity of the digenic epistatic network identified in this study suggests that many rare genes with minor effects were modulated by the core genes for yield heterosis. The signals of selection identified between the temperate and tropical hybrids indicated the presence of polygenic heterogeneity along the whole genome (**Figure 1C**), and in plants, GWPP and DTS are some examples of traits with a polygenic basis. Combining GWAS hits with the PPI networks, we found that the epistatic genes identified by GWAS interacted with many undetected background genes, indicating that genomic variations might cause the expression of many minor differential genes and molecular interactions between the two parents. Additionally, the PPI genes for GWPP were mainly related to photosynthesis, regulation of transcription, and protein complex assembly, suggesting that enhanced photosynthetic or biological pathways during development might be associated with hybrid vigor. The maize yield heterosis results from multiple QTL effects accumulated during the development of the hybrid plants (Xiao et al., 2021). In our study, many epistatic QTL were discovered simultaneously within network pathways for different traits, with nine heterosis QTL identified in common for GWPP and DTS in the temperate by tropical hybrids (**Supplementary Figure 9**). The

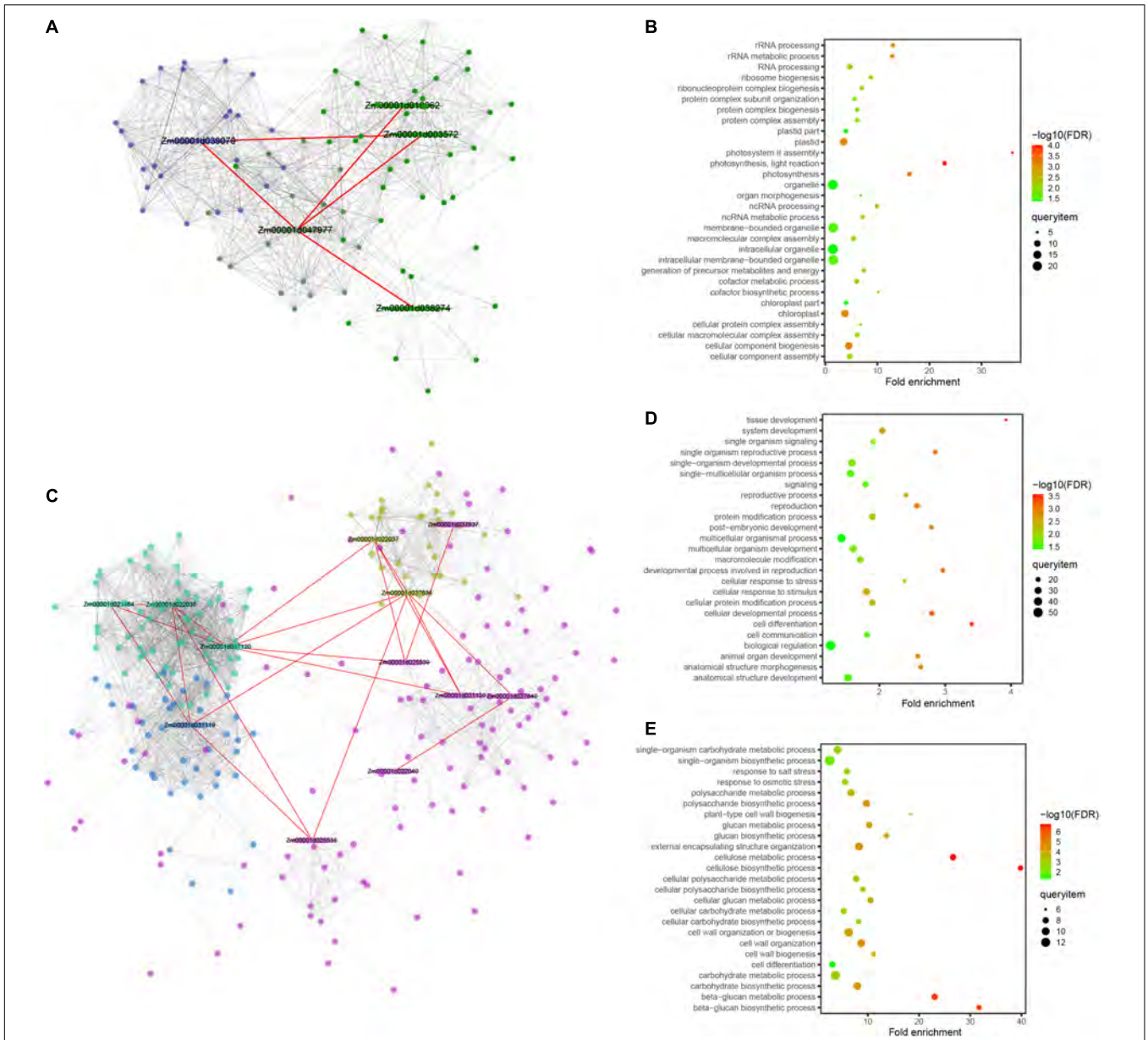

FIGURE 7 | Protein–protein interaction network and enrichment information of the modules for grain weight per plant (GWPP) and days to silking (DTS) in maize. Results are shown for the GWPP **(A,B)** and DTS **(C–E)**. **(A)** The *Zm00001d047977* gene interaction network has two modules and each module is marked with different colors. The red line indicates the protein–protein interaction network for the significant gene located by genome-wide association analysis. **(B)** The dark blue module shows enrichment in multiple developmental processes for GWPP. **(C)** The gene interaction network, including *Zm00001d037637*, *Zm00001d037640*, and *Zm00001d037636*, has four modules, marked with different colors, three of which have genes enriched in multiple developmental processes. **(D,E)** The pink and turquoise modules show enrichment in multiple developmental processes for DTS. The hexagon represents the core epistatic genes (first layer nodes), and the red line indicates the relationships of the core epistatic genes. Different colors represent module analysis using the Maize Interactome platform (second layer nodes).

floral transition might be a key stage in the formation of heterosis, where epistatic QTL are activated by parental contributions of alleles that counteract the recessive deleterious maternal alleles (Xiao et al., 2021). The correlation of heterosis between yield and many other traits suggests that yield heterosis reflects both the cumulative influence of heterosis with minor effects for many traits and the interaction through various molecular mechanisms (Flint-Garcia et al., 2009). Although our data and results were compelling, our study had some limitations. We obtained GWAS hits from the experimental sets of different sample sizes, which could have introduced bias. However, we mitigated this effect by taking the different significance thresholds for each experimental set. We suggest that future studies should use other methods to validate our candidate core genes, by deep sequencing to identify rare variants and wet-lab experiments to validate yield relevance.

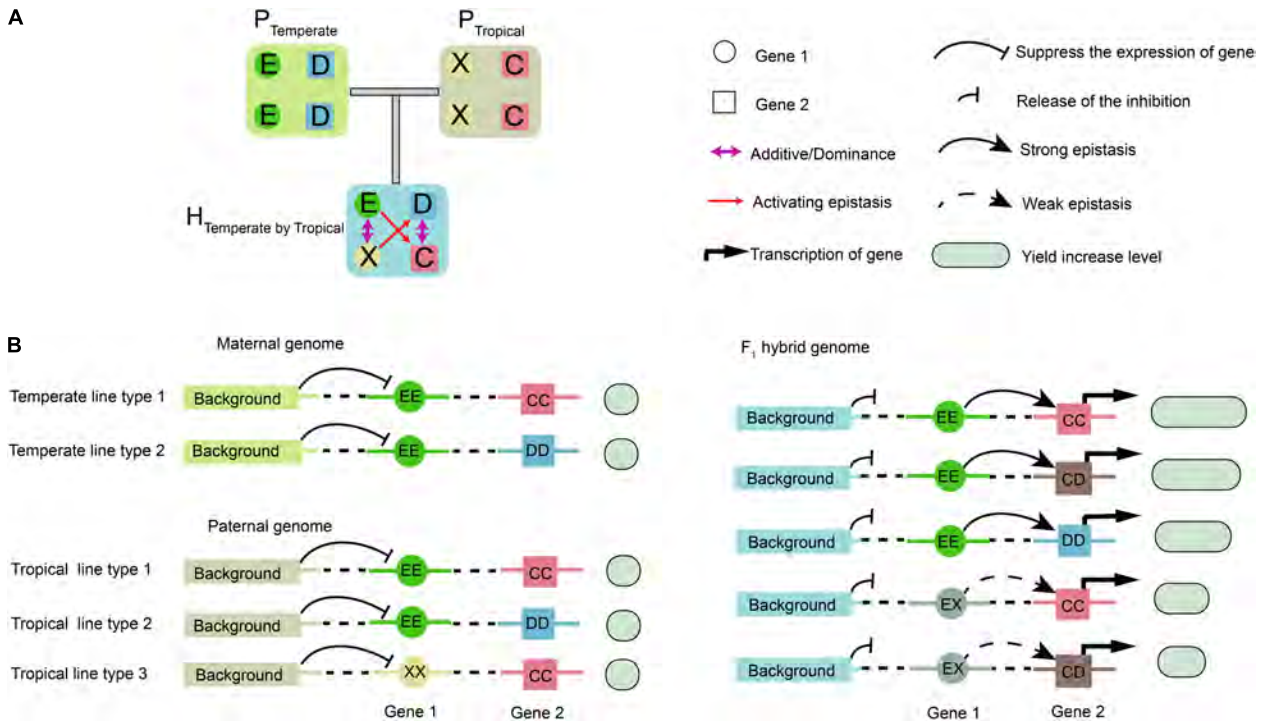

FIGURE 8 | Schematic illustration of epistatic effects. **(A)** Epistasis does not occur between temperate parental ($P_{Temperate}$) or tropical parental ($P_{Tropical}$) lines due to their homozygous genotypes. When two types of inbred lines are crossed, the genetic background in the hybrid changes, resulting in epistatic interaction between the two genetic loci, Gene 1 and Gene 2, which have additive and dominant effects. **(B)** A putative model for interpretation of the interactions between Gene 1, Gene 2, and background genes. In the parental inbreds, background genes repress the transcription of Gene 1. In the hybrid, the repression effect on Gene 1 is relieved, and its transcripts activate the expression of Gene 2. Then, transcription of Gene 2 is activated with different expression levels. The genetic background determines upstream protein–protein interactions specific to the F_1 hybrids, and the E, D, X, and C in a circle or square represent different alleles. The yield associated with the epistasis is measured by the sizes of the empty circles and boxes in light green.

Our GWAS and haplotype analyses indicate that epistasis contributes to the greater heterosis identified in the tropical by temperate hybrids. Epistasis might be related to various molecular interactions, and single or combined alterations of hybrid biological networks might contribute to heterosis to different degrees (Li et al., 2020). The complementary dominant gene expression of hybrids between transcriptional regulatory networks involved in biological pathways across developmental stages contributes to heterosis (Liu et al., 2021; Li et al., 2022). Many minor complementary dominant genes activate epistatic interactions with their PPI genes, resulting in a cascade of amplified phenotypic effects in the hybrids. Multiple alleles at Chr2.47114632 had different types of epistatic effects, producing a series of amplified effects on upstream and downstream gene regulation. This might explain why we detected many epistatic QTL through GWAS with a very strict significance threshold, although the overall contribution of complementary harmful alleles to heterosis was also found. The gene GRMZM2G147158 encoding calmodulin-binding protein 60 C (CBP60C) located at chr2.47114632 belongs to a plant-specific protein family that plays an important role in plant growth/development and biotic/abiotic stress responses, and CBP60 is a central transcriptional activator of immunity in *Arabidopsis* and positively regulates salicylic acid and abscisic acid biosynthesis (Wan et al., 2012; Li et al., 2021; Yu et al., 2021). Our results suggest that the concurrent detection of chr2.47114632 with the other four loci arose from different epistatic effects, and thus, the epistatic genes might be a central transcriptional activator to regulate downstream gene expression.

Designing optimal genotypic combinations and increasing the favorable alleles among parental lines might further enhance hybrid performance. In this study, we found that increasing parental heterotic genetic distance is necessary for maximizing heterosis. The mid-parent values only contributed to a fraction of hybrid performance in maize, while the lines with high GCA for yield were more suitable as parents for hybrid breeding (**Supplementary Figure 10**). Conversely, the mid-parent values accounted for a large proportion of hybrid performance in wheat hybrids (Zhao et al., 2013; Jiang et al., 2017; Boeven et al., 2020). In this study, mid-parent values were relatively stable across all cross combinations, and the increase in the performance of the hybrids was mainly contributed by mid-parent heterosis (**Supplementary Figures 10A,B**). With the increase in the mid-parent values, heterosis decreased at the beginning and then remained stable. Thus, whether hybrid yield can be improved with a further increase in the parental genetic distance while maintaining a certain level of parental

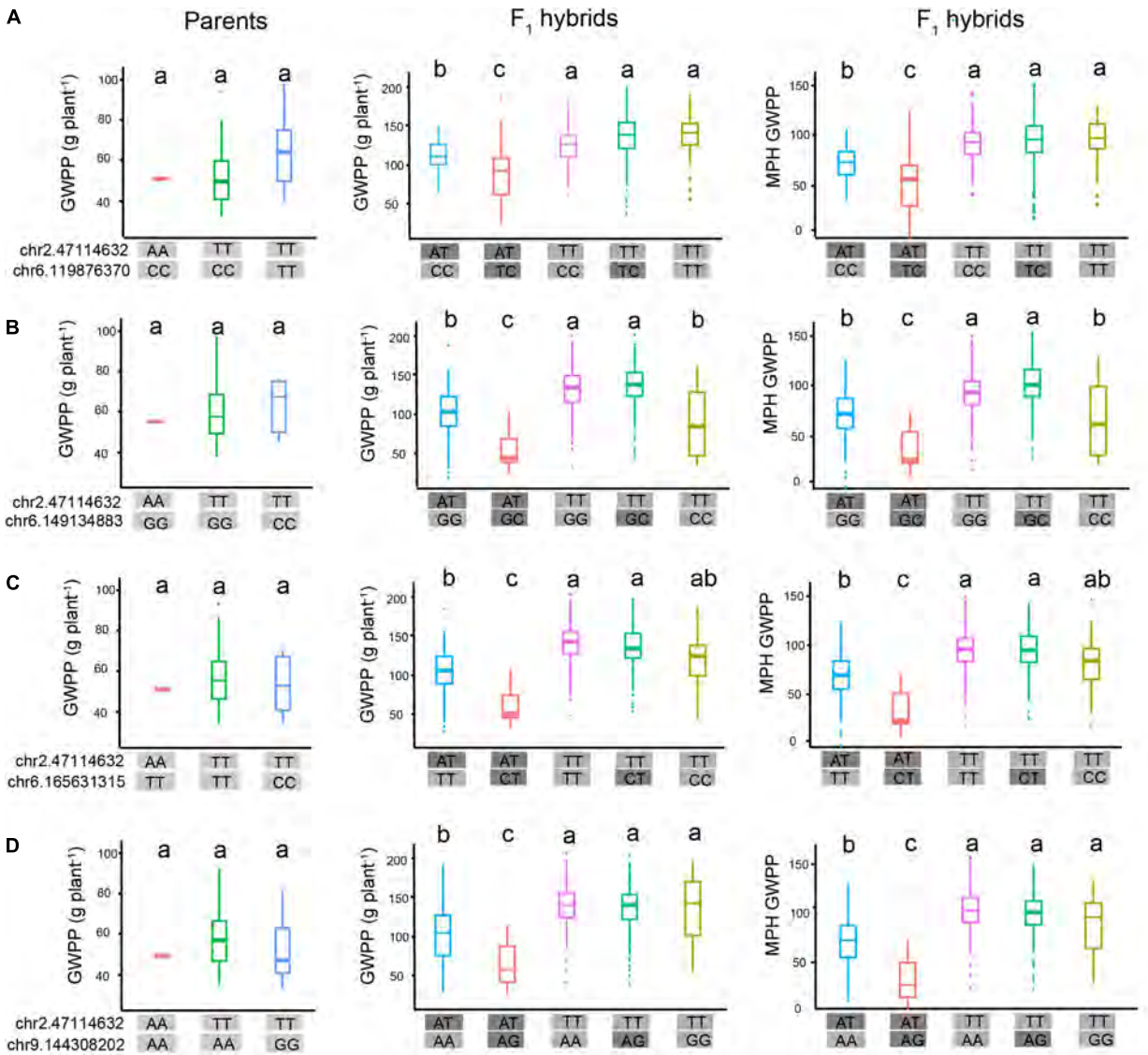

FIGURE 9 | Hypothetical model of epistatic effects affecting heterosis of grain weight per plant (GWPP). Epistatic interaction between chr2.47114632 and four loci contributes to the heterotic performance of GWPP in F_1 hybrids. **(A)** In the parental lines (left panel), the three haplotypes showed similar GWPP, indicating that there was no interaction between chr2.47114632 and chr6.119876370. In the F_1 hybrids (middle panel), the genotype chr2.47114632-TT (rose red boxes, green boxes, fluorescent green boxes) exhibited higher GWPP, indicating that chr2.47114632-TT activated a strong positive additive/dominance induced epistatic effect with the locus chr6.119876370 in F_1 hybrids, and chr2.47114632-TA exhibited lower GWPP (blue boxes, red boxes), indicating that chr2.47114632-TA activated a weak epistatic effect with the locus chr6.165631315 in F_1 hybrids. Panels **(B–D)** present the epistatic interactions between chr2.47114632 and three other loci (chr6.149134883, chr6.165631315, and chr9.144308202, respectively), contributing to the heterotic performance of GWPP in F_1 hybrids. The a, b, and c above the haplotype stick bars represent multiple comparisons by the Student–Newman–Keuls test with $\alpha = 0.05$.

performance is uncertain. With known heterotic groups, maize breeders usually use pedigree breeding for breeding inbred lines, by which dominant genes between parental lines from two heterotic groups can complement each other. However, early-generation selection lines are characterized by a high level of heterozygosity, making it impossible to select such dominant loci because of lower favorable allele frequencies and the complexity of epistasis. Thus, in the early generations, abiotic and biotic stress resistance, plant maturity, plant height, and other traits are prioritized for selection. In later generations, a large effective population is crucial for selecting desirable combinations of genotypes for grain yield.

DATA AVAILABILITY STATEMENT

The original contributions presented in this study are included in the article/**Supplementary Material**, further inquiries can be directed to the corresponding authors.

AUTHOR CONTRIBUTIONS

YX and ZS conceived and designed the experiments and wrote the manuscript. ZS, HW, and ZZ performed the experiments. ZS, YY, XL, and ZL analyzed the data. All authors contributed to the article and approved the submitted version.

FUNDING

This study was supported by the National Science Foundation of China (31760424) and The Scientific and Technological Project of Xinjiang Production and Construction Corps of China (2019AB021), agricultural scientific and technological innovation project of the Shandong Academy of Agricultural Sciences (CXGC2018E01), and open project of the National Engineering Research Center of Wheat and Maize/Shandong Technology Innovation Center of Wheat (2018LYZWS07).

ACKNOWLEDGMENTS

We thank the reviewers for valuable comments and suggestions that improved the manuscript and YX, Institute of Crop Sciences, Chinese Academy of Agricultural Sciences (CAAS) for technical assistance.

SUPPLEMENTARY MATERIAL

The Supplementary Material for this article can be found online at: https://www.frontiersin.org/articles/10.3389/fpls.2022.921608/full#supplementary-material

REFERENCES

Alves, F. C., Granato, ÍS. C., Galli, G., Lyra, D. H., Fritsche-Neto, R., and De Los Campos, G. (2019). Bayesian analysis and prediction of hybrid performance. *Plant Methods* 15:14.

Badu-Apraku, B., Oyekunle, M., Akinwale, R., and Aderounmu, M. (2013). Combining ability and genetic diversity of extra-early white maize inbreds under stress and nonstress environments. *Crop Sci.* 53, 9–26. doi: 10.2135/cropsci2012.06.0381

Bauman, L. F. (1959). Evidence of Non-Allelic Gene Interaction in Determining Yield, Ear Height, and Kernel Row Number in Corn 1. *Agron. J.* 51, 531–534. doi: 10.2134/agronj1959.00021962005100090007x

Birchler, J. A. (2015). Heterosis: the genetic basis of hybrid vigour. *Nat. Plants* 1:15020. doi: 10.1038/nplants.2015.20

Birchler, J. A., Yao, H., Chudalayandi, S., Vaiman, D., and Veitia, R. A. (2010). Heterosis. *Plant Cell* 22, 2105–2112. doi: 10.1105/tpc.110.076133

Boeven, P. H., Zhao, Y., Thorwarth, P., Liu, F., Maurer, H. P., Gils, M., et al. (2020). Negative dominance and dominance-by-dominance epistatic effects reduce grain-yield heterosis in wide crosses in wheat. *Sci. Adv.* 6:eaay4897. doi: 10.1126/sciadv.aay4897

Boggs, P. T., and Rogers, J. E. (1990). Orthogonal distance regression. *Contemp. Math.* 112, 183–194.

Bradbury, P. J., Zhang, Z., Kroon, D. E., Casstevens, T. M., Ramdoss, Y., and Buckler, E. S. (2007). TASSEL: software for association mapping of complex traits in diverse samples. *Bioinformatics* 23, 2633–2635. doi: 10.1093/bioinformatics/btm308

Butler, D. G., Cullis, B. R., Gilmour, A. R., and Gogel, B. J. (2009). *ASREMLQ23 R Reference Manual.* Release 3.0. Technical Report, Queensland Department of Primary Industries, Australia. Available online at: http://www.vsni.co.uk/downloads/asreml/release2/doc/asreml-R.pdf (accessed June 27, 2021).

Culverhouse, R., Klein, T., and Shannon, W. (2004). Detecting epistatic interactions contributing to quantitative traits. *Gen. Epidemiol.* 27, 141–152. doi: 10.1002/gepi.20006

Dagilis, A. J., Kirkpatrick, M., and Bolnick, D. I. (2019). The evolution of hybrid fitness during speciation. *PLoS Genet.* 15:e1008125. doi: 10.1371/journal.pgen.1008125

Danecek, P., Auton, A., Abecasis, G., Albers, C. A., Banks, E., DePristo, M. A., et al. (2011). The variant call format and VCFtools. *Bioinformatics* 27, 2156–2158. doi: 10.1093/bioinformatics/btr330

Doebley, J., Stec, A., and Gustus, C. (1995). teosinte branched1 and the origin of maize: evidence for epistasis and the evolution of dominance. *Genetics* 141, 333–346. doi: 10.1093/genetics/141.1.333

Doust, A. N., Lukens, L., Olsen, K. M., Mauro-Herrera, M., Meyer, A., and Rogers, K. (2014). Beyond the single gene: how epistasis and gene-by-environment effects influence crop domestication. *Proc. Natl. Acad. Sci. U.S.A* .111, 6178–6183. doi: 10.1073/pnas.1308940110

East, E. M. (1936). Heterosis. *Genetics* 21, 375–397. doi: 10.1093/genetics/21.4.375

Fiévet, J. B., Dillmann, C., and De Vienne, D. (2010). Systemic properties of metabolic networks lead to an epistasis-based model for heterosis. *Theor. Appl. Genet.* 120, 463–473. doi: 10.1007/s00122-009-1203-2

Flint-Garcia, S. A., Buckler, E. S., Tiffin, P., Ersoz, E., and Springer, N. M. (2009). Heterosis is prevalent for multiple traits in diverse maize germplasm. *PLoS One* 4:e7433. doi: 10.1371/journal.pone.0007433

Frankham, R. (1996). *Introduction to Quantitative Genetics*, 4th Edn. London: Longman.

Fu, D., Xiao, M., Hayward, A., Fu, Y., Liu, G., Jiang, G., et al. (2014). Utilization of crop heterosis: a review. *Euphytica* 197, 161–173.

Hallauer, A. R., Carena, M. J., and Filho, J. D. (2010). *Quantitative Genetics in Maize Breeding*. London: Springer Science & Business Media.

Han, L., Zhong, W., Qian, J., Jin, M., Tian, P., Zhu, W., et al. (2020). An Interactome Map of Maize (Zea mays L.). *Biol. Sci.* [preprint]. doi: 10.21203/rs.3.rs-88694/v2

Harper, L., Gardiner, J., Andorf, C., and Lawrence, C. J. (2016). "MaizeGDB: the maize genetics and genomics database," in *Plant Bioinformatics* (New York: Springer), 187–202.

Hochholdinger, F., and Baldauf, J. A. (2018). Heterosis in plants. *Curr. Biol.* 28, R1089–R1092. doi: 10.1016/j.cub.2018.06.041

Holm, S. (1979). A simple sequentially rejective multiple test procedure. *Scand. J. Statist.* 6, 65–70.

Hua, J., Xing, Y., Wu, W., Xu, C., Sun, X., Yu, S., et al. (2003). Single-locus heterotic effects and dominance by dominance interactions can adequately explain the genetic basis of heterosis in an elite rice hybrid. *Proc. Natl. Acad. Sci. U.S.A.* 100, 2574–2579. doi: 10.1073/pnas.0437907100

Huang, W., and Mackay, T. F. (2016). The genetic architecture of quantitative traits cannot be inferred from variance component analysis. *PLoS Genet.* 12:e1006421. doi: 10.1371/journal.pgen.1006421

Huang, X., Yang, S., Gong, J., Zhao, Y., Feng, Q., Gong, H., et al. (2015). Genomic analysis of hybrid rice varieties reveals numerous superior alleles that contribute to heterosis. *Nat. Commun.* 6:6258. doi: 10.1038/ncomms7258

Jiang, Y., Schmidt, R. H., Zhao, Y., and Reif, J. C. (2017). A quantitative genetic framework highlights the role of epistatic effects for grain-yield heterosis in bread wheat. *Nat. Genet.* 49, 1741–1746. doi: 10.1038/ng.3974

Jinks, J., and Jones, R. M. (1958). Estimation of the components of heterosis. *Genetics* 43, 223–234. doi: 10.1093/genetics/43.2.223

Jones, D. F. (1917). Dominance of linked factors as a means of accounting for heterosis. *Genetics* 2, 466–479. doi: 10.1093/genetics/2.5.466

Jung, M., Ching, A., Bhattramakki, D., Dolan, M., Tingey, S., Morgante, M., et al. (2004). Linkage disequilibrium and sequence diversity in a 500-kbp region around the adh1 locus in elite maize germplasm. *Theor. Appl. Genet.* 109, 681–689.

Kaeppler, S. (2012). Heterosis: many genes, many mechanisms—end the search for an undiscovered unifying theory. *ISRN Bot.* 2012:682824. doi: 10.5402/2012/682824

Lamkey, K. R., and Edwards, J. W. (1998). "Heterosis: theory and estimation," in *Proceedings of the 34th 1998 Illinois Corn Breeders' School*, Urbana, IL: University of Illinois 62–77.

Lamkey, K. R., and Edwards, J. W. (1999). "Quantitative genetics of heterosis," in *Proceedings of the International Symposium on the Genetics and Exploitation of Heterosis in Crops*, eds J. G. Coors and S. Pandey (Mexico: CIMMYT), 31–48.

Laude, T., and Carena, M. (2015). Genetic diversity and heterotic grouping of tropical and temperate maize populations adapted to the northern US Corn Belt. *Euphytica* 204, 661–677.

Li, D., Lu, X., Zhu, Y., Pan, J., Zhou, S., Zhang, X., et al. (2022). The multi-omics basis of potato heterosis. *J. Integr. Plant Biol.* 64, 671–687. doi: 10.1111/jipb.13211

Li, H., Jiang, S., Li, C., Liu, L., Lin, Z., He, H., et al. (2020). The hybrid protein interactome contributes to rice heterosis as epistatic effects. *Plant J.* 102, 116–128. doi: 10.1111/tpj.14616

Li, L. S., Ying, J., Li, E., Ma, T., Li, M., Gong, L. M., et al. (2021). Arabidopsis CBP60b is a central transcriptional activator of immunity. *Plant Physiol.* 186, 1645–1659. doi: 10.1093/plphys/kiab164

Lippert, C., Listgarten, J., Liu, Y., Kadie, C. M., Davidson, R. I., and Heckerman, D. (2011). FaST linear mixed models for genome-wide association studies. *Nat. Methods* 8, 833–835. doi: 10.1038/nmeth.1681

Liu, W., He, G., and Deng, X. W. (2021). Biological pathway expression complementation contributes to biomass heterosis in Arabidopsis. *Proc. Natl. Acad. Sci.* 118:e2023278118. doi: 10.1073/pnas.2023278118

Lu, Y., Shah, T., Hao, Z., Taba, S., Zhang, S., Gao, S., et al. (2011). Comparative SNP and haplotype analysis reveals a higher genetic diversity and rapider LD decay in tropical than temperate germplasm in maize. *PLoS One* 6:e24861. doi: 10.1371/journal.pone.0024861

Lu, Y., Yan, J., Guimaraes, C. T., Taba, S., Hao, Z., Gao, S., et al. (2009). Molecular characterization of global maize breeding germplasm based on genome-wide single nucleotide polymorphisms. *Theor. Appl. Genet.* 120, 93–115.

Ma, X., Tang, J., Teng, W., Yan, J., Meng, Y., and Li, J. (2007). Epistatic interaction is an important genetic basis of grain yield and its components in maize. *Mol. Breed.* 20, 41–51.

Möhring, J., and Piepho, H. P. (2009). Comparison of weighting in two-stage analysis of plant breeding trials. *Crop Sci.* 49, 1977–1988. doi: 10.2135/cropsci2009.02.0083

Oyekunle, M., Badu-Apraku, B., Hearne, S., and Franco, J. (2015). Genetic diversity of tropical early-maturing maize inbreds and their performance in hybrid combinations under drought and optimum growing conditions. *Field Crops Res.* 170, 55–65. doi: 10.1016/j.fcr.2014.10.005

Pérez, P., and De Los Campos, G. (2014). Genome-wide regression and prediction with the BGLR statistical package. *Genetics* 198, 483–495. doi: 10.1534/genetics.114.164442

Powers, L. (1944). An expansion of Jones's theory for the explanation of heterosis. *Am. Natural.* 78, 275–280. doi: 10.1086/281199

Purcell, S., Neale, B., Todd-Brown, K., Thomas, L., Ferreira, M. A., Bender, D., et al. (2007). PLINK: a tool set for whole-genome association and population-based linkage analyses. *Am. J. Hum. Genet.* 81, 559–575. doi: 10.1086/519795

R Core Team (2018). *R: A Language and Environment for Statistical Computing*. Vienna: R Foundation for Statistical Computing.

Rhode, J. M., and Cruzan, M. B. (2005). Contributions of heterosis and epistasis to hybrid fitness. *Am. Nat.* 166, E124–E139. doi: 10.1086/491798

Simon, A., Bierne, N., and Welch, J. J. (2018). Coadapted genomes and selection on hybrids: fisher's geometric model explains a variety of empirical patterns. *Evol. Lett.* 2, 472–498. doi: 10.1002/evl3.66

Tamura, K., Stecher, G., Peterson, D., Filipski, A., and Kumar, S. (2013). MEGA6: molecular evolutionary genetics analysis version 6.0. *Mol. Biol. Evol.* 30, 2725–2729. doi: 10.1093/molbev/mst197

Tian, H. Y., Channa, S. A., and Hu, S. W. (2016). Relationships between genetic distance, combining ability and heterosis in rapeseed (*Brassica napus* L.). *Euphytica* 213, 1–11.

Tian, S., Xu, X., Zhu, X., Wang, F., Song, X., and Zhang, T. (2019). Overdominance is the major genetic basis of lint yield heterosis in interspecific hybrids between *G. hirsutum* and *G. barbadense*. *Heredity* 123, 384–394.

Tian, T., Liu, Y., Yan, H., You, Q., Yi, X., Du, Z., et al. (2017). agriGO v2. 0: a GO analysis toolkit for the agricultural community, 2017 update. *Nucleic Acids Res.* 45, W122–W129. doi: 10.1093/nar/gkx382

Wan, D., Li, R., Zou, B., Zhang, X., Cong, J., Wang, R., et al. (2012). Calmodulin-binding protein CBP60 g is a positive regulator of both disease resistance and drought tolerance in Arabidopsis. *Plant Cell Rep.* 31, 1269–1281.

Wang, H., Xu, C., Liu, X., Guo, Z., Xu, X., Wang, S., et al. (2017). Development of a multiple-hybrid population for genome-wide association studies: theoretical consideration and genetic mapping of flowering traits in maize. *Sci. Rep.* 7:40239. doi: 10.1038/srep40239

Wei, X., and Zhang, J. (2018). The optimal mating distance resulting from heterosis and genetic incompatibility. *Sci. Adv.* 4:eaau5518. doi: 10.1126/sciadv.aau5518

Wright, S. (1984). *Evolution and The Genetics of Populations, Volume 1: Genetic and Biometric Foundations*. Chicago, IL: University of Chicago press.

Xiao, Y., Jiang, S., Cheng, Q., Wang, X., Yan, J., Zhang, R., et al. (2021). The genetic mechanism of heterosis utilization in maize improvement. *Genome Biol.* 22:148 doi: 10.1186/s13059-021-02370-7

Xu, C., Ren, Y., Jian, Y., Guo, Z., Zhang, Y., Xie, C., et al. (2017). Development of a maize 55 K SNP array with improved genome coverage for molecular breeding. *Mol. Breed.* 37:20.

Xu, S. (2013). Mapping quantitative trait loci by controlling polygenic background effects. *Genetics* 195, 1209–1222. doi: 10.1534/genetics.113.157032

Yang, J., Mezmouk, S., Baumgarten, A., Buckler, E. S., Guill, K. E., McMullen, M. D., et al. (2017). Incomplete dominance of deleterious alleles contributes substantially to trait variation and heterosis in maize. *PLoS Genet.* 13:e1007019. doi: 10.1371/journal.pgen.1007019

Yu, J., Pressoir, G., Briggs, W. H., Bi, I., Yamasaki, M., Doebley, J. F., et al. (2005). A unified mixed-model method for association mapping that accounts for multiple levels of relatedness. *Nat. Genet.* 38, 203–208. doi: 10.1038/ng1702

Yu, K., Wang, H., Liu, X., Xu, C., Li, Z., Xu, X., et al. (2020). Large-scale analysis of combining ability and heterosis for development of hybrid maize breeding strategies using diverse germplasm resources. *Front. Plant Sci.* 11:660. doi: 10.3389/fpls.2020.00660

Yu, Q., Liu, Y. L., Sun, G. Z., Liu, Y. X., Chen, J., Zhou, Y. B., et al. (2021). Genome-Wide Analysis of the Soybean Calmodulin-Binding Protein 60 Family and Identification of GmCBP60A-1 Responses to Drought and Salt Stresses. *Int. J. Mol. Sci.* 22:13501. doi: 10.3390/ijms222413501

Yu, S., Li, J., Xu, C., Tan, Y., Gao, Y., Li, X., et al. (1997). Importance of epistasis as the genetic basis of heterosis in an elite rice hybrid. *Proc. Natl. Acad. Sci. U.S.A.* 94, 9226–9231. doi: 10.1073/pnas.94.17.9226

Zhao, Y., Li, Z., Liu, G., Jiang, Y., Maurer, H. P., Würschum, T., et al. (2015). Genome-based establishment of a high-yielding heterotic pattern for hybrid wheat breeding. *Proc. Natl. Acad. Sci. U.S.A.* 112, 15624–15629. doi: 10.1073/pnas.1514547112

Zhao, Y., Zeng, J., Fernando, R., and Reif, J. C. (2013). Genomic prediction of hybrid wheat performance. *Crop Sci.* 53, 802–810. doi: 10.2135/cropsci2012.08.0463

Zhou, G., Chen, Y., Yao, W., Zhang, C., Xie, W., Hua, J., et al. (2012). Genetic composition of yield heterosis in an elite rice hybrid. *Proc. Natl. Acad. Sci. U.S.A.* 109, 15847–15852. doi: 10.1073/pnas.1214141109

Conflict of Interest: The authors declare that the research was conducted in the absence of any commercial or financial relationships that could be construed as a potential conflict of interest.

The reviewer KB declared a shared parent affiliation with the several authors ZS, HW, YY, XL, ZL, and YX to the handling editor at the time of review.

Publisher's Note: All claims expressed in this article are solely those of the authors and do not necessarily represent those of their affiliated organizations, or those of the publisher, the editors and the reviewers. Any product that may be evaluated in this article, or claim that may be made by its manufacturer, is not guaranteed or endorsed by the publisher.

frontiers | Frontiers in Plant Science

TYPE Original Research
PUBLISHED 22 August 2022
DOI 10.3389/fpls.2022.978941

OPEN ACCESS

EDITED BY
Manje S. Gowda,
International Maize and Wheat Improvement Center (CIMMYT), Kenya

REVIEWED BY
Tao Guo,
South China Agricultural University, China
Sibin Yu,
Huazhong Agricultural University, China
Mahender Anumalla,
International Rice Research Institute (IRRI), Philippines

*CORRESPONDENCE
Zhenhua Wang
zhenhuawang_2006@163.com
Jianfeng Weng
wengjianfeng@caas.cn

†These authors have contributed equally to this work and share first authorship

SPECIALTY SECTION
This article was submitted to Plant Breeding, a section of the journal Frontiers in Plant Science

RECEIVED 27 June 2022
ACCEPTED 29 July 2022
PUBLISHED 22 August 2022

CITATION
Zhou Y, Lu Q, Ma J, Wang D, Li X, Di H, Zhang L, Hu X, Dong L, Liu X, Zeng X, Zhou Z, Weng J and Wang Z (2022) Using a high density bin map to analyze quantitative trait locis of germination ability of maize at low temperatures.
Front. Plant Sci. 13:978941.
doi: 10.3389/fpls.2022.978941

Using a high density bin map to analyze quantitative trait locis of germination ability of maize at low temperatures

Yu Zhou[1†], Qing Lu[1†], Jinxin Ma[1], Dandan Wang[1], Xin Li[1], Hong Di[1], Lin Zhang[1], Xinge Hu[1], Ling Dong[1], Xianjun Liu[1], Xing Zeng[1], Zhiqiang Zhou[2], Jianfeng Weng[2]* and Zhenhua Wang[1]*

[1]Key Laboratory of Germplasm Enhancement, Physiology and Ecology of Food Crops in Cold Region, Ministry of Education, Northeast Agricultural University, Harbin, China, [2]Institute of Crop Science, Chinese Academy of Agricultural Sciences, Beijing, China

Low temperatures in the spring often lead to a decline in the emergence rate and uniformity of maize, which can affect yield in northern regions. This study used 365 recombinant inbred lines (RILs), which arose from crossing Qi319 and Ye478, to identify low-temperature resistance during the germination stage by measuring eight low-temperature-related traits. The quantitative trait locis (QTLs) were mapped using *R/qtl* software by combining phenotypic data, and the genotyping by sequencing (GBS) method to produce a high-density genetic linkage map. Twenty QTLs were detected during QTL mapping, of which seven QTLs simultaneously detected a consistent 197.10–202.30 Mb segment on chromosome 1. The primary segment was named *cQTL1-2*, with a phenotypic variation of 5.18–25.96% and a physical distance of 5.2 Mb. This combines the phenotype and genotype with the identification of seven chromosome segment substitution lines (CSSLs), which were derived from Ye478*Qi319 and related to *cQTL1-2*. The physical distance of *cQTL1-2* was reduced to approximately 1.9 Mb. The consistent meta-QTL *mQTL1* was located at 619.06 cM on chromosome 1, had a genetic distance of 7.27 cM, and overlapped with *cQTL1-2*. This was identified by combining the results of previous QTL studies assessing maize tolerance to low temperatures at the germination stage. An assessment of the results of the RIL population, CSSLs, and *mQTL1* found the consistent QTL to be *LtQTL1-1*. It was identified in bin1.06-1.07 at a confidence interval of between 200,400,148 and 201,775,619 bp. In this interval, qRT-PCR found that relative expression of the candidate genes *GRMZM2G082630* and *GRMZM2G115730* were both up-regulated in low-temperature tolerant lines and down-regulated in sensitive lines ($P < 0.01$).

KEYWORDS

maize, low temperature, germination, high-density linkage map, candidate gene

Introduction

Cold temperatures can affect the development, biochemistry, physiology, productivity, and quality of plants, making it one of the primary factors limiting the distribution of plants worldwide (Kocsy et al., 2011; Szalai et al., 2018). Maize (*Zea mays* L.) is an important crop, representing 40% of global cereal production[1] (Bouis and Welch, 2010). Maize is sensitive to cold temperatures, especially during its early growth, including the germination and seedling stages, because it originated in tropical and subtropical locations (Greaves, 1996; Verheul et al., 1996; Li et al., 2018).

When subjected to low temperatures, plant roots do not fully grow (Zhu et al., 2015). In *Arabidopsis thaliana*, growth of the main root is limited by low temperatures (Plohovska et al., 2016), while some genes, such as *CYTOKININ RESPONSE FACTOR2* (*CRF2*) and *CRF3*, serve vital functions and regulate the growth of the lateral roots of *A. thaliana* under low-temperature conditions (Jeon et al., 2016; Rativa et al., 2020). Some genes in the shoots and roots of maize and rice, such as *Adhl*, show a rapid increase in steady-state levels when exposed to low temperatures (Christie et al., 2021). The key issue affecting the ability of maize to germinate at low temperatures is appropriately identifying its phenotype. In a previous study, QTL mapping assessing the tolerance of maize to low temperatures mainly focused on traits related to the germination process, such as germination rate and germination index (Hu et al., 2016, 2017; Li et al., 2018), while little attention was paid to the growth of shoots and roots after germination.

The response of maize to low temperatures is governed by a complex quantitative genetic traits, controlled by multiple minor genes and easily affected by the environment. Many quantitative trait loci (QTLs) were detected in previous studies, such as a primary QTL on chromosome 6 that is related to cold tolerance. This QTL explains 37.4% of the differences in phenotypes during photo inhibition at low temperatures, and is related to the expression of six other traits (Fracheboud et al., 2004). Five meta-QTLs related to traits associated with the vigor of maize seeds at low temperatures were found on chromosomes 2, 3, 5, and 9 (Shi et al., 2016). Other QTLs, such as *mQTL1-1*, comprised seven QTLs associated with seedling and germination characteristics, including four QTLs under cold temperatures from a population produced by crossing a cold-intolerant (A661) inbred line with a cold-tolerant line (EP42), both of which were related to tolerance to low temperatures at the germination and seedling stages in small populations (Presterl et al., 2007; Rodrı'guez et al., 2014; Li et al., 2018). Previous results demonstrated that QTLs were distributed on 10 chromosomes in maize, and identified no major QTL related to tolerance to low temperatures at the germination stage. This could be because these QTLs are primarily related to the seedling stage. The identification traits (germination rate and germination index) were the same at the germination stage, while some significant traits related to shoots or roots were not included. Previous studies mostly used inbred lines from Europe or America with fewer molecular markers. The strains used in this study, Ye478 and Qi319, are important for breeding in China and respond differently to low temperatures. The 365 recombinant inbred lines (RILs) derived from Ye478 and Qi319 were sequenced using the genotyping by sequencing (GBS) method.

Several genes are associated with low-temperature responses in rice, *Arabidopsis thaliana*, and other plants, including CBFs, MYBs, and MPKs (Li et al., 2017a,b; Wang et al., 2019; Ye et al., 2019). The way in which the genes and related pathways of *A. thaliana* regulate tolerance to low temperatures is relatively clear. For example, PUB25 and PUB26 promote the tolerance of low temperature via degradation of the negative regulator MYB15, which is responsible for cold signaling in *A. thaliana* (Wang et al., 2019). ICE1 phosphorylation mediated by MPK3 and MPK6 regulates ICE1 in a negative manner, and BRASSINOSTEROID-INSENSITIVE2 negatively regulates ICE1 response to cold stress in *A. thaliana* (Li et al., 2017a; Ye et al., 2019). In rice, *COLD1* is a quantitative trait locus that allows *japonica* rice to tolerate frost by activating Ca^{2+} channels in response to low temperatures (Ma et al., 2015). The natural variations of *CTB4a* and *OsMADS57*, the transcription factors of MADS-box, were related to ATP content, while organogenesis genes could enhance the ability of rice to adapt to low temperatures (Zhang et al., 2017b; Chen et al., 2018). Genes related to low-temperature tolerance in maize, such as *ZmCDPK1*, *ZmSEC14p*, and *ZmMPK5* have been detected (Berberich et al., 1999; Kong et al., 2013; Wang et al., 2016). However, the genetic mechanism behind maize tolerance to low temperatures is still unclear. Therefore, it is necessary to perform additional research on how maize tolerates low temperatures.

This study used the genotypic and phenotypic data from 365 maize RILs, which were F_{11} individuals obtained from the self-cross of Ye478*Qi319. The purpose of this study is to (1) analyze QTLs related to low-temperature tolerance using R/qtl software and identify the primary QTL linked by multiple traits, (2) verify the consistent primary QTL linked by multiple traits using the contig substitution mapping method combining genotype and phenotype data of chromosome segment substitution lines (CSSLs), (3) analyze the consistent meta-mQTL data from previous studies, and (4) predict and verify candidate genes in the primary QTL confidence interval.

1 http://faostat.fao.org/

Materials and methods

Plant materials

Total of 365 lines were obtained from a hybrid of two well-known inbred maize strains, the cold-tolerant line Ye478 and the sensitive line Qi319, via single-seed origin of F_{11}. The two parent lines had significant differences in eight traits related to cold tolerance, including relative root volume (RRV), relative total length (RTL), relative shoot length (RSL), relative germination rate (RGR), relative root average diameter (RRAD), relative root length (RRL), relative root superficial area (RRSA), and relative simple vigor index (RSVI). Ye478, a dent maize, had an average RGR of 0.845 and an average RSVI of 0.715. In contrast, Qi319, a flint maize, was sensitive to cold, with averages of 0.449 and 0.257 for RGR and RSVI, respectively. Seven CSSLs were selected from the CSSL with donor parent Qi319 and recipient parent Ye478 and were used to verify the QTLs. The details of these seven CSSLs were displayed in **Supplementary Table 1** and **Supplementary Figure 1**.

Phenotypic evaluation

The seeds from both lines were sterilized with 1% sodium hypochlorite (NaClO) for 5 min and washed with distilled water. They were then soaked in tap water for 6 h and grown in paper rolls at 10°C chambers (treatment) and 25°C chambers (control) for 30 and 6 days in a dark environment, respectively. The chamber was ARC-36L2-E from PERCIVAL. A completely randomized design with three replicates was used for the germination experiment, with each replicate containing 50 seeds. Eight cold-related traits were measured after the seeds were placed in the chambers. The germination rate (GR) was expressed as the percentage of germinating plants out of the total number of seeds used. The root scanner (Epson Perfection V800 scanner) and analysis software (Regent WinRHIZO from Canada) were used to measure the following seven cold-related traits in germinated seedlings: shoot length (SL), root length (RL), root volume (RV), root superficial area (RSA), root average diameter (RAD), simple vigor index (SVI), and total length (TL). The mean of 10 seedlings were used to measure all these seven traits. For evaluation of seed germination ability at low temperatures, the ratio (relative value) of eight traits (RGR, RSL, RRL, RRV, RRSA, RRAD, RSVI, and RTL) were used as indicators for low-temperature tolerance in order to eliminate the differences in genetic background of the different materials. The ratios (relative performance) were calculated as the ratios of the mean values of measurements (n = 3) taken under low-temperature treatment conditions and normal temperature conditions (Zhang et al., 2020).

Phenotypic data analysis

The analysis of variance (ANOVA), as well as QTL mapping, was performed using the mean of all replicates. A combined ANOVA spanning several environments with the Mixed Linear Model procedure (PROC MLM) and Statistical Analysis System (SAS) software version 9.2 (SAS Institute, Cary NC, United States, 2009) were performed, which allowed us to approximate the variance. Linear regressions with significance levels of P = 0.05 were used to calculate Pearson's correlation coefficients (r) for each characteristic. Pearson correlation coefficients (r) between different traits were determined by linear regressions at the significance level p = 0.05, and calculated using SPSS20.0 (IBM corp., Armonk, NY, United States). The following equation was used to calculate the coefficients of variation (CV, %): CV = s/x. In this equation, "x" equals each trait's mean in a population and "s" is equals the standard deviation.

Mapping linkages

The GBS technology (The original genotypic datasets have become public in the NCBI database[2] under the accession PRJNA627044), were used with an Illumina 2500 platform and methods previously described to characterize the RIL population (Zhou et al., 2016). Total of 86,257 SNPs were identified and generated an ultra-high density linkage map using 4,602 bin markers (100-Kb intervals with no recombination events). The map had a total genetic distance of 1,533.72 cM, with an average distance of 0.33 cM between markers (Zhou et al., 2016). Composition-interval mapping (CIM) was used to identify the QTLs in the *R/qtl* package. The threshold of the logarithm of the odds (LOD) scores were determined using 1,000 permutations and a significance level of p = 0.05. These were used to evaluate the effects of the QTL. The QTLs with LOD figures higher than the threshold, which was 2.5, warranted additional study. The *ftqtl* function from the *R/qtl* package was used to assess the phenotypic variation of the identified QTLs. The consistent QTLs influencing multiple traits were named with the initial "c," which represents consistent, and the numbers in the name indicate chromosome and number.

Chromosome segment substitution lines materials and genotypic data screening

The population with 180 CSSLs were constructed with Ye478 as the female parent and Qi319 as the male parent.

2 https://www.ncbi.nlm.nih.gov/

These CSSLs were selected by backcrossing and marker-assisted selection technology by SSR and InDel marker encryption (Wang et al., 2018b). In this study, seven CSSLs with segments substitution of Qi319 in the major QTL of low-temperature tolerance were selected and used. In the seven CSSLs, six lines (CL6, CL9, CL14, CL17, CL18, and CL173) contain only one homozygous genomic segment of Qi319, respectively. However, line CL174 contain two genomic segments including a homozygous segment of Qi319 and a hybrid segment. The background recovery rates in seven CSSLs were all more than 96% (**Supplementary Figure 1**). The GR of each of the seven CSSLs were detected and the RGR was calculated to verify the accuracy of identification of the main effect QTL in the RIL population and to reduce the confidence interval of the QTL.

Meta-QTL analysis

The mapping information of 76 QTLs related to cold tolerance in the germination stage of maize were collected from recently published papers and our own research. This information included markers, traits, names, chromosomes, and Linkage Group selection (LGs). The original QTL maps to the reference map IBM2 2008 Neighbors were compared, which shares enough markers with other maps to make an accurate projection. As such, the IBM2 2008 Neighbors integrated QTLs from other populations. A homothetic function were used to project the QTLs to the reference map by estimating the most likely position and CI. The projected QTLs related to cold tolerance were used to construct a consensus map of cold-related traits with the BioMercator ver.2.1 software (Arcade et al., 2004). A meta-analysis using this software from different independent experiments, QTLs associated with similar LGs, and QTLs at neighboring intervals to generate an optimal QTL. While QTLs provided five different models, the best QTL model was the Akaike Information Criteria (AIC). This was considered the optimal QTL. The optimal QTL was close to the smallest AIC, while the mean R2 values of the original QTLs in the region explained the variance of the optimal QTL. The Meta-QTLs were named with the initial "m," which represent meta. The consistent QTLs and Meta-QTLs were named with the initial "Lt," which represent low-temperature, and the numbers in the name indicate chromosome and number.

Candidate gene prediction and identification

Based on the comprehensive analysis results of RIL population, CSSLs and Meta-QTL analysis, combined with MaizeGDB[3], NCBI database (see Text Footnote 2), and UniPort[4], the gene annotation function of B73 (B73 RefGen_v3) was searched for this major QTL segment. Well-annotated genes related to low-temperature tolerance and other abiotic stresses were obtained from *A. thaliana*, *Sorghum bicolor*, and *Oryza sativa*. Two genes were selected from our confident QTL interval in order to validate them with quantitative PCR (qPCR). A total of six maize inbred lines of Ye478 (tolerant), Qi319 (sensitive), ZYQ219 (tolerant), ZYQ011 (sensitive), CL082 (tolerant), and CL018 (sensitive) were used as test materials. Their relative germination rate phenotypes were listed in **Supplementary Table 2**. Two groups of seeds were soaked in tap water for 6 h and then grown at 10°C/25°C for 2 and 4 h in chambers, respectively. From each replication, 10 seeds were ground in liquid nitrogen to extract the total RNA with *TransZol*^{TM} Up Plus RNA Kit [TransGen Biotech (Beijing, China)]. They were then subjected to reverse transcription reaction of cDNA via RT MasterMix [TransGen Biotech (Beijing, China)], while qPCR analysis was performed on a *TransStart*® Tip Green qPCR SuperMix kit [TransGen Biotech (Beijing, China)]. **Supplementary Table 3** displays the primers used for qPCR. The Actin gene from maize was used for an internal control, and the mean of three replications was used to express the final gene. The candidate gene relative expression level was calculated using the $2^{-\Delta\Delta Ct}$ analytical method. And the gene expression was translated to $\log_2$(fold change).

Results

Phenotypic traits relating to tolerance of low temperatures

The descriptive statistics of the morphological traits at the germination stage in the RIL populations were displayed in **Table 1**. Two parental inbred lines showed highly significant differences ($P < 0.01$) in seven traits (RGR, RSL, RRL, RTL, RRSA, RRAD, RRV, and RSVI), except RRAD that showed a significant difference ($P < 0.05$). All traits were normally and continuously distributed in all 365 RILs, which also displayed quantitative inheritance. For example, RGR ranged from 0.088 to 0.993 and had a mean of 0.680 in the RIL population, and RSVI ranged from 0.036 to 0.765 and had a mean of 0.343. RSVI had the highest CV (0.365) in the RIL population, while RRAD (0.035) had the lowest CV. Within the RIL population, the broad-sense heritability (H^2) related to eight characteristics related to the germination stages spanned from 0.824 for RSVI to 0.907 for RRL (**Supplementary Table 4**).

Of the eight morphological traits relating to the germination stage analyzed in this study, several significant correlations were observed. The significant correlations between RSVI and six other traits were also been observed, which played an important

3 https://www.maizegdb.org/

4 https://www.uniprot.org/

10.3389/fpls.2022.978941

TABLE 1 QTLs identified for eight maize cold-related traits.

No.	QTL name	Chr.	Flanking markers	Interval (Mb)	Physical length (Mb)	LOD	PVE	ADD	Phenotype
(1)	*qRSVI1-1*	1	mk234-mk243	63.85–68.45	4.60	5.64	7.80	−0.25	RSVI
(2)	*qRGR1-1*	1	mk235-mk243	64.20–68.45	4.25	11.02	13.52	−0.14	RGR
(3)	*qRGR1-2*	1	mk445-mk466	197.10–201.95	4.85	5.03	8.05	−0.11	RGR
(4)	*qRRSA1-1*	1	mk445-mk465	197.10–201.60	4.50	5.17	5.18	−0.23	RRSA
(5)	*qRSL1-1*	1	mk446-mk466	197.75–201.95	4.20	4.19	6.06	−0.08	RSL
(6)	*qRRL1-1*	1	mk446-mk466	197.75–201.95	4.20	19.71	17.01	−0.42	RRL
(7)	*qRTL1-1*	1	mk446-mk466	197.75–201.95	4.20	19.71	20.36	−0.23	RTL
(8)	*qRRV1-1*	1	mk446-mk467	197.75–202.30	4.55	6.97	8.44	−0.33	RRV
(9)	*qRSVI1-2*	1	mk446-mk467	197.75–202.30	4.55	20.09	25.96	−0.16	RSVI
(10)	*qRRL3-1*	3	mk1225-mk1232	7.75–8.65	0.90	2.88	3.58	−0.17	RRL
(11)	*qRTL3-1*	3	mk1226-mk1227	7.90–8.05	0.15	2.69	3.79	−0.07	RTL
(12)	*qRSL3-1*	3	mk1295-mk1313	21.05–25.65	4.60	4.81	4.23	−0.08	RSL
(13)	*qRSL3-2*	3	mk1472-mk1489	164.10–169.00	4.90	5.65	6.47	−0.06	RSL
(14)	*qRRAD3-1*	3	mk1611-mk1639	206.80–211.75	4.95	7.40	8.37	0.01	RRAD
(15)	*qRRL7-1*	7	mk3161-mk3180	1.45–4.85	3.40	7.22	7.14	−0.25	RRL
(16)	*qRTL7-1*	7	mk3177-mk3193	3.65–8.40	4.75	6.46	6.39	−0.13	RTL
(17)	*qRSVI7-1*	7	mk3178-mk3194	3.80–8.75	4.95	3.86	3.59	−0.09	RSVI
(18)	*qRRAD8-1*	8	mk3839-mk3864	158.10–162.15	4.05	6.00	5.54	0.02	RRAD
(19)	*qRGR9-1*	9	mk3961-mk3984	1.35–5.75	4.40	4.90	5.07	−0.08	RGR
(20)	*qRGR10-1*	10	mk4539-mk4546	139.10–140.75	1.65	3.61	4.56	0.08	RGR

part in low-temperature resistance at the germination stage. The r values of these correlations were 0.76, 0.58, 0.48, 0.63, 0.30, and 0.34 for RGR, RSL, RRL, RTL, RRSA, and RRV, respectively. RRV displayed significant positive correlations with RRL (r = 0.51, $P < 0.01$), RSL (r = 0.27, $P < 0.01$), RTL (r = 0.45, $P < 0.01$), and RRSA (r = 0.51, $P < 0.01$). RRSA displayed significant positive correlations with RSL (r = 0.33, $P < 0.01$), RRL (r = 0.50, $P < 0.01$), and RTL (r = 0.49, $P < 0.01$). Three traits (RRL, RSL, and RTL) displayed significant positive correlations with each other ($P < 0.01$) (**Figure 1**).

Quantitative trait locis identification of low-temperature tolerance

Total of 19 QTLs were associated with eight traits in the control group, while 2, 4, 4, 2, 1, 2, 2, and 2 QTLs were associated with normal germination rate (NGR), normal shoot length (NSL), normal root length (NRL), normal total length (NTL), normal root superficial area (NRSA), normal root average diameter (NRAD), normal root volume (NRV), and normal simple vigor index (NSVI), respectively. These QTLs were detected on chromosomes 1, 2, 3, 4, 5, 7, 8, and 10, with LOD values ranging from 2.65 to 6.34, and the physical lengths from 0.25 to 2.80 Mb (**Supplementary Figure 2** and **Supplementary Table 5**).

A total of 20 QTLs were associated with eight relative traits, while 4, 3, 3, 3, 1, 2, 1, and 3 QTLs were associated with RGR, RSL, RRL, RTL, RRSA, RRAD, RRV, and RSVI (**Figure 2**), respectively. These QTLs were detected on chromosomes 1, 3, 7, 8, 9, and 10, with LOD values ranging from 2.69 to 20.09. Of these QTLs, more than 85% had a negative additive effect. This suggests that the parent Ye478's alleles resulted in higher phenotypic values. When assessed against the B73 RefGen_v3 genome, the confidence intervals for these QTLs averaged 3.93 Mb and ranged from 0.15 to 4.95 Mb. The individual QTLs explained 8.56% of the phenotypic variations, ranging from 3.58% (RRL, *qRRL3-1*) to 25.96% (RSVI, *qRSVI1-2*) for eight traits (**Table 1**).

Four stable or consistent QTLs were detected for at least two traits. Two consistent QTLs influencing multiple traits were found on chromosome 1. The *cQTL1-2* region (position 197.10–202.30 Mb on chromosome 1) possessed seven QTLs related to germination, with consistent QTLs of RGR, RSL, RRL, RTL, RRSA, RRV, and RSVI. These explained phenotypic variances from 5.18 to 25.96%, suggesting a close genetic relationship between the roots of the germinates and the indicators, possibly due to pleiotropy. *cQTL1-1* was found on chromosome 1 at position 63.85 to 68.45 Mb. It accounted for 7.80 and 13.52% of the respective total phenotypic variance for RSV and RGR (**Figure 3A**). The *cQTL3-1* with *qRRL3-1* and *qRTL3-1* were detected on chromosome 3 (**Figure 3B**). One consistent QTL (*cQRL7-1*) on chromosome 7, from 1.45 to 8.75, included three QTLs of *qRRL7-1*, *qRTL7-1*, and *qRSVI7-1*. These phenotypic variances ranged from 3.59 to 7.41% (**Figure 3C**).

Verification and fine mapping of quantitative trait locis with chromosome segment substitution lines

Two SSR markers umc1254 and umc2237 were added in *cQTL1-2* (chr1: 197.10–202.30 Mb) of a CSSLs population

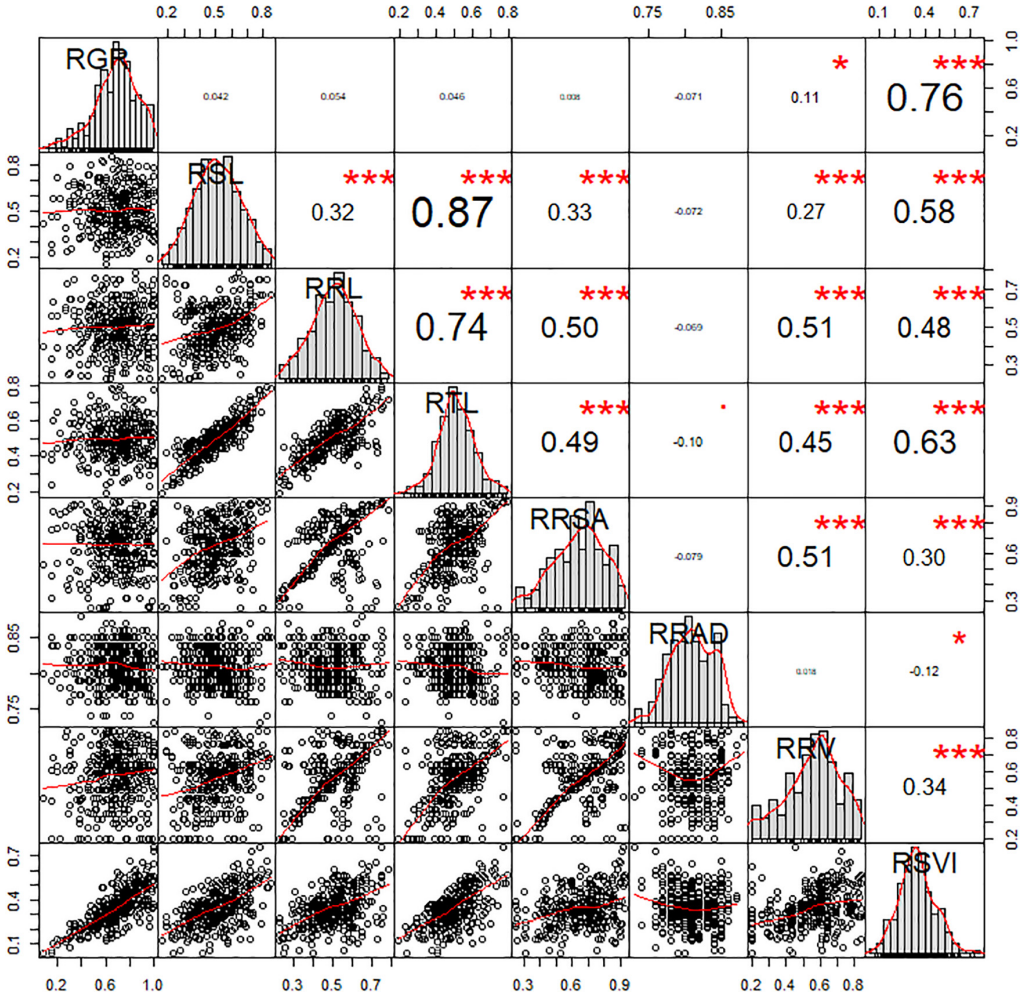

FIGURE 1
Correlation analysis of the RIL population related to low-temperature tolerance traits. The frequency distribution of each trait is shown on a central diagonal in the form of a histogram. Scatter plots of between each pair of traits are shown in the areas below the diagonal, and numerical correlation coefficients between each pair of traits are shown in the areas above in the diagonal. * and *** indicate significance at $p < 0.05$ and $p < 0.001$, respectively.

with 180 families which was constructed with Ye478 as the female parent and Qi319 as the male parent. In these CSSLs, the genotypes of CL174, CL017, CL006, and CL018 introduced Qi319 fragment from markers umc1254 to umc2237. However, the genotypes of CL014, CL009, and CL173 were still from the recurrent parent Ye478 fragment, and the imported Qi319 fragment was located near *cQTL1-2* (**Supplementary Table 1** and **Supplementary Figure 1**). To verify the consistency and narrow the consistent QTL range, seven CSSLs were analyzed with two major QTLs, which were constructed with the same parental inbred line. The RGR trait was used to verify *cQTL1-2*. The RGRs of the segment substitution lines CL174, CL017, CL006, and CL018, which were substituted with Qi319, were changed from 0.89 to 0.34–0.55. These were significantly different from the RGRs of Ye478 ($P < 0.001$). *cQTL1-2*, which controlled ability to germinate at low temperatures, was between the umc1254 and umc2237 markers (200,400,148–206,699,769 bp). Combined with *cQTL1-2*, the major QTL was from markers umc1254 and umc2505 (200,400,148–202,300,000 bp), with a confidence interval of 1,899,852 bp (**Figure 4**).

Meta-analysis verification of consistent QTL

The QTLs were distributed on all the ten chromosomes of maize in clusters of distribution (**Supplementary Figure 3** and **Supplementary Table 6**). The most QTLs (22) were detected on chromosome 1, while six QTLs were detected on chromosome 2, nine were detected on chromosome 3, four were detected on chromosome 4, seven were detected on

10.3389/fpls.2022.978941

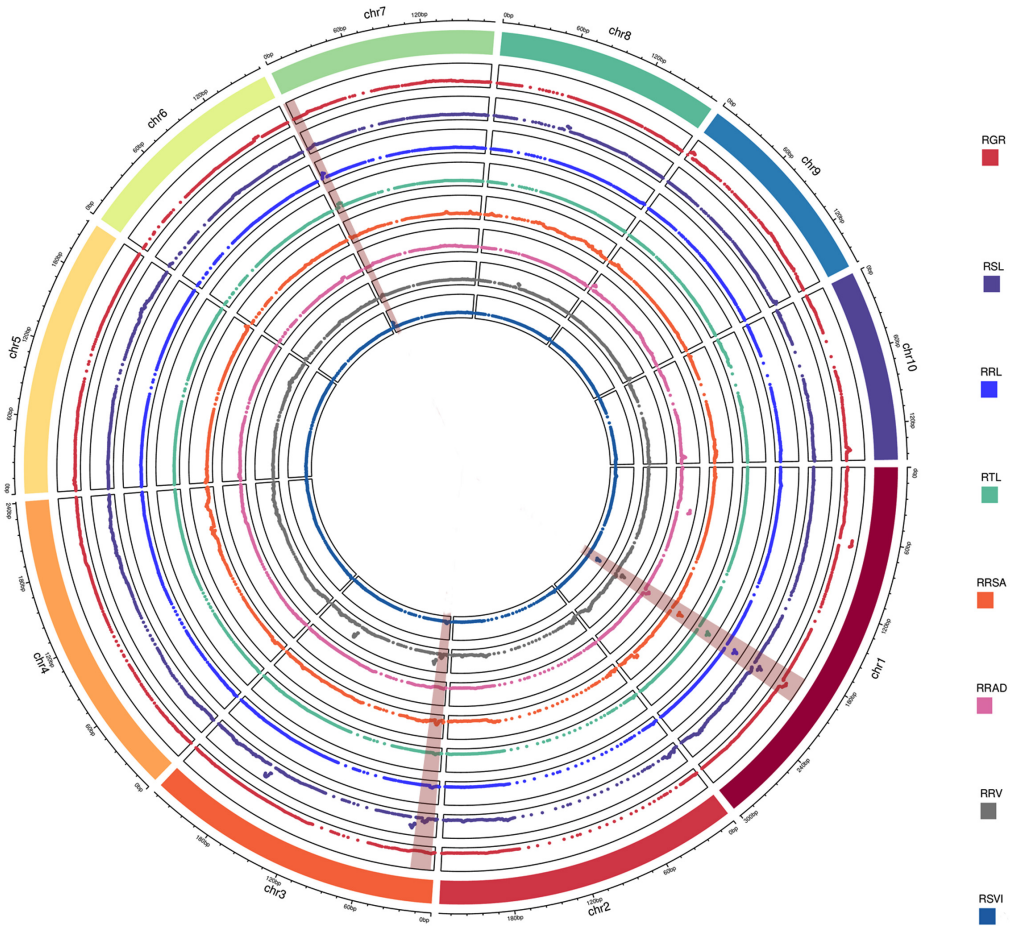

FIGURE 2
QTL analysis in the RIL population related to low-temperature tolerance traits. The outermost box with scale represents the 10 maize chromosomes. For each trait, different colors represent the eight different traits related to low-temperature tolerance (RGR, RSL, RRL, RTL, RRSA, RRAD, RRV, and RSVI). The red backgrounds of chromosomes 1, 3, and 7 represent consistent QTLs.

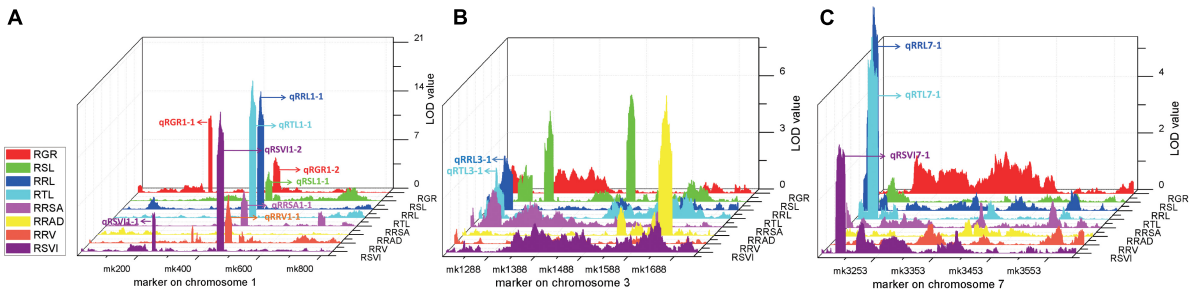

FIGURE 3
QTL map of consistent segments related to multiple low-temperature tolerance traits in the RIL population during germination. **(A)** QTL of eight phenotypes on chromosome 1, **(B)** QTL of eight phenotypes on chromosome 3, **(C)** QTL of eight phenotypes on chromosome 7. For each trait, different colors represent the eight different traits related to low-temperature tolerance (RGR, RSL, RRL, RTL, RRSA, RRAD, RRV, and RSVI).

chromosome 5, the least (three) were detected on chromosome 6, four were detected on chromosome 7, four were detected on chromosome 8, 12 were detected on chromosome 9, and five were detected on chromosome 10. These QTLs explained between 0.62 and 39.44% of phenotypic variation. A meta-QTL (*mQTL1*) was detected on chromosome 1, with 11 QTLs. These QTLs were co-located and distributed in clusters. The *mQTL1* was located on chromosome 1, from 199,674,463 to

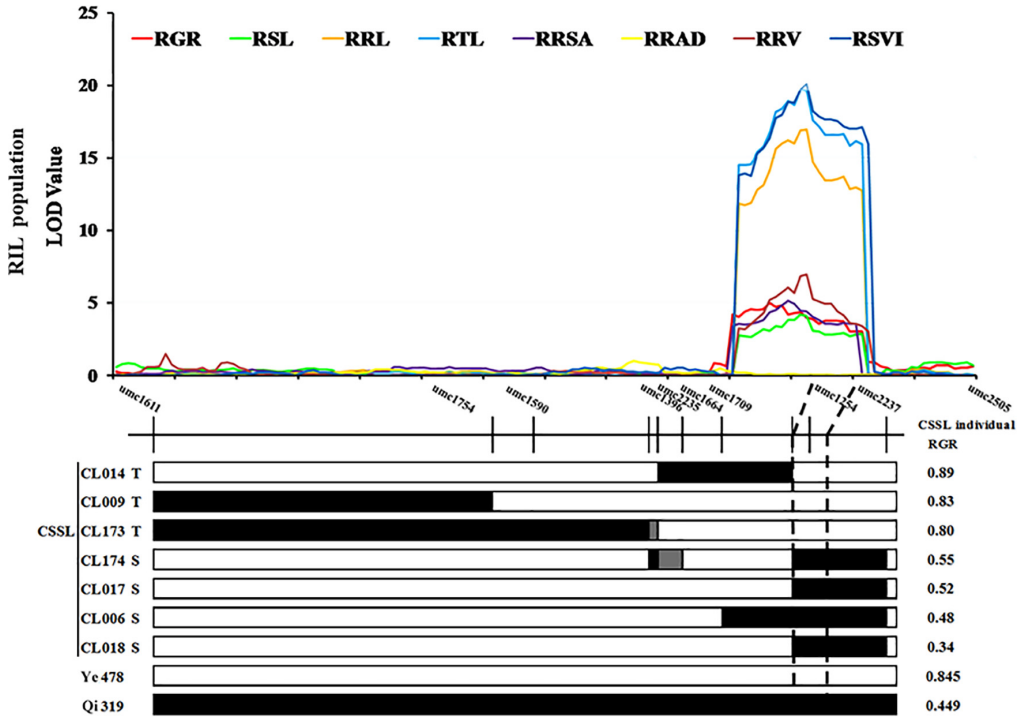

FIGURE 4
cQTL1-2 fine mapping in CSSL lines. White represents the homozygous segment of Ye478, black is the homozygous segment of Qi319, gray is the hybrid segment. T- material of tolerant line, S- material of sensitive line. For each trait, different colors of LOD value represent the eight different traits related to low-temperature tolerance (RGR, RSL, RRL, RTL, RRSA, RRAD, RRV, and RSVI) of the RIL population.

201,775,619 bp in bin 1.06–1.07 with molecular markers of ereb172 and tena2. Combined with the results of *cQTL1-2* and *mQTL1*, the consistent major low-temperature tolerance QTL (*LtQTL1-1*), which controls ability to germinate in maize, was on bin 1.06–1.07 on chromosome 1 at a range of 200,400,148–201,775,619 bp (**Figure 5**).

Quantitative PCR validation for candidate genes

Referring to B73 in MaizeGDB (see Text Footnote 3) RefGen_v3 genome annotation information, there were 66 genes in the *LtQTL1-1* confidence interval. Of these, 26 were annotated to be mainly related to transport, stress response, signal transduction, catalytic activity, binding activity, and cell components. Two candidate genes (*GRMZM2G082630* and *GRMZM2G115730*) within *LtQTL1-1* were similar to the genes relating to low-temperature adaptation published by BLAST analysis (**Supplementary Table 7**). qRT-PCR was used to confirm the levels of expression and confirm these two candidate genes. Of the six maize materials, there were two parental inbred lines, a low-temperature resistant and sensitive line, from RILs and CSSLs. These were used to detect the level of genetic expression under low temperatures. These two genes displayed significant positive expression levels in the low-temperature resistant lines (Ye478, ZYQ219m, and CL082) and negative expression levels in the low-temperature sensitive lines (Qi319, ZYQ011m, and CL018), 2 and 4 h following exposure to cold temperatures. *GRMZM2G082630* and *GRMZM2G115730* expression levels differed between the resistant and sensitive lines; further, expression levels of the two genes also showed significant differences between 2 and 4 h ($p < 0.01$) (**Figure 6**).

Discussion

Identification of traits related to low-temperature tolerance

Recent studies on plant stress resistance suggested that when plants are subjected to abiotic stress, their root structure changes to improve stress tolerance (Bao et al., 2014; Robbins and Dinneny, 2015). Therefore, root characteristics are an important measure of stress resistance. Research assessing the QTL mapping of the ability of maize to tolerate low temperature has mainly focused on traits related to germination, such as the germination rate and germination index (Hu et al., 2017; Li et al., 2018). Root traits such as length, fresh weight, dry weight, and

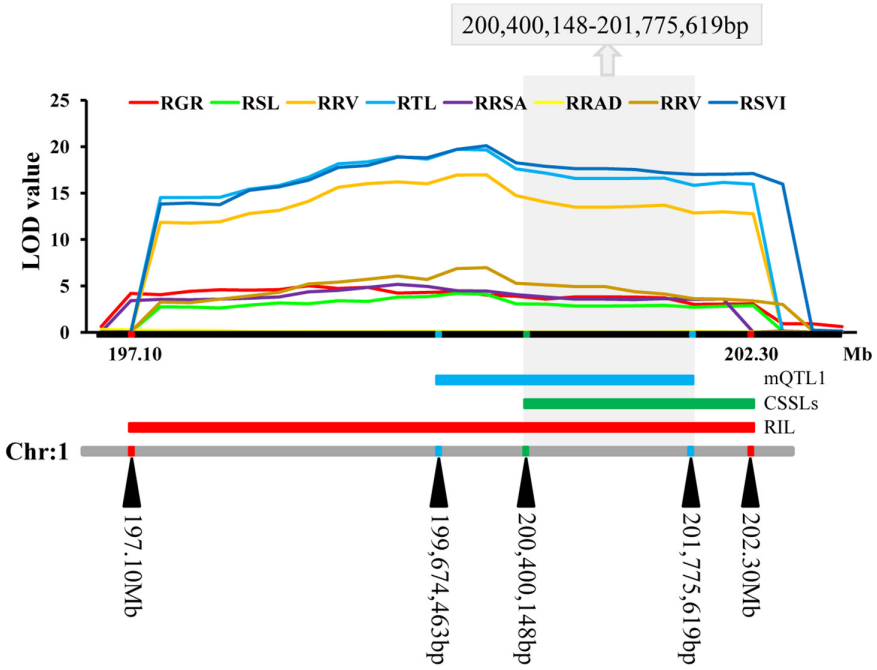

FIGURE 5
The consistent segments during the germination related to low-temperature. For each trait, different colors of LOD value represent the eight different traits related to low-temperature tolerance (RGR, RSL, RRL, RTL, RRSA, RRAD, RRV, and RSVI).

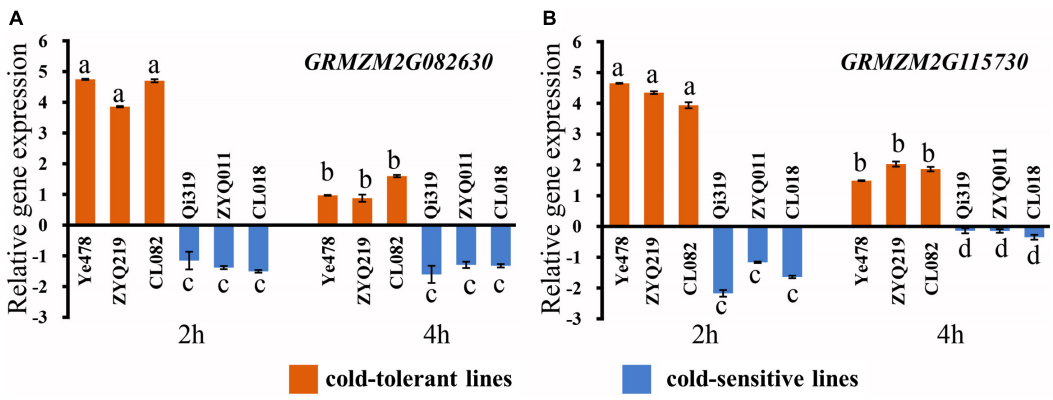

FIGURE 6
Relative expression of two candidate genes. **(A)** Relative expression of the candidate gene *GRMZM2G082630*, **(B)** relative expression of the candidate gene *GRMZM2G115730*. Different small letters within a gene indicate significant differences between the materials.

water content were primarily measured at the seedling stage (Jompuk et al., 2005; Presterl et al., 2007; Rodri'guez et al., 2014). Little attention was paid to root and shoot growth after the germination period; however, the root and shoot characteristics during the germination period help regulate the growth of maize (Hund et al., 2004). Thus, in the current study, eight traits including RGR, RSL, RRL, RTL, RRSA, RRAD, RRV, and RSVI were used to detect the QTLs of low temperatures during the germination period in maize. The results showed that RGR was significantly positively correlated with RSVI, while RSVI was also significantly positively correlated with RSL, RRL, RTL, RRSA, and RRV. However, the correlation between RRAD and other traits were not significant. The results of QTL mapping demonstrated that RGR, RSL, RRL, RTL, RRSA, RRV, and RSVI were all mapped to the main QTL segment (197.10–202.30 Mb on chromosome 1), and the contribution rate of each phenotype in this major QTL segment ranged from 5.18 to 25.96%. This indicates that the shoot and root traits were closely related to the species during seed germination. The seed germination rate should also be considered in QTL mapping, and the roots and

shoots at the germination stage are also related to the stress response of low-temperature tolerance in maize. Of the 20 QTLs mapped, root-related traits were important. When 15 QTLs were mapped, the phenotypic contribution rate ranged from 3.58 to 25.96%. Therefore, the root system plays a vital role in the adaptation of plants to stress conditions. Low temperatures can weaken, inhibit, and reduce root length, volume, and dry weight (Hodges et al., 1995; Bhosale et al., 2007; Rácz et al., 2007; Frascaroli and Landi, 2013, 2016). The results of this experiment were consistent with those of previous studies.

The advantages of bin map or high-throughput sequencing in QTL analysis

In plants, the bin map genetic linkage map obtained by high-throughput sequencing technology has a high-density and small QTL interval, and is widely used. Therefore, used a 2,500-locus bin map of the homologous group 5 in wheat to better understand the distribution and collinearity of its genes with that of rice (Linkiewicz et al., 2004). The researchers generated a high-resolution genetic map of the PmAS846 locus in order to assess the resistance of wheat to powdery mildew (Xue et al., 2012). The QTLs related to anaerobic germination tolerance and salt stress at early seedling stages in rice were also identified via high-density bin genetic map (Yang et al., 2019; Amoah et al., 2020). In maize, some RILs were constructed to identify QTLs and genes. One example is a set of 204 RILs (with parents Zheng58 and Chang7-2), which was the widely adopted Chinese hybrid ZD958 (Song et al., 2016). From this, 199 F_2 offspring were obtained by crossing the varieties SG-7 and SG-5 and genotyping them via GBS (Su et al., 2017), as well as a set of RILs derived from inbred lines Ye478 and Qi319 (Zhou et al., 2016). QTLs relating to yield, plant architecture, and seedling root system architecture traits were all mapped using the high-density linkage map (Courtial et al., 2013; Chen et al., 2016; Song et al., 2016; Su et al., 2017; Zhang et al., 2017a; Wang et al., 2018a). In this study, an ultra-high-density genetic linkage map (with 4,602 bin markers) and GBS high-throughput sequencing were used to perform QTL mapping. The low-temperature tolerance of these QTLs were mapped at the germination period to a range of 0.90-4.95Mb. The range of the mapped QTLs was smaller than others. The results were also stable, with several traits were located together, and the narrowed interval was suitable for further prediction of candidate genes.

The importance of chromosome segment substitution lines in QTL mapping

Chromosome segment substitution lines are one of the best methods of QTL mapping and are widely used in QTL analysis of agronomic and stress resistance traits in plants. CSSLs are most widely used in rice and for QTL mapping in maize. QTLs relating to the resistance of multiple diseases in maize were identified by CSSLs (Lopez-Zuniga et al., 2019). A set of 184 CSSLs and their inbred lines (Zheng58 and Xun9058) were used to identify maize kernel traits (Wang et al., 2018c). A set of 130 CSSLs were constructed with (donor parent Nongxi531 and recipient parent H21) to perform a QTL analysis of the number of kernel rows in maize. This demonstrated their true expression in different environments (Li et al., 2014). The CSSLs derived from Qi319 as donor and Ye478 were used to validate *qNCLB7.02*, which was the novel QTL related to resistance to the northern corn leaf (NCLB) (Wang et al., 2018b). However, there have yet been few reports on applying CSSL materials when mapping the QTLs related to maize tolerance of low temperatures. In this study, the RIL population was first constructed by Ye478*Qi319 to map QTLs related to tolerance to low temperatures in maize, in order to determine one or more traits. The linked consistent QTL segment is located on 197.10–202.30 Mb of chromosome 1, and the physical distance is 5.20 Mb. This QTL segment is named *cQTL1-2*. The CSSLs with the donor parent-introduced fragments near the *cQTL1-2* segment were subjected to phenotypic testing and the contig substitution mapping method was used to verify the accuracy of the *cQTL1-2* positioning of the RIL population. This was reduced to 200,400,148–202,300,000 bp, with a physical distance of about 1.9 Mb.

Comparative analysis of quantitative trait locis relating to maize tolerance of low temperatures

In this study, a linkage analysis of the RIL population were performed on eight low-temperature tolerance related traits and mapped a total of 20 QTLs located on different chromosomes. Of them, four were new QTLs that had not been previously mapped: *qRSL3-2*, *qRRAD8-1*, *qRGR9-1*, and *qRGR10-1*. The remaining 16 QTLs overlapped with QTLs known to be related to low-temperature tolerance, and this study narrowed the confidence interval of their positioning. This study assessed the QTLs of RGR, RSL, RRL, RTL, RRSA, RRV, and RSVI: *qRGR1-2*, *qRSL1-1*, *qRRL1-1*, *qRTL1-1*, *qRRSA1-1*, *qRRV1-1*, and *qRSVI1-2*. The mapped *cQTL1-2* segment of chromosome 1 (197.10–202.30 Mb) was consistent with QTLs (58.66 Mb) for shoot length, root length, and total length (Li et al., 2018), the phosphoric acid QTLs for enolpyruvate carboxylase activity (70 Mb) (Leipner and Mayer, 2008), the QTLs for φPSII traits (43 Mb) (Fracheboud et al., 2004), and the SNP related to chlorophyll content (PZE-101159230) (Revilla et al., 2016). In previous studies, the QTL was narrowed to 5.2 Mb (chr1: 197.10–202.30 Mb) from 43 to 70 Mb. In this experiment, the CSSLs were used to reduce the *cQTL1-2* to

approximately 1.9 Mb, using the contig substitution mapping method. This was used along with a meta-analysis to verify the accuracy of *cQTL1-2* and further reduce it to 1.38 Mb, which was named *LtQTL1-1* (200,400,148–201,775,619 bp). *LtQTL1-1* is the major QTL linked to multiple low-temperature tolerance traits and had a phenotypic contribution rate from 5.18 to 25.96%. Additionally, the SNP related to the chlorophyll content at low temperatures (PZE-101159230) (Revilla et al., 2016) was also located in our major QTL. The SNP-31 associated with relative water content at low temperatures was located in the *qRSL3-1* of our QTLs (Huang et al., 2013). The SNP (S7_1956860) associated with the relative number of days when germination rate reaches 50% was located in the QTL *qRRL7-1* (Hu et al., 2017).

Molecular function of two candidate genes

GRMZM2G082630 was the protein that codes for superfamily of basic Helix Loop Helix (bHLH) domain. The bHLH proteins were transcriptional regulators, and members of this superfamily with two functionally distinct regions, which were highly conserved: a basic DNA binding region and a helix-loop-helix (HLH) region. The characteristics of superfamily of bHLHs in *A. thaliana* were play important function of stress responses, light signal transduction, plant growth and development (Friedrichsen et al., 2002; Abe et al., 2003; Castelain et al., 2012; Liu et al., 2013; Yao et al., 2018). They were also participate in the crosstalk of hormone signaling, such as jasmonic acid (JA), salicylic acid (SA), abscisic acid (ABA), brassinosteroid (BR), and ethylene (ET) (Murre et al., 1989; Heim et al., 2003; Pires and Dolan, 2010; Feller et al., 2011), and they are critical for survival in the environment (Hao et al., 2021). Previous studies show that the homologous bHLH genes *bhlh068* of *O. sativa* and *bHLH112* of *A. thaliana* are important regulatory factor to response to salt stress (Chen et al., 2017). The *Nicotiana tabacum* plants which overexpressing *Ntbhlh123* can enhanced resistance of under low-temperature (Zhao et al., 2018). The genes *SbbHLH134*, *SbbHLH110,* and *SbbHLH101,* which have bHLH domain in *S. bicolor*, also can regulate flower and fruit development (Fan et al., 2021). *GRMZM2G115730* was encoded by the evolutionarily conserved protein with the Epsin N-Terminal Homology (ENTH) domain. The domain was a portion of structurally related ENTH, ANTH, or VHS domain in the N-terminal region and a variable C-terminal region, with the functions of transport vesicle (Feng et al., 2022). The ENTH domain protein family taken part in numerous plant processes, such as, response to abiotic stress, growth of pollen tube, growth and development. This domain could be detected in more than 30 *A. thaliana* proteins, which was involved in clathrin-related endomembrane trafficking of plants (Zouhar and Sauer, 2014). *OsMIP1* encoded a putative transmembrane protein with an ENTH/ANTH/VHS domain, and could respond to NaCl, PEG, and other abiotic stresses (Wang et al., 2017). ENTH family proteins might also plays an important role in the regulation of abiotic stress such as low-temperature. Therefore, two candidate genes, *GRMZM2G082630* and *GRMZM2G115730*, were screened for qRT-PCR validation.

Conclusion

This study performed QTL mapping of the 365 RILs which obtained from crossing Qi319 and Ye478. Major QTL was verified by seven CSSLs derived from Ye478*Qi319. And a meta-QTL analysis were performed of the ability of maize to tolerate low temperatures at the germination stage. The QTL *LtQTL1-1* related to tolerance of low temperatures at the germination stage was detected on bin1.06–1.07 of chromosome 1, at a confidence interval of between 200,400,148 and 201,775,619 bp. In this interval, the relative expression of the candidate genes *GRMZM2G082630* and *GRMZM2G115730* were significantly different ($p < 0.01$) from that of materials with different low-temperature tolerances. Both genes were up-regulated in low-temperature-tolerant varieties and down-regulated in low-temperature-sensitive varieties.

Data availability statement

The datasets presented in this study can be found in online repositories. The names of the repository/repositories and accession number(s) can be found below: https://www.ncbi.nlm.nih.gov/, PRJNA627044.

Author contributions

YZ, QL, and DW performed the experiments and wrote the manuscript. JM, XL, HD, LZ, LD, XJL, XZ, and ZZ took participate in the experiments. ZW, JW, and YZ designed the experiments and revised the manuscript. All authors read and approved the manuscript.

Funding

This research was jointly funded by the National Key Research and Development Program (2021YFD1201001), Backbone of Young Talent Scholar Project (to YZ, 20XG23), Natural Science Foundation Project of Heilongjiang Province

(C2018014), and Engineering Technology Research Center of Maize Germplasm Resources Innovation on Cold land of Heilongjiang Province.

Acknowledgments

We thank Xinhai Li for providing the plant materials.

Conflict of interest

The authors declare that the research was conducted in the absence of any commercial or financial relationships that could be construed as a potential conflict of interest.

Publisher's note

Supplementary material

The Supplementary Material for this article can be found online at: https://www.frontiersin.org/articles/10.3389/fpls.2022.978941/full#supplementary-material

References

Abe, H., Urao, T., Ito, T., Seki, M., Shinozaki, K., and Yamaguchi-Shinozaki, K. (2003). Arabidopsis AtMYC2 (bHLH) and AtMYB2 (MYB) function as transcriptional activators in abscisic acid signaling. *Plant Cell* 15, 63–78. doi: 10.1105/tpc.006130

Amoah, N. K. A., Akromah, R., Kena, A. W., Manneh, B., Dieng, I., and Bimpong, I. K. (2020). QTLs for tolerance to salt stress at the early seedling stage in rice (*Oryza sativa* L.) using a newly identified donor 'Madina Koyo'. *Euphytica* 216, 16–20. doi: 10.1007/s10681-020-02689-5

Arcade, A., Labourdette, A., Falque, M., Mangin, B., Chardon, F., Charcosset, A., et al. (2004). BioMercator: integrating genetic maps and QTL towards discovery of candidate genes. *Bioinformatics* 20, 2324–2326. doi: 10.1093/bioinformatics/bth230

Bao, Y., Aggarwalb, P., Robbins, N. E., Sturrocke, C. J., Thompsone, M. C., Tan, H. Q., et al. (2014). Plant roots use a patterning mechanism to position lateral root branches toward available water. *Proc. Natl. Acad. Sci U S A.* 25, 9319–9324. doi: 10.1073/pnas.1400966111

Berberich, T., Sano, H., and Kusano, T. (1999). Involvement of a MAP kinase, ZmMPK5, in senescence and recovery from low-temperature stress in maize. *Mol. Gen. Genet.* 262, 534–542. doi: 10.1007/s004380051115

Bhosale, S. U., Rymen, B., Beemster, G. T., Melchinger, A. E., and Reif, J. C. (2007). Chilling tolerance of Central European maize lines and their factorial crosses. *Ann. Bot.* 100, 1315–1321. doi: 10.1093/aob/mcm215

Bieluszewski, T., Sura, W., Dziegielewski, W., Bieluszewska, A., Lachance, C., Kabza, M., et al. (2022). NuA4 and H2A.Z control environmental responses and autotrophic growth in *Arabidopsis*. *Nat. Commun.* 13, 277–296. doi: 10.1038/s41467-021-27882-5

Bouis, H. E., and Welch, R. M. (2010). Biofortification - a sustainable agricultural strategy for reducing micronutrient malnutrition in the global south. *Crop Sci.* 50, S20–S32. doi: 10.3389/fgene.2020.00414

Castelain, M., Le Hir, R., and Bellini, C. (2012). The non-DNA-binding bHLH transcription factor PRE3/bHLH135/ATBS1/TMO7 is involved in the regulation of light signaling pathway in Arabidopsis. *Physiol. Plant.* 145, 450–460. doi: 10.1111/j.1399-3054.2012.01600.x

Chen, H. C., Hsieh-Feng, V., Liao, P. C., Cheng, W. H., Liu, L. Y., Yang, Y. W., et al. (2017). The function of OsbHLH068 is partially redundant with its homolog, AtbHLH112, in the regulation of the salt stress response but has opposite functions to control flowering in *Arabidopsis*. *Plant Mol. Biol.* 94, 531–548. doi: 10.1007/s11103-017-0624-6

Chen, L., Li, C. H., Li, Y. X., Song, Y. C., Zhang, D. F., Wang, T. Y., et al. (2016). Quantitative trait loci mapping of yield and related traits using a high-density genetic map of maize. *Mol. Breed.* 36, 134–148. doi: 10.1007/s11032-016-0545-0

Chen, L. P., Zhao, Y., Xu, S. J., Zhang, Z. Y., Xu, Y. Y., Zhang, J. Y., et al. (2018). OsMADS57 together with OsTB1 coordinates transcription of its target OsWRKY94 and D14 to switch its organogenesis to defense for cold adaptation in rice. *New Phytol.* 218, 219–231. doi: 10.1111/nph.14977

Chou, W. L., Chung, Y. L., Fang, J. C., and Lu, C. A. (2016). Novel interaction between CCR4 and CAF1 in rice CCR4-NOT deadenylase complex. *Plant Mol. Biol.* 93, 79–96. doi: 10.1007/s11103-016-0548-6

Christie, P. J., Hahn, M., and Walbot, V. (2021). Low-Temperature accumulation of alcohol dehydrogenase-1 mRNA and protein activity in maize and rice seedlings. *Plant Physiol.* 1991, 699–706. doi: 10.1104/pp.95.3.699

Courtial, A., Thomas, J., Reymond, M., Me'chin, V., Grima-Pettenati, J., and Barrie're, Y. (2013). Targeted linkage map densification to improve cell wall related QTL detection and interpretation in maize. *Theor. Appl. Genet.* 126, 1151–1165. doi: 10.1007/s00122-013-2043-7

del Campillo, E., Abdel-Aziz, A., Crawford, D., and Patterson, S. E. (2004). Root cap specific expression of an endo-β-1,4-D-glucanase (cellulase): a new marker to study root development in *Arabidopsis*. *Plant Mol. Biol.* 56, 309–323. doi: 10.1007/s11103-004-3380-3

Faik, A., Price, N. J., Raikhel, N. V., and Keegstra, K. (2002). An Arabidopsis gene encoding an α-xylosyltransferase involved in xyloglucan biosynthesis. *Proc. Natl. Acad. Sci. U S A.* 99, 7797–7802. doi: 10.1073/pnas.102644799

Fan, Y., Yang, H., Lai, D., He, A., Xue, G., Feng, L., et al. (2021). Genome-wide identification and expression analysis of the bHLH transcription factor family and its response to abiotic stress in sorghum [*Sorghum bicolor* (L.) Moench]. *BMC Genomics* 22:415. doi: 10.1186/s12864-021-07652-9

Feller, A., Machemer, K., Braun, E. L., and Grotewold, E. (2011). Evolutionary and comparative analysis of MYB and bHLH plant transcription factors. *Plant J.* 66, 94–116. doi: 10.1111/j.1365-313X.2010.04459.x

Feng, Y., Hiwatashi, T., Minamino, N., Ebine, K., and Ueda, T. (2022). Membrane trafficking functions of the ANTH/ENTH/VHS domain-containing proteins in plants. *FEBS Lett.* Online ahead of print. doi: 10.1002/1873-3468.14368

Fracheboud, Y., Jompuk, C., Ribaut, J. M., Stamp, P., and Leipner, J. (2004). Genetic analysis of cold-tolerance of photosynthesis in maize. *Plant. Mol. Biol.* 56, 241–253. doi: 10.1007/s11103-004-3353-6

Frascaroli, E., and Landi, P. (2013). Divergent selection in a maize population for germination at low temperature in controlled environment: study of the direct response, of the trait inheritance and of correlated responses in the field. *Theor. Appl. Genet.* 126, 733–746. doi: 10.1007/s00122-012-2014-4

Frascaroli, E., and Landi, P. (2016). Cold tolerance in field conditions, its inheritance, agronomic performance and genetic structure of maize lines divergently selected for germination at low temperature. *Euphytica* 209, 771–788. doi: 10.1007/s10681-016-1680-8

Friedrichsen, D. M., Nemhauser, J., Muramitsu, T., Maloof, J. N., Alonso, J., Ecker, J. R., et al. (2002). Three redundant brassinosteroid early response genes encode putative bHLH transcription factors required for normal growth. *Genetics* 162, 1445–1456. doi: 10.1093/genetics/162.3.1445

Greaves, J. A. (1996). Improving suboptimal temperature tolerance in maize the search for variation. *J. Exp. Bot.* 47, 307–323. doi: 10.1093/jxb/47.3.307

Hao, Y., Zong, X., Ren, P., Qian, Y., and Fu, A. (2021). Basic Helix-Loop-Helix (bHLH) transcription factors regulate a wide range of functions in *Arabidopsis*. *Int. J. Mol. Sci.* 22, 7152–7171. doi: 10.3390/ijms22137152

Heim, M. A., Jakoby, M., Werber, M., Martin, C., Weisshaar, B., and Bailey, P. C. (2003). The basic helix-loop-helix transcription factor family in plants: a genome-wide study of protein structure and functional diversity. *Mol. Biol. Evol.* 20, 735–747. doi: 10.1093/molbev/msg088

Hodges, D. M., Hamilton, R. I., and Charest, C. (1995). A chilling response test for early growth phase maize. *Agron. J.* 87, 970–974. doi: 10.2134/agronj1995.00021962008700050033x

Hu, G. H., Li, Z., Lu, Y. C., Li, C. X., Gong, S. C., Yan, S. Q., et al. (2017). Genome-wide association study Identifed multiple genetic loci on chilling resistance during germination in maize. *Sci Rep.* 7:10840. doi: 10.1038/s41598-017-11318-6

Hu, S. D., Lübberstedt, T., Zhao, G. W., and Lee, M. (2016). QTL mapping of low-temperature germination ability in the maize IBM Syn4 RIL population. *PLoS One* 11:e0152795. doi: 10.1371/journal.pone.0152795

Huang, J., Zhang, J. H., Li, W. Z., Hu, W., Duan, L. C., Feng, Y., et al. (2013). Genome-wide association analysis of ten chilling tolerance indices at the germinationand seedling stages in maize. *J. Integr. Plant Biol.* 55, 735–744. doi: 10.1111/jipb.12051

Hund, A., Fracheboud, Y., Soldati, A., Frascaroli, E., Salvi, S., and Stamp, P. (2004). QTL controlling root and shoot traits of maize seedlings under cold stress. *Theor. Appl. Genet.* 109, 618–629. doi: 10.1007/s00122-004-1665-1

Jeon, J., Cho, C., Lee, M. R., Van Binh, N., and Kim, J. (2016). CYTOKININ RESPONSE FACTOR2 (CRF2) and CRF3 regulate lateral root development in response to cold stress in *Arabidopsis*. *Plant Cell* 28, 1828–1843. doi: 10.1105/tpc.15.00909

Jompuk, C., Fracheboud, Y., Stamp, P., and Leipner, J. (2005). Mapping of quantitative trait loci associated with chilling tolerance in maize (*Zea mays* L.) seedlings grown under field conditions. *J. Exp. Bot.* 56, 1153–1163. doi: 10.1093/jxb/eri108

Kameoka, T., Okayasu, T., Kikuraku, K., Ogawa, T., Sawa, Y., Yamamoto, H., et al. (2021). Cooperation of chloroplast ascorbate peroxidases and proton gradient regulation 5 is critical for protecting *Arabidopsis* plants from photo-oxidative stress. *Plant J.* 107, 876–892. doi: 10.1111/tpj.15352

Kocsy, G., Pál, M., Soltész, A., Szalai, G., Boldizsár, Á, Kovács, V., et al. (2011). Low temperature and oxidative stress in cereals. *Acta. Agron. Hungarica* 59, 169–189. doi: 10.1556/AAgr.59.2011.2.7

Kong, X. P., Lv, W., Jiang, S. S., Zhang, D., Cai, G. H., Pan, J. W., et al. (2013). Genome-wide identification and expression analysis of calcium-dependent protein kinase in maize. *BMC Genomics* 14:433. doi: 10.1186/1471-2164-14-433

Leipner, J., and Mayer, E. (2008). QTL mapping in maize seedlings reveals little relevance of C4 cycle enzymes and antioxidants for genotypic differences in chilling tolerance of photosynthesis. *Maydica* 53, 269–277.

Li, F., Jia, H. T., Liu, L., Zhang, C. X., Liu, Z. J., and Zhang, Z. X. (2014). Quantitative trait loci mapping for kernel row number using chromosome segment substitution lines in maize. *Genet. Mol. Res.* 13, 1707–1716. doi: 10.4238/2014.January.17.1

Li, H., Ding, Y. L., Shi, Y. T., Zhang, X. Y., Zhang, S. Q., Gong, Z. Z., et al. (2017a). MPK3- and MPK6-Mediated ICE1 phosphorylation negatively regulates ICE1 stability and freezing tolerance in *Arabidopsis*. *Dev. Cell.* 43, 630–642. doi: 10.1016/j.devcel.2017.09.025

Li, H., Ye, K. Y., Shi, Y. T., Cheng, J. K., Zhang, X. Y., and Yang, S. H. (2017b). BZR1 positively regulates freezing tolerance via CBF-dependent and CBF-Independent pathways in *Arabidopsis*. *Mol. Plant.* 10, 545–559. doi: 10.1016/j.molp.2017.01.004

Li, X., Wang, G., Fu, J., Li, L., Jia, G., Ren, L., et al. (2018). QTL mapping in three connected populations reveals a set of consensus genomic regions for low temperature germination ability in *Zea mays* L. *Front. Plant Sci.* 9:65. doi: 10.3389/fpls.2018.00065

Linkiewicz, A. M., Qi, L. L., Gill, B. S., Ratnasiri, A., Echalier, B., Chao, S., et al. (2004). A 2500-locus bin map of wheat homoeologous group 5 provides insights on gene distribution and colinearity with rice. *Genetics* 168, 665–676. doi: 10.1534/genetics.104.034835

Liu, Y., Chen, X., Xue, S., Quan, T., Cui, D., Han, L., et al. (2021). SET DOMAIN GROUP 721 protein functions in saline-alkaline stress tolerance in the model rice variety Kitaake. *Plant Bio. J.* 19, 2576–2588. doi: 10.1111/pbi.13683

Liu, Y., Li, X., Li, K., Liu, H., and Lin, C. (2013). Multiple bHLH proteins form heterodimers to mediate CRY2-dependent regulation of flowering-time in *Arabidopsis*. *PLoS Genet.* 9:e1003861. doi: 10.1371/journal.pgen.1003861

Lopez-Zuniga, L. O., Petra, W., Scott, D., Weldekidan, T., Kolkman, J. M., Nelson, R., et al. (2019). Using maize chromosome segment substitution line populations for the identification of loci associated with multiple disease resistance. *G3-Genes Genomes Genet.* 9, 189–201.

Ma, Y., Dai, X. Y., Xu, Y. Y., Luo, W., Zheng, X. M., Zeng, D. L., et al. (2015). COLD1 confers chilling tolerance in rice. *Cell* 160, 1209–1221. doi: 10.1016/j.cell.2015.01.046

McDonnell, M. M., Burkhart, S. E., Stoddard, J. M., Wright, Z. J., Strader, L. C., and Bartel, B. (2016). The early-acting peroxin PEX19 is redundantly encoded. farnesylated, and essential for viability in *Arabidopsis thaliana*. *PLoS One* 11:e0148335. doi: 10.1371/journal.pone.0148335

Moon, Y. K., Hong, J. P., Cho, Y. C., Yang, S. J., An, G., and Kim, W. T. (2009). Structure and expression of OsUBP6, an ubiquitin-specific protease 6 homolog in rice (*Oryza sativa* L.). *Mol. Cells* 28, 463–472. doi: 10.1007/s10059-009-0138-4

Murre, C., McCaw, P. S., and Baltimore, D. (1989). A new DNA binding and dimerization motif in immunoglobulin enhancer binding, daughterless, MyoD, and myc proteins. *Cell* 56, 777–783. doi: 10.1016/0092-8674(89)90682-x

Nishikawa, Y., Yamamoto, H., Okegawa, Y., Wada, S., Sato, N., Taira, Y., et al. (2012). PGR5-dependent cyclic electron transport around PSI contributes to the redox homeostasis in chloroplasts rather than CO2 fixation and biomass production in rice. *Plant Cell Physiol.* 53, 2117–2126. doi: 10.1093/pcp/pcs153

Ohyama, A., Tominaga, R., Toriba, T., and Tanaka, W. (2022). D-type cyclin OsCYCD3;1 is involved in the maintenance of meristem activity to regulate branch formation in rice. *J. Plant Physiol.* 270:153634. doi: 10.1016/j.jplph.2022.153634

Pires, N., and Dolan, L. (2010). Origin and diversification of basic-helix-loop-helix proteins in plants. *Mol. Biol. Evol.* 27, 862–874.

Plohovska, S. G., Yemets, A. I., and Blume, Y. B. (2016). Influence of cold on organization of actin filament in various cell types root *Arabidopsis thaliana*. *Tsitol Genet.* 50, 65–71.

Presterl, T., Ouzunova, M., Schmidt, W., Möller, E. M., Röber, F. K., Knaak, C., et al. (2007). Quantitative trait loci for early plant vigour of maize grown in chilly environments. *Theor. Appl. Genet.* 114, 1059–1070. doi: 10.1007/s00122-006-0499-4

Rácz, F., Hadi, G., Szõke, C., Záborszky, S., and Marton, C. L. (2007). Cold tolerance of seed from inbred maize lines sown at various sowing dates in different years. *Cereal Res. Commun.* 35, 697–700.

Rativa, A. G. S., Junior, A. T. A., Friedrich, D. S., Gastmann, R., Lamb, T. I., Silva, A. S., et al. (2020). Root responses of contrasting rice genotypes to low temperature stress. *J. Plant. Physiol.* 255:153307. doi: 10.1016/j.jplph.2020.153307

Revilla, P., Rodríguez, V. M., Ordás, A., Rincent, R., Charcosset, A., Giauffret, C., et al. (2016). Association mapping for cold tolerance in two large maize inbred panels. *BMC Plant Biol.* 16:127. doi: 10.1186/s12870-016-0816-2

Ribaudo, C. M., Cura, J. A., and Cantore, M. L. (2017). Activation of a calcium-dependent protein kinase involved in the *Azospirillum growth* promotion in rice. *World J. Microbiol. Biotechnol.* 33, 22–30. doi: 10.1007/s11274-016-2186-1

Robbins, N. E. II, and Dinneny, J. R. (2015). The divining root: moisture-driven responses of roots at the micro- and macro-scale. *J. Exp. Bot.* 66, 2145–2154. doi: 10.1093/jxb/eru496

Rodri'guez, V. M., Butroi'n, A., Rady, M. O. A., Soengas, P., and Revilla, P. (2014). Identification of quantitative trait loci involved in the response to cold stress in maize (*Zea mays* L.). *Mol. Breed* 33, 363–371.

Shi, Y., Li, G. H., Tian, Z. Q., Wang, Z. Y., Wang, X. B., Zhu, Y. G., et al. (2016). Genetic dissection of seed vigour traits in maize (*Zea mays* L.) under low-temperature conditions. *J. Genet.* 95, 1017–1022. doi: 10.1007/s12041-016-0714-2

Song, W. B., Wang, B. B., Hauck, A. L., Dong, X. M., Li, J. P., and Lai, J. S. (2016). Genetic dissection of maize seedling root system architecture traits using an ultra-high density bin-map and a recombinant inbred line population. *J. Integr. Plant Biol.* 58, 266–279. doi: 10.1111/jipb.12452

Su, C. H., Wang, W., Gong, S. L., Zuo, J. H., Li, S. J., and Xu, S. Z. (2017). High density linkage map construction and mapping of yield trait QTLs in maize (*Zea mays*) using the genotyping-by-sequencing (GBS) technology. *Front Plant. Sci.* 8:706. doi: 10.3389/fpls.2017.00706

Szalai, G., Majláth, I., Pál, M., Gondor, O. K., Rudnóy, S., Oláh, C., et al. (2018). Janus-Faced nature of light in the cold acclimation processes of maize. *Front. Plant Sci.* 9:850. doi: 10.3389/fpls.2018.00850

Tan, Q. K., and Irish, V. F. (2006). The *Arabidopsis* zinc finger-homeodomain genes encode proteins with unique biochemical properties that are coordinately expressed during floral development. *Plant Physiol.* 140, 1095–1108. doi: 10.1104/pp.105.070565

Taniguchi, M., Taniguchi, Y., Kawasaki, M., Takeda, S., Kato, T., Sato, S., et al. (2002). Identifying and characterizing plastidic 2-Oxoglutarate/Malate and dicarboxylate transporters in *Arabidopsis thaliana*. *Plant Cell Physiol.* 43, 706–717. doi: 10.1093/pcp/pcf109

Taylor, N. L., Howell, K. A., Heazlewood, J. L., Tan, T. Y., Narsai, R., Huang, S., et al. (2010). Analysis of the rice mitochondrial carrier family reveals anaerobic accumulation of a basic amino acid carrier involved in arginine metabolism during seed germination. *Plant Physiol.* 154, 691–704. doi: 10.1104/pp.110.162214

Tsugama, D., Fujino, K., Liu, S., and Takano, T. (2020). A GDSL-type esterase/lipase gene, GELP77, is necessary for pollen dissociation and fertility in *Arabidopsis*. *Biochem. Biophys. Res. Commun.* 526, 1036–1041. doi: 10.1016/j.bbrc.2020.03.179

Verheul, M. J., Picatto, C., and Stamp, P. (1996). Growth and development of maize (*Zea mays* L.) seedlings under chilling conditions in the field. *Eur. J. Agron.* 5, 31–43.

Wang, B. B., Liu, H., Liu, Z. P., Dong, X. M., Guo, J. J., Li, W., et al. (2018a). Identification of minor effect QTLs for plant architecture related traits using super high density genotyping and large recombinant inbred population in maize (*Zea mays*). *BMC Plant Biol.* 18:17. doi: 10.1186/s12870-018-1233-5

Wang, J. J., Xu, Z. N., Yang, J., Lu, X. H., Zhou, Z. Q., Zhang, C. S., et al. (2018b). qNCLB7.02, a novel QTL for resistance to northern corn leaf blight in maize. *Mol. Breed.* 38, 54–65.

Wang, Y. F., Zhang, X. G., Shi, X., Sun, C. R., Jin, J., Tian, R. M., et al. (2018c). Heterotic loci identified for maize kernel traits in two chromosome segment substitution line test populations. *Sci. Rep.* 8, 11101–11115. doi: 10.1038/s41598-018-29338-1

Wang, L., Guo, C. K., Ren, D., and Ma, H. (2017). Molecular evolution and expression analysis of the osmip1 response to abiotic stress. *Chinese Bull. Botany* 52, 43–53.

Wang, X., Ding, Y. L., Li, Z. Y., Shi, Y. T., Wang, J. L., Hua, J., et al. (2019). PUB25 and PUB26 promote plant freezing tolerance by degrading the cold signaling negative regulator MYB15. *Dev. Cell.* 51, 222–235. doi: 10.1016/j.devcel.2019.08.008

Wang, X. Y., Shan, X. H., Xue, C. M., Wu, Y., Su, S. Z., Li, S. P., et al. (2016). Isolation and functional characterization of a cold responsive phosphatidylinositol transfer-associated protein, ZmSEC14p, from maize (*Zea may* L.). *Plant Cell Rep.* 35, 1671–1686. doi: 10.1007/s00299-016-1980-4

Weijers, D., Franke-van Dijk, M., Vencken, R. J., Quint, A., Hooykaas, P., and Offringa, R. (2001). An *Arabidopsis* Minute-like phenotype caused by a semi-dominant mutation in a RIBOSOMAL PROTEIN S5 gene. *Development* 128, 4289–4289. doi: 10.1242/dev.128.21.4289

Xue, F., Ji, W. Q., Wang, C. Y., Zhang, H., and Yang, B. J. (2012). High-density mapping and marker development for the powdery mildew resistance gene PmAS846 derived from wild emmer wheat (*Triticum turgidum* var. dicoccoides). *Theor. Appl. Genet.* 124, 1549–1560. doi: 10.1007/s00122-012-1809-7

Yang, J., Sun, K., Li, D., Luo, L., Liu, Y., Huang, M., et al. (2019). Identification of stable QTLs and candidate genes involved in anaerobic germination tolerance in rice via high-density genetic mapping and RNA-Seq. *BMC Genomics* 20:355. doi: 10.1186/s12864-019-5741-y

Yang, J., Zhang, T., Mao, H., Jin, H., Sun, Y., and Qi, Z. (2020). A Leymus chinensis histidine-rich Ca2+-binding protein binds Ca2+/Zn2+ and suppresses abscisic acid signaling in *Arabidopsis*. *J. Plant Physiol.* 252:153209. doi: 10.1016/j.jplph.2020.153209

Yao, X., Cai, Y., Yu, D., and Liang, G. (2018). bHLH104 confers tolerance to cadmium stress in *Arabidopsis thaliana*. *J. Integr. Plant Biol.* 60, 691–702. doi: 10.1111/jipb.12658

Ye, K. Y., Li, H., Ding, Y. L., Shi, Y. T., Song, C. P., Gong, Z. Z., et al. (2019). BRASSINOSTEROID-INSENSITIVE2 negatively regulates the stability of transcription factor ICE1 in response to cold stress in *Arabidopsis*. *Plant Cell* 31, 2682–2696.

Yun, J., Kim, Y. S., Jung, J. H., Seo, P. J., and Park, C. M. (2012). The AT-hook motif-containing protein AHL22 regulates flowering initiation by modifying FLOWERING LOCUS T chromatin in *Arabidopsis*. *J. Biol. Chem.* 287, 15307–15316. doi: 10.1074/jbc.M111.318477

Zhang, C. S., Zhou, Z. Q., Yong, H. J., Zhang, X. C., Hao, Z. F., Zhang, F. J., et al. (2017a). Analysis of the genetic architecture of maize ear and grain morphological traits by combined linkage and association mapping. *Theor. Appl. Genet.* 130, 1011–1029. doi: 10.1007/s00122-017-2867-7

Zhang, Z. Y., Li, J. J., Pan, Y. H., Li , J., Zhou, L., Shi , H., et al. (2017b). Natural variation in CTB4a enhances rice adaptation to cold habitats. *Nat. Commun.* 8:14788. doi: 10.1038/ncomms14788

Zhang, H., Zhang, J. Y., Xu, Q. Y., Wang, D. D., Di, H., Huang, J., et al. (2020). Identification of candidate tolerance genes to low-temperature during maize germination by GWAS and RNA-seq approaches. *BMC Plant Biol.* 20:333. doi: 10.1186/s12870-020-02543-9

Zhao, H., Ma, B., Duan, K. X., Li, X. K., Lu, X., Yin, C. C., et al. (2020). The GDSL lipase MHZ11 modulates ethylene signaling in rice roots. *Plant Cell* 32, 1626–1643.

Zhao, Q., Xiang, X., Liu, D., Yang, A., and Wang, Y. (2018). Tobacco transcription factor NtbHLH123 confers tolerance to cold stress by regulating the NtCBF pathway and reactive oxygen species homeostasis. *Front. Plant Sci.* 9:381. doi: 10.3389/fpls.2018.00381

Zheng, T., Dai, L., Liu, Y., Li, S., Zheng, M., Zhao, Z., et al. (2021). Overexpression populus d-Type cyclin gene PsnCYCD1;1 influences cell division and produces curved leaf in *Arabidopsis thaliana*. *Int. J. Mol. Sci.* 22, 5837–5850. doi: 10.3390/ijms22115837

Zhou, L., Liu, Z., Liu, Y., Kong, D., Li, T., Yu, S., et al. (2016). A novel gene OsAHL1 improves both drought avoidance and drought tolerance in rice. *Sci. Rep.* 6:30264. doi: 10.1038/srep30264

Zhou, Z. Q., Zhang, C. S., Zhou, Y., Hao, Z. F., Wang, Z. H., Zeng, X., et al. (2016). Genetic dissection of maize plant architecture with an ultra-high density bin map based on recombinant inbred lines. *BMC Genomics* 17:178. doi: 10.1186/s12864-016-2555-z

Zhu, J., Zhang, K. X., Wang, W. S., Gong, W., Liu, W. C., Chen, H. G., et al. (2015). Low temperature inhibits root growth by reducing auxin accumulation via ARR1/12. *Plant Cell Physiol.* 56, 727–736. doi: 10.1093/pcp/pcu217

Zou, W., Li, G., Jian, L., Qian, J., Liu, Y., and Zhao, J. (2021). Arabidopsis SMC6A and SMC6B have redundant function in seed and gametophyte development. *J. Exp. Bot.* 72, 4871–4887. doi: 10.1093/jxb/erab181

Zouhar, J., and Sauer, M. (2014). Helping hands for budding prospects: ENTH/ANTH/VHS accessory proteins in endocytosis, vacuolar transport, and secretion. *Plant Cell* 26, 4232–4244. doi: 10.1105/tpc.114.131680

frontiers | Frontiers in Plant Science

TYPE Mini Review
PUBLISHED 20 September 2022
DOI 10.3389/fpls.2022.952146

OPEN ACCESS

EDITED BY
Rogelio Santiago Carabelos,
Spanish National Research Council (CSIC), Spain

REVIEWED BY
Amit Kumar Mishra,
Mizoram University, India
Aykut Saglam,
Karadeniz Technical University, Turkey
Iqbal Hussain,
Government College University, Faisalabad, Pakistan

*CORRESPONDENCE
Laura Serna
laura.serna@uclm.es

SPECIALTY SECTION
This article was submitted to Plant Physiology, a section of the journal Frontiers in Plant Science

RECEIVED 24 May 2022
ACCEPTED 29 August 2022
PUBLISHED 20 September 2022

CITATION
Serna L (2022) Maize stomatal responses against the climate change. *Front. Plant Sci.* 13:952146. doi: 10.3389/fpls.2022.952146

Maize stomatal responses against the climate change

Laura Serna*

Facultad de Ciencias Ambientales y Bioquímica, Universidad de Castilla-La Mancha, Toledo, Spain

Drought and heat, in the context of climate change, are expected to increase in many agricultural areas across the globe. Among current abiotic stresses, they are the most limiting factors that influence crop growth and productivity. Maize is one of most widely produced crops of the world, being the first in grain production with a yield that exceeded 1.1 billion tons in 2021. Despite its wide distribution in semi-arid regions, it is highly vulnerable to climate change, which triggers important losses in its productivity. This article explores how maize yield may persevere through climate change by focusing on the stomatal regulation of gas exchange. The emerging picture unravels that maize copes with drought stress by reducing stomatal size and stomatal pore area, and increasing stomatal density, which, in turn, reduces transpiration and photosynthetic rate. When drought and heat co-occur, heat enhances stomatal response to drought stress. To avoid plant heat damage, the decline in stomatal aperture could trigger the expansion of the distance of action, from the longitudinal leaf veins, of ZmSHR1, which might act to positively regulate ZmSPCHs/ZmICE1 heterodimers, increasing the stomatal density. Only when drought is not very severe, elevated CO_2 levels reduce yield losses. The knowledge of the upcoming climate changes together with the prediction of the developmental and physiological stomatal responses will allow not only to anticipate maize yield in the next years, but also to contribute to the correct decision-making in the management of this important crop.

KEYWORDS

climate change, drought, heat, maize, productivity, stomata

Introduction

Drought and heat stresses are the major limiting factors for crops growth and productivity (Fahad et al., 2017; Gupta et al., 2020; Jaldhani et al., 2022), and they cause the greatest annual loss of crops (Lipiec et al., 2013; Ray et al., 2015; Gupta et al., 2020). Worryingly, climate change, resulting from increasing emissions of greenhouse gases, is threatening crops yield, and food security, through increased temperatures and alterations of rainfall patterns (IPCC, 2021). The changes in rainfall patterns, which agree with climate models (Räisänen, 2002; Kharin et al., 2007; Wetherald, 2010; Fischer et al., 2013), are decreasing the frequency of the storms and increasing their intensity in many regions of the planet (Räisänen, 2002; Kharin et al., 2007; IPCC, 2013).

This substitution of evenly distributed rainfall for an increased precipitation variability increases the risk of drought due to loss of water through runoff. Elevated temperatures also contribute to inducing drought because the rapid water loss from plant tissues and soil surface, and when they are too elevated can induce direct damage on crops (Wahid et al., 2007). Drought and heat stresses, both individually and in combination, have a deep impact on the agricultural sector, which, unfortunately, translates into a strong threat to food security.

One of the world's most widely produced crops is maize, being the first in grain production with a production that exceeded 1.1 billion tons in 2021 (FAS, USDA, 2022). It belongs to the grass family *Poaceae*, which includes more than 10,000 species (Kellogg, 1998), with other important crops such as wheat (*Triticum aestivum*), rice (*Oryza sativa*), or barley (*Hordeum vulgare*). Maize was domesticated from teosinte (*Zea mays* ssp. *Parviglumis*), at the tropical Balsas River valley in Mexico (Matsuoka et al., 2002; van Heerwaarden et al., 2011), and continued to spread north and south across the Americas (Matsuoka et al., 2002). Currently, it is cultivated across a wider area than any other major crop, being the United States, China, and Brazil the top producers (FAO, 2021; **Figure 1A**). Besides its primary use for food, it can also be processed into a variety of industrial products, including glue, industrial alcohol, and fuel ethanol (Ranum et al., 2014). Sixty one percent of global maize production is used as livestock feed and 13% for human consumption (OECD/FAO, 2021; **Figure 1B**). Despite the low percentage used directly for human consumption, it is an essential element of the diet of millions of people in Sub-Saharan Africa, where its use is expected to increase because the rapid growth of its population (OECD/FAO, 2021).

Despite its adaptation to a wide array of agro-ecologies, which explains its wide distribution, maize is highly vulnerable to climate change. It is cultivated in semi-arid environments, facing drought, heat, and combinations of these factors (Cairns et al., 2012; Zhao et al., 2016). Rojas et al. (2019), for example, by analyzing both the annual mean precipitation and specific growing seasons and areas found that reduced precipitation will impact, before 2040, maize production in southern Africa and Europe. Considering that the variability of precipitation is an essential factor because water availability during a given stage of plant developmental influences plant production at later stages of the life cycle (Brouwer and Heibloem, 1986; Kranz et al., 2008; Al-Kaisi and Broner, 2009; Hashim et al., 2012; Halubok and Yang, 2020), it is likely that more regions of the globe with maize crops will be concerned. In addition, in the context of climate change, not only changes in rainfall patterns affect maize growth, but also increases in temperature. Certainly, it is known that temperatures above 35°C negatively impact the vegetative and reproductive growth of maize, from germination to grain filling (Hatfield et al., 2011). The Russian invasion of Ukraine will also affect maize production, with a decline of Ukraine maize production for 2022/2023 of 54% relative to last year (FAS, USDA, 2022). Moreover, the impact of climate change on maize will be more pronounced considering that global population is predicted to rise, in the least drastic scenario, from 7.7 billion currently to 9,7 billion in 2050 (Adam, 2021). The greatest climatic impact, in addition, falls on South Africa (SADC, 2016; Rojas et al., 2019), where maize is an essential element of the diet of its population (SADC, 2016; OECD/FAO, 2021), and where, together with other regions in Southern Africa, the persistent socioeconomic vulnerability enhances the negative impact of climate change (Leichenko and O'Brien, 2002; Niang et al., 2015).

This article explores the consequences of climate change on both maize productivity and stomatal development (stomatal density and stomatal size) and function. Drought, through alterations in the stomatal development and function, reduces both transpiration and photosynthetic rate (Zhao et al., 2015; Hussain et al., 2019). When drought and heat co-occur, plants experience a reduction in transpiration rate, photosynthetic rate, and biomass accumulation, which are more severe than those induced by drought stress individually (Hussain et al., 2019). In addition, the alterations in stomatal function are physiologically buffered, to avoid plant heat damage, with changes in the stomatal density possibly induced by the expansion of the distance of action, from the longitudinal leaf veins, of ZmSHR1. Given that crop yields must improve despite the potentially negative consequences of increasing temperatures and changing precipitation patterns, this stomatal response to climate change alerts about the future of maize cultivation, and it demands a search for solutions to deal with the impact of climate change on its productivity. Even more so considering that only when drought is not very severe, maize benefits from increased CO_2 levels reducing yield losses (Webber et al., 2018). This mitigation of the drastic effects of drought is due to a reduction in stomatal transpiration, which improves water use efficiency, and consequently, the water content of the soil (Long et al., 2004; Leakey et al., 2006, 2009; Ghannoum, 2009; Manderscheid et al., 2014).

Effects of drought and heat on maize crop productivity

Although there are other factors that affect maize production, drought and heat are, without a doubt, two of the most important. Certainly, there are several works that show the relevance of these factors on maize yield in distinct parts of the world (**Table 1**). Maitah et al. (2021), for example, demonstrated the influence of precipitation, from 2002 to 2019, on maize yield in the Czechia. They found that both total yield and yield rate increased from 1961 to 2010, but they dropped after 2010, just when precipitation also decreased. After 2010, there was also a trend of increasing temperature that correlates with a decrease in total yield and yield rate

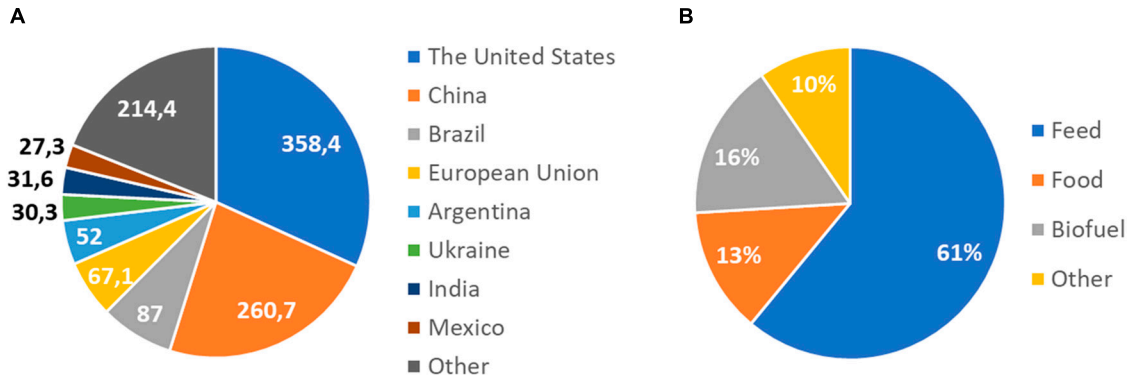

FIGURE 1
World maize production and uses. **(A)** Maize production by country in 2020/2021. The United States, China, and Brazil are the top producers. Production is expressed in million metric tons. Data source: USDA, Foreign Agricultural Service, Global Market Analysis. **(B)** Global uses of maize in 2021. Maize is used as food and animal feed, and as a source of biofuel. It can also be processed into a wide range of useful chemicals. Data source: OECD/FAO, 2021; forecast.

(Maitah et al., 2021). Data from more than 20,000 historical maize trials in Africa, from 1999 to 2007, combined with daily temperature and precipitation data, showed that each additional degree day above 30°C reduced the final yield by 1% under optimal rainfed conditions, and by 1.7% under drought ones (Lobell et al., 2011). This is telling us that the ability of maize to cope with rising temperatures depends on the availability of water. Certainly, plant cooling takes place through transpiration (Curtis, 1936), which needs soil moisture. Outside Europe and Africa, specifically in Khyber Pakhtunkhwa (Pakistan), an analysis of maize yield between years 1996 and 2015 also showed that precipitation has a positive effect in maize productivity, while elevated temperatures have a deleterious impact (Khan et al., 2019). In the United States, maize yield losses, from 1959 to 2004, were due to increased evaporative demand and subsequent water supply depletion, which was induced by high temperatures (Lobell et al., 2013). Together, this suggests that, at least up to a certain temperature, drought, induced by a deficiency of precipitation or elevated temperatures, causes a decrease in maize productivity.

Estimations of the effect of drought and heat on maize yield in various regions of the world, from mid- to late-21st century, have been also realized (**Table 1**). In Europe, climate change by 2050 will reduce maize yield by 20% (Webber et al., 2018). In addition, drought stress versus heat stress is the main driver of losses for maize yield, even in low-yielding years (Webber et al., 2018). In agreement with modeling analysis (Schauberger et al., 2017), elevated CO_2 concentration will be able to mitigate such losses only when drought is not too severe (Webber et al., 2018). It is also expected a drop of 10.1% in maize yield toward the middle of the century in Turkey, and it is associated to drought and/or heat stress (Dellal et al., 2011). In sub-Saharan Africa, maize yield was estimated for two 10-year periods, 2056–2065 and 2081–2090, unraveling changes from $>+6$ to $<-33\%$ (Waha et al., 2013). The authors found that the importance of changes in temperature and precipitation in maize yield will depend on the study region. For example, in southern parts of Mozambique and Zambia, the Sahel and parts of eastern Africa, a reduction of the wet season precipitation will cause a decrease in maize yield, prevailing over the effect of increased temperatures (Waha et al., 2013). Although, as the authors suggested, the model may have underestimated the damage that elevated temperatures will produce. Projections of changes in precipitation and temperature in the United States showed that maize yield, by 2050 and relative to 2013–2017 period, will reduce by 39–68% depending on the climate scenario (Yu et al., 2021). When the authors incorporated to the model the estimated effects of climate-neutral technological advances, the net change in yield ranged from (−)13 to 62%, questioning, interestingly, the usefulness of scientific efforts in adapting crops to extreme conditions of heat and drought (Yu et al., 2021). Considering the total maize production in the world, twenty-first-century projections using state-of-the-art climate and crop model suites, but excluding changing farming practices, and adaptations such as breeding hardier crop varieties, suggest that mean maize productivity, at the end-of-century, will shift from +5 to −6% (SSP126) and from +1 to −24% (SSP585) (Jägermeyr et al., 2021).

Despite some models omit CO_2 fertilization effect (Dellal et al., 2011; Waha et al., 2013), which alleviates yield losses when drought is not too intense (Webber et al., 2018), drought and heat are reducing, and will continue to do so, maize yield in many regions of the world. The intensity of this effect depends not only on the genotypes, but also on environmental conditions and, therefore, on time and location of these crops. The inclusion in the models of changing farming practices, adaptations such as breeding hardier crop varieties and economic incentives is essential to anticipate the effect of

TABLE 1 Observations and estimations of maize yield and drivers of its change.

Region	Period	Drivers of yield changes and effect on yield	References
Czechia	2002–2019	Decrease in precipitation and increase in temperature decreased from 7.73 t/ha (2001–2010) to 7.67 (2011–2019) maize yield, even considering technological and management improvement in production	Maitah et al., 2021
Africa	1999–2007	Each additional degree day spend above 30°C, changed the final yield by −1% under optimal rainfed conditions, and by −1.7% under drought ones	Lobell et al., 2011
Khyber Pakhtunkhwa	1996–2015	Increase in precipitation increased maize yield, and increase in temperature decreased maize yield	Khan et al., 2019
The United States	1959–2004	Increase in evaporative demand induced by elevated temperatures decreased maize yield	Lobell et al., 2013
Europe	2050	Drought will change maize yield −20%	Webber et al., 2018
Turkey	2050	Drought and heat will change maize yield −10.1%	Dellal et al., 2011
Sub-Saharan Africa	2056–2065 and 2081–2090	Drought or heat, depending on space, will change maize yield from >+6 to <−33%	Waha et al., 2013
The United States	2050	Drought or heat, depending on the climate scenario, will change maize yield from −39 to −68% (relative to 2013–2017). And from −13 to +62% (relative to 2013–2017), incorporating to the model the estimated effects of climate-neutral technological advances	Yu et al., 2021
World	End-of-century	Climate change will change maize yield from +5 to −6% (SSP126) and from +1 to −24% (SSP585), excluding changing farming practices and maize adaptations	Jägermeyr et al., 2021

climate change on maize crop yield and to design strategies for its mitigation. Because in the next 50 years climate extreme events will alternate with normal ones (IPCC, 2021), and varieties adapted only to extreme events reduce their yield (Yu et al., 2021), there is an urgent need not to make varieties more resilient to extreme drought and heat, but to adapt these varieties to a wide variety of conditions.

Maize stomatal response to drought and heat stresses

Plants have developed multiple responses at the developmental, physiological, and molecular levels that enable them to escape, avoid, and/or tolerate unfavorable environmental conditions (Gupta et al., 2020; Chávez-Arias et al., 2021). Avoidance of drought and/or heat stress damage includes changes in stomatal number and/or function (Gupta et al., 2020; Chávez-Arias et al., 2021). Stomatal pores open to absorb CO_2 for photosynthesis, and close to prevent water loss through transpiration (Blatt et al., 2017). It is widely known that drought stress induces stomatal closure reducing water loss (Taiz and Zeiger, 2006). However, in some regions of the world, maize not only faces low water availability, but also elevated temperatures (Hu et al., 2015; Zhao et al., 2016). For a century, it has been known that transpiration reduces leaf temperature (Curtis, 1936). Therefore, stomatal closure to prevent transpiration, also triggers leaf heating. But how does maize solve the dilemma of avoiding water loss and, at the same time, heating the leaves when growing under both drought and high temperatures?

Specifically in maize, with the typical grass stomata consisting of two dumbbell-shaped guard cells (Stebbins and Shah, 1960; Serna, 2011), severe water deficit (40–50% field capacity) leads to a decrease in the size and opening of the stomata and an increase in stomatal density (Zhao et al., 2015; **Figure 2A**). The latter is possibly associated with the need for cooling through transpiration. Anyway, this stomatal response to drought negatively impacts stomatal conductance, photosynthetic rate and transpiration (Zhao et al., 2015; Hussain et al., 2019). The reduction in the stomatal size has an important advantage because it increases the speed of stomatal movement (Aasamaa et al., 2001; Hetherington and Woodward, 2003), resulting in a decrease in water loss by transpiration. But it also implies a reduction in the assimilation of photosynthetic CO_2, and in the yield of the

plant. Nonetheless, the negative correlation between stomatal density and transpiration rate in maize is stronger than that with photosynthetic rate, indicating that leaf water use efficiency tends to increase (Zhao et al., 2015). As expected, when the temperature increases, the stomatal aperture area does too, which increases the stomatal conductance and the rate of transpiration (Zheng et al., 2013), avoiding the heating of the leaves. Hussain et al. (2019) also found that heat stress (38°C for 15 days) increases the rate of transpiration, but it decreases the photosynthetic rate (these changes were not statistically significant). This decrease in photosynthetic rate is obviously due to non-stomatal limitations, such as alterations in electron transport capacity and activity (Way and Oren, 2010; Zafar et al., 2018). Certainly, exceeding 35°C degrades maize chlorophyll (Hatfield et al., 2011; Hussain et al., 2019), and compromises protein activity with strong impact on carbon assimilation (Chaves et al., 2016). However, the combination of heat and drought generates a reduction in stomatal conductance, transpiration rate, photosynthetic rate, biomass accumulation and, ultimately, yield, with these reductions being more severe than those induced only under drought stress (Hussain et al., 2019). Therefore, heat enhances the stomatal response to drought, possibly associated with a reduction in stomatal pore area accompanied by an increase in stomatal density, which in turn reduces transpiration, but it also increases leaf temperature (**Figure 2A**). This reduction in transpiration associated with high water use efficiency has costs in terms of lower rates of CO_2 assimilation and reduced yield, possibly through a direct decrease in CO_2 uptake, and an increase in leaf temperature that negatively impacts protein activity. Taking theses stomatal responses into account, it is likely that the increased frequency of extreme events induced by climate change, such as heat waves, will exacerbate maize yield loss.

Only under certain drought conditions, maize benefits from elevated CO_2 levels

Climate change includes not only rising temperatures, changes in precipitation patterns and increasing frequency of extreme weather events, but also increased atmospheric concentrations of CO_2. In maize, heat enhances the stomatal response to drought, decreasing water loss through transpiration (Hussain et al., 2019). This protective response to drought has costs in terms of lower CO_2 assimilation, which is manifested by a decrease in the photosynthetic rate and, by extension, in the accumulation of biomass (Hussain et al., 2019). Will maize benefit from increased CO_2 levels, avoiding a decline in growth and yield, when water is scarce, and temperatures rise?

Increased atmospheric concentrations of CO_2 stimulate photosynthesis and yield of C3 species (Long et al., 2004; Leakey et al., 2009; Kimball, 2016). However, C4 species concentrate CO_2 at the site of Rubisco, and the enzyme is saturated with the current CO_2 levels (Furbank et al., 1989; Jenkins et al., 1989; von Caemmerer and Furbank, 2003; Ghannoum, 2009). Therefore, the increase of CO_2 concentration should not induce any effect on the photosynthetic rate of these plant species. Agree with this, several works have shown the insensitivity of C4 species, including maize (Leakey et al., 2006; Markelz et al., 2011; Manderscheid et al., 2014; Ruiz-Vera et al., 2015), to increases in CO_2 levels under sufficient water supply (Leakey et al., 2009; Kimball, 2016), and except for one paper showing that maize benefits from CO_2 enrichment (Driscoll et al., 2006). However, while the effects of increased temperature on photosynthesis and growth of well-watered maize plants remain unchanged at elevated CO_2 levels compared to current ones (Kim et al., 2007), when water becomes limiting, increased levels of atmospheric CO_2 levels improve their photosynthesis and growth (Leakey et al., 2006; Markelz et al., 2011; Manderscheid et al., 2014). However, and according to model analysis (Schauberger et al., 2017), CO_2 levels can alleviate the negative impact of drought only when it is not too severe (Webber et al., 2018).

In C4 species, the alleviation of the negative effects of drought under elevated CO_2 levels is due to a reduction in stomatal transpiration, improving water use efficiency and, consequently, the water content of the soil (Long et al., 2004; Leakey et al., 2006, 2009; Ghannoum, 2009; Manderscheid et al., 2014). However, this reduction in transpiration, on the other hand, increases leaf temperature (Curtis, 1936; Kimball et al., 1999; Gray et al., 2016), which may intensify heat stress, impacting maize yield (Ruiz-Vera et al., 2015). Therefore, maize may benefit from increased CO_2 levels only when the drought is not too severe, and temperatures do not reach very extreme values.

Possible molecular mechanism of maize stomatal development in response to climate change

Changes in stomatal density can greatly impact a plant's water use efficiency and, consequently, drought tolerance. Grasses develop their stomata in rows positioned at the flanks of underlying longitudinal leaf veins (Stebbins and Shah, 1960). This position of stomatal files may result from an inhibitory signal transmitted from the vein to overlying epidermal cells and/or from an inductive signal transmitted to epidermal cells at a specific distance from the vein (Hernandez et al., 1999). One such candidate for

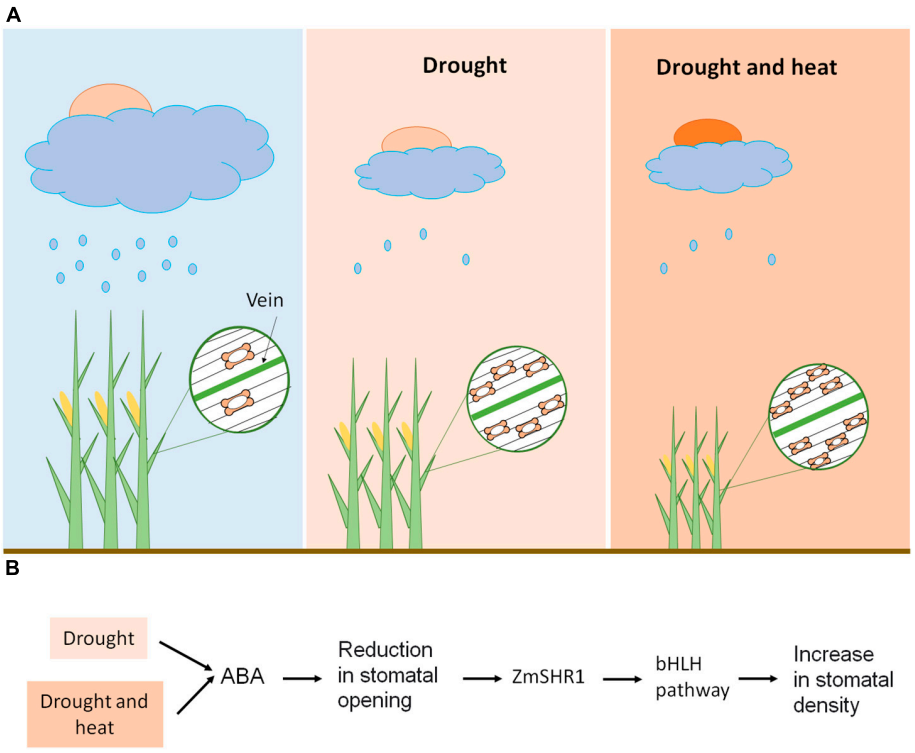

FIGURE 2
Maize stomatal response to climate change. **(A)** Heat enhances the maize stomatal responses to drought stress. Drought reduces stomatal size and opening, and increases stomatal density, which, in turn, reduces transpiration and photosynthetic rate. When drought and heat coexist, plants experience a reduction in transpiration rate and photosynthetic rate, possibly related to a reduction in stomatal size and opening, accompanied by an increase in stomatal density. This triggers a reduction in biomass accumulation, which is more severe than that induced by drought stress. **(B)** Possible molecular mechanisms of stomatal response to climate change. Drought stress, individually or in combination with high temperatures, reduces stomatal opening by increasing abscisic acid (ABA) levels. This stomatal response could trigger the increase of the distance of action of ZmSHR1 from the longitudinal leaf veins. ZmSHR1 might act to positively regulate ZmSPCHs/ZmICE1 heterodimers, increasing the number of stomatal files and, consequently, the stomatal density.

this inductive signal is *ZmSHR1*, since transgenic rice lines expressing this gene in an expanded domain, compared to the vascular-specific expression domain of its orthologous *OsSHR2* gene, produce supernumerary stomatal files between veins (Schuler et al., 2018).

In *Arabidopsis*, entry into stomatal lineage is controlled by the basic helix-loop-helix (bHLH) protein SPEECHLESS (AtSPCH) and its more distantly related bHLH heterodimer partners INDUCER OF CBF EXPRESSION1 (AtICE1) and SCREAM2 (AtSCRM2) (MacAlister et al., 2007; Kanaoka et al., 2008). Proteins encoded by the duplicated *SPCH* homologs in *Brachypodium*, BdSPCH1 and BdSPCH2, also redundantly control stomatal lineage initiation, with loss-of-function of both *BdSPCH1/2* (*bdspch1 bdspch2*) triggering a stomata-less phenotype, and gain-of-function by overexpression of *BdSPCH2* inducing ectopic stomatal development in new cell files (Raissig et al., 2016). In addition, *BdICE1*, but not *BdSCRM2*, drives stomatal lineage initiation (Raissig et al., 2016). This suggests that BdSPCHs/BdICE1 heterodimers regulate entry into the stomatal lineage. In maize, there are three copies of *SPCH*-like genes and one copy of *ICE1/AtSCRM2*-like genes (McKown and Bergmann, 2020), suggesting that stomatal initiation is also controlled by ZmSPCHs/ZmICE1 heterodimers.

ZmSHR1, through an unknown mechanism, might act to positively regulate these ZmSPCHs/ZmICE1 heterodimers in epidermal files that flank leaf veins and, thus, to promote stomatal initiation (**Figure 2B**). Thus, drought stress, by increasing abscisic acid (ABA) levels, reduces stomatal opening (Munemasa et al., 2015; Zhao et al., 2015), which, to avoid plant heat damage, could increase the number of stomatal files and, consequently, the stomatal density, by expanding the expression domain of *ZmSHR1* (**Figure 2B**). Drought could also decrease the stomatal distance within epidermal files, but the molecular mechanism behind this regulation is unknown. Under adequate water supply, *ZmSHR1* expression in expanded domains by genetic manipulation would produce supernumerary stomatal rows between veins and, consequently, increased stomatal density. This would reduce excess heat by

increasing transpiration and would, possibly, improve maize yield.

Future considerations

Climate change is increasing the frequency of extreme events such as heat waves (IPCC, 2021). The heat is intensifying the effect of the drought in maize by decreasing gaseous exchange through the production of smaller stomata and reducing their opening (Zhao et al., 2015; Hussain et al., 2019). Since photosynthesis is saturated at current CO_2 levels in C4 species (Kimball, 2016), this response could be beneficial in mitigating hydraulic demand. However, decreased transpiration will increase leaf temperature, which will cause damage to plants in specific locations of the planet. Under this climatic context, the combination of plant breeding and agronomic management is required to avoid yield losses. Under adequate water supply, targeted genetic manipulation through the production of genotypes characterized by an increase in stomatal size and/or density could regulate leaf temperature by increasing transpiration, thus preventing tissue damage. However, under water restrictions, close monitoring of plant temperature could prevent tissue damage caused by, for example, heat waves, through timely irrigation. Earlier sowing could also help rainfed maize adapt to climate change in some regions with higher water demand in warmer periods. Even more if we consider that the greatest yield losses occur when drought stress prevails in the pre-tasseling stage (Anjum et al., 2017), and high temperatures near the anthesis stage (Gabaldón-Leal et al., 2016). In any case, adaptation strategies must be local, and they must consider both agronomic management and well-adapted genotypes.

Since varieties adapted only to extreme drought and/or heat reduce their yield (Yu et al., 2021), selection or production of varieties more resilient to extreme events, but also adapted to a wide variety of conditions, is essential to avoid yield losses. To achieve this, genetic modifications aimed at modifying stomatal density and/or opening could be combined with those aimed at modifying enzymes that regulate the photosynthetic process. For example, as Pignon and Long (2020) suggested, maize mutants with reduced carbonic anhydrase activity could be combined with transgenic maize overexpressing Rubisco to improve photosynthesis and water use efficiency under elevated CO_2 levels. In addition, the combination of modifications in these characters with others that are not related to the stomatal response could improve the adaptation of maize to climate change.

Author contributions

The author confirms being the sole contributor of this work and has approved it for publication.

Acknowledgments

The author is grateful to Lee Robertson of INIA for his constructive comments, which greatly helped to improve the manuscript. The author also acknowledges support by the Castilla-La Mancha University.

Conflict of interest

The author declares that the research was conducted in the absence of any commercial or financial relationships that could be construed as a potential conflict of interest.

Publisher's note

All claims expressed in this article are solely those of the author and do not necessarily represent those of her affiliated organization, or those of the publisher, the editors and the reviewers. Any product that may be evaluated in this article, or claim that may be made by its manufacturer, is not guaranteed or endorsed by the publisher.

References

Aasamaa, K., Sober, A., and Rahi, M. (2001). Leaf anatomical characteristics associated with shoot hydraulic conductance, stomatal conductance and stomatal sensitivity to changes of leaf water status in temperate deciduous trees. *Aust. J. Plant Physiol.* 28, 765–774. doi: 10.1071/PP00157

Adam, D. (2021). How far will global population rise? Researchers can't agree. *Nature* 597, 462–465. doi: 10.1038/d41586-021-02522-6

Al-Kaisi, M. M., and Broner, I. (2009). *Crop water use and growth stages*. Fort Collins, CO: Colorado State University Extension.

Anjum, S. A., Ashraf, U., Tanveer, M., Khan, I., Hussain, S., Shahzad, B., et al. (2017). Drought induced changes in growth, osmolyte accumulation and antioxidant metabolism of three maize hybrids. *Front. Plant Sci.* 8:69. doi: 10.3389/fpls.2017.00069

Blatt, M. R., Brodribb, T. J., and Torii, K. U. (2017). Small pores with a big impact. *Plant Physiol.* 174, 467–469. doi: 10.1104/pp.17.00642

Brouwer, C., and Heibloem, M. (1986). *Irrigation water management: Irrigation water needs*. Rome: Food and Agriculture Organization.

Cairns, J. E., Sonder, K., Zaidi, P. H., Verhulst, N., Mahuku, G., Babu, R., et al. (2012). Maize production in a changing climate: Impacts, adaptation, and mitigation strategies. *Adv. Agron.* 114, 1–58. doi: 10.1016/B978-0-12-394275-3.00006-7

Chaves, M. M., Costa, J. M., Zarrouk, O., Pinheiro, C., Lopes, C. M., and Pereira, J. S. (2016). Controlling stomatal aperture in semi-arid regions – The dilemma of saving water or being cool? *Plant Sci.* 251, 54–64. doi: 10.1016/j.plantsci.2016.06.015

Chávez-Arias, C. C., Ligarreto-Moreno, G. A., Ramírez-Godoy, A., and Restrepo-Díaz, H. (2021). Maize responses challenged by drought, elevated daytime temperature and arthropod herbivory stresses: A physiological, biochemical and molecular view. *Front. Plant Sci.* 12:702841. doi: 10.3389/fpls.2021.702841

Curtis, O. F. (1936). Transpiration and the cooling of leaves. *Am. J. Bot.* 23, 7–10. doi: 10.2307/2436384

Dellal, D., McCarl, B. A., and Butt, T. (2011). The economic assessment of climate change on Turkish agriculture. *J. Environ. Prot. Ecol.* 12, 376–385.

Driscoll, S. P., Prins, A., Olmos, E., Kunert, K. J., and Foyer, C. H. (2006). Specification of adaxial and abaxial stomata, epidermal structure and photosynthesis to CO2 enrichment in maize leaves. *J. Exp. Bot.* 57, 381–390. doi: 10.1093/jxb/erj030

Fahad, S., Bajwa, A. A., Nazir, U., Anjum, S. A., Farooq, A., Zohaib, A., et al. (2017). Crop production under drought and heat stress: Plant responses and management options. *Front. Plant. Sci.* 8:1147. doi: 10.3389/fpls.2017.01147

FAO (2021). *Biannual report on global food markets*. Rome: Food Outlook. doi: 10.4060/cb7491

Fischer, E. M., Beyerle, U., and Knutti, R. (2013). Robust spatially aggregated projections of climate extremes. *Nat. Clim. Change* 3, 1033–1038. doi: 10.1038/nclimate2051

Furbank, R. T., Jenkins, C. L., and Hatch, M. D. (1989). CO2 concentrating mechanism of C4 photosynthesis: Permeability of isolated bundle sheath cells to inorganic carbon. *Plant Physiol.* 91, 1364–1371. doi: 10.1104/pp.91.4.1364

Gabaldón-Leal, C., Webber, H., Otegui, M. E., Slafer, G. A., Ordóñez, R. A., Gaiser, T., et al. (2016). Modelling the impact of heat stress on maize yield formation. *Field Crops Res.* 198, 226–237. doi: 10.1016/j.fcr.2016.08.013

Ghannoum, O. (2009). C4 photosynthesis and water stress. *Ann. Bot.* 103, 635–644. mcn093 doi: 10.1093/aob/

Gray, S., Dermody, O., Klein, S., Locke, A. M., McGrath, J. M., Paul, R. E., et al. (2016). Intensifying drought eliminates the expected benefits of elevated carbon dioxide for soybean. *Nat. Plants* 2:16132. doi: 10.1038/nplants.2016.132

Gupta, A., Rico-Medina, A., and Caño-Delgado, A. I. (2020). The physiology of plant responses to drought. *Science* 368, 266–269. doi: 10.1126/science.aaz7614

Halubok, M., and Yang, Z.-L. (2020). Estimating crop and grass productivity over the United States using satellite solar-induced chlorophyll fluorescence, precipitation and soil moisture data. *Remote Sens.* 12:3434. doi: 10.3390/rs12203434

Hashim, M., Siam, N., Al-Dosari, A., Asl-Gaadi, K., Patil, V., Tola, E., et al. (2012). Determination of water requirement and crop water productivity of crops grown in the Makkah region of Saudi Arabia. *Aust. J. Basic Appl. Sci.* 6, 196–206.

Hatfield, J. L., Boote, K. J., Kimball, B. A., Ziska, L. H., Izaurralde, R. C., Ort, D., et al. (2011). Climate impacts on agriculture: Implications for crop production. *Agron. J.* 103, 351–370. doi: 10.2134/agronj2010.0303

Hernandez, M. L., Passas, H. J., and Smith, L. G. (1999). Clonal analysis of epidermal patterning during maize leaf development. *Dev. Biol.* 216, 646–658. doi: 10.1006/dbio.1999.9429

Hetherington, A. M., and Woodward, F. I. (2003). The role of stomata in sensing and driving environmental change. *Nature* 424, 901–908. doi: 10.1038/nature01843

Hu, X., Wu, L., Zhao, F., Zhang, D., Li, N., Zhu, G., et al. (2015). Phosphoproteomic analysis of the response of maize leaves to drought, heat and their combination stress. *Front. Plant Sci.* 6:298. doi: 10.3389/fpls.2015.00298

Hussain, H. A., Men, S., Hussain, S., Chent, Y., Ali, S., Zhang, S., et al. (2019). Interactive effects of drought and heat stresses on morpho-physiological attributes, yield, nutrient uptake and oxidative status in maize hybrids. *Sci. Rep.* 9:3890. doi: 10.1038/s41598-019-40362-7

IPCC (2013). "Climate change 2013: The physical science basis," in *Contribution of working group I to the fifth assessment report of the intergovernmental panel on climate change*, eds T. F. Stocker, D. Qin, G.-K. Plattner, M. Tignor, S. K. Allen, J. Boschung, et al. (Cambridge: Cambridge University Press).

IPCC (2021). "Climate change 2021: The physical science basis," in *Contribution of working group I to the sixth assessment report of the intergovernmental panel on climate change*, eds V. Masson-Delmotte, P. Zhai, A. Pirani, S. L. Connors, C. Péan, S. Berger, et al. (Cambridge: Cambridge University Press).

Jägermeyr, J., Müller, C., Ruane, A. C., Elliott, J., Balkovic, J., Castillo, O., et al. (2021). Climate impacts on global agriculture emerge earlier in new generation of climate and crop models. *Nat. Food* 2, 873–885. doi: 10.1038/s43016-021-00400-y

Jaldhani, V., Sanjeeva Rao, D., Beulah, P., Nagaraju, P., Suneetha, K., Veronica, N., et al. (2022). "Drought and heat stress combination in a changing climate," in *Climate change and crop stress*, eds K. Arun (Cambridge, MA: Academic Press), 33–70. doi: 10.1016/B978-0-12-816091-6.00002-X

Jenkins, C. L., Furbank, R. T., and Hatch, M. D. (1989). Mechanism of c(4) photosynthesis: A model describing the inorganic carbon pool in bundle sheath cells. *Plant Physiol.* 91, 1372–1381. doi: 10.1104/pp.91.4.1372

Kanaoka, M. M., Pillitteri, L. J., Fujii, H., Yoshida, Y., Bogenschutz, N. L., Takabayashi, J., et al. (2008). SCREAM/ICE1 and SCREAM2 specify three cell-state transitional steps leading to Arabidopsis stomatal differentiation. *Plant Cell* 20, 1775–1785. doi: 10.1105/tpc.108.060848

Kellogg, E. A. (1998). Relationships of cereal crops and other grasses. *Proc. Natl. Acad. Sci. U.S.A.* 95, 2005–2010. doi: 10.1073/pnas.95.5.2005

Khan, A., Ali, S., Shah, S. A., Khan, A., and Ullah, R. (2019). Impact of climate change on maize productivity in Khyber Pakhtunkhwa, Pakistan. *Sarhad J. Agric.* 35, 594–601. doi: 10.17582/journal.sja/2019/35.2.594.601

Kharin, V. V., Zwiers, F. W., Zhang, X. B., and Hegerl, G. C. (2007). Changes in temperature and precipitation extremes in the IPCC ensemble of global coupled model simulations. *J. Clim.* 20, 1419–1444. doi: 10.1175/JCLI4066.1

Kim, S. H., Gitz, D. C., Sicherb, R. C., Baker, J. T., Timlin, D. J., and Reddy, V. R. (2007). Temperature dependence of growth, development, and photosynthesis in maize under elevated CO2. *Environ. Exp. Bot.* 61, 224–236. envexpbot.2007.06.005 doi: 10.1016/j

Kimball, B. A. (2016). Crop responses to elevated CO2 and interactions with H2O, N, and temperature. *Curr. Opin. Plant Biol.* 31, 36–43. doi: 10.1016/j.pbi.2016.03.006

Kimball, B. A., LaMorte, R. L., Pinter, P. J., Wall, G. W., Hunsaker, D. J., Adamsen, F. J., et al. (1999). Free-air CO2 enrichment and soil nitrogen effects on energy balance and evapotranspiration of wheat. *Water Resour. Res.* 35, 1179–1190. doi: 10.1016/j.agrformet.2004.01.005

Kranz, W. L., Irmak, S., Van Donk, S. J., Yonts, C. D., and Martin, D. L. (2008). *Irrigation management for Corn in Neb Guide G1850*. Lincoln, NE: University of Nebraska-Lincoln, 1–8.

Leakey, A. D. B., Ainsworth, E. A., Bernacchi, C. J., Rogers, A., Long, S. P., and Ort, D. R. (2009). Elevated CO2 effects on plant carbon, nitrogen, and water relations: Six important lessons from FACE. *J. Exp. Bot.* 60, 2859–2876. erp096 doi: 10.1093/jxb/

Leakey, A. D. B., Uribelarrea, M., Ainsworth, E. A., Naidu, S. L., Rogers, A., Ort, D. R., et al. (2006). Photosynthesis, productivity, and yield of maize are not affected by open-air elevation of CO2 concentration in the absence of drought. *Plant Physiol.* 140, 779–790. doi: 10.1104/pp.105.073957

Leichenko, R. M., and O'Brien, K. L. (2002). The dynamics of rural vulnerability to global change: The case of southern Africa. *Mitig. Adapt. Strat. Glob. Change* 7, 1–18. doi: 10.1023/A:1015860421954

Lipiec, J., Doussan, C., Nosalewicz, A., and Kondracka, K. (2013). Effect of drought and heat stresses on plant growth and yield: A review. *Int. Agrophys.* 27, 463–477. doi: 10.2478/intag-2013-0017

Lobell, D., Bänziger, M., Magorokosho, C., and Vivek, B. (2011). Nonlinear heat effects on African maize as evidenced by historical yield trials. *Nat. Clim. Change* 1, 42–45. doi: 10.1038/nclimate1043

Lobell, D., Hammer, G., McLean, G., Messina, C., Roberts, M. J., and Schlenker, W. (2013). The critical role of extreme heat for maize production in the United States. *Nat. Clim. Change* 3, 497–501. doi: 10.1038/nclimate1832

Long, S. P., Ainsworth, E. A., Rogers, A., and Ort, D. R. (2004). Rising atmospheric carbon dioxide: Plants FACE the future. *Annu. Rev. Plant Biol.* 55, 591–628. 031903.141610 doi: 10.1146/annurev.arplant.55

MacAlister, C. A., Ohashi-Ito, K., and Bergmann, D. C. (2007). Transcription factor control of asymmetric cell divisions that establish the stomatal lineage. *Nature* 445, 537–540. doi: 10.1038/nature05491

Maitah, M., Malec, K., and Maitah, K. (2021). Influence of precipitation and temperature on maize production in the Czech republic from 2002 to 2019. *Sci. Rep.* 11:10467. doi: 10.1038/s41598-021-89962-2

Manderscheid, R., Erbs, M., and Weigel, H.-J. (2014). Interactive effects of free-air CO2 enrichment and drought stress on maize growth. *Eur. J. Agron.* 52, 11–21. doi: 10.1016/j.eja.2011.12.007

Markelz, R. J. C., Strellner, R. S., and Leakey, A. D. B. (2011). Impairment of C4 photosynthesis by drought is exacerbated by limiting nitrogen and ameliorated by elevated CO2 in maize. *J. Exp. Bot.* 62, 3235–3246. doi: 10.1093/jxb/err056

Matsuoka, Y., Vigouroux, Y., Goodman, M. M., Sanchez, G. J., Buckler, E., and Doebley, J. (2002). A single domestication for maize shown by multilocus microsatellite genotyping. *Proc. Natl. Acad. Sci. U.S.A.* 99, 6080–6084. doi: 10.1073/pnas.052125199

McKown, K. H., and Bergmann, D. C. (2020). Stomatal development in the grasses: Lessons from models and crops (and crop models). *New Phytol.* 227, 1636–1648. doi: 10.1111/nph.16450

Munemasa, S., Hauser, F., Park, J., Waadt, R., Brandt, B., and Schroeder, J. I. (2015). Mechanisms of abscisic acid-mediated control of stomatal aperture. *Curr. Opin. Plant Biol.* 28, 154–162. doi: 10.1016/j.pbi.2015.10.010

Niang, I., Ruppel, O. C., Abdrabo, M. A., Essel, A., Lennard, C., Padgham, J., et al. (2015). "Africa," in *Climate change 2014: Impacts, adaptation, and vulnerability. Part b: Regional aspects. contribution of working group II to the fifth assessment report of the intergovernmental panel on climate change*, eds V. R. Barros, C. B. Field, D. J Dokken, M. D Mastrandrea, K. J Mach, E. Bilir, et al. (Cambridge: Cambridge University Press), 1199–1265.

OECD/FAO (2021). *OECD-FAO agricultural outlook 2021-2030*. Paris: FAO/OECD Publishing.

Pignon, C. P., and Long, S. P. (2020). Retrospective analysis of biochemical limitations to photosynthesis in 49 species: C4 crops appear still adapted to pre-industrial atmospheric [CO2]. *Plant Cell Environ.* 43, 2606–2622. doi: 10.1111/pce.13863

Räisänen, J. (2002). CO2-Induced changes in interannual temperature and precipitation variability in 19 CMIP2 experiments. *J. Clim.* 15, 2395–2411. doi: 10.1175/1520-04422002015<2395:CICIIT<2.0.CO;2

Raissig, M. T., Abrash, E., Bettadapur, A., Vogel, J. P., and Bergmann, D. C. (2016). Grasses use an alternatively wired bHLH transcription factor network to establish stomatal identity. *Proc. Natl. Acad. Sci. U.S.A.* 113, 8326–8331. doi: 10.1073/pnas.1606728113

Ranum, P., Peña-Rosas, J. P., and Garcia-Casal, M. N. (2014). Global maize production, utilization, and consumption. *Ann. N.Y. Acad. Sci.* 1312, 105–112. doi: 10.1111/nyas.12396

Ray, D. K., Gerber, J. S., Macdonald, G. K., and West, P. C. (2015). Climate variation explains a third of global crop yield variability. *Nat. Commun.* 6:5989. doi: 10.1038/ncomms6989

Rojas, M., Lambert, F., Ramirez-Villegas, J., and Challinor, A. J. (2019). Emergence of robust precipitation changes across crop production areas in the 21st century. *Proc. Natl. Acad. Sci. U.S.A.* 116, 6673–6678. doi: 10.1073/pnas.1811463116

Ruiz-Vera, U. M., Siebers, M. H., Drag, D. W., Ort, D. R., and Bernacchi, C. J. (2015). Canopy warming caused photosynthetic acclimation and reduced seed yield in maize grown at ambient and elevated CO2. *Glob. Change Biol.* 21, 4237–4279. doi: 10.1016/j.eja.2017.01.002.g

SADC (2016). *Over 41.4 million people in southern Africa are food insecure*. Available online at: https://www.sadc.int/news-events/news/over-414-million-people-southern-africaare-food-insecure/ (accessed June 13, 2022).

Schauberger, B., Archontoulis, S., Arneth, A., Balkovic, J., Ciais, P., Deryng, D., et al. (2017). Consistent negative response of US crops to high temperatures in observations and crop models. *Nat. Commun.* 8:13931. doi: 10.1038/ncomms13931

Schuler, M. L., Sedelnikova, O. V., Walker, B. J., Westhoff, P., and Langdale, J. A. (2018). SHORTROOT-mediated increase in stomatal density has no impact on photosynthetic efficiency. *Plant Physiol.* 176, 757–772. doi: 10.1104/pp.17.01005

Serna, L. (2011). Stomatal development in *Arabidopsis* and grasses: Differences and commonalities. *Int. J. Dev. Biol.* 55, 5–10. doi: 10.1387/ijdb.103094ls

Stebbins, G. L., and Shah, S. S. (1960). Developmental studies of cell differentiation in the epidermis of monocotyledons. II. Cytological features of stomatal development in the Gramineae. *Dev. Biol.* 2, 477–500. doi: 10.1016/0012-1606(60)90050-6

Taiz, L., and Zeiger, E. (2006). *Plant physiology*, 4th Edn. Sunderland, MA: Sinauer Associates.

USDA (2022). *World agricultural production*. Circular Series, WAP 5-22. Washington, DC: Foreign Agricultural Service.

van Heerwaarden, J., Doebley, J., Briggs, W. H., Glaubitz, J. C., Goodman, M. M., Sanchez, J., et al. (2011). Genetic signals of origin, spread, and introgression in a large sample of maize landraces. *Proc. Natl. Acad. Sci. U.S.A.* 108, 1088–1092. doi: 10.1073/pnas.1013011108

von Caemmerer, S., and Furbank, R. T. (2003). The C4 pathway: An efficient CO2 pump. *Photosynth. Res.* 77, 191–207. doi: 10.1023/a:1025830019591

Waha, K., Müller, C., and Rolinski, S. (2013). Separate and combined effects of temperature and precipitation change on maize yields in sub-Saharan Africa for mid- to late-21st century. *Glob. Planet. Change* 106, 1–12. doi: 10.1016/j.gloplacha.2013.02.009

Wahid, A., Gelani, S., Ashraf, M., and Foolad, M. R. (2007). Heat tolerance in plants: An overview. *Environ. Exp. Bot.* 61, 199–223. doi: 10.1016/j.envexpbot.2007.05.011

Way, D. A., and Oren, R. (2010). Differential responses to changes in growth temperature between trees from different functional groups and biomes: A review and synthesis of data. *Tree Physiol.* 30, 669–688. doi: 10.1093/treephys/tpq015

Webber, H., Ewert, F., Olesen, J. E., Müller, C., Fronzek, S., Ruane, A. C., et al. (2018). Diverging importance of drought stress for maize and winter wheat in Europe. *Nat. Commun.* 9:4249. doi: 10.1038/s41467-018-06525-2

Wetherald, R. (2010). Changes of time mean state and variability of hydrology in response to a doubling and quadrupling of CO2. *Clim. Change* 102, 651–670. doi: 10.1007/s10584-009-9701-4

Yu, C., Miao, R., and Khanna, M. (2021). Maladaptation of U.S. corn and soybeans to a changing climate. *Sci. Rep.* 11:12351. doi: 10.1038/s41598-021-91192-5

Zafar, S. A., Hameed, A., Nawaz, M. A., Ma, W., Noor, M. A., Hussain, M., et al. (2018). Mechanisms and molecular approaches for heat tolerance in rice (*Oryza sativa* L.) under climate change scenario. *J. Integr. Agric.* 17, 726–738. doi: 10.1016/S2095-3119(17)61718-0

Zhao, F., Zhang, D., Zhao, Y., Wang, W., Yang, H., Tai, F., et al. (2016). The difference of physiological and proteomic changes in maize leaves adaptation to drought, heat, and combined both stresses. *Front. Plant Sci.* 7:1471. doi: 10.3389/fpls.2016.01471

Zhao, W., Sun, Y., Kjelgren, R., and Liu, X. (2015). Response of stomatal density and bound gas exchange in leaves of maize to soil water deficit. *Acta Physiol. Plant.* 37:1704. doi: 10.1007/s11738-014-1704-8

Zheng, Y., Xu, M., Hou, R., Shen, R., Qiu, S., and Ouyang, Z. (2013). Effects of experimental warming on stomatal traits in leaves of maize (*Zea may* L.). *Ecol. Evol.* 3, 3095–3111. doi: 10.1002/ece3.674

frontiers | Frontiers in Plant Science

TYPE Original Research
PUBLISHED 07 October 2022
DOI 10.3389/fpls.2022.995815

OPEN ACCESS

EDITED BY
Ana Butron,
Misión Biológica de Galicia, (CSIC), Spain

REVIEWED BY
Deshu Lin,
Fujian Agriculture and Forestry University, China
Thomas L. Slewinski,
Bayer CropScience, Belgium

*CORRESPONDENCE
Yunling Peng
pengyl@gsau.edu.cn

SPECIALTY SECTION
This article was submitted to Plant Breeding, a section of the journal Frontiers in Plant Science

RECEIVED 16 July 2022
ACCEPTED 21 September 2022
PUBLISHED 07 October 2022

CITATION
Zhang Y, Ji X, Xian J, Wang Y and Peng Y (2022) Morphological characterization and transcriptome analysis of leaf angle mutant *bhlh112* in maize [*Zea mays* L.]. *Front. Plant Sci.* 13:995815. doi: 10.3389/fpls.2022.995815

Morphological characterization and transcriptome analysis of leaf angle mutant *bhlh112* in maize [*Zea mays* L.]

Yunfang Zhang[1,2,3], Xiangzhuo Ji[1,2,3], Jinhong Xian[1], Yinxia Wang[1,2,3] and Yunling Peng[1,2,3]*

[1]College of Agronomy, Gansu Agricultural University, Lanzhou, China, [2]Gansu Provincial Key Laboratory of Aridland Crop Science, Gansu Agricultural University, Lanzhou, China, [3]Gansu Key Laboratory of Crop Improvement & Germplasm Enhancement, Gansu Agricultural University, Lanzhou, China

Leaf angle is an important agronomic trait in maize [*Zea mays* L.]. The compact plant phenotype, with a smaller leaf angle, is suited for high-density planting and thus for increasing crop yields. Here, we studied the ethyl methane sulfonate (EMS)-induced mutant *bhlh112*. Leaf angle and plant height were significantly decreased in *bhlh112* compared to the wild-type plants. After treatment of seedlings with exogenous IAA and ABA respectively, under the optimal concentration of exogenous hormones, the variation of leaf angle of the mutant was more obvious than that of the wild-type, which indicated that the mutant was more sensitive to exogenous hormones. Transcriptome analysis showed that the *ZmbHLH112* gene was related to the biosynthesis of auxin and brassinosteroids, and involved in the activation of genes related to the auxin and brassinosteroid signal pathways as well as cell elongation. Among the GO enrichment terms, we found many differentially expressed genes (DEGs) enriched in the cell membrane and ribosomal biosynthesis, hormone biosynthesis and signaling pathways, and flavonoid biosynthesis, which could influence cell growth and the level of endogenous hormones affecting leaf angle. Therefore, *ZmbHLH112* might regulate leaf angle development through the auxin signaling and the brassinosteroid biosynthesis pathways. 12 genes related to the development of leaf were screened by WGCNA; In GO enrichment and KEGG pathways, the genes were mainly enriched in rRNA binding, ribosome biogenesis, Structural constituent of ribosome; *Arabidopsis* ribosome RNA methyltransferase CMAL is involved in plant development, likely by modulating auxin derived signaling pathways; The free 60s ribosomes and polysomes in the functional defective mutant *rice minute-like1* (*rml1*) were significantly reduced, resulting in plant phenotypic diminution, narrow leaves, and growth retardation; Hence, ribosomal subunits may play an important role

in leaf development. These results provide a foundation for further elucidation of the molecular mechanism of the regulation of leaf angle in maize.

KEYWORDS

maize (Zea mays L.), *bhlh112* mutant, transcriptomics, exogenous hormones, co-expression network

1 Introduction

Maize (*Zea mays* L.) is one of the three largest food crops grown in China (Yang et al., 2019). It is also a common feed for animals and the raw material for various industrial products (He et al., 2020). Since 2012, maize has become the most produced food crop in the world, and together with wheat and rice, it plays an important role in ensuring national food security and meeting market demand (Zhao et al., 2016).

Plant height and leaf angle are important plant architecture traits: plant height is closely related to lodging resistance, and leaf angle is closely associated with canopy structure and photosynthetic efficiency under high planting density. It is important to improve plant lodging resistance and increase canopy photosynthetic area when planting in high densities to improve yield. Previous research has shown that phytohormones, such as auxin indole-3-acetic acid (IAA), gibberellins (GAs), and brassinosteroids (BRs) are involved in regulating the leaf inclination. IAA is critical to the development of leaf morphology in maize, and interacts with light (white, red, and blue) or ethylene in regulation of leaf declination (Fellner et al., 2003). In addition, the regulatory pathways of auxin signaling and BR biosynthesis are also included (Liu et al., 2019), and GAs genes interact with BR genes to modulate the leaf angle (Li et al., 2020). Two rice (*Oryza sativa* L.) auxin response factors (ARFs), OsARF6 and OsARF17, which are highly expressed in lamina joint tissues, control flag leaf angle in response to auxin (Huang et al., 2021). And rice LEAF INCLUSION1 (LC1), an IAA amide synthase, maintains auxin homeostasis by binding excess IAA with various amino acids, and then regulates the leaf angle (Zhao et al., 2013). In addition, Li et al. found that ABA regulate lamina joint inclination in rice by the BR biosynthesis pathway and BR signal transduction (Li et al., 2019a).

Basic helix-loop-helix (bHLH) transcription factor (TF) is a major regulatory factor, which is one of the largest TF family, and widely distributed among eukaryotic kingdoms. The bHLH domain generally contains approximately 60 amino acids and possesses two functionally distinct regions: a basic region and a helix-loop-helix (HLH) region (Guo and Wang, 2017). The basic region is located at the N-terminus along with a DNA-binding motif, and the HLH region contains two amphipathic α-helices separated by a loop region of variable length which could act as a dimerization domain that promotes protein-protein interactions and forms homo-dimers or hetero-dimers (Massari and Murre, 2000).

Studies have clarified that bHLH TFs play a regulatory role in plant growth and development (Heang and Sassa, 2012; Endo et al., 2016), response to a variety of abiotic stresses (Li et al., 2007; Ogo et al., 2007) and signal transduction (Friedrichsen et al., 2002; Huq and Quail, 2002; Zhang et al., 2011). The rice bHLH TF OsBIM1 has been reported to positively regulate leaf angle by promoting brassinolide signal transduction (Tian et al., 2021). The maize bHLH (ZmbHLH) TF PTF1 can promote lateral root elongation and assist with abscisic acid (ABA) biosynthesis, signal transduction, and drought tolerance (Li et al., 2019b). In addition, *bHLH* genes in plants have also found to be involved in the biosynthesis pathways of anthocyanins (Wang et al., 2018).

At present, the regulation functions of bHLH TF of leaf angle are widely studied in rice, but important questions remain. In this study, we obtained the *ZmbHLH112* mutant *bhlh112* by ethyl methane sulfonate (EMS) mutagenesis of wild-type B73, which displays a relatively small leaf angle. Maize mutant *bhlh112* and wild-type B73 were analyzed using RNA-Seq sequencing. Our findings will provide useful information for further studies in maize plant type breeding to clarify the functions of bHLH TF in diverse growth and development processes.

2 Materials and methods

2.1 Plant materials and planting conditions

Mutant *bhlh112* (EMS3-03e012) with altered expression of maize leaf angle was obtained from the maize EMS mutant library of Qilu Normal University (http://elabcaas.cn/memd/). The mutant *bhlh112* was planted in the experimental field of Gansu Agricultural University, we used mutant *bhlh112* to continuously backcross B73 for 2 generations and then self-bring for one generation to clear the mutant background. We then used the Sanger Method to preserve the mutated sites during background removal and observe the mutant phenotypes. The experiment was arranged in a complete

randomized block design with replicated three time, and technique of the alternately planting of wide (70 cm) and narrow (40 cm) row spacing was used with plant spacing of 25 cm (75000 seeds ha^{-1}). B73 germplasm material was provided by the Maize Breeding Research Group of the Agricultural College of Gansu Agricultural University. The experiment was carried out at the State Key Laboratory of Aridland Crop Science, Gansu Agricultural University.

2.2 Bioinformatics analysis of *ZmbHLH112*

We used the NCBI database to find the gene sequence and amino acid sequence encoded by *ZmbHLH112*, DNAMAN software to analyze the *ZmbHLH112* sequence and sequence alignment, ClustalW programs to perform multiple alignment of amino acid sequences, and MEGA7.0 software to construct multiple alignment results generated by the ClustalW Phylogenetic tree; Using the Neighbor-joining method with select Pairwise deletion, bootstrap set to 1000.

2.3 Mutant phenotype analysis

After pollination, three plants of wild-types and mutant with look similar were selected in each plot, respectively, the field phenotypic data (plant height, ear height, chlorophyll, stem diameter, and branch number of tassels) were measured; Meanwhile, ten wild-type and mutants with similar appearance were selected and their ear leaf angle, a leaf angle above the ear, a leaf angle below the ear were measured respectively. Mature ears were harvested at the end of September of the same year and dried to safe moisture before threshing. At that time, the single ear weight, ear length, ear diameter, grain type, grain color, and 100 grain weight were measured, the values shown are averages from three biological replicates. Leaf area size (LAS= LL x LW x 0.75) and leaf direction value (LOV = Σ (90 - θ i) x (Lf/LL)/N were calculated; θ i: leaf angle value; Lf: leaf spacing; LL: leaf length; N: number of leaves above the ear) (Zhang et al., 2021a).

2.4 Identification of the homozygous mutant *bhlh112*

We used mutant *bhlh112* to continuously backcross B73 for 2 generations and then self-bring for one generation as the experimental material, DNA was extracted from V3 stage leaves of the mutant *bhlh112* and wild-type B73. Primer premier 5.0 was used to design primers: forward primer: GGAGTTCTGGCACCCTACAT; reverse primer: TTTGGGCG GCATCATGATTT. Using wild-type and mutant DNA as the template, PCR amplification was carried out with Easy-Taq enzyme. The reaction system (20 μL) included Easy Taq 10 μL, ddH_2O 7 μL, forward and reverse primers 1 μL each, and DNA template 1 μL. Amplification conditions were pre-denaturation at 94°C for 4 min, 94°C for 1 min, 56°C for 30 s, 72°C for 1 min, after 35 cycles, extension at 72°C for 10 min. PCR amplification products were sent to Shanghai Sangon Biotech Company for sequencing, and the mutation sites were determined by DNAMAN analysis.

2.5 Expression pattern analysis of *ZmbHLH112*

2.5.1 Extraction of total RNA and synthesis of first strand cDNA

The root, stem, old leaves, new leaves, and the leaf occipital part of the second leaf of maize B73 at the V3 stage were collected and frozen in liquid nitrogen. Three biological replicates for each sampling part in this study.The SteadyPure plant RNA extraction kit was used to extract total RNA and the RNA concentration, purity, and integrity were examined using advanced molecular biology equipment. cDNA (including gDNA) was synthesized by M-MLV (Moloney murine leukemia virus) reverse transcription kit, provided by Accurate Biology Company. Reverse transcription conditions: 37°C for 15 min, 85°C for 5 sec, and 4°C.

2.5.2 Quantitative real-time PCR (qRT-PCR)

We used the SYBR ® Green Pro Taq HS Premixed qPCR kit was used for qRT-PCR, and the internal reference gene Actin (forward primer: TGAAACCTTCGAATGCCCAG, reverse primer: GATTGGAACCGTGTGGCTCA; *ZmbHLH112*: forward primer: TAACGGCGACACGAAGCAAGAC, reverse primer: CTCCAAATGTAGGGTGCCAGAACTC). The reaction system was 20 μL: 2xSYBR ® Green Pro Taq HS Premix 10 μL; cDNA 1 μL, forward primer 0.4 μL and reverse primer 0.4 μL, RNase free water 8.2 μL. This was amplified by Illumina qRT-PCR; $2^{-\Delta\Delta CT}$ calculated the relative expression of genes (Livak and Schmittgen, 2001). Reaction conditions: 95 °C for 30 sec, followed by cycling for 40 rounds of 95°C for 5 sec, 60°C for 30 sec.

2.6 Screening the optimal concentration of exogenous hormones

The maize seeds were planted with vermiculite in a flower pot with a diameter of 10 cm and placed in an artificial climate room (12 h light/12 h dark, 28°C, 65% RH) to determine the phenotypic and physiological characteristics of the seedlings. Two hormone treatment groups were set up in this experiment; (1) ABA application at four concentrations: B73 and *bhlh112*

with 0 μmol·L^{-1} (control), 1 μmol·L^{-1}, 10 μmol·L^{-1} and 50 μmol·L^{-1}; (2) IAA application at five concentrations: B73 and *bhlh112* are set to 0 μmol·L^{-1} (control), 1 μmol·L^{-1}, 10 μmol·L^{-1}, 100 μmol·L^{-1} and 500 μmol·L^{-1}. Treatment with exogenous plant hormones was carried out from the normal watering to the V1 stage of the seedlings. The treatment was conducted once every other day, with 50 mL poured each time, and the leaves of the corn seedlings sprayed with the corresponding hormones. The leaf angle of each treatment was measured at the V3 stage to screen the optimal concentration of exogenous hormones. 2 cm of the leaf occipital part of the V3 stage at the optimal concentration was collected and frozen in liquid nitrogen, and sent it to Lianchuan biological company for sequencing.

2.7 RNA-seq library construction and sequencing

For RNA-seq analysis, the second leaf occipital part of the wild-type and mutant plants at the V3 stage were harvested and frozen in liquid nitrogen. Three biological replicates for each genotype and three pooled samples for each replicate were tested in this study. The total RNA of the sample was extracted with TRIzol (Thermo Fisher, 15596018), and the RNA was isolated and purified according to the manufacturer's instructions. The quantity and purity of total RNA was controlled with NanoDrop ND-1000 (NanoDrop, Wilmington, DE, USA), and the integrity of RNA was detected with Bioanalyzer 2100 (Agilent, CA, USA); Illumina Novaseq™ 6000 (LC Bio Technology CO., Ltd. Hangzhou, China) was used for double ended sequencing according to the standard operating procedures. Clean Data bases produced by each sample more than 43 million; About 94.37% - 97.95% of the clean data can be compared to the number of reads on the reference genome (RefGen_v4) of B73, about 90.48% - 94.27% can only be compared to the number of reads at one position of the genome, and only about 3.51% - 5.14% of the clean data can be compared to the number of reads at multiple positions of the genome. The size of the filtered data accounted for 97.69% of the original data size. The percentage of bases with a quality value of Q≥30 is 97.74% and above. The data presented in the study are deposited in the SRA at NCBI repository, accession number PRJNA856349.

2.8 qRT-PCR validation of the DEGs

In order to verify the reliability of the DEGs, the differentially expressed genes in different comparison groups were selected for qRT-PCR. The method was the same as in 2.5.2; the primer sequence in the Table 1.

2.9 Co-expression network analysis for module construction

Co-expression networks were constructed using the WGCNA package in R. We selected genes with FPKM ≥ 10, gene expression values were imported into WGCNA to construct co-expression modules with default settings, TOM Type was unsigned, used the picksoftthreshold function to select the appropriate soft threshold β = 18, selected the threshold value close to 0.9 of the fitting curve, and constructed the scale-free network distribution. We associated the merged modules with phenotypic traits, selected the genes of the core module top30 according to the weighted values, constructed the protein interaction network between genes with the string website, and drew the network diagram with Cytoscape function.

3 Results

3.1 Identification of the *ZmbHLH112* Gene

The *ZmbHLH112* (*Zm00001d043248*) gene (LOC100277655) is located on maize chromosome 3, with a total length of 1525bp, including 1158bp CDs sequence,

TABLE 1 Primer design sequence.

Gene name	Forward Primer (5'→3')	Reverse Primer (5'→3')
Zm00001d009985	GCAAGGTGCGCTCCTTCTTCTG	ACGAGAGAGACGAGGACGACAAG
Zm00001d022435	CGATGACGACTACGACTACGACTTG	TTGATCCTGATGGCTCCCGAGTC
Zm00001d016719	CACCAAGCTGCTGCTGCTCATG	GCTCTTGCCGTTGACCCTGAAG
Zm00001d018150	AAGAAGGTTGGTAGCGGCAAGAAG	CGACCGGATTAGCTTCCACCATG
Zm00001d019629	GCGAGATGAGGCTCAGCAACTTC	CGCAACGCTTCCAGGTACTCAG
Zm00001d009687	ACCAATCTCCACCGCCTCAT	GAAGGCATGGACGAGGACGA
Zm00001d032024	CGGGAACAAGTGGTCGCTCATC	ACGTGCGTGTTCCAGTAGTTCTTG
Zm00001d007175	TGGACGAGCCACTGATCTCC	CGGTGGACGAGGAGGTTGAT

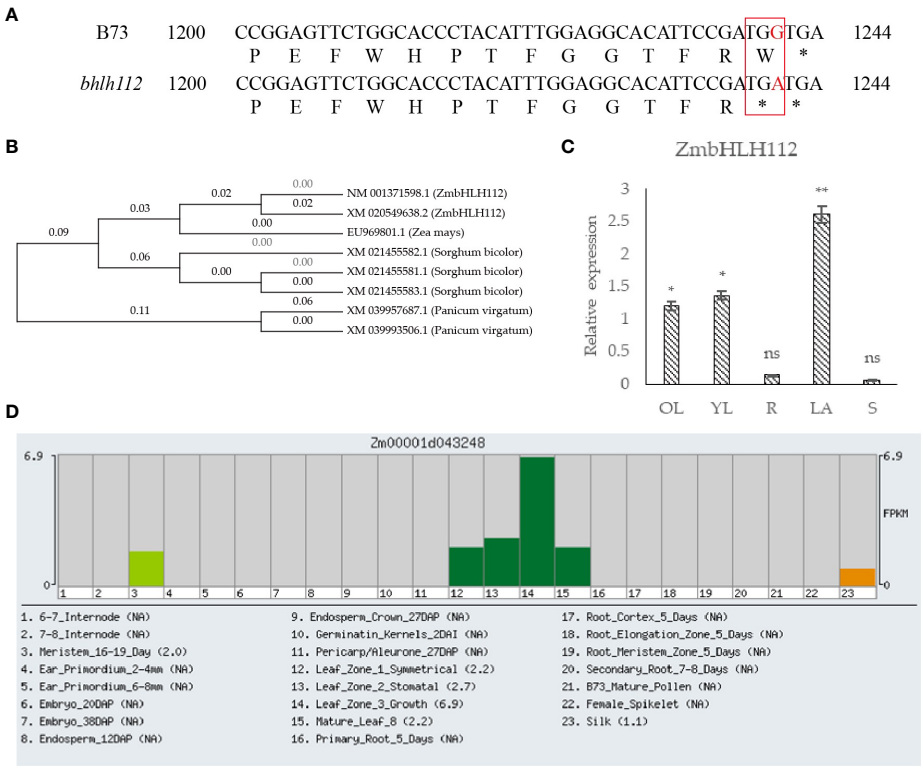

FIGURE 1
Analysis of the *ZmbHLH112* gene in maize. **(A)** Partial sequence alignment of the *ZmbHLH112* gene in mutants *bhlh112* and B73. **(B)** Evolutionary tree of the *ZmbHLH112* gene. **(C)** Relative expression of *ZmbHLH112* in different tissues. **(D)** Gene Expression Atlas of the *ZmbHLH112* gene from Maize GDB. OL, old leaves; YL, young leaves; R, roots; LA, the leaf occipital part of the second leaf at the V3 stage; S: stems. ** indicates $P < 0.01$, * indicates $P < 0.05$. ns indicates not significant.

encoding 385 amino acids. The protein sequence of *ZmbHLH112* was analyzed by Blast in the NCBI database; we found that it had the highest homology with sorghum bicolor (XM_021455582.1 and XM_021455581.1). The above plant protein sequences were compared by MEGA7.0 software, and then a phylogenetic tree was constructed (Figure 1B). The 1241th base G of *ZmbHLH112* gene in the mutant *bhlh112* was replaced with A (Figure 1A), whereby tryptophan (TGG) was mutated into termination codon (TGA). The mutation at this base leads to the differences in maize phenotype and physiological structure. In order to verify the expression specificity of the *ZmbHLH112* gene in different maize tissues, the expression patterns of the *ZmbHLH112* gene in maize roots, stems, old leaves (second leaf at the V3 stage), young leaves (fourth leaf at the V3 stage) and the leaf occipital part of the second leaf were detected by quantitative real-time polymerase chain reaction (qRT-PCR) analysis. *ZmbHLH112* had the highest relative expression of the leaf occipital part of the second leaf; relative expression was the lowest in roots and stems (Figure 1C). The *ZmbHLH112* gene was related to the development of meristem, leaf, and silk according to the Maize GDB website (https://www.maizegdb.org/) (Figure 1D). These results showed that this gene could regulate the development of maize leaves and the leaf occipital part.

3.2 Phenotypic and grain characters of *bhlh112*

Phenotypic analysis of mutant *bhlh112* and its wild-type B73 showed that significant reductions in plant height and ear height were observed in the *bhlh112* mutant when compared to the wild-type, with 31.93% and 19.41% reductions observed at the mature stage, respectively (Figures 2A, D). The leaf angles also significantly differed; the average leaf angle of the mutant was smaller than that of the wild-type (Figure 2B). We measured the ear leaf angle, a leaf angle above the ear, and a leaf angle below the ear, and observed 16.70%, 25.00%, and 18.36% reductions in these leaf angles, respectively, in *bhlh112* at the mature stage (Figures 2C, E). Compared to the wild-type, the single ear weight, ear length, and ear diameter of the mutant decreased by 35.96%, 22.09%, and 6.48%, ear rows, number of rows and ear shaft weight decreased 10.28%, 6.96% and 22.89%, respectively; And, the 100-kernel weight increased by 3.25% (Figure 2F). In

TABLE 2 Field phenotypic traits of mutant *bhlh112* and B73.

Traits	B73	*bhlh112*
Plant height/cm	250.39 ± 0.87a	170.44 ± 4.94b
Ear height/cm	108.78 ± 1.95a	87.67 ± 1.26b
Stem diameter/mm	22.29 ± 0.38a	18.03 ± 0.69b
Tassel branch number	8.89 ± 0.35a	3.44 ± 0.44b
Chlorophyll	50.14 ± 1.64a	34.92 ± 0.69b
Leaf length/cm	78.54 ± 2.08a	63.34 ± 1.61b
Leaf width/cm	9.23 ± 0.18a	7.16 ± 0.23b
Leaf orientation value	5.35 ± 0.28a	7.03 ± 0.43b
Leaf area size/cm2	545.56 ± 23.84a	341.78 ± 17.31b

a, b indicated significant differences between materials. $P < 0.05$.

TABLE 3 Field grain traits of mutant *bhlh112* and B73.

Traits	B73	*bhlh112*
Ear length/cm	10.87 ± 0.49a	8.47 ± 0.70b
Ear coarse/cm	3.97 ± 0.32a	3.37 ± 0.25b
Ear rows	16.67 ± 1.15a	12.67 ± 1.15b
Number of rows	26.67 ± 1.15a	22.33 ± 1.53a
Ear weight/g	81.52 ± 6.98a	52.21 ± 1.06b
Kernel weight/g	66.66 ± 3.27a	45.28 ± 0.59a
100-kernel weight/g	41.53 ± 3.56a	44.68 ± 0.61a
Shaft weight/g	14.86 ± 1.80a	6.92 ± 0.09b
Shaft coarse/cm	2.77 ± 0.21a	2.27 ± 0.21b

a, b indicated significant differences between materials. $P < 0.05$.

summary, the phenotypes of mutants and wild-type differed in many dimensions (Tables 2, 3).

3.3 Screening of optimum concentrations of different exogenous plant hormones

In order to further understand the regulation of bHLH TF of maize leaf angle and the effect of exogenous hormones on leaf angle development, we treated mutant *bhlh112* and the wild-type with the exogenous hormones ABA and IAA, and observed leaf angles at the V3 stage. When treated with 0 μmol·L^{-1} ABA (control), the leaf angle of B73 was larger than that of *bhlh112* (Figure 3A), which was consistent with the results from field data, which also showed a smaller leaf angle of the mutant *bhlh112*. However, with increasing ABA concentration, the leaf angle of *bhlh112* and B73 increased first and then decreased, and reached a maximum at 10 μmol·L^{-1}, indicating that this is the preferred treatment concentration. At this concentration, the leaf angles

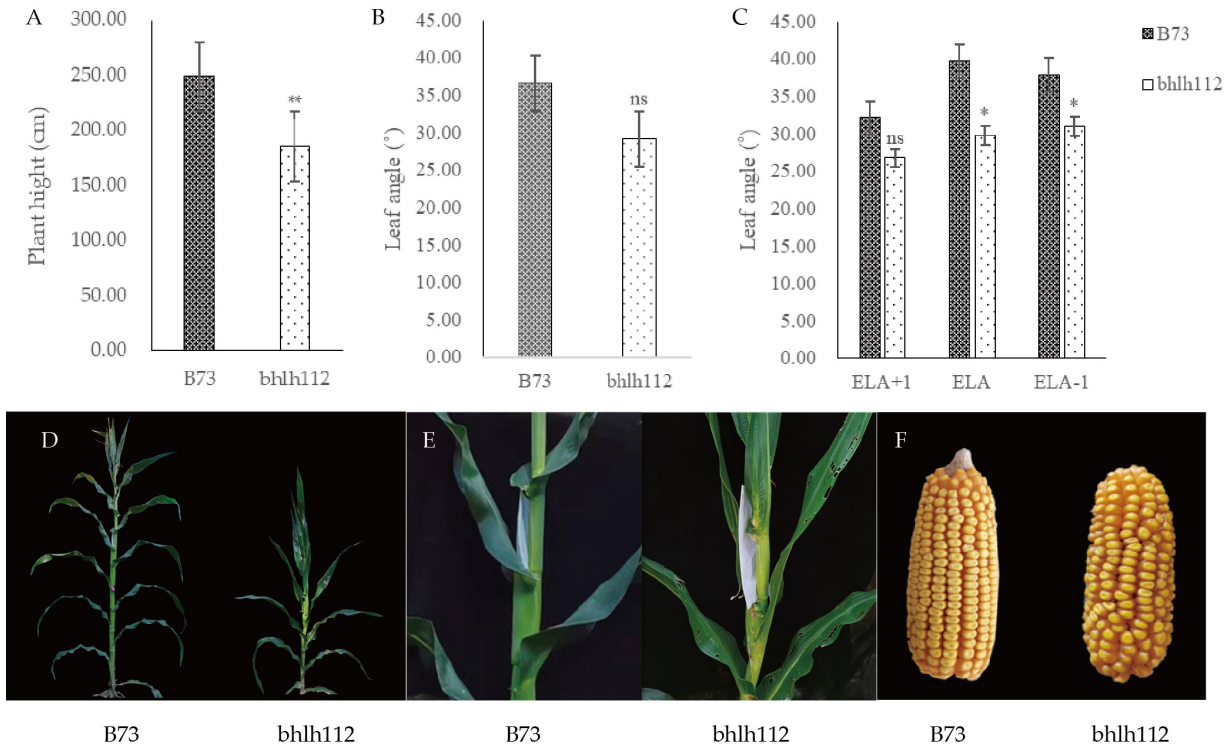

FIGURE 2
Analysis of index of wild-type and mutant *bhlh112*. **(A)** Plant height of mutant and wild-type; **(B)** Leaf angle of mutant and wild-type; **(C)** Three ear-leaf-angle of mutant and wild-type at the mature stage. ELA: ear leaf angle; ELA+1: a leaf angle above the ear; ELA-1: a leaf angle below the ear; ns indicates not significant; **(D)** Plants at silking stage; **(E)** Corresponding leaf angle in **(D)**; **(F)** Mature ear of wild type and mutant. * indicates $P < 0.05$. ** indicates $P < 0.01$.

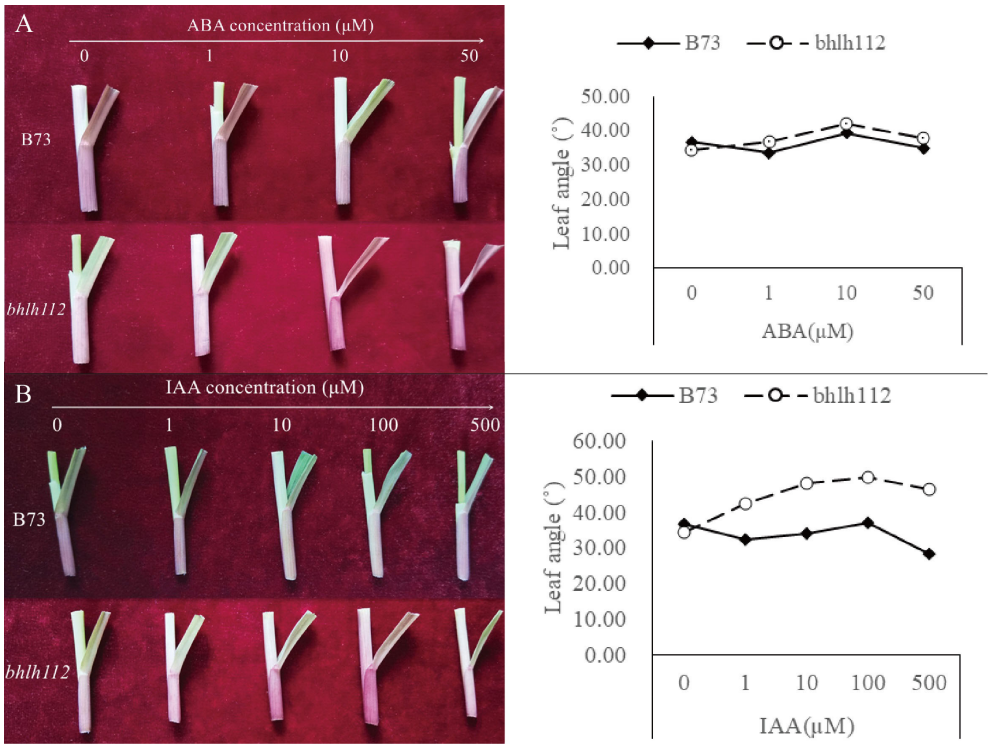

FIGURE 3
Effects of ABA and IAA on leaf angle in maize. **(A)** Changes in leaf angle from different concentrations of ABA in mutant and wild-type V3 stage. **(B)** Changes in leaf angle from different concentrations of IAA in the mutant and wild-type V3 stage.

were 42.15° and 39.33° in the mutant *bhlh112* and the wild-type, respectively, which represents a respective increase of 22.29% and 7.325%, compared with the control. When treated with increased concentrations of exogenous IAA, the leaf angle of *bhlh112* and B73 increased first and then decreased (Figure 3B). When exogenous IAA was 100 μmol·L^{-1}, the leaf angles of *bhlh112* and B73 reached the maximum, 49.92° and 37.03° respectively, which was an increase of 44.83% and 1.05% respectively compared with the control. In general, the mutant *bhlh112* was more sensitive to different exogenous plant hormones than was the wild-type B73.

3.4 Transcriptomic analyses of *bhlh112* and B73

In order to understand the transcriptome network underlying the *ZmbHLH112* gene mutation, high-throughput RNA-seq was performed for mutant *bhlh112* and the wild-type B73. Fold changes >= 2 (|log2FC| >= 1) was used as the change threshold, and q < 0.05 (q value is the correction value of p value) was used as the standard for screening DEGs. In the control group, a total of 944 DEGs were identified. Among them, 386 genes were significantly up-regulated, and 558 genes were significantly down-regulated, accounting for 40.89% and 59.11%, respectively, of the DEGs (Figure 4A and Table S1). In *bhlh112* and B73 under 10 μmol·L^{-1} exogenous ABA treatment, a total of 1045 DEGs were identified, with 191 genes up-regulated and 854 genes down-regulated, accounting for 18.28% and 81.72% of the total DEGs, respectively (Figure 4B and Table S2). When *bhlh112* and B73 were treated with 100 μmol·L^{-1} exogenous IAA, a total of 663 DEGs were identified, and the number of up-regulated and down-regulated genes were 237 and 426, accounting for 35.75% and 64.25% of the total DEGs, respectively (Figure 4C and Table S3); *bhlh112* and B73 were treated with 0 μmol·L^{-1} and 10 μmol·L^{-1} exogenous ABA, and a total of 465 and 692 DEGs were identified, of which the numbers of up-regulated genes were 34 and 431, accounting for 7.31% and 92.68% of the total DEGs, respectively, and the numbers of down-regulated genes were 547 and 145, accounting for 79.05% and 20.95% of the total DEGs respectively (Figures 4D, E, Tables S4, S5). *bhlh112* and B73 were treated with 0 μmol·L^{-1} and 100 μmol·L^{-1} exogenous IAA, and a total of 650 and 721 DEGs were identified respectively, of which the numbers of up-regulated genes were 356 and 556, accounting for 54.77% and 45.23% of the total DEGs, respectively, and the numbers of down-regulated genes were 294 and 165, accounting for 77.12% and 22.88% of the total DEGs, respectively (Figures 4F, G, Tables S6, S7). Further observation of the number of DEGs between each comparison group showed that there were some differences in the responses of the mutant *bhlh112* and B73 to different exogenous plant hormones (Figure 4H).

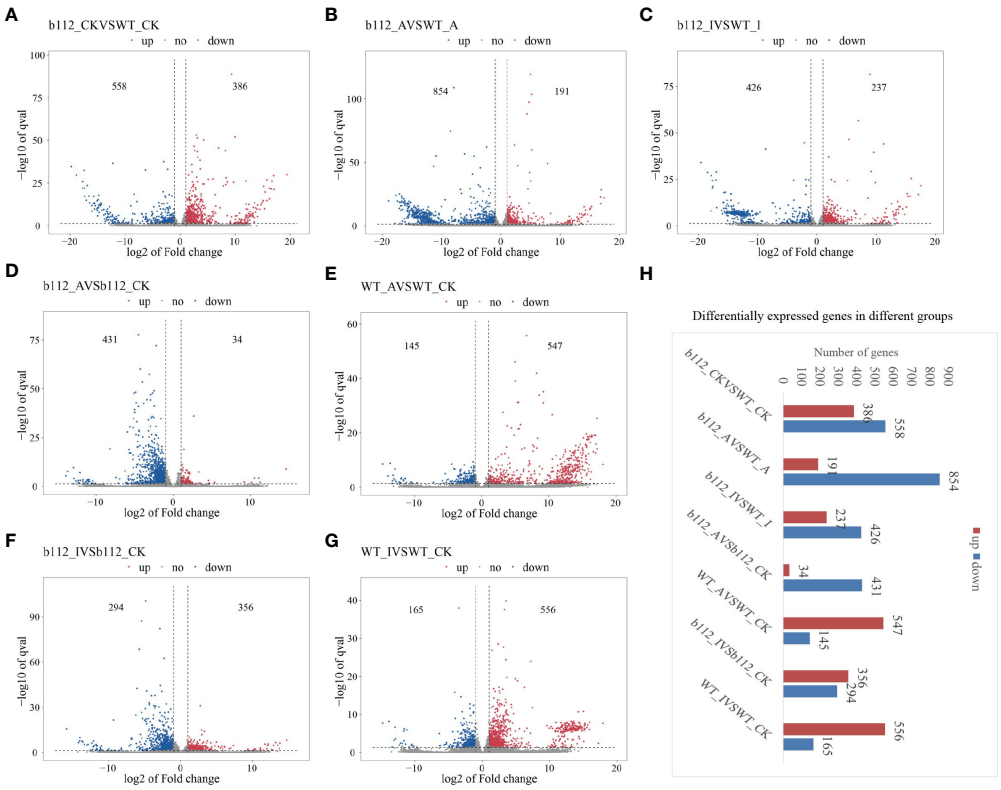

FIGURE 4
DEGs between *bhlh112* and the wild-type. **(A)** Number of DEGs of *bhlh112* and B73 under the control treatment; **(B)** Number of DEGs of *bhlh112* and B73 under 10 μmol·L^{-1} exogenous ABA treatment; **(C)** Number of DEGs of *bhlh112* and B73 under 100 μmol·L^{-1} exogenous IAA treatment; **(D)** Number of DEGs of *bhlh112* under 0 μmol·L^{-1} and 10 μmol·L^{-1} exogenous ABA treatment; **(E)** Number of DEGs of B73 under 0 μmol·L^{-1} and 10 μmol·L^{-1} exogenous ABA treatment; **(F)** Number of DEGs of *bhlh112* under 0 μmol·L^{-1} and 100 μmol·L^{-1} exogenous IAA treatment; **(G)** Number of DEGs of B73 under 0 μmol·L^{-1} and 100 μmol·L^{-1} exogenous IAA treatment; **(H)** DEGs across different groups. control = CK = 0 μmol·L^{-1} ABA = 0 μmol·L^{-1} IAA.

3.5 GO terms and KEGG pathways analysis of leaf angle in *bhlh112*

Both GO terms and KEGG pathways were used to elucidate the functional annotations of the DEGs (Figures 5, 6). Annotation functions of GO terms were mainly divided into three categories: biological processes (BP), cellular components (CC), and molecular functions (MF). The up-regulated DEGs were significantly represented in 209 BP terms, 114 CC terms, and 31 MF terms; the down-regulated DEGs were significantly represented in 33 BP terms, 312 CC terms, and 206 MF terms. Compared with the wild-type B73, in the mutant *bhlh112*, the most significantly enriched GO terms mainly included the BP terms "oxylipin biosynthetic process", "aromatic compound biosynthetic process", "regulation of jasmonic acid mediated signaling pathway" and "regulation of defense response"; the CC terms "extracellular region" and "apoplast"; the MF terms "dioxygenase activity", "oxidoreductase activity", "O-methyltransferase activity" and "serine-type endopeptidase inhibitor activity" (Figure 5). KEGG enrichment analysis revealed that "Plant hormone signal transduction", "MAPK signaling pathway-plant" and "Plant-pathogen interaction" were the most overrepresented pathways in the up-regulated DEGs, while "DNA replication", "Lipid metabolism", "Nucleotide excision repair", and "Mismatch repair" were the main pathways in the down-regulated DEGs (Figure 6). These results showed that the expression level of genes related to plant hormone signal transduction, MAPK signaling pathway-plant, and response to wounding were increased in the mutant *bhlh112*, and the expression level of genes related to genetic information processing were inhibited.

3.6 Pathway enrichment analysis of *bhlh112* and B73 with exogenous ABA

We performed pathway enrichment analysis on all DEGs in wild-type B73 and the mutant *bhlh112* (Figures 5B, 6B). Under

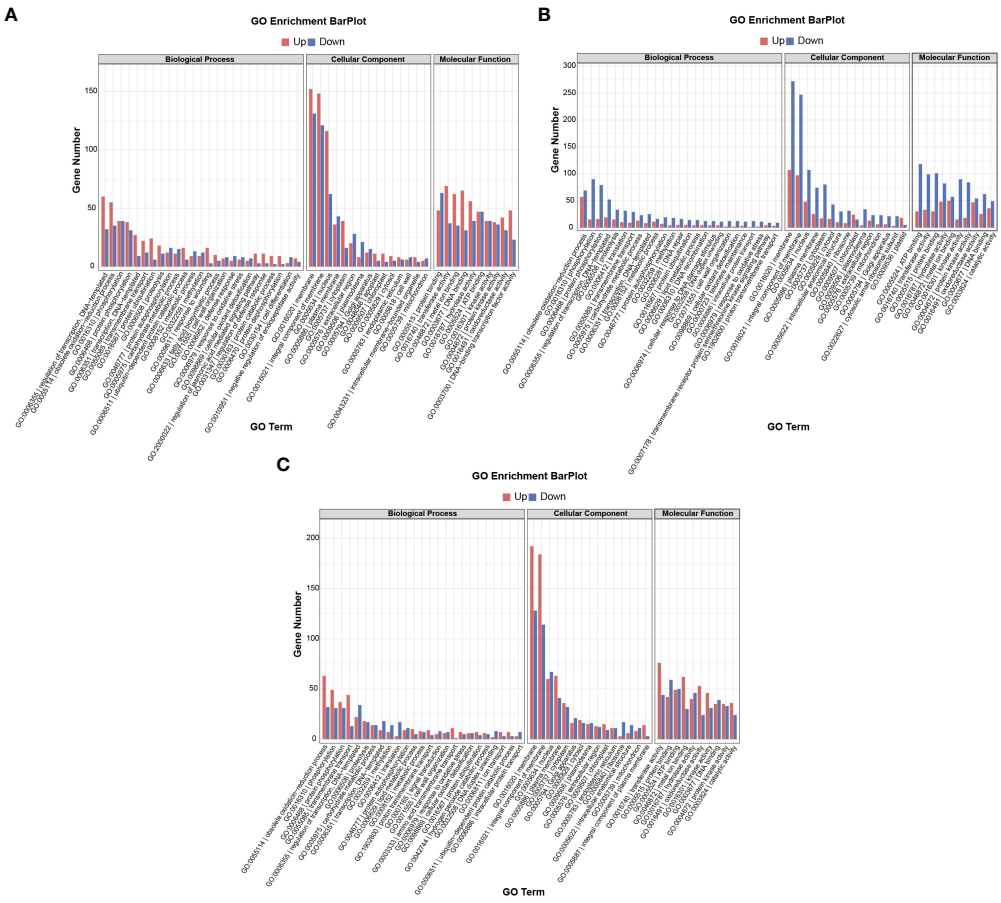

FIGURE 5
GO term annotations of DEGs in B73 and *bhlh112* under the different treatments. **(A)** b112_CKvsB73_CK; **(B)** b112_AvsB73_A; **(C)** b112_IvsB71_I. CK = control, A = exogenous ABA, I = exogenous IAA.

ABA treatment, compared with B73, *bhlh112* had 61, 3, and 123 significantly up-regulated DEGs involved in biological processes, cell composition, and molecular functions ($q<0.05$), and 76, 21, and 207 significantly down-regulated DEGs for these three categories. For BP, DEGs were enriched in the "obsolete oxidation-reduction process", "tryptophan biosynthetic process", and "negative regulation of endopeptidase activity". The enriched CC terms were primarily "cytosolic small ribosomal subunit", "anthranilate synthase complex", and "plasmodesma". The enriched MF terms were "oxidoreductase activity", "hydrolase activity", "protein kinase activity", "phosphate ion transmembrane transporter activity", and "catalytic activity". Further KEGG enrichment analysis revealed that up-regulated genes were enriched in "Stilbenoid, diarylheptanoid and gingerol biosynthesis", "Linoleic acid metabolism", and "Phenylpropanoid biosynthesis"; down-regulated genes were enriched in "Benzoxazinoid biosynthesis" and "Plant hormone signal transduction". These results suggest that exogenous ABA may be involved in leaf angle development of the mutant *bhlh112* through plant hormone signal transduction, lipid metabolism, and biosynthesis of secondary metabolites.

3.7 Pathway enrichment analysis of *bhlh112* and B73 with exogenous IAA

Under IAA treatment (Figures 5C, 6C), compared with B73, the mutant *bhlh112* had the significantly enriched BP terms "amino acid transmembrane transport", "obsolete oxidation-reduction process", "cellulose biosynthetic process", "exocyst assembly", "cell surface receptor signaling pathway" and "hexose transmembrane transport"; enriched CC terms were "plasma membrane" and "plasmodesma"; MF terms were "oxidoreductase activity", "monooxygenase activity", "amino acid transmembrane transporter activity", "carbohydrate: proton symporter activity" and "protein histidine kinase binding".

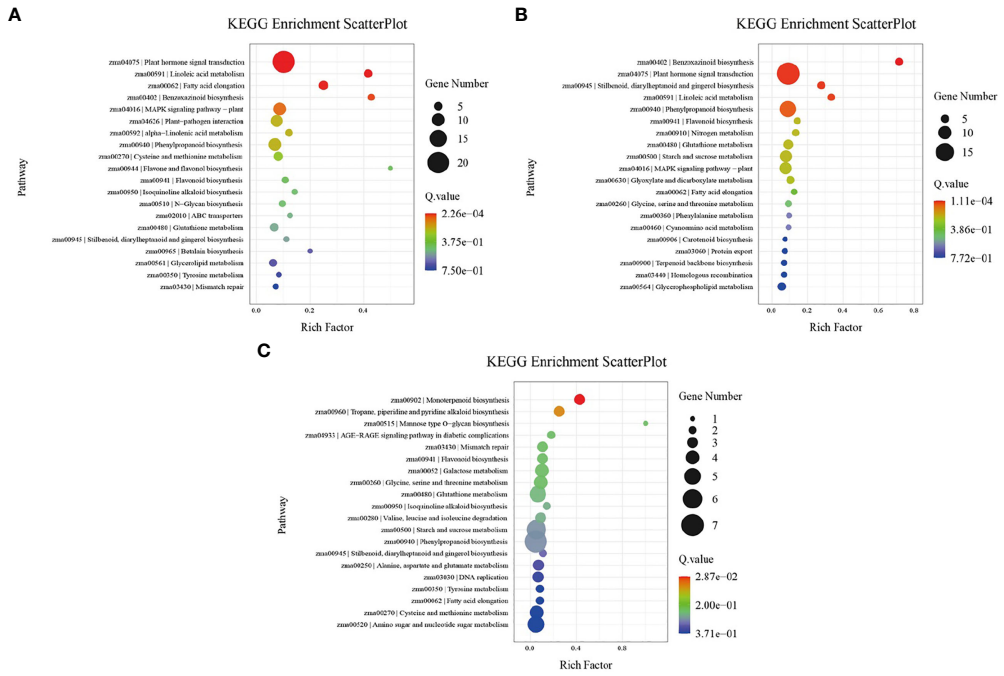

FIGURE 6
KEGG pathway enrichment analysis of DEGs in B73 and *bhlh112* under the different treatments. **(A)** b112_CKvsB73_CK; **(B)** b112_AvsB73_A; **(C)** b112_IvsB71_I. CK = control, A = exogenous ABA, I = exogenous IAA.

3.8 Validation of DEGs by qRT-PCR analysis

The expression levels of some DEGs were evaluated by qRT-PCR in order to validate the reliability of the RNA-seq data (Figure 7). We found that 8 DEGs exhibited the same trends in both the RNA-Seq and qRT-PCR results, indicating that the RNA-seq data was reliable (y = 1.9244x+0.2667, R^2 = 0.6608).

3.9 Weighted correlation network analysis (WGCNA)

3.9.1 Construction of modules associated with leaf angle of maize based on WGCNA

In order to identify the correlation between the genes obtained by RNA-seq and the phenotypic data of maize leaf angle (LA), the DEGs with FPKM ≥ 10 were selected, and a total of 8994 DEGs were screened to construct the co-expression network. Used the threshold value close to 0.9 of the fitting curve (Figures 8A, B), and constructed the scale-free network distribution (Figures 8C, D). A total of 15 modules meeting the conditions were screened, of which the white module had the highest correlation with the leaf angle of maize (Figures 8E, F). These 15 modules were analyzed by correlation and cluster analysis (Figures 8G-I), and they were clustered into 3 categories at 1.0

3.9.2 Identification of hub genes and construction of the PPI network

In order to further screen the genes related to leaf angle, a total of 63 genes were screened for the white module based on | GS | >0.2 and | MM | >0.8 (GS: Gene significance for body weight; MM: Module Membership in white module) (Table S8). A protein-protein interaction (PPI) network was constructed using the STRING database with a combined score of >0.4. In addition, the PPI network was constructed with the genes with the weighted value of top30 (Figure 9). The PPI relationship between them was predicted by using the STRING database, and retaining the combined_score > 0.4, the PPI network of 12 hub genes was obtained (Table 4). The interconnected lines between genes represent co-expression interrelations, and the PPI network diagram was drawn by Cytoscape (Figure 10).

To further study the functions of leaf angle related genes, the 12 hub genes of this module were analyzed by GO enrichment and KEGG pathways. In GO analysis, the genes were mainly enriched in “Peptide metabolic process”, “rRNA binding”, “Structural constituent of ribosome”, “Structural molecule activity”, “Mitochondrial large ribosomal subunit”, “Mitochondrial ribosome”, “Plastoglobule”, “Large ribosomal

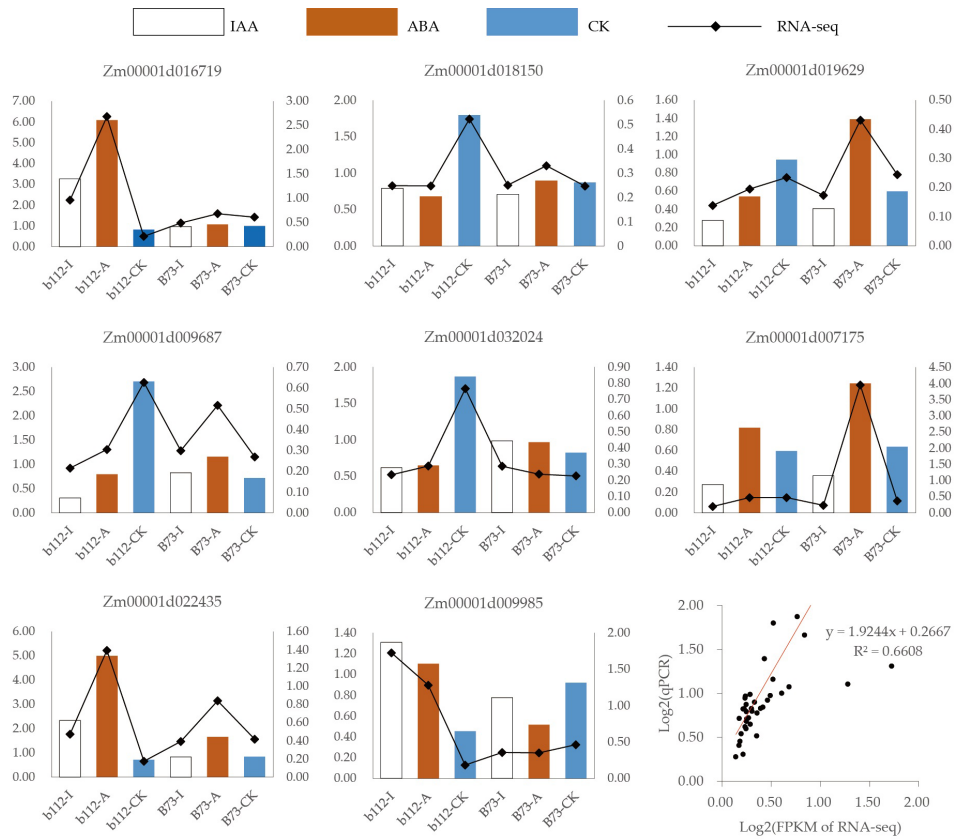

FIGURE 7
qRT-PCR was performed using 8 randomly selected DEGs. Bar and line graphs represent the qRT-PCR and RNA-Seq data, respectively.

subunit", and "Mitochondrial matrix". In KEGG pathway analysis, the hub genes were mainly involved in "Ribosome".

4 Discussion

4.1 *ZmbHLH112* gene regulates maize leaf angle development

Leaf angle is an important agronomic trait in maize, with a smaller leaf angle allowing higher planting density, leading to more efficient light capture and higher yields (Tross et al., 2021). Cao et al. (Cao et al., 2020) cloned maize bHLH TF ZmIBH1-1 by map-based cloning, and found that it was a negative regulator of leaf angle. The combined transcriptomics results revealed 59 ZmIBH1-1-modulated target genes, which were mainly related to the cell wall, cell development, and hormones. Compared with the wild-type, the rice *lc2* (*rice leaf invocation2 (LC2*, three alleles)) mutant has a larger leaf angle due to increased division of paraxial epidermal cells in leaf joints. However, *LC2* is mainly expressed in the lamina joint during leaf development, and is particularly induced by the phytohormones abscisic acid, gibberellin acid, auxin, and brassinosteroids. The mutant lc2 had changed expression level of genes related to cell division and plant hormones due to the lack of the *LC2* gene, resulting in the change of leaf angle (Zhao et al., 2010). These results suggested that the smaller leaf angle of the mutant *bhlh112* compared with wild-type B73 may be caused by the lack of the *ZmbHLH112* gene. In order to verify this hypothesis, we used qRT-PCR to verify the relative expression of *ZmbHLH112*. The relative expression of this gene was the highest in the wild-type leaf angle, indicating that the gene has a regulatory effect on the development of the leaf angle in maize. Transcriptome analysis showed that auxin signal transduction, protein kinase activity, and membrane-related gene expression were down-regulated, which was consistent with the findings of previous studies, indicating that the

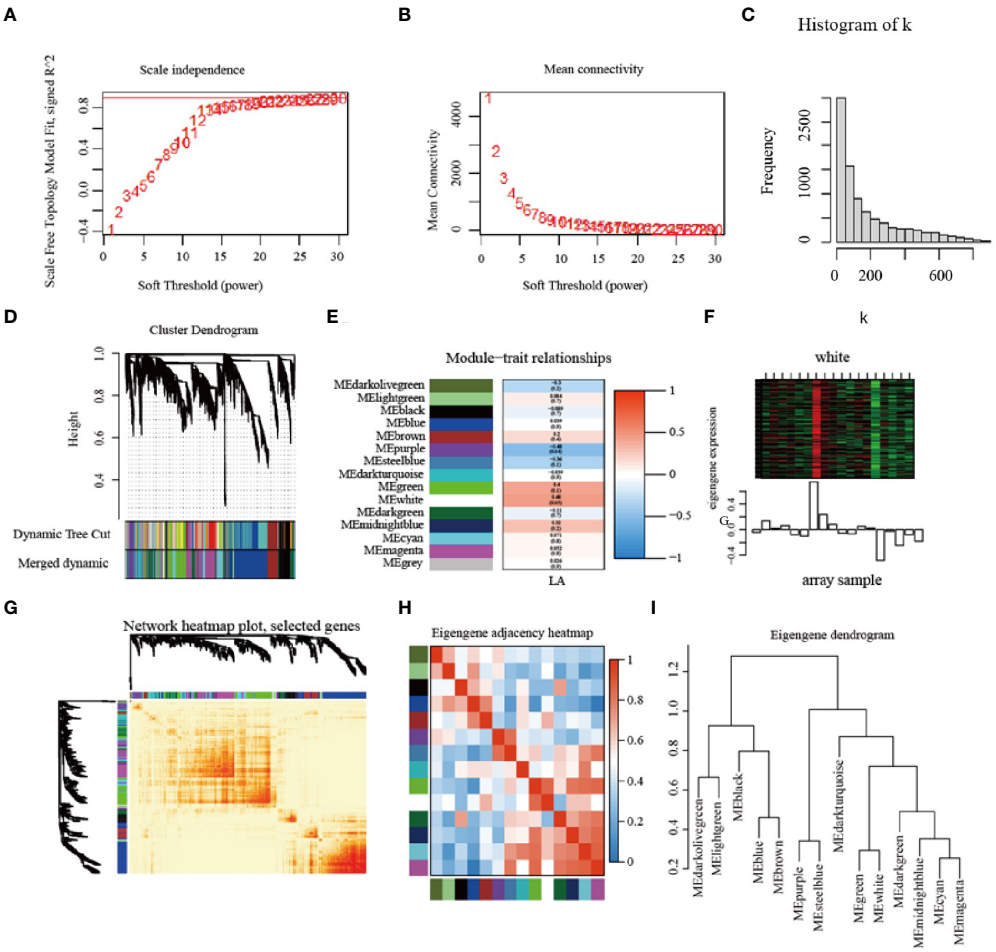

FIGURE 8
Construction of modules based on weighted gene co-expression network analysis. **(A–C)** Soft power value screening of differentially expression genes for LA related co-expression modules; **(D)** Establishment of the cluster dendrogram in LA co-expression mod-ules. **(E)** The correlation between modules and LA; **(F)** White module; **(G)** Network heatmap; **(H, I)** Module clustering. LA = leaf angle.

smaller leaf angle of mutant *bhlh112* was also related to the differential expression of this gene.

4.2 Effect of exogenous IAA on maize leaf angle

The auxin indoleacetic acid (IAA) is critical in regulating the adaxial/abaxial cell growth of leaves in *Arabidopsis* (Ali et al., 2020); it also regulates the growth of *Arabidopsis* hypocotyls by affecting the expression of auxin response factor related genes (Reed et al., 2018). In the current study, the leaf angles of mutant *bhlh112* and wild-type B73 maize V3 stage reached the maximum under 100 μmol·L^{-1} exogenous IAA treatment. Transcriptome analysis showed that, compared with the control, the DEGs in the mutant *bhlh112* were involved in plant hormone signal transduction, flavonoid biosynthesis and some amino acid biosynthesis, with redox activity, hydrolase activity and transmembrane transporter activity, and were also cell membrane components. In addition, the DEGs in the wild-type participate in the cell membrane component, lipid metabolism process, flavonoid biosynthetic process and the composition of plasmodesmata and membrane, and have oxidoreductase activity and catalytic activity. Flavonoids are secondary metabolites, which play a variety of functions in plants and can regulate auxin transport (Mierziak et al., 2014). Our results showed that both the mutant and wild-type genes were involved in flavonoids biosynthesis, which indicated that exogenous IAA may cause an imbalance of endogenous auxin in plants, and flavonoids may be a regulator of auxin homeostasis in maize seedlings. At the same time, differential expression of genes related to cell development and plant hormone signal transduction caused the changes to maize leaf angle.

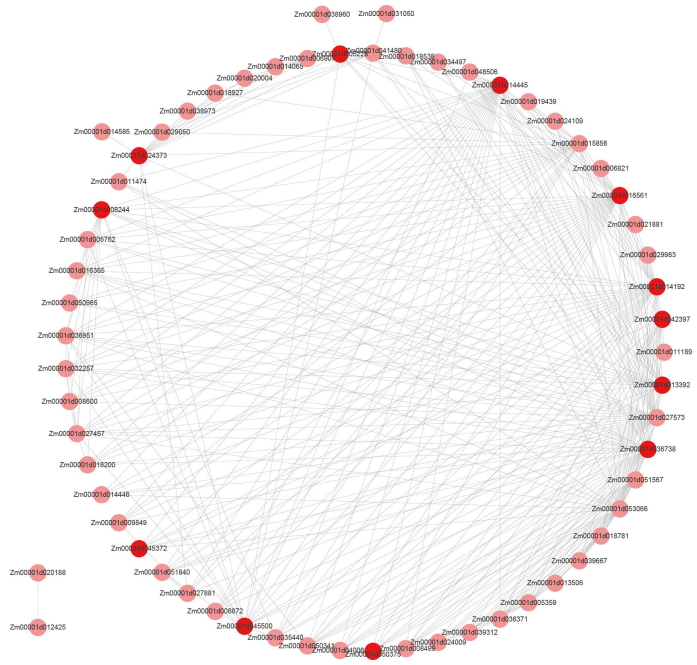

FIGURE 9
Co-expression regulatory network analysis of the white module. Red represents hub genes.

Glucosyltransferase *UGT74D1* affects leaf positioning through modulating auxin homeostasis and regulating transcription of related genes (Jin et al., 2021). *Rice LEAF INCLUSION1 (LC1)*, an IAA amide synthase, maintains auxin homeostasis by binding excess IAA with various amino acids, and then regulates the leaf angle (Zhao et al., 2013). Leaf invocation3 (LC3) containing the SPOC domain cooperatively regulates auxin signals by interacting with LIP1 (LC3-interacting protein 1, a HIT zinc finger domain-containing protein), and maintains auxin homeostasis to regulate lamina joint development in rice (Chen et al., 2018). These results indicate that maintenance of auxin homeostasis play an essential role in regulating leaf angle.

4.3 Effect of exogenous ABA on maize leaf angle

As an important plant hormone, abscisic acid (ABA) participates in the regulation of the physiological processes

TABLE 4 The 12 hub genes of the protein-protein interaction network.

GeneID	ProteinID	Gene description
Zm00001d045500	GRMZM2G048557_P01	39S ribosomal protein L47
Zm00001d013392	GRMZM2G046055_P01	probable histone H2AXa
Zm00001d005228	pco061453, pza02939	Ribosomal protein L22p/L17e-like
Zm00001d024373	GRMZM2G178807_P01	60S ribosomal protein L7-like
Zm00001d050375	csu614a	uncharacterized LOC100285226
Zm00001d045372	GRMZM2G050971_P01	iron-sulfur assembly protein IscA
Zm00001d014445	GRMZM5G845129_P01	protein ACTIVITY OF BC1 COMPLEX KINASE 7, chloroplastic
Zm00001d016561	pco145004	uncharacterized LOC100286235
Zm00001d014192	GRMZM2G120579_P01	uncharacterized LOC100276033
Zm00001d008244	GRMZM2G120857_P01	3-isopropylmalate dehydrogenase
Zm00001d042397	GRMZM2G432390_P01	ABC transporter B family member 26, chloroplastic
Zm00001d036738	GRMZM2G442804_P03	S-adenosyl-L-methionine-dependent methyltransferase superfamily protein

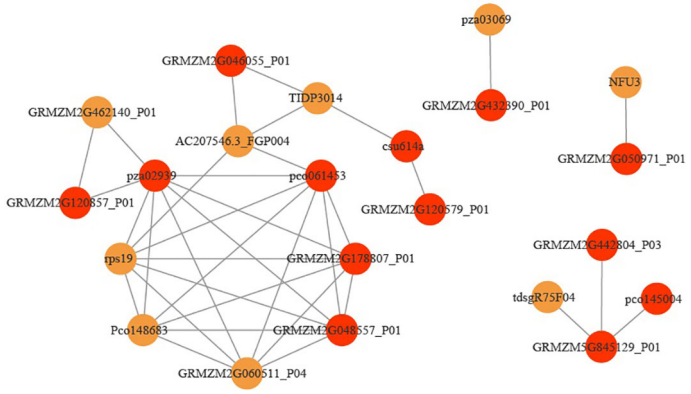

FIGURE 10
Co-expression regulatory network analysis of the hub genes. Red represents hub genes.

required to respond to various abiotic stresses in plants (Huang et al., 2017). ABA can regulate seed development, maturation, and dormancy (Verslues and Zhu, 2007). Under drought stress, ABA can induce stomatal closure and reduce water loss (Guajardo et al., 2016). It also has a defensive effect in plant immunity (Xie et al., 2018). However, there have been very few studies on ABA regulation of plant leaf angle. Li et al. found that ABA regulates the leaf angle of rice by the BR biosynthesis pathway and BR signal transduction (Li et al., 2019a). Here, we found that the leaf angle of mutant *bhlh112* and wild-type maize V3 stage reached the maximum under treatment with 10 μmol·L^{-1} exogenous ABA. Transcriptome analysis showed that, compared with the control, in the mutant *bhlh112*, the up-regulated DEGs mainly enriched the ribosome structural components, small ribosomal subunits, and membranes and membrane components; down-regulated DEGs mainly enriched plasmodesmata, auxin and abscisic acid signaling pathways, membrane transporter activity, and redox activity. In the wild-type, the up-regulated genes mainly enriched catalytic activity, serine pyruvate transaminase activity, glycine biosynthesis pathway and peroxisome, while the down-regulated genes enriched methyltransferase activity, hydrolase activity, lignin biosynthesis pathway, cell wall biogenesis, and cell wall components. These results suggest that ABA may regulate the development of leaf angle through the expression of these differentially expressed genes.

In addition, transcriptome analysis found that most of the differentially expressed genes were oxidoreductase, transferase, hydrolase and ribosome components; there were also genes involved in plant hormone signal transduction, such as *IAA24* (*Zm00001d018973*), a member of the *AUX/IAA* family, and genes related to cell wall structure, including *Zm00001d017033*, is a glycine-rich cell wall structural protein. Therefore, we speculate that ABA may regulate maize leaf angle through IAA signal transduction or BR biosynthesis (Li et al., 2019a).

4.4 *ZmbHLH112* modulates leaf angle through auxin and BR signaling

The development of leaf angle is affected by many factors, including the regulation of exogenous plant hormones and genes. Previous studies have shown that gene regulation occurs mainly through the auxin and brassinolide signal pathways, which then adjust the inclination of the leaf angle (Liu et al., 2019; Tian et al., 2021). The bHLH TFs play a variety of regulatory roles in plant growth and development. Dong et al. (Dong et al., 2018) found that 6 members of the *bHLH* family share a conserved function in regulating the flag leaf angle in rice. This study found that the *ZmbHLH112* gene can repress the expression of *Aux/IAA* related genes (auxin/indole-3-acid acid transcription repressors), promote the binding of auxin response factor (ARF) and DNA, and then regulate the elongation of the leaf angle cells. Aux/IAA and ARF the central components of the auxin signaling pathway and play an important role in auxin mediated growth and development (Liscum and Reed, 2002). Aux/IAA, Gretchen Hagen3 (GH3), and small auxin-up RNA (SAUR) are three types of auxin response genes. SAUR can be rapidly induced by exogenous auxin to promote plant growth and development. We found that exogenous IAA or ABA treatment caused the differential expression of SAUR (Figures 11, 12) (Li et al., 2017; Zhang et al., 2021b). The GH3 protein catalyzes conjugation of amino acids with free IAA, jasmonic acid (JA), and salicylic acid (SA), and auxin response elements (AuxRE) exist in its promoter region. The binding of auxin response factors (ARFs) with AuxRE can regulate the expression of GH3 related genes, regulate auxin homeostasis in plants, and affect the development of the leaf angle (Yu et al., 2018). In addition, we found that in the mutant *bhlh112*, exogenous IAA and ABA treatment caused down-regulation of *TCH4* related genes in the BR biosynthesis pathway; Xyloglucan endoglucokinase/hydrolase (XTH) encoded by the *TCH4* gene is

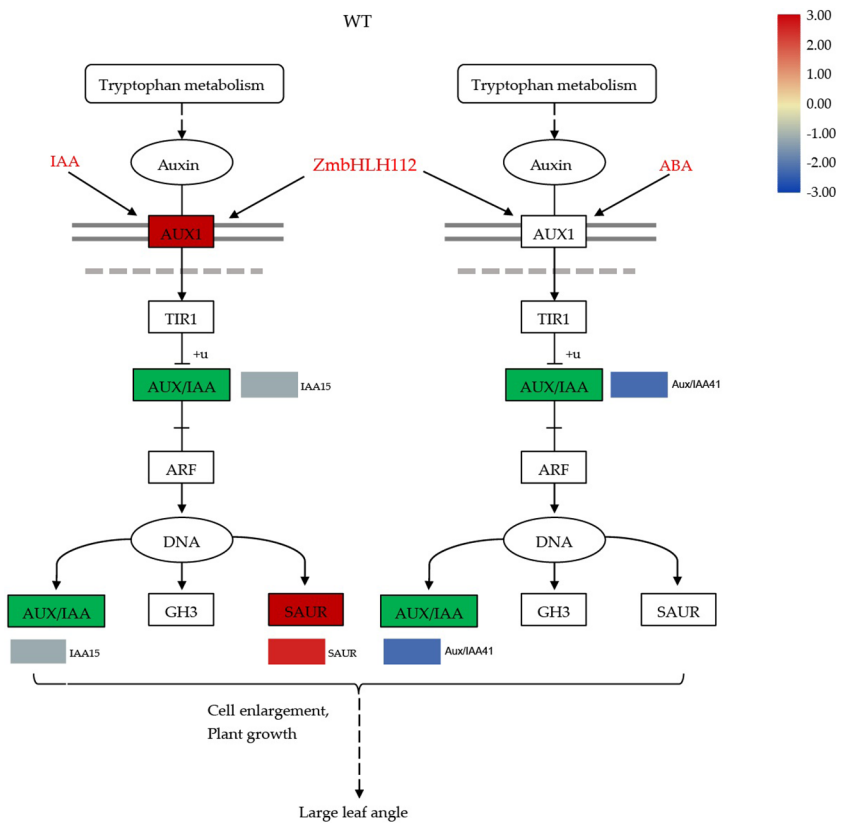

FIGURE 11
Molecular model for the regulation of maize leaf angle development by *ZmbHLH112*. *ZmbHLH112* mediates the auxin signaling pathway. WT: wild-type B73.

the primary component that acts on the cell wall and plays an essential role in plant morphogenesis (Iliev et al., 2002; Zhang et al., 2022). In conclusion, this study revealed that the *ZmbHLH112* gene of the bHLH transcription factor family acts on genes related to cell elongation and cell wall formation in the leaf angle of maize, and regulates the inclination of the leaf angle through the auxin signaling and BR biosynthesis pathways.

4.5 Co-expression network in maize leaf angle

By comparing RNA-seq with maize seeding leaf angle traits, 12 hub genes were identified. The GO enrichment KEGG pathway analysis of these genes showed that most genes had ribosome structure molecular activity, rRNA binding activity, or mitochondrial large ribosomal subunit activity. We speculate that these hub genes may play a role in regulating maize leaf angle through modifying some characteristics of ribosomes. The significant expression of ribosomal subunit related genes was also found when application of exogenous ABA regulated the leaf angle of mutant *bhlh112*, which further indicated that ribosomal subunits may play an important role in leaf development.

The rice gene *RML1* encodes a ribosomal large subunit protein 3B (RPL3B). The free 60s ribosomes and polysomes in the functional defective mutant *rice minute-like1* (*rml1*) were significantly reduced, resulting in plant phenotypic diminution, narrow leaves, and growth retardation. Those results showed that the ribosomal protein RPL3B is required for maintaining normal leaf morphology and plant architecture in rice through its regulation of ribosome biogenesis (Zheng et al., 2016). *Arabidopsis* rRNA methyltransferase CMAL (Chloroplast MraW-Like) is involved in plant development, likely by modulating auxin derived signaling pathways. Knockout of the *CMAL* gene leads to chloroplast functional defects, as well as abnormalities in leaf and root development and in the overall plant morphology (Zou et al., 2020). Kojima et al. identified a new nucleolar protein G-patch domain protein1 (GDP1) in *Arabidopsis*, which is involved in the ribosome biosynthesis pathway. GDP1 functional deletion mutation causes a proliferation defect in leaf primordium cells, and in the adaxial

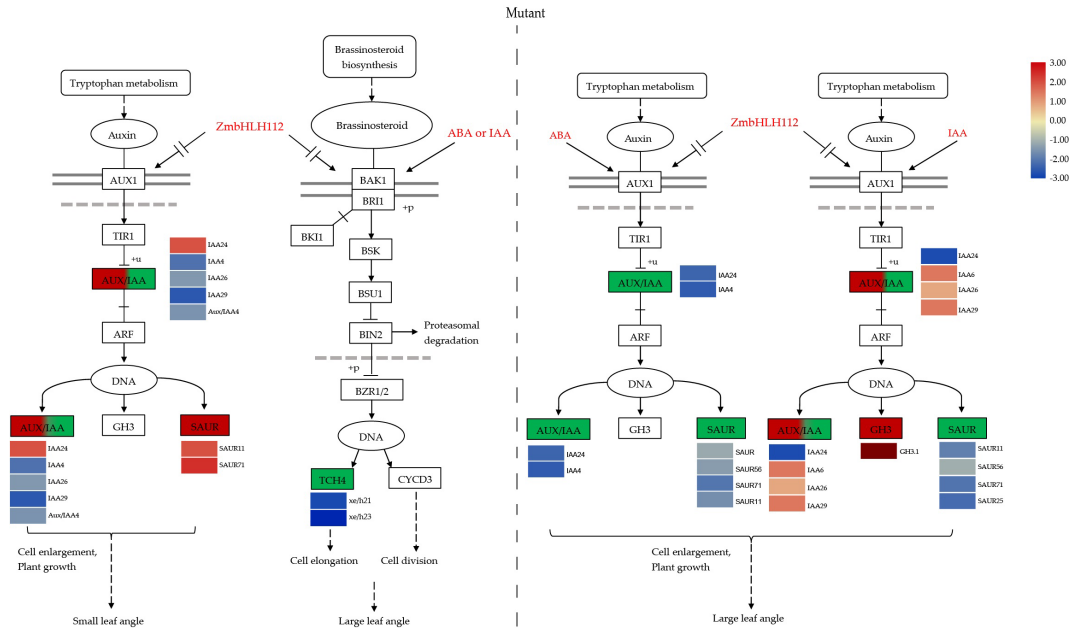

FIGURE 12
Two signaling pathways regulating maize leaf angle in the mutant *bhlh112*: the auxin signaling and BR biogenesis pathways. Mutant: *bhlh112*.

- abaxial polarity regulation of leaves (Kojima et al., 2017). These results showed that the large ribosomal subunit could regulate the development of plant leaves; however, the molecular mechanism of leaf angle adjustment needs further study.

5 Conclusions

In this study, the wild-type B73 produced the mutant *bhlh112* by EMS-induction. Our results showed that the 1241st base G of the *ZmbHLH112* gene in the mutant was mutated into A, whereby tryptophan was mutated into termination codon. Compared with the wild-type, the mutant *bhlh112* had lower plant height and smaller leaf angles. Wild-type and mutant seedlings were treated with exogenous IAA and ABA to screen the optimal concentrations of each, and the functions of *ZmbHLH112* were analyzed by transcriptome sequencing. The results showed that *ZmbHLH112* is related to auxin signal transduction and BR biosynthesis, and involved in the activation of auxin and brassinolide signal pathway related genes and cell growth. Further transcriptome analysis showed that genes involved in cell wall, cell membrane development, plant hormone signal transduction, ribosome biosynthesis, and flavonoid biosynthesis were differentially expressed between the mutant *bhlh112* and wild-type B73, resulting in the change in leaf angles in the mutant. The co-expression network was constructed by WGCNA, and 12 hub genes related to the development of leaf angle were screened; In GO enrichment and KEGG pathways, the genes were mainly enriched in rRNA binding, ribosome biogenesis, Structural constituent of ribosome; Result showed that ribosomal subunits may play an important role in leaf development. This study provides an important finding allowing further elucidation of the molecular mechanism of regulation of leaf angle in maize.

Data availability statement

The data presented in the study are deposited in the SRA at NCBI repository, accession number PRJNA856349. https://dataview.ncbi.nlm.nih.gov/object/PRJNA856349?reviewer=7t6aa2bj0no68d49hjr5bbbkpv.

Author contributions

YP designed the experiments. YZ wrote the manuscript. YZ performed the experiments and analyzed data. XJ, JX, and YW participated in the planting and identification of experimental materials and the critical reading and discussion of the manuscript. All authors contributed to the article and approved the submitted version.

Funding

This research was supported by the industrial support plan for colleges and universities of Gansu, China (No. 2022CYZC-

46), the Fuxi Talent Project of Gansu Agricultural University, China (No. GAUFX-02Y09), and the Lanzhou Science and Technology Bureau (No. 2020-RC-122).

Acknowledgments

We thank the reviewers for the critical review of the manuscripts, and Peng Yunling for her guidance and revision.

Conflict of interest

The authors declare that the research was conducted in the absence of any commercial or financial relationships that could be construed as a potential conflict of interest.

Publisher's note

Supplementary material

The Supplementary Material for this article can be found online at: https://www.frontiersin.org/articles/10.3389/fpls.2022.995815/full#supplementary-material

References

Ali, S., Khan, N., and Xie, L. (2020). Molecular and hormonal regulation of leaf morphogenesis in arabidopsis. *Int. J. Mol. Sci.* 21, 5132. doi: 10.3390/ijms21145132

Cao, Y., Zeng, H., Ku, L., Ren, Z., Han, Y., Su, H., et al. (2020). ZmIBH1-1 regulates plant architecture in maize. *J. Exp. Bot.* 71, 2943–2955. doi: 10.1093/jxb/eraa052

Chen, S. H., Zhou, L. J., Xu, P., and Xue, H. W. (2018). SPOC domain-containing protein leaf inclination3 interacts with LIP1 to regulate rice leaf inclination through auxin signaling. *PloS Genet.* 14, e1007829. doi: 10.1371/journal.pgen.1007829

Dong, H. J., Zhao, H., Li, S. L., Han, Z. M., Hu, G., Liu, C., et al. (2018). Genome-wide association studies reveal that members of bHLH subfamily 16 share a conserved function in regulating flag leaf angle in rice (*Oryza sativa*). *PloS Genet.* 14, e1007323. doi: 10.1371/journal.pgen.1007323

Endo, T., Fujii, H., Sugiyama, A., Nakano, M., Nakajima, N., Ikoma, Y., et al. (2016). Overexpression of a citrus basic helix-loop-helix transcription factor (CubHLH1), which is homologous to arabidopsis activation-tagged bri1 suppressor 1 interacting factor genes, modulates carotenoid metabolism in transgenic tomato. *Plant Sci.* 243, 35–48. doi: 10.1016/j.plantsci.2015.11.005

Fellner, M., Horton, L. A., Cocke, A. E., Stephens, N. R., Ford, E. D., and Van Volkenburgh, E. (2003). Light interacts with auxin during leaf elongation and leaf angle development in young corn seedlings. *Planta* 216, 366–376. doi: 10.1007/s00425-002-0881-7

Friedrichsen, D. M., Nemhauser, J., Muramitsu, T., Maloof, J. N., Alonso, J., Ecker, J. R., et al. (2002). Three redundant brassinosteroid early response genes encode putative bHLH transcription factors required for normal growth. *Genetics* 162, 1445–1456. doi: 10.1093/genetics/162.3.1445

Guajardo, E., Correa, J. A., and Contreras-Porcia, L. (2016). Role of abscisic acid (ABA) in activating antioxidant tolerance responses to desiccation stress in intertidal seaweed species. *Planta* 243, 767–781. doi: 10.1007/s00425-015-2438-6

Guo, X. J., and Wang, J. R. (2017). Global identification, structural analysis and expression characterization of bHLH transcription factors in wheat. *BMC Plant Biol.* 17, 90. doi: 10.1186/s12870-017-1038-y

Heang, D., and Sassa, H. (2012). Antagonistic actions of HLH/bHLH proteins are involved in grain length and weight in rice. *PloS One* 7, e31325. doi: 10.1371/journal.pone.0031325

He, H. Y., Hu, Q., Li, R., Pan, X. B., Huang, B. X., and He, Q. J. (2020). Regional gap in maize production, climate and resource utilization in China. *Field Crops Res.* 254, 107830. doi: 10.1016/j.fcr.2020.107830

Huang, Y., Sun, M. M., Ye, Q., Wu, X. Q., Wu, W. H., and Chen, Y. F. (2017). Abscisic acid modulates seed germination *via* ABA INSENSITIVE5-mediated PHOSPHATE1. *Plant Physiol.* 175, 1661–1668. doi: 10.1104/pp.17.00164

Huang, G., Hu, H., Van De Meene, A., Zhang, J., Dong, L., Zheng, S., et al. (2021). AUXIN RESPONSE FACTORS 6 and 17 control the flag leaf angle in rice by regulating secondary cell wall biosynthesis of lamina joints. *Plant Cell* 33, 3120–3133. doi: 10.1093/plcell/koab175

Huq, E., and Quail, P. H. (2002). PIF4, a phytochrome-interacting bHLH factor, functions as a negative regulator of phytochrome b signaling in arabidopsis. *EMBO J.* 21, 2441–2450. doi: 10.1093/emboj/21.10.2441

Iliev, E. A., Xu, W., Polisensky, D. H., Oh, M. H., Torisky, R. S., Clouse, S. D., et al. (2002). Transcriptional and posttranscriptional regulation of arabidopsis TCH4 expression by diverse stimuli. roles of cis regions and brassinosteroids. *Plant Physiol.* 130, 770–783. doi: 10.1104/pp.008680

Jin, S. H., Hou, B. K., and Zhang, G. Z. (2021). The ectopic expression of arabidopsis glucosyltransferase UGT74D1 affects leaf positioning through modulating indole-3-acetic acid homeostasis. *Sci. Rep.* 11, 1154. doi: 10.1038/s41598-021-81016-x

Kojima, K., Tamura, J., Chiba, H., Fukada, K., Tsukaya, H., and Horiguchi, G. (2017). Two nucleolar proteins, GDP1 and OLI2, function as ribosome biogenesis factors and are preferentially involved in promotion of leaf cell proliferation without strongly affecting leaf adaxial-abaxial patterning in arabidopsis thaliana. *Front. Plant Sci.* 8, 2240. doi: 10.3389/fpls.2017.02240

Li, X., Liu, G., Geng, Y., Wu, M., Pei, W., Zhai, H., et al. (2017). A genome-wide analysis of the small auxin-up RNA (SAUR) gene family in cotton. *BMC Genomics* 18, 815. doi: 10.1186/s12864-017-4224-2

Li, Z., Liu, C., Zhang, Y., Wang, B., Ran, Q., and Zhang, J. (2019b). The bHLH family member ZmPTF1 regulates drought tolerance in maize by promoting root development and abscisic acid synthesis. *J. Exp. Bot.* 70, 5471–5486. doi: 10.1093/jxb/erz307

Li, Q. F., Lu, J., Zhou, Y., Wu, F., Tong, H. N., Wang, J. D., et al. (2019a). Abscisic acid represses rice lamina joint inclination by antagonizing brassinosteroid biosynthesis and signaling. *Int. J. Mol. Sci.* 20, 4908. doi: 10.3390/ijms20194908

Li, H., Sun, J., Xu, Y., Jiang, H., Wu, X., and Li, C. (2007). The bHLH-type transcription factor AtAIB positively regulates ABA response in arabidopsis. *Plant Mol. Biol.* 65, 655–665. doi: 10.1007/s11103-007-9230-3

Li, X., Wu, P. F., Lu, Y., Guo, S. Y., Zhong, Z. J., Shen, R. X., et al. (2020). Synergistic interaction of phytohormones in determining leaf angle in crops. *Int. J. Mol. Sci.* 21, 5052. doi: 10.3390/ijms21145052

Liscum, E., and Reed, J. W. (2002). Genetics of Aux/IAA and ARF action in plant growth and development. *Plant Mol. Biol.* 49, 387–400. doi: 10.1023/A:1015255030047

Liu, K. Y., Cao, J., Yu, K. H., Liu, X. Y., Gao, Y. J., Chen, Q., et al. (2019). Wheat TaSPL8 modulates leaf angle through auxin and brassinosteroid signaling. *Plant Physiol.* 181, 179–194. doi: 10.1104/pp.19.00248

Livak, K. J., and Schmittgen, T. D. (2001). Analysis of relative gene expression data using real-time quantitative PCR and the 2(-delta delta C(T)) method. *Methods* 25, 402–408. doi: 10.1006/meth.2001.1262

Massari, M. E., and Murre, C. (2000). Helix-loop-helix proteins: regulators of transcription in eucaryotic organisms. *Mol. Cell Biol.* 20, 429–440. doi: 10.1128/MCB.20.2.429-440.2000

Mierziak, J., Kostyn, K., and Kulma, A. (2014). Flavonoids as important molecules of plant interactions with the environment. *Molecules* 19, 16240–16265. doi: 10.3390/molecules191016240

Ogo, Y., Itai, R. N., Nakanishi, H., Kobayashi, T., Takahashi, M., Mori, S., et al. (2007). The rice bHLH protein OsIRO2 is an essential regulator of the genes involved in fe uptake under fe-deficient conditions. *Plant J.* 51, 366–377. doi: 10.1111/j.1365-313X.2007.03149.x

Reed, J. W., Wu, M. F., Reeves, P. H., Hodgens, C., Yadav, V., Hayes, S., et al. (2018). Three auxin response factors promote hypocotyl elongation. *Plant Physiol.* 178, 864–875. doi: 10.1104/pp.18.00718

Tian, Q., Luan, J., Guo, C., Shi, X., Deng, P., Zhou, Z., et al. (2021). Corrigendum to "A bHLH protein, OsBIM1, positively regulates rice leaf angle by promoting brassinosteroid signaling". *Biochem. Biophys. Res. Commun.* 581, 120. doi: 10.1016/j.bbrc.2021.10.044

Tross, M. C., Gaillard, M., Zwiener, M., Miao, C., Grove, R. J., Li, B., et al. (2021). 3D reconstruction identifies loci linked to variation in angle of individual sorghum leaves. *PeerJ* 9, e12628. doi: 10.7717/peerj.12628

Verslues, P. E., and Zhu, J. K. (2007). New developments in abscisic acid perception and metabolism. *Curr. Opin. Plant Biol.* 10, 447–452. doi: 10.1016/j.pbi.2007.08.004

Wang, P., Su, L., Gao, H., Jiang, X., Wu, X., Li, Y., et al. (2018). Genome-wide characterization of bHLH genes in grape and analysis of their potential relevance to abiotic stress tolerance and secondary metabolite biosynthesis. *Front. Plant Sci.* 9, 64. doi: 10.3389/fpls.2018.00064

Xie, K., Li, L., Zhang, H., Wang, R., Tan, X., He, Y., et al (2018). Abscisic acid negatively modulates plant defence against rice black-streaked dwarf virus infection by suppressing the jasmonate pathway and regulating reactive oxygen species levels in rice. *Plant Cell Environ.* 41, 2504–2514. doi: 10.1111/pce.13372

Yang, X. Q., Zhi, H., Zhang, H., and Sun, J. M. (2019). Research progress on chemical constituents, pharmacological activity and utilization status of different parts of corn. *Jilin J. Chin. Med.* 39, 837–840. doi: 10.13463/j.cnki.jlzyy.2019.06.038

Yu, D., Qanmber, G., Lu, L., Wang, L., Li, J., Yang, Z., et al. (2018). Genome-wide analysis of cotton GH3 subfamily II reveals functional divergence in fiber development, hormone response and plant architecture. *BMC Plant Biol.* 18, 350. doi: 10.1186/s12870-018-1545-5

Zhang, Q. Q., Zhu, J. H., Ni, Y. M., and Zhang, Z. L. (2011). The structure and function of plant bHLH transcription factors. *J. Trop. Subtropical Bot.* 19, 84–90.

Zhang, M., Jin, Y., Ma, Y., Zhang, Q., Wang, Q., Jiang, N., et al. (2021a). Identification of QTLs and candidate genes associated with leaf angle and leaf orientation value in maize (Zea mays l.) based on GBS. *Trop. Plant Biol.* 14, 34–49. doi: 10.1007/s12042-020-09270-3

Zhang, H., Yu, Z., Yao, X., Chen, J., Chen, X., Zhou, H., et al. (2021b). Genome-wide identification and characterization of small auxin-up RNA (SAUR) gene family in plants: evolution and expression profiles during normal growth and stress response. *BMC Plant Biol.* 21, 4. doi: 10.1186/s12870-020-02781-x

Zhang, C., He, M., Jiang, Z., Liu, L., Pu, J., Zhang, W., et al. (2022). The xyloglucan Endotransglucosylase/Hydrolase gene XTH22/TCH4 regulates plant growth by disrupting the cell wall homeostasis in arabidopsis under boron deficiency. *Int. J. Mol. Sci.* 23, 1250. doi: 10.3390/ijms23031250

Zhao, S. Q., Hu, J., Guo, L. B., Qian, Q., and Xue, H. W. (2010). Rice leaf inclination2, a VIN3-like protein, regulates leaf angle through modulating cell division of the collar. *Cell Res.* 20, 935–947. doi: 10.1038/cr.2010.109

Zhao, J. R., Wang, R. H., and Liu, X. X. (2016). Current situation of maize industry and development trend of biological breeding in China *Biotechnology & Business* 3, 45–52.

Zhao, S. Q., Xiang, J. J., and Xue, H. W. (2013). Studies on the rice LEAF INCLINATION1 (LC1), an IAA-amido synthetase, reveal the effects of auxin in leaf inclination control. *Mol. Plant* 6, 174–187. doi: 10.1093/mp/sss064

Zheng, M., Wang, Y., Liu, X., Sun, J., Wang, Y., Xu, Y., et al. (2016). The RICE MINUTE-LIKE1 (RML1) gene, encoding a ribosomal large subunit protein L3B, regulates leaf morphology and plant architecture in rice. *J. Exp. Bot.* 67, 3457–3469. doi: 10.1093/jxb/erw167

Zou, M., Mu, Y., Chai, X., Ouyang, M., Yu, L. J., Zhang, L., et al. (2020). The critical function of the plastid rRNA methyltransferase, CMAL, in ribosome biogenesis and plant development. *Nucleic Acids Res.* 48, 3195–3210. doi: 10.1093/nar/gkaa129

frontiers | Frontiers in Plant Science

TYPE Correction
PUBLISHED 24 November 2022
DOI 10.3389/fpls.2022.1089402

OPEN ACCESS

EDITED AND REVIEWED BY
Ana Butron,
Spanish Council for Scientific Research (MBG-CSIC), Spain

*CORRESPONDENCE
Yunling Peng
pengyl@gsau.edu.cn

SPECIALTY SECTION
This article was submitted to Plant Breeding, a section of the journal Frontiers in Plant Science

RECEIVED 04 November 2022
ACCEPTED 14 November 2022
PUBLISHED 24 November 2022

CITATION
Zhang Y, Ji X, Xian J, Wang Y and Peng Y (2022) Corrigendum: Morphological characterization and transcriptome analysis of leaf angle mutant *bhlh112* in maize [*Zea mays* L.]. *Front. Plant Sci.* 13:1089402. doi: 10.3389/fpls.2022.1089402

Corrigendum: Morphological characterization and transcriptome analysis of leaf angle mutant *bhlh112* in maize [*Zea mays* L.]

Yunfang Zhang[1,2,3], Xiangzhuo Ji[1,2,3], Jinhong Xian[1], Yinxia Wang[1,2,3] and Yunling Peng[1,2,3]*

[1]College of Agronomy, Gansu Agricultural University, Lanzhou, China, [2]Gansu Provincial Key Laboratory of Aridland Crop Science, Gansu Agricultural University, Lanzhou, China, [3]Gansu Key Laboratory of Crop Improvement & Germplasm Enhancement, Gansu Agricultural University, Lanzhou, China

KEYWORDS

maize (*Zea mays* L.), *bhlh112* mutant, transcriptomics, exogenous hormones, co-expression network

A Corrigendum on

Morphological characterization and transcriptome analysis of leaf angle mutant *bhlh112* in maize [*Zea mays* L.]

by Zhang Y, Ji X, Xian J, Wang Y and Peng Y (2022) Front. Plant Sci. 13:995815. doi: 10.3389/fpls.2022.995815

In the published article, there were 2 errors. A sentence in the **Conclusions** of the article was not revised in time, resulting in a difference from the analysis of the results in the text. This sentence previously stated:

"Our results showed that the 1241st base G of the *ZmbHLH112* gene in the mutant was mutated into A, and glycine was mutated into aspartic acid."

The corrected sentence appears below:

"Our results showed that the 1241st base G of the *ZmbHLH112* gene in the mutant was mutated into A, whereby tryptophan was mutated into termination codon."

There was also an error in the caption of Figure 2. This sentence previously stated:

"(E) Corresponding leaf angle in (D, F) Mature ear of wild type and mutant."

The corrected sentence appears below:

"(E) Corresponding leaf angle in D; (F) Mature ear of wild type and mutant."

The authors apologize for these errors and state that this does not change the scientific conclusions of the article in any way. The original article has been updated.

Publisher's note

frontiers | Frontiers in Plant Science

TYPE Original Research
PUBLISHED 26 October 2022
DOI 10.3389/fpls.2022.992799

OPEN ACCESS

EDITED BY
Manje S. Gowda,
The International Maize and Wheat Improvement Center (CIMMYT), Kenya

REVIEWED BY
Darshan Sharma,
Department of Primary Industries and Regional Development of Western Australia (DPIRD), Australia
Frank White,
University of Florida, United States

*CORRESPONDENCE
Pengcheng Li
pcli@yzu.edu.cn
Siyi Guo
guosiyi@henu.edu.cn

†These authors have contributed equally to this work

SPECIALTY SECTION
This article was submitted to Plant Breeding, a section of the journal Frontiers in Plant Science

RECEIVED 13 July 2022
ACCEPTED 30 September 2022
PUBLISHED 26 October 2022

CITATION
Zhang X, Zhu T, Li Z, Jia Z, Wang Y, Liu R, Yang M, Chen Q-B, Wang Z, Guo S and Li P (2022) Natural variation and domestication selection of *ZmSULTR3;4* is associated with maize lateral root length in response to salt stress.
Front. Plant Sci. 13:992799.
doi: 10.3389/fpls.2022.992799

Natural variation and domestication selection of *ZmSULTR3;4* is associated with maize lateral root length in response to salt stress

Xiaomin Zhang[1,2†], Tianze Zhu[3,4†], Zhi Li[1,2†], Zhongtao Jia[5], Yunyun Wang[3,4], Runxiao Liu[2], Mengling Yang[2], Qing-Bin Chen[1,2], Zhenjie Wang[1], Siyi Guo[1,2*] and Pengcheng Li[3,4*]

[1]Sanya Institute, Henan University, Sanya, Hainan, China, [2]State Key Laboratory of Crop Stress Adaptation and Improvement, School of Life Sciences, Henan University, Kaifeng, China, [3]Jiangsu Key Laboratory of Crop Genetics and Physiology/Key Laboratory of Plant Functional Genomics of the Ministry of Education/Jiangsu Key Laboratory of Crop Genomics and Molecular Breeding, Yangzhou University, Yangzhou, China, [4]Jiangsu Co-Innovation Center for Modern Production Technology of Grain Crops, Yangzhou University, Yangzhou, China, [5]Key Laboratory of Plant-Soil Interactions, Ministry of Education (MOE), College of Resources and Environmental Sciences, National Academy of Agriculture Green Development, China Agricultural University, Beijing, China

Soil salinity is a major constraint that restricts crop productivity worldwide. Lateral roots (LRs) are important for water and nutrient acquisition, therefore understanding the genetic basis of natural variation in lateral root length (LRL) is of great agronomic relevance to improve salt tolerance in cultivated germplasms. Here, using a genome-wide association study, we showed that the genetic variation in *ZmSULTR3;4*, which encodes a plasma membrane-localized sulfate transporter, is associated with natural variation in maize LRL under salt stress. The transcript of *ZmSULTR3;4* was found preferentially in the epidermal and vascular tissues of root and increased by salt stress, supporting its essential role in the LR formation under salt stress. Further candidate gene association analysis showed that DNA polymorphisms in the promoter region differentiate the expression of *ZmSULTR3;4* among maize inbred lines that may contribute to the natural variation of LRL under salt stress. Nucleotide diversity and neutrality tests revealed that *ZmSULTR3;4* has undergone selection during maize domestication and improvement. Overall, our results revealed a regulatory role of *ZmSULTR3;4* in salt regulated LR growth and uncovered favorable alleles of *ZmSULTR3;4*, providing an important selection target for breeding salt-tolerant maize cultivar.

KEYWORDS

maize (*Zea mays*), natural variation, salt stress, lateral root length, domestication selection, *ZmSULTR3;4*

Introduction

Maize (*Zea mays* L.) is a particularly important cereal crop planted worldwide, providing key resources for human food, animal feed and industrial products. Maize yield, however, is vulnerable to various environmental stresses. Among them, salt stress, which can be induced by excessive irrigation practices as well as factors related to climate change, could have a severe impact on corn production and has attracted increasing attention from researchers worldwide (Zhu, 2016; Ismail and Horie, 2017). A considerable number of studies have demonstrated that salt accumulation in soil solution not only provokes water deficit and nutrient imbalance, but also causes ionic toxicity to plant cells. This leads to plant metabolism disorder, impaired oxidation–reduction system, decreased photosynthesis, and ultimately suppressed plant growth and development (Yang and Guo, 2018; Van Zelm et al., 2020). In particular, severe salt stress occurring during the seedling stage is detrimental to developing seedlings (Sandhu et al., 2020; Chen et al., 2021). For instance, studies have shown that maize is hypersensitive to salinity stress (Farooq et al., 2015; Luo et al., 2019). Therefore, it is essential to identify the genetic variation contributing to maize salt tolerance in order to genetically improve the trait.

Previous studies have revealed that the exclusion of Na^+ from the shoot is critical to the salt tolerance of crops. Allelic variation affecting the transcription of *HKT1*, *CIPK13* and *HAK4* has been reported to play a key role in sodium exclusion and, therefore, salinity tolerance (Rus et al., 2006; Munns et al., 2012; Roy et al., 2013; Zhang et al., 2019). Recently, *ZmSTL1*, a dirigent protein that confers variation in casparian strip thickness, was demonstrated to regulate transpiration-dependent Na^+ exclusion, thereby improving the salt tolerance of maize plants (Wang et al., 2022). Another widely used proxy for salinity tolerance is the developmental plasticity of roots in response to salt stress (Julkowska et al., 2017; Li et al., 2021). Plant roots not only provide anchorage and participate in the uptake of water and mineral nutrients, but also act as the first organ sensing the salinity stress (Villordon et al., 2014; Wang et al., 2021). In the model plant Arabidopsis, the root system comprises a single embryonically formed primary root (PR) and several post-embryonically developed LRs of different orders. These traits describe the overall three-dimensional structure of root system, which enables plants to optimize resource acquisition and stress avoidance/escape (Julkowska et al., 2017; Jia and Von Wiren, 2020). LRs are specified in the pericycle cells of plants, with the exception in cereals that endodermal cells also contribute to LR formation (Van Norman et al., 2013; Yu et al., 2016). In general, LR development involves three developmental processes: LR primordium (LRP) initiation, LRP establishment and progression, and postemergence elongation (Casimiro et al., 2003). All these LR developmental checkpoints are highly susceptible to intrinsic and external environmental cues, such as nutrient availability and soil salinity (Karlova et al., 2021; Jia et al., 2022).

Maize establishes a typical fibrous root system composed of embryonic PR, seminal roots (SRs) as well as post-embryonic shoot-borne crown roots (CRs) and brace roots (BRs). All these root types undergo higher-order branching of LRs that greatly extend the exploration of soil volume (Bellini et al., 2014). Growth inhibition of maize root system as a whole by salt stress has been reported, although root-type specific plastic response has been observed (Zhang et al., 2015). Since lateral roots play an important role in water use efficiency, ion exclusion, and acquisition of water and macronutrients from soil, it is reasonable that changes in LR growth are of great adaptive value to plant survival under salt stress conditions (Faiyue et al., 2010; Ristova and Busch, 2014). Therefore, understanding the genetic components and exploring the natural variants that can enhance LR growth are of great importance for breeding stress-resilient crops.

In the present study, we showed by genome-wide association study (GWAS) that *ZmSULTR3;4* is associated with natural variation in LRL under salt stress condition. *ZmSULTR3;4* encodes a plasma membrane (PM)-localized sulfate transporter, with a preferential expression in the epidermal and vascular tissues of root. We further re-sequenced *ZmSULTR3:4* in 32 teosintes, 71 landraces, and 280 inbred lines, and a gene-based association analysis was conducted in inbred lines. The objectives of this study aimed to (1) identify natural variations in *ZmSULTR3:4* associated with LRL under salt stress condition; (2) examine the *ZmSULTR3:4* nucleotide diversity among teosintes, landraces, and inbred lines. (3) explore the role of *ZmSULTR3:4* in maize domestication and improvement. These findings may lay a foundation for further development of molecular markers for the genetic improvement of maize tolerance to soil salinilty.

Materials and methods

Plant materials and phenotypic evaluation

In this study, 32 teosintes, 71 landraces, and 280 maize inbred lines were used to evaluate LR length (LRL) at the seedling stage. LRL was collected with a paper roll system as previously described (Li et al., 2021). Briefly, seeds of uniform size were sterilized in 10% (v/v) H_2O_2 solution for 20 min following by washing with distilled water at least three times. They were then soaked in saturated $CaSO_4$ for 6 h to synchronize germination, and further placed on moist filter paper for germination at 28°C and 80% relative humidity for 2 days in darkness. Afterwards, eight uniformly germinating seeds were transferred to the paper, which were vertically placed in a 39.5 × 29.5 × 22.5 cm black incubators containing 7.5 L

Hoagland nutrient solution. The Hoagland nutrient solution were consisted of 2.0 mM $Ca(NO_3)_2$, 0.75 mM K_2SO_4, 0.65 mM $MgSO_4$, 0.1 mM KCl, 0.25mM KH_2PO_4, 1×10^{-3} mM H_3BO_3, 1×10^{-3} mM $MnSO_4$, 1×10^{-4} mM $CuSO_4$, 1×10^{-3} mM $ZnSO_4$, 5×10^{-6} mM $(NH_4)_6Mo_7O_{24}$ and 0.1 mM Fe-EDTA. Five days after germination, the distilled water was replaced with Hoagland solution supplemented with or without 100 mmol·L^{-1} NaCl. The nutrient solution was refreshed every other day. Six individuals were harvested 14 days after germination. The roots were separated from the shoots and stored at 4°C. Then, the roots were scanned and analyzed using WinRHIZO software (Pro 2004b, Canada). Each treatment contained two independent biological replicates.

GWAS and *ZmSULTR3;4*-candidate gene-based association mapping

A GWAS of maize LRL was performed by analyzing a maize natural population comprising 280 inbred lines (Li et al., 2019). LRL data were obtained from two replicated experiments. The association mapping panel was genotyped by genotyping-by-sequencing (GBS). After a quality control step (missing rate ≤ 20%), a total of 140,714 genomic single nucleotide polymorphisms (SNPs) were used for the GWAS with a minor allele frequency (MAF) ≥ 0.05, and their association with LRL was calculated by TASSEL 5.0 (Bradbury et al., 2007). The standard mixed linear model (MLM) was used, in which population structure (Q) and kinship (K) were estimated according to previous research (Bradbury et al., 2007; Liu et al., 2013). The genome-wide significant threshold was set as 1.96×10^{-5} (1/n, n represents the effective number of SNPs) as previously described (Li et al., 2021).

Genomic DNA was extracted from young leaves of teosintes, landraces, and inbred lines using the cetyltrimethylammonium bromide (CTAB) method. *ZmSULTR3;4*-based association mapping was performed with 280 maize inbred lines. The *ZmSULTR3;4* gene was resequenced using targeted sequence capture technology on the NimbleGen platform by Beijing Genomics Institute (BGI) Life Tech Co., China (Choi et al., 2009). The genomic sequence of *ZmSULTR3;4* (*GRMZM2G444801*) of the B73 inbred line was used as a reference for target sequence capture. Polymorphisms including SNPs and insertions/deletions (InDels) with a minor allele frequency (MAF) ≥ 0.05 were extracted and their associations with LRL was analyzed by TASSEL 5.0 using the standard MLM.

Sequence analysis, genetic diversity analysis and neutral evolution test

MAFFT software was used to align the *ZmSULTR3;4* gene sequences, and BioEdit was used for manual improvement (Katoh and Standley, 2013). The gene features (5'-untranslated region (UTR), 3'-UTR, introns and exons) were demarcated according to the gene annotations of MaizeGDB (B73, AGPv3.31). DNASP 5.0 software was employed for sequence polymorphism analysis, genetic diversity analysis and neutral evolution test (Librado and Rozas, 2009). π and θ were used to evaluate the genetic diversity within individual population. The Tajima's D as well as Fu and Li's test were applied in the neutrality tests (Tajima and Genetics, 1989; Fu and Li, 1993).

Identification of ZmSULTR proteins in the maize genome and phylogenetic analysis

Twenty-four sulfate transporter protein sequences from Arabidopsis and rice were used as references to search for ZmSULTR proteins in MaizeGDB (http://www.maizegdb.org/). The 12 SULTR proteins in Arabidopsis were downloaded from TAIR 10 (http://www.arabidopsis.org), and 12 SULTR proteins in rice were retrieved from the Phytozome database v10.0 (http://www.phytozome.net/eucalyptus.php). The full-length amino acid sequences of 32 SULTR members identified above were aligned with the Clustal X 1.83 software. Finally, the phylogenetic tree was constructed using the neighbor-joining method in MEGA-X with the default parameters.

Expression profiling and RNA-seq analysis

The expression profiling of eight *ZmSULTR*s in various tissues were analyzed using the previously reported genome-wide gene expression profile of maize inbred line B73. A concise description of the tissues collected and sampling to create the gene atlas is presented in Table 1 and Table S1 of the published article (Sekhon et al., 2011). Expression data of 15 tissues from 60 developmental stages were collected and combined. The average normalized expression values of each gene in different tissues were obtained. For maize RNA-seq analysis, the uniform seeds of the maize inbred line B73 were selected and sterilized with 10% H_2O_2 for 30 min. The seeds were rinsed three times with distilled water to remove H_2O_2 from the surface of the seeds. The sterilized seeds were soaked in saturated $CaSO_4$ for 6 h to promote germination and then placed on moist filter paper at 28°C and 80% relative humidity for two days. Eight germinated seeds were rolled up with brown germinating paper. The hydroponic experiment was conducted in an incubator at 28/22°C (day/night) with a relative humidity of 60% and a light intensity of 400 μmol.m^{-2}.s^{-1}. Hoagland solution was used instead of distilled water on day 3. At the same time, PEG 8000 solution (-0.8 MPa) was added to simulate soil drought stress, and the incubator was set at 40°C as the daytime temperature and 35°C for night to simulate a hot

10.3389/fpls.2022.992799

TABLE 1 List of parameters for the nucleotide polymorphism analysis of *ZmSULTR3;4*.

Parameters	Upstream	5'UTR	Coding region	3'UTR	Downstream	Entire region
Total length of amplicons (bp)	2252	255	5054	412	742	8715
Number of all of the sequence vanants	454	33	497	46	89	1119
Frequency of all of the sequence variants	0.202	0.129	0.098	0.112	0.120	0.128
Number of nucleotide substitutions (bp)	356	19	391	23	55	844
Frequency of polymorphic sites per bp	0.158	0.075	0.077	0.056	0.074	0.097
Number of InDels	98	14	106	23	34	275
Number of InDel sites	846	42	504	69	261	1722
Average InDel length	12.48	4.429	5.472	3.826	10.382	8.385
Frequency of indels per bp	0.044	0.055	0.021	0.056	0.046	0.032
$\pi \times 1000$	17.83	1.76	7.02	8.34	5.65	9.15
$\theta \times 1000$	46.72	15.11	16.04	12.28	40.68	23.33
Tajima's D	-1.893*	-2.240**	-1.723	-0.825	-2.466**	-1.874*
Fu and Li's D *	-7.103**	-6.419**	-6.774**	-3.334**	-4.077**	-7.360**
Fu and Li's F *	-5.049**	-5.7003**	-4.753**	-2.780*	-3.996**	-5.072**

*denotes statistical significance at the $p < 0.05$ level; ** denotes statistical significance at the $p < 0.01$ level.

environment or 15°C as the daytime temperature and 10°C for night to simulate a cold environment. For the salt stress, the distilled water was replaced with Hoagland solution supplemented with 100 mmol·L^{-1} NaCl. Two independent biological replicates were set for each treatment. Tissues were collected from 30 roots and pooled for RNA-seq analysis. Total RNA was extracted using TRIzol reagent (Biotopped), and RNA integrity was assessed by a Bioanalyzer 2100 (Agilent). The 100-bp paired-end Illumina sequencing was performed at Berry Genomics (Beijing).

For qPCR analysis of *ZmSULTR3;4*, root samples of A404 and A207 were collected after 24 h treatment with or without 100 mmol·L^{-1} NaCl. The growth procedure of plants were identical to phenotypic screening of LRL in natural population. Total RNA was isolated as mentioned above. cDNA was obtained using M-MLV Reverse Transcriptase, and qRT–PCR was performed using a SYBR Premix Ex Taq Kit (Takara) on a Step One System (Applied Biosystems, Shanghai, China). The $2^{-\Delta\Delta Ct}$ was used to calculate the relative expression of gene. Primer used for *ZmSULTR3;4* and *ZmUBI2* as internal control were listed in Supplementary Table S1.

RNA *in situ* hybridization

Tissue embedding and RNA *in situ* hybridization were conducted as described by Gu et al., 2013. Briefly, the root tissues of 7-d-old hydroponically grown B73 plants were fixed in FAA for 12 h at 4°C. Then, the root tissues were embedded, and sectioned with a sliding slicer. The slides were dewaxed, digested with proteinase K (Roche), dehydrated with gradient ethanol, and hybridized by sense and antisense probes. After being washed, the slides were incubated with anti-digoxigenin-AP Fab fragments. Finally, the immunological detection was performed using the NBT/BCIP. The digoxigenin (DIG)-labeled RNA probes were listed in Supplementary Table S1.

Subcellular localization and transient promoter activity assay of *ZmSULTR3;4*

The protoplast transient expression system were used for protein subcellular localization and promoter activity analysis. The coding sequence (CDS) of *ZmSULTR3;4* was cloned into *pGreenII-Ubi : GFP* vector by the *BamH* I site for protein subcellular localization. Protoplasts were isolated and collected from 14-day-old etiolated leaves of maize inbred lines (B73) as previously described (Yoo et al., 2007; Zhang et al., 2020). After a 14 h incubation, transformed protoplasts were counterstained with membrane dye FM4-64 (10 μM) for 1 min and then imaged with a confocal microscope (Leica TCS SP5).

For promoter activity assay, the ~1.3-kb and ~0.8-kb promoter fragments of *ZmSULTR3;4* were amplified from A404 and A207, respectively, and inserted in the upstream of *LUC* gene in the *pGreenII 0800-LUC* vector cleaved by the *Spe* I site. The transfection of protoplasts was conducted as above described. The Renilla luciferase (REN) driven by the 35S promoter was used as internal control to calculate the transfection efficiency. The detection of LUC signals were carried out as previously described (Chen et al., 2022). Four biological replicates were set up for each construct.

Statistical analysis

The unpaired two-tailed Student's *t* test was used to compare the differences in gene expression levels, LRL, and LUC acivity

between the control and experimental groups. The Tajima's D as well as Fu and Li's test were applied to determine whether *ZmSULTR3:4* underwent selection. The data were considered different based on a threshold values of $p < 0.05$ and $p < 0.01$, as indicated by * and **, respectively.

Results

ZmSULTR3;4 is associated with LRL under salt stress condition

In our previous study, considerable phenotypic variation in LRL was revealed by analyzing a natural maize population under normal and salt stress conditions (Li et al., 2021). To further identify genes associated with variation in maize LRL, GWAS were performed on a natural maize population consisting of 280 inbred lines under normal and salt stress condition. Using a standard mixed linear model (MLM) incorporating population structure (Q) and kinship (K) as covariates, two SNPs within *GRMZM2G444801* on chromosome 9 were identified to be associated with LRL under salt stress condition, but not under normal condition (Figure 1 and Supplementary Figure S1). *GRMZM2G444801* encodes a protein phylogenetically closely related AtSULTR3;4 in Arabidopsis (Figure 2A). The gene therefore was named *ZmSULTR3;4*. Notably, the expression of *ZmSULTR3;4* in roots was upregulated by salt treatment in six randomly selected inbred lines (Supplementary Figure S2), suggesting that *ZmSULTR3;4* may play a key role in plant salt tolerance.

Expression patterns of *ZmSULTRs* and response to various stresses

Using Arabidopsis SULTR protein sequences as query to blast against maize database, eight putative *SULTR* genes were identified in the maize genome (Figure 2A). *SULTR* genes have been shown to play key roles in plant development, as well as in response to stress. To gain insights into the function of *ZmSULTR* genes, the tissue-specific expression patterns from the available transcriptomic data of maize B73 were evaluated. An expression heatmap of the eight *ZmSULTR* genes in different tissues at various developmental stages was constructed under normal growth condition. The results indicated that all *ZmSULTRs* showed a broad expression pattern in the tissues analyzed (Figure 2B). Additionally, genes clustered together showed similar expression patterns. Genes in class I were expressed at relatively high levels in the shoot apical meristem (SAM), young stems, internodes, tassels, anthers, and leaves but at low levels in endosperm and 16- to 24-day whole seeds. Genes in class II were expressed at relatively high levels in the silk, husk, seeds, and 2- to 14-day whole seeds but at low levels in the germinating seeds.

Transcriptome analysis was further conducted using maize seedling leaves to evaluate responses of *ZmSULTR* genes to different abiotic stresses, including salt, drought, heat, and cold. The results showed that *ZmSULTR3;4*, *ZmSULTR3;1* and *ZmSULTR1;3* were strongly induced by heat stress. *ZmSULTR3;3* and *ZmSULTR1;2* were induced by salt and cold, while they were downregulated by heat. In addition, *ZmSULTR3;5* was upregulated by drought and cold, but downregulated by salt and heat. Interestingly, the expression of *ZmSULTR1;1* and *ZmSULTR2;1* was downregulated by all types of stresses (Figure 2C). The expression of the eight *ZmSULTR* genes in response to salt stress was further examined in the roots of maize plants under salt stress condition (Figure 2D). Strong upregulation was found for *ZmSULTR1;2*, *ZmSULTR3;4*, and *ZmSULTR3;5* in the roots, hinting that these three genes may play a critical role in the root response to salt stress. In contrast, transcript level of *ZmSULTR1;1/1;3/2;1/3;1/3;3* were reduced upon salt treatment. Collectively, these results indicate that *ZmSULTRs* may play important roles in plant development and adaptation to different types of stresses.

Given the strong association of *ZmSULTR3;4* with LRL under salt stress (Figure 1), we focus our study on *ZmSULTR3;4* in the present study. To gain insights into the function of *ZmSULTR3;4*, we then probe the tissue-specific expression of *ZmSULTR3;4* in roots of B73 using *in situ* mRNA hybridization. Results indicated that the sense probes of *ZmSULTR3;4* did not produce detectable hybridization signals (Figure 3A), while the strong signal of the antisense probe demonstated that *ZmSULTR3;4* was highly expressed in epidermal cells of the apical root zone and preferentially in the stele, especially in the pericycle cells and xylem parenchyma, but was absent in the cortex. Consistently, maize microarray data in the eFP browser confirmed that *ZmSULTR3;4* was highly expressed in the stele of roots and faintly expressed in the cortex (Supplementary Figure 4). We further transiently expressed *ZmSULTR3;4*-GFP fusion under the control of the strong constitutive *ZmUbi* promoter in maize leaf protoplasts to investigate the subcellular localization of *ZmSULTR3;4*. The Green fluorescence signal of ZmSULTR3;4-GFP overlapped well with the membrane marker FM4-64, indicating that ZmSULTR3;4 is a plasma membrane-bound protein (Figure 3B).

Expression variation of *ZmSULTR3;4* associates with LRL under salt stress condition

The association of SNPs in *ZmSULTR3;4* with LRL and transprtional upregulation of *ZmSULTR3;4* by salt stress

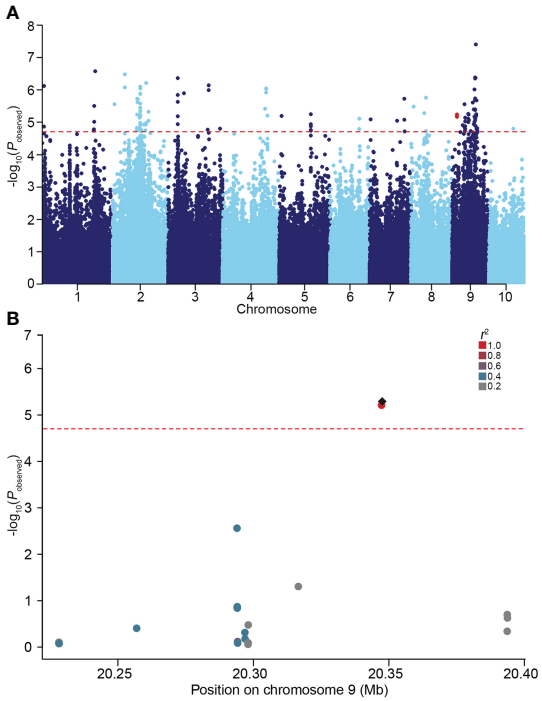

FIGURE 1
GWAS performed on the lateral root length (LRL) of maize under 100 mM NaCl condition. **(A)** Manhattan plot for the GWAS. The red dotted line represents the significance threshold ($P = 1.96 \times 10^{-5}$). Two SNPs located in *ZmSULTR3;4* were highlighted in red. **(B)** Local manhattan plot of the *ZmSULTR3;4* genomic region on chromosome 9. The 0.1-Mb genomic region on both sides of the most significant SNP was displayed. The most significant SNP was highlighted with a black diamond, while others were shown by dots and colored according to their LD (r^2) with the most significant SNP.

promote us to further investigate how *ZmSULTR3;4* contributes to maize tolerance to salt. We therefore resequenced a 6.9-kb genomic fragment spanning the promoter to the 3'-UTR region of *ZmSULTR3;4* in 280 maize inbred lines. In total, 90 SNPs and 20 InDels (MAF ≥ 0.05) were detected (Supplementary Table S2). *ZmSULTR3;4* gene-based association analysis revealed nine polymorphisms (SNP-777, -705, -649, -563, -461, -400, -344, and -159 and InDel-202) in the promoter region were associated with LRL ($P < 4.55 \times 10^{-4}$). Among them, SNP-649 explained the most phenotypic variation ($r^2 = 6.63\%$) in LRL. The nine DNA polymorphisms were in high LD ($r^2 > 0.8$), and divided the whole collection to two major haplotypes (Hap1 and Hap2) (Figures 4A, B). Statistically, the LRL of Hap2 inbred lines was on average longer than that of Hap1 under salt stress condition, suggesting that Hap1 is salt-sensitive, while Hap2 is salt-tolerant (Figure 4C).

Several significant genetic variations in the promoter region of *ZmSULTR3;4* suggests that expression variation of *ZmSULTR3;4* may be causal for the natural variation of LRL under salt stress. Therefore, *ZmSULTR3;4* expression was comprehensively analyzed in 167 maize inbred lines. The results indicated that the Hap2 inbred lines on average exhibits higher transcript level of *ZmSULTR3;4* than that of Hap1 inbred lines (Supplementary Figure 3), suggesting that differential expression of *ZmSULTR3;4* may contribute to the natural variation of LRL under salt stress. To further verify whether the genetic variation of promoter region contribute to the differential expression of *ZmSULTR3;4*, we assessed the promoter activity of two inbred lines contrasting in their sensitivity to salt stress using a transient expression system in maize protoplasts. Two promoter fragments (~0.8 kb or ~1.3 kb) of *ZmSULTR3;4* were cloned from the salt-sensitive inbred line A404 (Hap1) and the salt-tolerant inbred line A207 (Hap2) to drive the expression of luciferase (*LUC*) reporter gene and then were transformed into the maize protoplasts (Figure 5A). As shown by LUC expression, a stronger promoter activity was detected for $ZmSULTR3;4^{A207}$ than that of $ZmSULTR3;4^{A404}$ under both normal and salt stress conditions (Figure 5B). Furthermore, qRT–PCR analysis also indicated that the *ZmSULTR3;4* transcript level in A207 was higher than that in A404 under both normal and salt stress conditions (Figure 5C). Collectively, these data suggest that the natural genetic variation in the 0.8-kb promoter region differentiates the expression level of *ZmSULTR3;4*, which further conferred natural variation in maize salt tolerance.

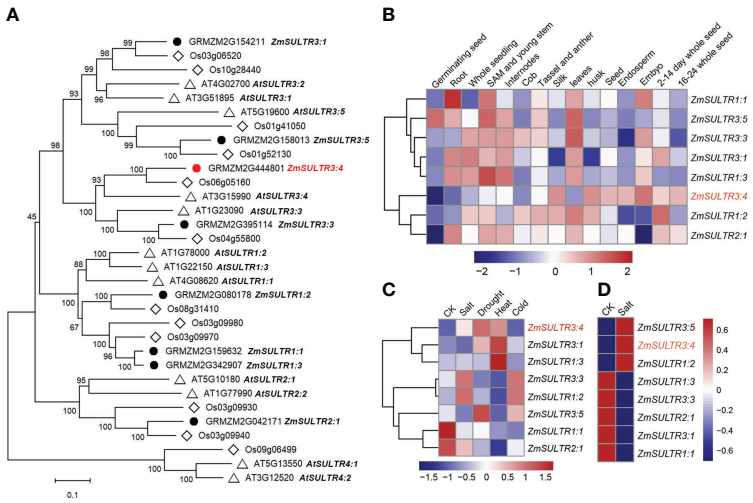

FIGURE 2
Phylogenetic and expression patterns of *ZmSULTR* genes in different types of tissue and stress response. **(A)** The phylogenetic tree of putative SULTR transporters in Arabidopsis, rice and maize. The neighbor-joining tree was constructed by MEGA-X with 1000 bootstrap values and the Poisson model. The scale denoted the branch lengths. The gene identifiers and annotation were illustrated as black dots for maize, diamonds for rice, and triangles for Arabidopsis, respectively. **(B)** A heatmap showing the transcript levels of 8 *ZmSULTRs* in fifteen different tissues at various developmental stages. Normalized gene expression values were indicated in different colors. **(C)** Expression patterns of *ZmSULTR* genes in the leaves of 7-d-old hydroponically grown maize plants in response to salt, drought, heat, and cold stresses. The bar color represents the Z score of the FPKM of each gene under five treatments. **(D)** Expression patterns of *ZmSULTR* genes in the roots of 7-d-old hydroponically grown maize plants under salt stress conditions. The bar color for the Z score of the FPKM of each gene is shown on the right.

ZmSULTR3;4 undergoes natural selection during maize domestication and improvement

Nucleotide diversity reflects the historical process of maize domestication and artificial selection (Buckler and Thornsberry, 2002; Li et al., 2022; Yamasaki et al., 2007). To explore the evolutionary history of *ZmSULTR3;4*, we resequenced it in 32 teosintes, 71 maize landraces and 280 inbred lines. A 8715-bp genomic region was analyzed, including 2252-bp upstream, 255-bp 5′-UTR, 5054-bp coding region, 412-bp o 3′-UTR, and 742-bp downstream region, respectively (Table 1). A total of 1119 polymorphic sites were detected in all the varieties, comprising 844 SNPs and 275 InDels. The average frequencies of SNPs and InDels of the gene as a whole were 0.097 and 0.032, respectively. We observed that the upstream region and 3′-UTR showed the highest frequencies of SNPs and InDels, with a value of 1 per 6.33 bp and 1 per 17.86 bp, respectively. The nucleotide diversity analysis indicated that the overall nucleotide diversity ($\pi \times 1000$) of *ZmSULTR3;4* was 9.15. Among the five investigated regions of *ZmSULTR3;4*, upstream region had the highest nucleotide diversity, with a $\pi \times 1000$ value of 17.83, while the lowest $\pi \times 1000$ value (1.76) was observed in the 5′-UTR (Table 1). We also compared the sequence conservation (C) and nucleotide diversity within three populations. The results show that the total C and $\pi \times 1000$ values were 0.83 and 9.15, respectively (Figure 6A). Among three populations, landrace and inbred line exhibited higher conservation ($C_L = 0.854$ and $C_I = 0.860$) but lower nucleotide diversity ($\pi \times 1000_L = 8.55$ and $\pi \times 1000_I = 5.98$) than teosinte ($C_T = 0.838$ and $\pi \times 1000_T = 23.35$). Furthermore, teosintes have higher nucleotide diversity across the whole gene regions compared with inbred lines and landraces, with the most significant divergence observed in the promoter region, suggesting higher selective pressure in the promoter region of *ZmSULTR3;4* during maize domestication (Figure 6B). Neutrality tests including Tajima's D as well as Fu and Li's tests were further applied to test whether *ZmSULTR3;4* underwent selection during maize domestication. We observed that Tajima's D and Fu and Li's values were not different within individual population, while Tajima's D values of all test regions except for the coding region and 3′-UTR were significantly negative across three population. Likewise, Fu and Li's values of all test regions were less than 0 (Table 1). We further analyzed the allele frequency of SNP-649 in teosintes, landraces, and inbred lines, considering that SNP-649 contributed the most to phenotypic variation. The frequency of salt-tolerant allele SNP-649^A was increased from 9.38% in teosinte to 74.65% and 88.21% in landrace and inbred lines, respectively (Figure 6C). These results collectively suggest that *ZmSULTR3;4* underwent purifying selection during maize domestication.

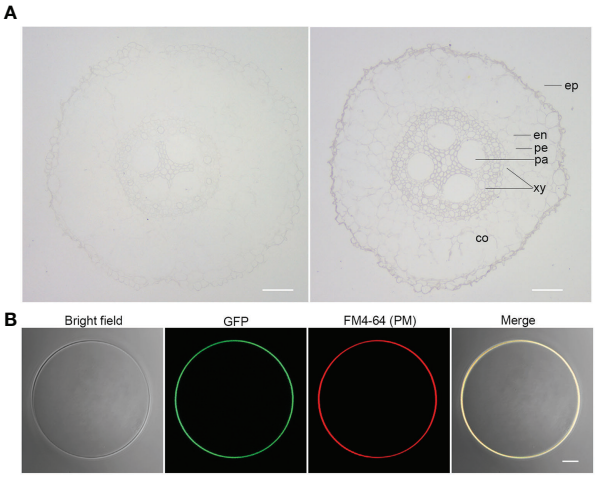

FIGURE 3
Tissue-specific expression and subcellular localization analysis of *ZmSULTR3;4*. **(A)** The tissue-specific expression of *ZmSULTR3:4* detected *via in situ* RNA hybridization in the roots of 7-d-old hydroponically grown maize seeldings. The tissue-specific expression of *ZmSULTR3;4* was detected using DIG-labeled RNA sense probes (left) and antisense probes (right). Ep, epidermis; en, endodermis; pe, pericycle; xy, xylem; pa, parenchyma; co, cortex. Bar = 100 μm. **(B)** ZmSULTR3:4 is localized exclusively in the plasma membrane (PM). The *Ubi : ZmSULTR3:4-GFP* expression cassette was transfected into maize B73 protoplasts. The transformed protoplasts were stained with FM4-64 stain for 1 min to marker the PM. Bar = 5 μm.

Discussion

Soil salinity is a wide-spread constraint that limits plant growth and productivity. Therefore, it is of great significance to excavate important salt tolerance genes and elucidate their molecular regulatory mechanisms in salt tolerance. The root system, which is in direct contact with complex and changeable soil environment, is the first organ to encounter salt stress (Pierik and Testerink, 2014). Previous researches on the effect of salinity on root development showed that LR growth is more sensitive to salt than PR growth (Duan et al., 2013; Julkowska et al., 2017; Li et al., 2021). In maize, lateral roots account for most of the total root length (Lynch, 2013). Therefore, LRL can serve as an important trait for mapping salt tolerance QTLs and regulatory genes (Julkowska et al., 2017; Li et al., 2021).

Although many QTLs responsible for salt tolerance have been excavated (Cui et al., 2014; Zhang et al., 2018), the contribution of natural variation to phenotypic variations remains largely unknown. Numerous studies have shown that GWAS can successfully fine-map the QTLs that underlie complex quantitative traits in crops (Jia et al., 2019; Kuhlmann et al., 2020; Zhang et al., 2020). Maize is a kind of out-pollination crop, the genetic linkage disequilibrium (LD) decays very fast, and is estimated to be ≤ 2 kb in diverse inbred lines due to the high rate of recombination (Yan et al., 2009; Wang et al., 2016). In the present study, we performed LD-based GWAS of salt tolerance using 140,714 high-quality and dense SNP markers, with LD decreased to 0.2 at a distance between SNPs of approximately 50 kb, allowing for high-resolution QTL mapping (Li et al., 2021). we found that two SNPs in the *ZmSULTR3;4* gene was relevant to maize LRL under salt stress. When scanning the 0.1-Mb genomic region on both sides of the two SNPs, there were no other polymorphisms that are associated with maize LRL under salt stress. Therefore, it is plausible that *ZmSULTR3;4* is the only causal gene. Notably, the upregulated expression of *ZmSULTR3;4* by salt stress implies a positive role of *ZmSULTR3;4* in regulating LR growth and salt tolerance. Thus, the association of *ZmSULTR3:4* with salt tolerance seemed to be reliable, which might enhance our understanding of the genetic basis for maize salt tolerance.

Previous study also revealed that SULTRs in maize might play roles in adaptation to sulfur deficiency and adverse environmental conditions (Huang et al., 2018). In fact, several *SULTR3s* were identified to involve in in sulfate absorption and stress response. For instance, SULTR3;1 has been shown to localize in the chloroplast, and its loss decreases the sulfate uptake of the chloroplast (Chen et al., 2019). *SULTR3;5* was reported to play a role in root-to-shoot sulfate transport, with the mutation of *SULTR3;5* resulting in more sulfate accumulation in roots under low-sulfur conditions (Kataoka et al., 2004). While annotated as sulfate transporter, members in SULTR3 subfamily differs greatly in their substrate specificity. For example, the mutation of *OsSULTR3;3* reduces the concentions of sulfate and phosphate and modified the metabolic profile in rice grains (Zhao et al., 2016). Instead of transporting sulfate, vascular cambium-localized plasma membrane-bound *AtSPDT/AtSULTR3;4* and *OsSPDT* were demonstrated to transport Pi and mediate preferential

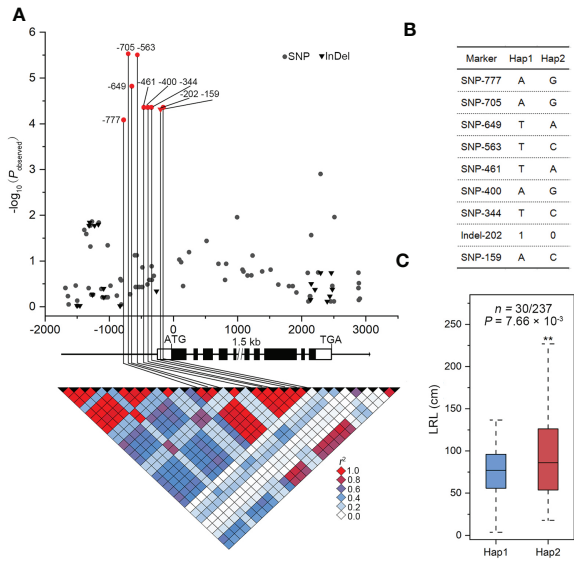

FIGURE 4
Genetic variation in *ZmSULTR3:4* is associated with the lateral root length (LRL) of maize seedlings under salt stress conditions. **(A)** Association analysis between the genetic variation of *ZmSULTR3:4* and the LRL of maize seedlings under salt stress. Black dots represent SNPs, and triangles denote InDels. The position of the start codon (ATG) is defined as "+1". The 5'- and 3'-UTRs and exons of *ZmSULTR3:4* are shown as open and filled boxes, respectively. The black lines represent gene promoters and introns. The *p value* is shown on a -$\log_{10}$ scale. The nine significant polymorphisms in the promoter are connected to the pairwise LD diagram with black vertical lines, illustrating that the nine variants are in strong LD (r^2 >0.8). **(B)** Significant markers of *ZmSULTR3:4* associated with LRL in different haplotypes. **(C)** The distribution of i LRL under salt stress conditions. n is the number of inbred lines belonging to each haplotype. Statistical significance was determined using a two-sided *t test*. "**"denotes statistical significance at the p < 0.01 level.

distribution of phosphorus (P) to young tissues (Chen et al., 2019; Ding et al., 2020). *ZmSULTR3;4*, the closest ortholog of *AtSULTR3;4*, is also localized to the PM, suggesting there may be a conserved function in different plant species. The preferential expression of *ZmSULTR3;4* in the epidermal and vascular tissues of roots indicates that it may play an important role in transporting mineral elements to young tissues, allowing them to withstand malnutrition caused by high salt levels. Further research will be necessary to understand the *in planta* function of *ZmSULTR3;4*.

Then, we resequenced the *ZmSULTR3;4* gene to verify the results of association analysis and more accurately identify genetic variation related to maize salt tolerance. The results revealed nine significant genetic variants residing in the 0.8-kb promoter region of *ZmSULTR3;4*. Although nine significant natural variations were located in the *ZmSULTR3;4* promoter, the inbred lines mainly classified into two haplotypes. Compared with the inbred lines of Hap1, the inbred lines of Hap2 showed longer LRs under slat stress, suggesting that $ZmSULTR3;4^{Hap2}$ allele would be valuable in breeding program seeking to improve salt tolerance in maize germplasms. Consistent with the longer LR length in $ZmSULTR3;4^{Hap2}$ allele, we observed also higher *ZmSULTR3;4* expression in the $ZmSULTR3;4^{Hap2}$ inbred lines, suggesting that allelic variants in the promoter region may impact the transcript level of *ZmSULTR3;4* that confers different sensitivity to salt in maize population. Luciferase (LUC) and β-glucuronidase (GUS) are routinely used as reporters for the quantitative measurement of gene expression in transient expression using mesophyll protoplasts (Yoo et al., 2007; Tian et al., 2019). Supporting this conclusion, LUC activity driven by the 0.8-kb and 1.3-kb promoter fragments of $ZmSULTR3;4^{Hap2}$ was greater than that of $ZmSULTR3;4^{Hap1}$ promoter fragment, suggesting that functional allele resides in 0.8-kb promoter region. In fact, numerous studies have shown that regulatory polymorphisms upstream of genes as a major driver that differentiates gene expression and lead to changes in plant phenotypes (Salvi et al., 2007; Mao et al., 2015; Wang et al., 2016; Jia et al., 2020; 2021). For example, genetic variations in the promoter region of *ZmVPP1* and *ZmNAC111* regulate the gene expression, which is closely associated with variation of plant drought tolerance (Mao et al., 2015; Wang et al., 2016). An insertion upstream of *Vgt1* (*Vegetative to generative transition 1*) represses gene expression and affects maize flowering-time (Salvi et al., 2007). Unfortunately, the strong LD among these nine SNPs prohibits us to identify the causal functional allele associated with natural variation of LR length. In future precise nucleotide substitution of these nine variants will allow to fine-map the causal variant differentiating the expression of *ZmSULTR3;4*.

Genetic and archeological evidence has suggested that maize was domesticated from its wild ancestor, teosinte, in southwestern Mexico about 9000 years ago. The bottleneck

10.3389/fpls.2022.992799

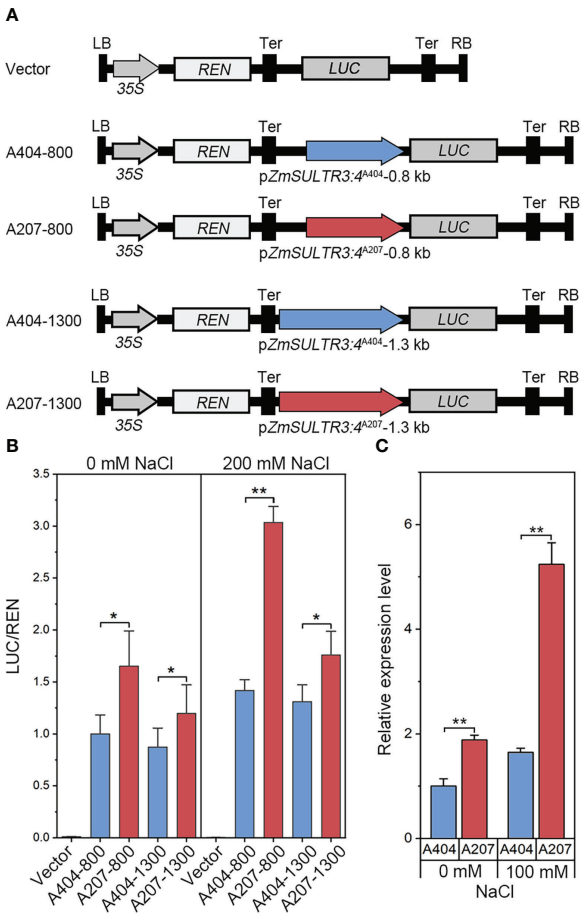

FIGURE 5
LUC enzyme activity driven by 0.8-kb and 1.3-kb promoter fragments of *ZmSULTR3:4*^{A404} and *ZmSULTR3:4*^{A207} under normal and salt stress conditions. **(A)** Vector diagram used to detect the effect of genetic variation of the promoter region on *ZmSULTR3:4* expression. A404-800, A207-800, A404-1300, and A207-1300 constructs harbor the promoter fragments of different *ZmSULTR3:4* alleles, including 800 bp from A404, 800 bp from A207, 1300 bp from A404, and 1300 bp from A207. **(B)** Transient expression assays of different promoter fragments from two. *35S:Renilla luciferase* was used as a positive control for transfection efficiency. Statistical significance was determined by a two-sided *t test*: $*p < 0.05$, $**p < 0.01$. **(C)** Relative expression of *ZmSULTR3:4* in roots of 14-d-old hydroponically grown A404 and A207 inbred lines under normal and 100 mM NaCl conditions.

effect of domestication resulted in a stark decrease in nucleotide diversity (Wang et al., 2017; Allaby et al., 2019). The rich genetic diversity is the basis of crop genetic improvement (Yan et al., 2011). In this research, nucleotide polymorphisms of *ZmSULTR3;4* were analyzed in teosintes, landraces, and inbred lines through resequencing. The genetic diversity of *ZmSULTR3:4* in teosintes, landraces and maize inbred lines decreased in turn, suggesting that approximately three-quarters of the genetic diversity in the *ZmSULTR3:4* genome was lost during the domestication process. Moreover, the apparent reduction of nucleotide polymorphisms in the promoter region of *ZmSULTR3:4* suggested that this region might have been subjected to greater selection pressure. The neutrality tests also revealed that *ZmSULTR3;4* might be selected during maize domestication and improvement. Indeed, the frequency of the favourable allele of *ZmSULTR3;4* increased gradually during the domestication from teosinte to landraces, and the improvement from landraces to maize inbred lines, which strongly reflects a breeding history involving selection. Similarly, a few yield- or stress-related genes, *e.g.*, *tb1*, *KRN4*, and *bZIP68*, have been reported undergone strong artificial selection during maize genetic improvement (Studer et al., 2011; Liu et al., 2015; Li et al., 2022). Although the salt-induced expression pattern of *ZmSULTR1:2* and *ZmSULTR3:5* was similar to that of *ZmSULTR3:4* in the roots, our GWAS analysis did not reveal an association between these two genes and the phenotype, which may be due to the limitation of population material or the choice of traits for salinity tolerance. New populations and phenotypic traits need to be developed to reveal the genetic architecture of maize salt stress response. Some important genes

10.3389/fpls.2022.992799

A

Poopulation	*Hd*	Dens.	C	π × 1000	θ × 1000	Tajima's D	D	F
Teosintes	1.000	85	0.838	23.35	32.640	-1.103	-1.844	-1.886
Landraces	1.000	38	0.854	8.55	11.610	-0.921	-2.102	-1.942
Inbreds	0.880	22	0.860	5.98	5.280	0.413	0.334	0.444
All	0.935	97	0.830	9.15	23.330	-1.874*	-7.360**	-5.072**

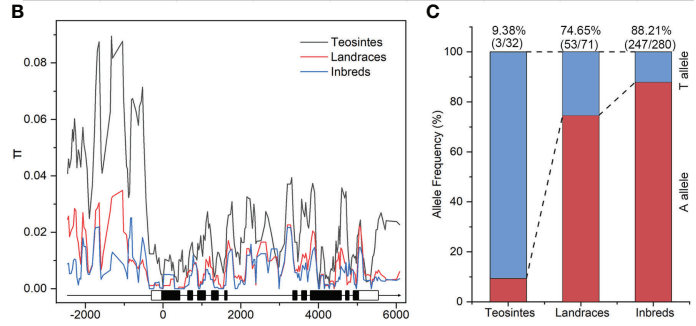

FIGURE 6
Analysis of nucleotide diversity (π) and allele frequency of *ZmSULTR3;4* in teosinte, landrace, and inbred lines. **(A)** Evaluation of nucleotide polymorphisms and neutrality tests of *ZmSULTR3;4*. *Hd* represents haplotype diversity; Dens. denotes the number of single nucleotide polymorphisms (SNPs) per 1000 bp; C represents sequence conservation; D and F represent Fu and Li's D* and F*, respectively. Asterisks indicate statistical significance at the level of $*p < 0.05$, and $**p < 0.01$. **(B)** Nucleotide diversity (π) of teosinte, landrace, and inbred lines. The sliding window method was used to calculate π with a window size of 100 bp and a step size of 25 bp. A schematic illustrating the genomic region of *ZmSULTR3;4*, encompassing the upstream promoter region, introns (black lines), exons (filled boxes), and the 5'- and 3'-UTRs (open boxes). **(C)** Detection of allele frequency of SNP-705 in teosinte, landrace, and inbred lines. Number in the brackets indicated the count of accessions carrying the corresponding allele within respective population.

or loci responsible for salt mediated LR growth may also be missed in our GWAS due to SNP density and low frequency of some markers as well as the lacking of structure variations such as presence/absence variations (PAVs) and copy number variations (CNVs) in our genotype datesets. To our knowledge, *ZmSULTR3;4* was the first gene identified to play a regulatory role in salt-regulated LR growth and underwent domestication and improvement in maize. The biological function and regulatory network of *ZmSULTR3;4* need to be further investigated using approaches such as CRISPR-Cas9 and overexpression. Although some progress has been made in the study of plant SULTRs, the function of SULTRs in maize is still poorly understood. It is also unclear whether other *ZmSULTR* members were under selection during maize domestication and improvement. Further research is required to understand the biological function and selective characteristic of *ZmSULTRs*. Collectively, the identified natural variants and elite haplotype of *ZmSULTR3;4* may be used to improve maize root traits and salinity tolerance by molecular breeding.

Data availability statement

The original contributions presented in the study are publicly available. This data can be found here: NCBI, PRJNA683126.

Author contributions

XZ, PL, TZ, and ZL performed the experiments and drafted the manuscript. PL, ZJ, and SG conceived the experiment and revised the manuscript. XZ, MY, RL, ZW, and QC analyzed the data. All authors reviewed and approved this submission.

Funding

This research was supported by the National Natural Science Foundation of China (32201726 and 31972487), the Open Project Funding of the State Key laboratory of Crop Stress Adaptation and Improvement, the Science and Technology Development Plan Project of Henan Province (212102110152 and 222102110006), the High-end Talent Project of Yangzhou University, Qing Lan Project of Jiangsu Province, and the Priority Academic Program Development of Jiangsu Higher Education Institutions (PAPD).

Conflict of interest

The authors declare that the research was conducted in the absence of any commercial or financial relationships that could be construed as a potential conflict of interest.

Publisher's note

Supplementary material

The Supplementary Material for this article can be found online at: https://www.frontiersin.org/articles/10.3389/fpls.2022.992799/full#supplementary-material

SUPPLEMENTARY FIGURE 1
GWAS performed on lateral root length (LRL) under normal growth condition. The red horizontal dashed line depicted the significance threshold ($P = 1.96 \times 10^{-5}$).

SUPPLEMENTARY FIGURE 2
The relative expression level of *ZmSULTR3;4* in response to salt stress in roots of six hydroponically grown maize inbred lines. The data represented the mean of two replicates.

SUPPLEMENTARY FIGURE 3
Transcript level of *ZmSULTR3;4* in roots of different maize inbred lines under normal growth condition. Statistical significance was detected by a two-sided *t-test*; $^{**}p < 0.01$.

SUPPLEMENTARY FIGURE 4
Relative expression of *ZmSULTR3;4* in the different developmental zones of primary roots. The data were retrieved from the Maize eFP Browser (http://bar.utoronto.ca/efp_maize/cgi-bin/efpWeb.cgi).

References

Allaby, R. G., Ware, R. L., and Kistler, L. (2019). A re-evaluation of the domestication bottleneck from archaeogenomic evidence. *Evol. Appl.* 12, 29–37. doi: 10.1111/eva.12680

Bellini, C., Pacurar, D. I., and Perrone, I. (2014). Adventitious roots and lateral roots: similarities and differences. *Annu. Rev. Plant Biol.* 65, 639–666. doi: 10.1146/annurev-arplant-050213-035645

Bradbury, P. J., Zhang, Z., Kroon, D. E., Casstevens, T. M., and Buckler, E. S. J. B. (2007). TASSEL: Software for association mapping of complex traits in diverse samples. *Bioinformatics* 23 (19), 2633–2635. doi: 10.1093/bioinformatics/btm308

Buckler, E. S., and Thornsberry, J. M. (2002). Plant molecular diversity and applications to genomics. *Curr. Opin. Plant Biol.* 5, 107–111. doi: 10.1016/s1369-5266(02)00238-8

Casimiro, I., Beeckman, T., Graham, N., Bhalerao, R., Zhang, H., Casero, P., et al. (2003). Dissecting arabidopsis lateral root development. *Trends Plant Sci.* 8 (4), 165–171. doi: 10.1016/S1360-1385(03)00051-7

Chen, W., Chen, L., Zhang, X., Yang, N., Guo, J., Wang, M., et al. (2022). Convergent selection of a WD40 protein that enhances grain yield in maize and rice. *Science* 375 (6587), eabg7985. doi: 10.1126/science.abg7985

Chen, M. X., Lu, C. C., Sun, P. C., Nie, Y. X., Tian, Y., Hu, Q. J., et al. (2021). Comprehensive transcriptome and proteome analyses reveal a novel sodium chloride responsive gene network in maize seed tissues during germination. *Plant Cell Environ.* 44 (1), 88–101. doi: 10.1111/pce.13849

Chen, Z., Zhao, P. X., Miao, Z. Q., Qi, G. F., Wang, Z., Yuan, Y., et al. (2019). SULTR3s function in chloroplast sulfate uptake and affect ABA biosynthesis and the stress response. *Plant Physiol.* 180 (1), 593–604. doi: 10.1104/pp.18.01439

Choi, M., Scholl, U. I., Ji, W., Liu, T., Tikhonova, I. R., Zumbo, P., et al. (2009). Genetic diagnosis by whole exome capture and massively parallel DNA sequencing. *Proc. Natl. Acad. Sci. U.S.A.* 106 (45), 19096–19101. doi: 10.1073/pnas.0910672106

Cui, D., Wu, D., Somarathna, Y., Xu, C., Li, S., Li, P., et al. (2014). QTL mapping for salt tolerance based on snp markers at the seedling stage in maize (*Zea mays* l.). *Euphytica* 203, 273–283. doi: 10.1007/s10681-014-1250-x

Ding, G., Lei, G. J., Yamaji, N., Yokosho, K., Mitani-Ueno, N., Huang, S., et al. (2020). Vascular cambium-localized *AtSPDT* mediates xylem-to-phloem transfer of phosphorus for its preferential distribution in arabidopsis. *Mol. Plant* 13 (1), 99–111. doi: 10.1016/j.molp.2019.10.002

Duan, L., Dietrich, D., Ng, C. H., Chan, P. M., Bhalerao, R., Bennett, M. J., et al. (2013). Endodermal ABA signaling promotes lateral root quiescence during salt stress in arabidopsis seedlings. *Plant Cell* 25 (1), 324–341. doi: 10.1105/tpc.112.107227

Faiyue, B., Vijayalakshmi, C., Nawaz, S., Nagato, Y., Taketa, S., Ichii, M., et al. (2010). Studies on sodium bypass flow in lateral rootless mutants *lrt1* and *lrt2*, and crown rootless mutant *crl1* of rice (*Oryza sativa* l.). *Plant Cell Environ.* 33 (5), 687–701. doi: 10.1111/j.1365-3040.2009.02077.x

Farooq, M., Hussain, M., Wakeel, A., and Siddique, K. H. M. (2015). Salt stress in maize: effects, resistance mechanisms, and management. a review. *Agron. Sustain. Dev.* 35, 461–481. doi: 10.1007/s13593-015-0287-0

Fu, Y. X., and Li, W. H. J. G. (1993). Statistical tests of neutrality of mutations. *Genetics* 133 (3), 693–709. doi: 10.1093/genetics/133.3.693

Gu, R., Duan, F., An, X., Zhang, F., Von Wiren, N., and Yuan, L. (2013). Characterization of AMT-mediated high-affinity ammonium uptake in roots of maize (*Zea mays* l.). *Plant Cell Physiol.* 54 (9), 1515–1524. doi: 10.1093/pcp/pct099

Huang, Q., Wang, M., and Xia, Z. (2018). The *SULTR* gene family in maize (*Zea mays* l.): Gene cloning and expression analyses under sulfate starvation and abiotic stress. *J. Plant Physiol.* 220, 24–33. doi: 10.1016/j.jplph.2017.10.010

Ismail, A. M., and Horie, T. (2017). Genomics, physiology, and molecular breeding approaches for improving salt tolerance. *Annu. Rev. Plant Biol.* 68, 405–434. doi: 10.1146/annurev-arplant-042916-040936

Jia, Z., Giehl, R. F. H., Meyer, R. C., Altmann, T., and Von Wiren, N. (2019). Natural variation of *BSK3* tunes brassinosteroid signaling to regulate root foraging under low nitrogen. *Nat. Commun.* 10, 2378. doi: 10.1038/s41467-019-10331-9

Jia, Z., Giehl, R. F. H., and Von Wiren, N. (2022). Nutrient-hormone relations: Driving root plasticity in plants. *Mol. Plant* 15, 86–103. doi: 10.1016/j.molp.2021.12.004

Jia, Z. T., Bienert, M. D., von Wirén, N., and Bienert, G. P. (2021). Genome-wide association mapping identifies HvNIP2;2/HvLsi6 accounting for efficient boron transport in barley. . *Physiol. Plant* 171 (4), 809–822. doi: 10.1111/ ppl.13340

Jia, Z. T., Giehl, R., and von Wirén, N. (2020). The root foraging response under low nitrogen depends on DWARF1- mediated brassinosteroid biosynthesis. *Plant Physiol.* 183 (3), 998–1010. doi: 10.1104/pp.20.00440

Jia, Z., and Von Wiren, N. (2020). Signaling pathways underlying nitrogen-dependent changes in root system architecture: from model to crop species. *J. Exp. Bot.* 71, 4393–4404. doi: 10.1093/jxb/eraa033

Julkowska, M. M., Koevoets, I. T., Mol, S., Hoefsloot, H., Feron, R., Tester, M. A., et al. (2017). Genetic components of root architecture remodeling in response to salt stress. *Plant Cell* 29 (12), 3198–3213. doi: 10.1105/tpc.16.00680

Karlova, R., Boer, D., Hayes, S., and Testerink, C. (2021). Root plasticity under abiotic stress. *Plant Physiol.* 187, 1057–1070. doi: 10.1093/plphys/kiab392

Kataoka, T., Hayashi, N., Yamaya, T., and Takahashi, H. (2004). Root-to-shoot transport of sulfate in arabidopsis. evidence for the role of *SULTR3;5* as a component of low-affinity sulfate transport system in the root vasculature. *Plant Physiol.* 136 (4), 4198–4204. doi: 10.1104/pp.104.045625

Katoh, K., and Standley, D. M. (2013). MAFFT multiple sequence alignment software version 7: improvements in performance and usability. *Mol. Biol. Evol.* 30 (4), 772–780. doi: 10.1093/molbev/mst010

Kuhlmann, M., Meyer, R. C., Jia, Z., Klose, D., Krieg, L.-M., Von Wirén, N., et al. (2020). Epigenetic variation at a genomic locus affecting biomass accumulation under low nitrogen in *Arabidopsis thaliana*. *Agronomy* 10, 636. doi: 10.3390/agronomy10050636

Librado, P., and Rozas, J. J. B. (2009). DnaSP v5 : A software for comprehensive analysis of DNA polymorphism data. *Bioinformatics* 25 (11), 1451–1452. doi: 10.1093/bioinformatics/btp187

Li, Z., Fu, D., Wang, X., Zeng, R., Zhang, X., Tian, J., et al. (2022). Natural variation in the *bZIP68* promoter modulates cold tolerance and was targeted during maize domestication. *Plant Cell* 34 (8), koac137. doi: 10.1093/plcell/koac137

Liu, L., Du, Y., Shen, X., Li, M., Sun, W., Huang, J., et al. (2015). *KRN4* controls quantitative variation in maize kernel row number. *PloS Genet.* 11, e1005670. doi: 10.1371/journal.pgen.1005670

Liu, S., Wang, X., Wang, H., Xin, H., Yang, X., Yan, J., et al. (2013). Genome-wide analysis of *ZmDREB* genes and their association with natural variation in drought tolerance at seedling stage of *Zea mays* l. *PloS Genet.* 9, e1003790. doi: 10.1371/journal.pgen.1003790

Li, P., Wei, J., Wang, H., Fang, Y., Yin, S., Xu, Y., et al. (2019). Natural variation and domestication selection of *ZmPGP1* affects plant architecture and yield-related traits in maize. *Genes (Basel)* 10 (9), 664. doi: 10.3390/genes10090664

Li, P., Yang, X., Wang, H., Pan, T., Wang, Y., Xu, Y., et al. (2021). Genetic control of root plasticity in response to salt stress in maize. *Theor. Appl. Genet.* 134 (5), 1475–1492. doi: 10.1007/s00122-021-03784-4

Luo, X., Wang, B., Gao, S., Zhang, F., Terzaghi, W., and Dai, M. (2019). Genome-wide association study dissects the genetic bases of salt tolerance in maize seedlings. *J. Integr. Plant Biol.* 61 (6), 658–674. doi: 10.1111/jipb.12797

Lynch, J. P. (2013). Steep, cheap and deep: an ideotype to optimize water and n acquisition by maize root systems. *Ann. Bot.* 112 (2), 347–357. doi: 10.1093/aob/mcs293

Mao, H., Wang, H., Liu, S., Li, Z., Yang, X., Yan, J., et al. (2015). A transposable element in a *NAC* gene is associated with drought tolerance in maize seedlings. *Nat. Commun.* 6, 8326. doi: 10.1038/ncomms9326

Munns, R., James, R. A., Xu, B., Athman, A., Conn, S. J., Jordans, C., et al. (2012). Wheat grain yield on saline soils is improved by an ancestral na^+ transporter gene. *Nat. Biotechnol.* 30 (4), 360–364. doi: 10.1038/nbt.2120

Pierik, R., and Testerink, C. (2014). The art of being flexible: how to escape from shade, salt, and drought. *Plant Physiol.* 166 (1), 5–22. doi: 10.1104/pp.114.239160

Ristova, D., and Busch, W. (2014). Natural variation of root traits: from development to nutrient uptake. *Plant Physiol.* 166 (2), 518–527. doi: 10.1104/pp.114.244749

Roy, S. J., Huang, W., Wang, X. J., Evrard, A., Schmockel, S. M., Zafar, Z. U., et al. (2013). A novel protein kinase involved in na^+ exclusion revealed from positional cloning. *Plant Cell Environ.* 36 (3), 553–568. doi: 10.1111/j.1365-3040.2012.02595.x

Rus, A., Baxter, I., Muthukumar, B., Gustin, J., Lahner, B., Yakubova, E., et al. (2006). Natural variants of *AtHKT1* enhance na^+ accumulation in two wild populations of arabidopsis. *PloS Genet.* 2 (12), e210. doi: 10.1371/journal.pgen.0020210

Salvi, S., Sponza, G., Morgante, M., Tomes, D., Niu, X., Fengler, K. A., et al. (2007). Conserved noncoding genomic sequences associated with a flowering-time quantitative trait locus in maize. *Proc. Natl. Acad. Sci. U.S.A.* 104 (27), 11376–11381. doi: 10.1073/pnas.0704145104

Sandhu, D., Pudussery, M. V., Kumar, R., Pallete, A., Markley, P., Bridges, W. C., et al. (2020). Characterization of natural genetic variation identifies multiple genes involved in salt tolerance in maize. *Funct. Integr. Genomics* 20 (2), 261–275. doi: 10.1007/s10142-019-00707-x

Sekhon, R. S., Lin, H., Childs, K. L., Hansey, C. N., Buell, C. R., Leon, N. D., et al. (2011). Genome-wide atlas of transcription during maize development. *Plant J.* 66 (4), 553–563. doi: 10.1111/j.1365-313X.2011.04527.x

Studer, A., Zhao, Q., Ross-Ibarra, J., and Doebley, J. (2011). Identification of a functional transposon insertion in the maize domestication gene *tb1*. *Nat. Genet.* 43, 1160–1163. doi: 10.1038/ng.942

Tajima,, and Genetics, F. J. (1989). Statistical method for testing the neutral mutation hypothesis by DNA polymorphism. *Genetics* 123 (3), 585–595. doi: 10.1093/genetics/123.3.585

Tian, J., Wang, C., Xia, J., Wu, L., Xu, G., Wu, W., et al. (2019). Teosinte ligule allele narrows plant architecture and enhances high-density maize yields. *Science* 365, 658–664. doi: 10.1126/science.aax5482

Van Norman, J. M., Xuan, W., Beeckman, T., and Benfey, P. N. (2013). To branch or not to branch: the role of pre-patterning in lateral root formation. *Development* 140 (21), 4301–4310. doi: 10.1242/dev.090548

Van Zelm, E., Zhang, Y., and Testerink, C. (2020). Salt tolerance mechanisms of plants. *Annu. Rev. Plant Biol.* 71, 403–433. doi: 10.1146/annurev-arplant-050718-100005

Villordon, A. Q., Ginzberg, I., and Firon, N. (2014). Root architecture and root and tuber crop productivity. *Trends Plant Sci.* 19 (7), 419–425. doi: 10.1016/j.tplants.2014.02.002

Wang, L., Beissinger, T. M., Lorant, A., Ross-Ibarra, C., Ross-Ibarra, J., and Hufford, M. B. (2017). The interplay of demography and selection during maize domestication and expansion. *Genome Biol.* 18 (1), 215. doi: 10.1186/s13059-017-1346-4

Wang, Y., Cao, Y., Liang, X., Zhuang, J., Wang, X., Qin, F., et al. (2022). A dirigent family protein confers variation of casparian strip thickness and salt tolerance in maize. *Nat. Commun.* 13 (1), 2222. doi: 10.1038/s41467-022-29809-0

Wang, Y., Sun, H., Wang, H., Yang, X., Xu, Y., Yang, Z., et al. (2021). Integrating transcriptome, co-expression and QTL-seq analysis reveals that primary root growth in maize is regulated *via* flavonoid biosynthesis and auxin signal transduction. *J. Exp. Bot.* 72 (13), 4773–4795. doi: 10.1093/jxb/erab177

Wang, X., Wang, H., Liu, S., Ferjani, A., Li, J., Yan, J., et al. (2016). Genetic variation in *ZmVPP1* contributes to drought tolerance in maize seedlings. *Nat. Genet.* 48 (10), 1233–1241. doi: 10.1038/ng.3636

Yamasaki, M., Wright, S. I., and Mcmullen, M. D. (2007). Genomic screening for artificial selection during domestication and improvement in maize. *Ann. Bot.* 100 (5), 967–973. doi: 10.1093/aob/mcm173

Yang, Y., and Guo, Y. (2018). Unraveling salt stress signaling in plants. *J. Integr. Plant Biol.* 60 (9), 796–804. doi: 10.1111/jipb.12689

Yan, J., Shah, T., Warburton, M. L., Buckler, E. S., McMullen, M. D., and Crouch, J. (2009). Genetic characterization and linkage disequilibrium estimation of a global maize collection using SNP markers. *PloS One* 4, e8451. doi: 10.1371/journal.pone.0008451

Yan, J., Warburton, M., and Crouch, J. (2011). Association mapping for enhancing maize (*Zea mays* l.) genetic improvement. *Crop Sci.* 51 (2), 433–449. doi: 10.2135/cropsci2010.04.0233

Yoo, S. D., Cho, Y. H., and Sheen, J. (2007). Arabidopsis mesophyll protoplasts: a versatile cell system for transient gene expression analysis. *Nat. Protoc.* 2 (7), 1565–1572. doi: 10.1038/nprot.2007.199

Yu, P., Gutjahr, C., Li, C., and Hochholdinger, F. (2016). Genetic control of lateral root formation in cereals. *Trends Plant Sci.* 21 (11), 951–961. doi: 10.1016/j.tplants.2016.07.011

Zhang, M., Cao, Y., Wang, Z., Wang, Z. Q., Shi, J., Liang, X., et al. (2018). A retrotransposon in an HKT1 family sodium transporter causes variation of leaf na^+ exclusion and salt tolerance in maize. *New Phytol.* 217, 1161–1176. doi: 10.1111/nph.14882

Zhang, M., Kong, X., Xu, X., Li, C., Tian, H., and Ding, Z. (2015). Comparative transcriptome profiling of the maize primary, crown and seminal root in response to salinity stress. *PloS One* 10 (3), e0121222. doi: 10.1371/journal.pone.0121222

Zhang, M., Liang, X., Wang, L., Cao, Y., Song, W., Shi, J., et al. (2019). A HAK family na^+ transporter confers natural variation of salt tolerance in maize. *Nat. Plants* 5 (12), 1297–1308. doi: 10.1038/s41477-019-0565-y

Zhang, X., Mi, Y., Mao, H., Liu, S., Chen, L., and Qin, F. (2020). Genetic variation in *ZmTIP1* contributes to root hair elongation and drought tolerance in maize. *Plant Biotechnol. J.* 18, 1271–1283. doi: 10.1111/pbi.13290

Zhao, H., Frank, T., Tan, Y., Zhou, C., Jabnoune, M., Arpat, A. B., et al. (2016). Disruption of *OsSULTR3;3* reduces phytate and phosphorus concentrations and alters the metabolite profile in rice grains. *New Phytol.* 211 (3), 926–939. doi: 10.1111/nph.13969

Zhu, J. K. (2016). Abiotic stress signaling and responses in plants. *Cell* 167 (2), 313–324. doi: 10.1016/j.cell.2016.08.029

frontiers | Frontiers in Plant Science

TYPE Original Research
PUBLISHED 28 November 2022
DOI 10.3389/fpls.2022.1010030

OPEN ACCESS

EDITED BY
Manje S. Gowda,
The International Maize and Wheat Improvement Center (CIMMYT), Kenya

REVIEWED BY
Xingliang Ma,
University of Saskatchewan, Canada
Jaindra Nath Tripathi,
International Institute of Tropical Agriculture (IITA), Kenya

*CORRESPONDENCE
Peter M. Rogowsky
peter.rogowsky@ens-lyon.fr

†These authors have contributed equally to this work

SPECIALTY SECTION
This article was submitted to Plant Physiology, a section of the journal Frontiers in Plant Science

RECEIVED 02 August 2022
ACCEPTED 03 November 2022
PUBLISHED 28 November 2022

CITATION
Fierlej Y, Jacquier NMA, Guille L, Just J, Montes E, Richard C, Loue-Manifel J, Depège-Fargeix N, Gaillard A, Widiez T and Rogowsky PM (2022) Evaluation of genome and base editing tools in maize protoplasts. *Front. Plant Sci.* 13:1010030. doi: 10.3389/fpls.2022.1010030

Evaluation of genome and base editing tools in maize protoplasts

Yannick Fierlej[1,2†], Nathanaël M. A. Jacquier[1†], Loïc Guille[1], Jérémy Just[1], Emilie Montes[1], Christelle Richard[1], Jeanne Loue-Manifel[1], Nathalie Depège-Fargeix[1], Antoine Gaillard[2], Thomas Widiez[1] and Peter M. Rogowsky[1*]

[1]Laboratoire Reproduction et Développement des Plantes, Univ Lyon, Ecole Normale Supérieure (ENS) de Lyon, Université Claude Bernard (UCB) Lyon 1, Centre National de la Recherche Scientifique (CNRS), Institut National de Recherche pour l'Agriculture, l'alimentation et l'Environnement (INRAE), Lyon, France, [2]Department Research and Development, MAS Seeds, Haut-Mauco, France

Introduction: Despite its rapid worldwide adoption as an efficient mutagenesis tool, plant genome editing remains a labor-intensive process requiring often several months of *in vitro* culture to obtain mutant plantlets. To avoid a waste in time and money and to test, in only a few days, the efficiency of molecular constructs or novel Cas9 variants (clustered regularly interspaced short palindromic repeats (CRISPR)-associated protein 9) prior to stable transformation, rapid analysis tools are helpful.

Methods: To this end, a streamlined maize protoplast system for transient expression of CRISPR/Cas9 tools coupled to NGS (next generation sequencing) analysis and a novel bioinformatics pipeline was established.

Results and discussion: Mutation types found with high frequency in maize leaf protoplasts had a trend to be the ones observed after stable transformation of immature maize embryos. The protoplast system also allowed to conclude that modifications of the sgRNA (single guide RNA) scaffold leave little room for improvement, that relaxed PAM (protospacer adjacent motif) sites increase the choice of target sites for genome editing, albeit with decreased frequency, and that efficient base editing in maize could be achieved for certain but not all target sites. Phenotypic analysis of base edited mutant maize plants demonstrated that the introduction of a stop codon but not the mutation of a serine predicted to be phosphorylated in the bHLH (basic helix loop helix) transcription factor ZmICEa (INDUCER OF CBF EXPRESSIONa) caused abnormal stomata, pale leaves and eventual plant death two months after sowing.

KEYWORDS

genome editing, plant biotechnology, protoplast, sgRNA scaffold, stomatal development, targeted mutagenesis, CRISPR/Cas9, *Zea mays*

Introduction

Genome editing using clustered regularly interspaced short palindromic repeats (CRISPR)/CRISPR-associated protein 9 (Cas9) technology has rapidly become the preferred tool to generate mutants for functional genomics in microbes, animals and plants (Adli, 2018; Chen et al., 2019; Schindele et al., 2020). The success of CRISPR/Cas9 technology over earlier meganuclease, zinc finger or transcription activator-like effector nuclease (TALEN) techniques is mainly due to the fact that the recognition of the target sequence in the genome is mediated by fully foreseeable DNA/RNA base pairing rather than less predictable DNA/protein interactions. In its original context of bacterial defense the Cas9 nuclease forms a complex with two RNA molecules, the CRISPR RNA (crRNA) and the trans-activating crRNA (tracrRNA) (Jinek et al., 2012), which for biotechnological applications were linked together into a single-guide RNA (sgRNA) (Mali et al., 2013). Cas9 expression is driven either by constitutive or tissue-specific promoters transcribed by RNA polymerase II, whereas the sgRNA is generally under the control of U3 or U6 promoters transcribed by RNA polymerase III.

In plants, the most widely use of the technology is targeted mutagenesis, which is achieved by a CRISPR/Cas9-mediated double strand break of the DNA. Due to the random nature of error-prone cellular DNA repair, only the site but not the nature of the mutation is predetermined. In 2019, 97% of the publications were based on this approach and only 3% used true genome editing, which copies the modified, predetermined sequence of a repair matrix into the genome (Modrzejewski et al., 2019). This preference is due to the fact that the molecular nature of the mutation is not crucial for the generation of loss-of-function mutants and that the repair of nuclease-mediated double strand breaks by non-homologous end joining (NHEJ) or microhomology-mediated end joining (MMEJ) leading to targeted mutagenesis is approximately two orders of magnitude more frequent than repair by homologous recombination (HR) using a repair matrix (Huang and Puchta, 2019). More recently, new variants of the CRISPR/Cas9 technology such as base editing or prime editing have emerged that allow to predetermine the precise nature of the mutation, albeit with certain limitations. These variants are based on a nickase version of the Cas9 that cuts only one and not both DNA strands, and which is fused to a protein domain with enzymatic action, for example to a cytidine and/or adenine deaminase domain for C and/or A base editing (Shimatani et al., 2017; Zong et al., 2017; Yan et al., 2018; Li et al., 2020), or to a reverse transcriptase domain for prime editing (Hua et al., 2020; Lin et al., 2020; Xu et al., 2022).

Another limitation of the initial CRISPR/Cas9 technology was the protospacer adjacent motif (PAM), *i.e.* the need for the triplet NGG downstream of the targeted site in the genome. Both the use of other RNA-guided nuclease such as Cas12a/CPF1 with its PAM sequence TTTN located upstream of the target (Zetsche et al., 2015), and the molecular engineering of Cas9 leading to the xCas9 (Hu et al., 2018) and Cas9-NG variants (Nishimasu et al., 2018) markedly enlarged the number of sites amenable to genome editing in a given genome. After initial exemplification in human cell lines, all of these improvements have been successfully transferred to plants and are now available for plant genome editing (Chen et al., 2019), including the latest development referred to as PAM-less genome editing (Ren et al., 2021).

The production of edited plants is a time consuming and labor-intensive process, which generally involves the *in vitro* culture of hundreds of calli over several months. This created a need for rapid, reliable and cost-efficient evaluation methods both for the implementation of novel genome editing tools and the day to day test of sgRNA designs. In fact, in maize, for example, CRISPR/Cas9-mediated mutation rates show important variations between genes and between guides in a given gene (Doll et al., 2019), despite ever improving bioinformatics tools for the design of sgRNAs. With a size of 2.3 Gb and over 32,000 predicted genes the B73 maize reference genome is of intermediate size for angiosperms and behaves as a diploid despite important remnants of its allotetraploid origin (Schnable et al., 2009). Protoplasts are an attractive test system, since a large number of cells can be transformed in parallel to provide in depth insight in the efficiency of a molecular construct within one or two days (Lin et al., 2018). In maize, protoplast systems have been used for the initial setup of the technology with a marker gene (Feng et al., 2016), the codon-optimization of the Cas9 protein and the validation of an endogenous maize U6 snRNA promoter (Zhu et al., 2016), the test of new vector sets (Xing et al., 2014; Gentzel et al., 2020), the establishment of a DNA-free protocol based on pre-assembled ribonucleoprotein complexes (RNPs) composed of purified recombinant Cas9 enzyme and *in vitro* transcribed guide RNA (gRNA) molecules (Sant'Ana et al., 2020) and the evaluation of targeted base editing (Zong et al., 2017).

Here we used a streamlined maize protoplast system coupled to a novel NGS analysis pipeline to evaluate the efficiency of different sgRNA scaffolds, novel Cas9 variants with relaxed PAM sequences and cytidine base editing. Selected constructs were also used in stable maize transformation.

Materials and methods

Plant material and growth conditions

The maize (*Zea mays*) inbred line A188 (Gerdes and Tracy, 1993) and derived transgenic or edited plants were grown in 15 m^2 growth chambers that fulfil the French S2 safety standards for the culture of transgenic plants (Gilles et al., 2021). The

photoperiod consisted of 16 h light and 8 h darkness in a 24 h diurnal cycle. Temperature was set to 26°C/17°C (day/night) during the first 3 months after sowing and then to 28°C/19°C for the remaining month of the life cycle. The relative humidity was controlled at 55% (day) and 65% (night). Seeds were germinated in 0.2 l of Favorit MP Godets substrate (Eriterre, Saint-André-de-Corcy) and transferred after 2 weeks to 8 l of Favorit Argile TM + 20% perlite substrate (Eriterre, Saint-André-de-Corcy) and watered with a nutritional solution composed of 1.2 g/l Peters® Excel Hard Water Grow Special 18-10-1+2 MgO+TE (ICL Limas, France) and 0.04 g/l Micromax (ICL Limas, France). The insertional mutant *Zmicea::Mu* (UFmu-02855) of the UniformMU collection (Settles et al., 2007) was obtained from the stock center of the maize genetics cooperation. All plants were propagated by hand pollination.

Protoplast extraction and transformation

Maize protoplast extraction and transformation were performed with a protocol adapted from (Wolter et al., 2017) with line A188 (Figure 1A). Briefly, 12-15 days old seedlings were grown in soil with a 16 h photoperiod and the youngest fully expanded leaves (Figure 1B) of 4 healthy plants were transferred into a 94 mm Petri dish with 15 ml of enzyme mix (0.6 mannitol, 10mM MES pH 5.7, 1.5% w/v Cellulase R-10, 0.75% w/v Macerozyme R-10, 0.1% w/v Pectolyase Y-23, 10mM $CaCl_2$, 0.1% v/v BSA) and cut in 1 mm stripes parallel to the midrib (Figure 1C). The stripes were arranged in a monolayer and vacuum infiltrated at -500 mbar for 30 min in the dark at room temperature followed by incubation at 26°C with shaking (20 rpm) for 4 h.

The protoplasts were filtered through a 70 µm cell strainer, collected by centrifugation at 100 g and resuspended in 2 ml W5 buffer (154 mM NaCl, 125 mM $CaCl_2$, 5 mM KCl, 2 mM MES pH 5.7, Figure 1D). The protoplasts were layered on a sucrose cushion (Banks and Evans, 1976) and centrifuged for 10 min at 200 g to eliminate cell debris (Figure 1E). The protoplasts were washed in four times their volume of W5, centrifuged for 5 min at 100 g, resuspended in W5 and put on ice for 30 min. In the meantime, the protoplasts were counted, usually yielding 3-4 x 10^6 cells. The protoplasts were centrifuged at 100 g for 5 min and resuspended in MMG buffer (0.4 M mannitol, 15 mM $MgCl_2$, 4 mM MES pH5.7) to a 2.5 x 10^6 cells ml^{-1} density.

Each transformation was performed in a 2 ml Eppendorf tube adding the three following solutions in that order, mixing gently but thoroughly: 500 000 protoplasts (200 µl), 1.62 x 10^{23} copies of plasmid DNA (NucleoBond® Xtra Maxi, Machery-Nagel Hœrdt, France) and 250 µl polyethylene glycol (PEG) solution (40% w/v PEG 4000, 0.2 M mannitol, 0.1 M $CaCl_2$). After 15 min of incubation in the dark at room temperature, 800 µl of W5 was added and the tubes were centrifuged for 3 min at 100 g. The pellet was resuspended in 2 ml W5 and the protoplasts were transferred in 24 well cell culture plates and incubated for 48 h at 26°C in the dark.

The protoplast transformation efficiency was calculated by dividing the number of cells expressing green fluorescent protein (GFP; parallel transformation with plasmid L1036 promoting GFP expression under the control of the constitutive cassava vein mosaic virus (*CsVMV*) promoter, Figure 1F) by the total number of viable cells using an Axio Imager M2 fluorescence microscope (Zeiss, Figure 1G). Protoplasts were pelleted for 3 min at 100 g and the pellets stored at -80°C.

Vectors for targeted mutagenesis and base editing

The original vectors harboring different Cas9 derivatives and/or scaffolds (Supplementary Table S1) were derived from L1609, an integrative plasmid harboring the Cas9 cassette, an empty site for sgRNA1 and a Basta resistance cassette, and L1611, a small plasmid used for initial cloning of sgRNA2 (Doll et al., 2019).

Stable maize transformation

Agrobacterium-mediated transformation of inbred line A188 was performed according to a published protocol (Ishida et al., 2007). Briefly, immature 13 DAP embryos were co-cultivated with Agrobacterium and glufosinate-resistant type I calli (hard and compact) selected on auxin containing media. After suppression of auxin, shoots were initiated in the presence of cytokinin and gibberellin inhibitors. Roots were obtained in the absence of hormones. Finally, the plantlets were transferred to soil (see above). The precise composition of the different *in vitro* culture media and the respective incubation times are summarized in Supplementary Table S2.

DNA extraction and amplification

DNA extractions from transformed protoplasts (500 000 protoplasts) or from leaf punches (5 punches of 25 mm^2) of stably transformed plantlets (10 DAS) were performed with a Biosprint 96 robot (Qiagen) and a DNeasy 96 plant kit (Qiagen). The gene-specific parts of the primers (Supplementary Figure S1) and melting temperatures used to amplify the target regions around the CRISPR/Cas9 binding site with Phusion™ High-Fidelity DNA Polymerase (Thermo Scientific) are indicated in Supplementary Table S3.

10.3389/fpls.2022.1010030

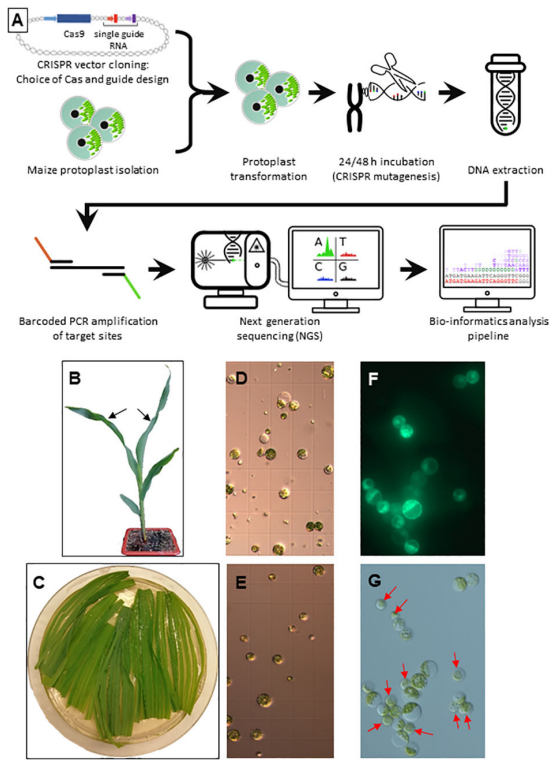

FIGURE 1
Protoplast isolation and transformation **(A)** Overview of the developed workflow. **(B)** Germination at 4 leaf stage. The two youngest leaves used for protoplast isolation are indicated by black arrows. **(C)** Longitudinally sliced leaf pieces during enzymatic digestion. **(D, E)** Protoplast preparations before **(D)** and after **(E)** purification on a sucrose gradient. **(F, G)** Protoplasts 48 h after transformation with a GFP control plasmid in UV light **(F)** and visible light **(G)**. Red arrows indicate non-transformed protoplasts.

Molecular characterization of stable maize transformants

Transfer DNA (T-DNA) integrity was checked as previously described (Gilles et al., 2017). Molecular characterization of the sites targeted by genome editing involved, for each targeted gene, PCR amplification with specific primers (Supplementary Table S3) on DNA extracted from leaves of T0 plants, followed by Sanger sequencing. In T1 plants segregation of Cas9 bearing T-DNA was evaluated by PCR amplification of the *Bar* gene, checking the presence and quality of genomic DNA by PCR amplification of the GRMZM2G136559 (Zm00001eb386680) control gene (Doll et al., 2019).

Library construction and sequencing

Protoplast PCR products spanning the CRISPR/Cas9 target site and carrying tails with homology to NGS adapters (Supplementary Figure S1) were gel purified, cleaned with the NucleoSpin Gel and PCR Clean-up kit (Machery-Nagel Hœrdt, France) and quantified with the Qubit dsDNA high-sensitivity assay (Thermo-Fischer). Libraries were constructed with Index5/Index7 adapters, quality controlled with a High Sensitivity D1000 ScreenTape Assay on an Agilent Tapestation and sequenced in multiplex (12 libraries) with a NextSeq 500/550 Mid Output v2 kit (300 cycles) on an Illumina NextSeq500 platform in paired-end mode.

NGS analysis

Software of the Illumina NextSeq500 platform was used to assign raw read sequences to libraries based on the indexes and to trim the NGS adapters. For subsequent analysis, a 7-step bioinformatics pipeline mixing existing programs and custom-made scripts was built (Figure 2, https://gitbio.ens-lyon.fr/rdp/crispr_proto_maize). In the first step the paired-end reads were assembled with PEAR software (Zhang et al., 2014, version 0.9.10). The assembled reads were quality checked using fastQC (http://www.bioinformatics.babraham.ac.uk/projects/fastqc, version 0.11.7) and trimmed using fastq-mcf (https://github.com/ExpressionAnalysis/ea-utils, version 1.04.676). To avoid problems in downstream sequence alignments, sequences containing one or several undetermined nucleotides (N) after this step (on average, 0.02% of the output sequences) were eliminated from further analysis despite their overall acceptable quality. For the third step of the pipeline a specifically developed Python program was used to trim the 5-nt tags at both extremities of the sequence and to concatenate their sequences to the sequence name. This program then identified identical sequences, counted their number of occurrences and adjusted this count if not only the sequences but also the tags were identical, *i.e.* the sequences were PCR duplicates, corresponding in fact to a single initial editing event. At the end of this step the obtained file (in FASTA format) contained one sequence for each group of identical sequences and their counts. The next step consisted in the pairwise alignment of the representatives of the different groups of reads with the reference sequence using the Needleman & Wunsch algorithm, as implemented in the 'needle' program from EMBOSS (Needleman and Wunsch, 1970, Rice et al., 2000; version 6.6.0.0, with scoring matrix EDNAFULL83 and options "-gapopen 10.0 -gapextend 0.5"). After the alignment, another Python program identified the different mutations and computed their frequencies. These quantitative data contained in this file were used in the last step of the pipeline to create a logo (Figure 2).

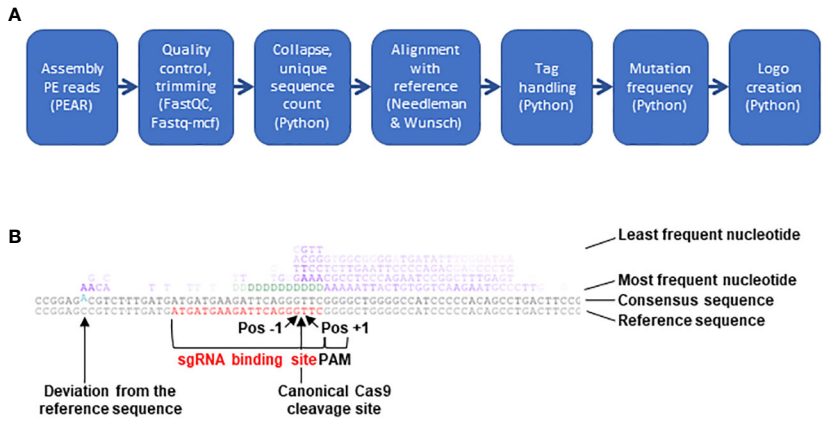

FIGURE 2
NGS analysis pipeline. **(A)** Schematic presentation of the 7 steps constituting the bioinformatics pipeline built to analyze CRISPR/Cas9-mediated mutations. **(B)** Example of mutation logo. The logo shows from the bottom to the top the reference sequence (sgRNA binding site in red), the consensus of all sequences (differences to the reference sequence in blue and offset) and the most frequent nudeotide at mutated sites. The following lines represent other nucleotides with decreasing frequency. In the upper 4 lines insertions and mismatches are indicated by the four bases G, A, T and C (in purple) and deletions (absence of a base at a given position) by aD (in green). The intensity of each letter is proportional to its frequency. The position of the canonical Cas9 cleavage site 3 nudeotides upstream of the PAM is indicated by an arrow. Pos-1, first base to the left of the cleavage site; Pos+1, first base to the right of the cleavage site.

Results

Coupling of protoplast transformation with NGS provides deep insight in the CRISPR/Cas9 mutation landscape

To reliably evaluate genome editing by CRISPR/Cas9 in maize protoplasts, a robust experimental system yielding protoplasts with a good viability at high density was established. Comparative tests of several parameters incited us to use as starting material young leaves of soil born germinations, which were easier to obtain in large quantity and without the risk of contamination than *in vitro* germinations or Black Mexican Sweet (BMS) cell cultures (Figure 1). Other important choices to increase the overall yield and/or viability were the tenderness of the leaves (the two youngest leaves at the 4 to 5 leaf stage, Figure 1B), the addition of pectolyase to the enzyme mix containing also cellulase and macerozyme, the vacuum infiltration of the enzyme mix, a purification step on a sucrose cushion, the use of polyethylene glycol (PEG) rather than electroporation for DNA uptake, ultrapure plasmid DNA without salts and simple deep freezing rather than grinding of protoplasts prior to DNA extraction (see Materials and Methods for details). The transformation rate was calculated by transforming a protoplast aliquot with a plasmid expressing a *GFP* reporter gene under the control of the constitutive *CsVMV* promoter (Figure 1).

After incubation for 24 to 48 h allowing transcription, translation and action of the CRISPR/Cas9 tool, total DNA was extracted from protoplasts. To assess the different types of mutations caused by a given construct in a pool of protoplasts, the target site was amplified with a proof-reading enzyme by site-specific PCR and the PCR product subjected to NGS sequencing (Figure 1A). In addition to the maize-specific part, the primers contained a 5 nt tag with a random sequence and part of the Illumina adapter (Supplementary Figure S1). The random nature of the tag allowed to distinguish NGS sequence reads originating from independent amplifications of the target site (different tags) or representing the same PCR product (identical tag). This tag is not to be confused with the index added during the second amplification with the full Illumina adapter, which allowed multiplexing of libraries in a single flow cell. The raw sequence data obtained were deposited at EBI under the accession number PRJEB56234.

To analyze the type and frequency of CRISPR/Cas9-mediated mutations, a 7-step bioinformatics pipeline combining existing programs and custom-made scripts was developed (Figure 2A) and made available (https://gitbio.ens-lyon.fr/rdp/crispr_proto_maize). The overlapping paired-end mode was chosen to enhance sequence quality and allow the processing of slightly larger PCR products compared to single read mode. After classical pairing with PEAR (Zhang et al., 2014), quality control with FASTQC (Andrews, 2010) and trimming of remaining adapter sequences with Fastq-mcf (Aronesty, 2013), the tags at the 5' and 3' ends of the sequences were removed with a Python script and added to the sequence name. In the next step, unique sequences were counted and extracted for alignment with the non-mutated reference sequence. After testing several alternatives such as

BLAST, Bowtie or Smith & Waterman, pairwise alignments with the reference sequence were performed with the Needleman & Wunsch algorithm using a custom score matrix and suitable gap opening and extension penalties, since it (i) allowed systematic alignment over the entire length of the reference sequence and (ii) satisfactorily handled even important size differences between the mutated and the reference sequence. The next step allowed to quantify by a Python script the different types of mutations (deletion, insertion, mismatch) for each position of the reference sequence, excluding the primer regions and distinguishing the 20 nt CRISPR/Cas9 range corresponding to the sgRNA binding site from the rest of the amplified sequence. Finally, the types and positions of the mutations were summarized in a logo (Figure 2B). Together with an original assembly of the tools, the logo was the most distinctive feature of the pipeline (Supplementary Table S4, Guell et al., 2014; Boel et al., 2016; Park et al., 2016; Pinello et al., 2016; Wang et al., 2017; Liu et al., 2019).

This experimental system was used to analyze the CRISPR/Cas9 mutation landscape at 14 different target sites (Supplementary Table S3). On average, nearly 15 million sequence reads were obtained for each target. An average 99.2% success rate of the PEAR step and a 99.3% success rate of the combined FASTQC/Fastq-mcf step were indicators for excellent sequence quality (Supplementary Table S5). The collapse to unique sequences reduced the number of reads to 11% on average, rendering the time-consuming pairwise alignment step easily feasible. After several tests, the (modifiable) default minimal value of the Needleman & Wunsch score needed for a sequence to be retained for subsequent steps was fixed to 200, which was a compromise between exhaustiveness to include even large deletions or insertions and specificity to exclude PCR products not related to the target site. When applying this default threshold, on average 8.2% of the unique sequences were eliminated (Supplementary Table S5). The next step was to count the occurrences for each unique sequence in the initial read sets either with or without consideration of the 5-nt tag. Considering the mutation rate at every single position of the 14 analyzed amplicons, the highest difference ever observed with or without consideration of the tag was a 2.1-fold decrease when considering the 5 nt-tag. This suggested that there was no strong over-representation of particular PCR products and that the relative values obtained with or without tag were very similar. In the last step the table with numerical values was exploited to create a visual representation of the results (mutation logo, as exemplified in Figure 2B). With regard to the canonical Cas9 cleavage site 3 nucleotides upstream of the PAM site, the positions of mutations will be indicated with increasing negative or positive numbers to the left (upstream) or to the right (downstream) of the cleavage site throughout this manuscript (Figure 2B).

Theoretical considerations indicate that the observed final counts are only semi-quantitative values under our experimental setup. The transformation of 500 000 protoplasts allows at the most 1 million (diploid genome) independent mutations. Since each amplicon was sequenced with a depth of 15 million reads, this indicates that on average a given mutation was independently amplified 15 times with different 5-nt tags. Considering that only 80 ng of protoplast DNA (containing approximately 66 000 genomes) was amplified, the real effect was even much stronger. This limitation needs to be kept in mind when analyzing the numbers presented in the following chapters.

Mutagenesis tendencies in selected *ZmSWEET* genes

In order to validate our quick transient protoplast transformation to gather information on CRISPR/Cas9 efficiency, we targeted three genes from the *Sugars Will Eventually Be Exported Transporter* (*SWEET*) family, previously identified as expressed at an embryo/endosperm interface (Doll et al., 2020): *ZmSWEET14a* (Zm00001e011125), *ZmSWEET14b* (Zm00001e021494) and *ZmSWEET15a* (Zm00001e022582). Each gene was targeted with two sgRNAs, which were identical for the paralogous genes *ZmSWEET14a* and *ZmSWEET14b* showing very high sequence homology (Supplementary Table S3). For NGS analysis, gene specific primers were designed to amplify the two targets in *ZmSWEET14a* and in *ZmSWEET14b* with a single amplicon of 199 bp and 194 bp, respectively. For *ZmSWEET15a*, only the mutagenesis events at the sgRNA1 target were analyzed.

To assess the general sgRNA design efficiency, the occurrence of mutations (deletions, insertions and mismatches) starting or ending within the 20-nt target regions was compared to the occurrence of mutations originating outside of the targets. All five targets considered, the number of deletions and insertions per base was at least 11 times and up to 567 times higher within the 20-nt target than in the rest of the amplicon. The number of mismatches was also slightly higher within all targets except for the sgRNA2 target in *ZmSWEET14a* (Supplementary Table S5). Please note that sgRNA1 contained an additional A at its 5'-end, which was not present at the genomic target site, to allow efficient transcription from the OsU3 promoter (Supplementary Table S3).

Although the sgRNA target sequences were identical between *ZmSWEET14a* and *ZmSWEET14b* the type of deletions observed within the target range of sgRNA1 showed contrasted results between the two genes (Figure 3A). For example, a deletion at position -2 to -1 was 10 times more frequent for *ZmSWEET14b* as compared to *ZmSWEET14a*. In contrast, the type of deletions observed at sgRNA2 target followed the same trends for the two genes with the highest frequency observed for a CC deletion at position -2 to -1 (Figure 3A). For *ZmSWEET15a*, the usual -1 position had the highest deletion frequency (25%), followed by positions -5 to -2

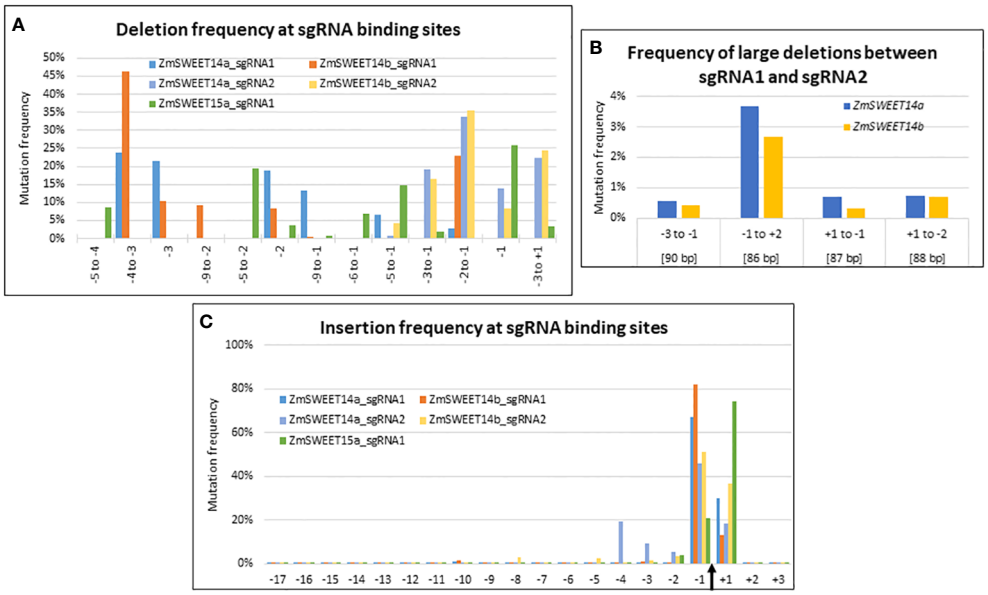

FIGURE 3
CRISPR/Cas9-induced mutations landscape in ZmSWEET genes. **(A–C)** Graphs indicating the deletion and insertion frequency in Zm00001e011125 (ZmSWEET14a), Zm00001e021494 (ZmSWEET14b) and Zm00001e022582 (ZmSWEET15a). **(A)** Frequency of selected deletions. **(B)** Frequencies of large deletions observed between the two target sites in Zm00001e011125 (ZmSWEET14a) and Zm00001e021494 (ZmSWEET14b). Positions are relative to the Cas9 cleavage sites of each target. Values in brackets indicate the length of the deletions. **(C)** Frequency of insertions at all positions of the target sequences. The Cas9 cleavage site is indicated by a black arrow. The numbers of the x-axis indicate the position of the mutations relative to this cleavage site.

(20%) and -5 to -1 (15%) (Figure 3A). The efficiency of sgRNA2 (~85%) to generate deletions in *ZmSWEET14a* and *ZmSWEET14b* was far greater than the one of sgRNA1 (~9%) (Supplementary Figure S2A).

Large deletions between the two targets sites of *ZmSWEET14a* and *ZmSWEET14b* represented ~5% of all deletions observed for each gene, with the highest frequency observed for the 86 bp deletion between position -1 of the first target and position +2 of the second target (Figure 3B).

The vast majority of insertions concerned positions -1 and +1 for all 5 targets, the values at position -1 being higher with the exception of *ZmSWEET15a* (Figure 3C). There was a good correspondence for sgRNA1 and sgRNA2 targets between *ZmSWEET14a* and *ZmSWEET14b*. The efficiencies of the two sgRNAs to generate insertions in *ZmSWEET14a* and *ZmSWEET14b* were balanced in *ZmSWEET14a* with ~47% and ~53%, whereas sgRNA2 was more efficient in *ZmSWEET14b* (~77%) than in *ZmSWEET14a* (~23%). The imbalance for sgRNA2 was reminiscent of the one observed for deletions (Supplementary Figure S2B).

The two vectors used to target *ZmSWEET14a*, *ZmSWEET14b* and *ZmSWEET15a* in protoplasts were used in parallel to generate stable transformants (Supplementary Table S6). All nine T0 *Zmsweet14a/14b* mutant plants bared mutations at the sgRNA2 target site for each gene and only one plant had a mutation at the sgRNA1 target site in *ZmSWEET14b* (a 1 bp insertion at position -1). The analysis of 8 events (for one event Sanger sequencing could not be interpreted) at the sgRNA2 target site in *ZmSWEET14a* revealed that all events were bi-allelic. The most frequent ones with 62.5% (10/16) and 18.75% (3/16) were a 1 bp insertion at position -1 and a 1 bp deletion at position -1, respectively. In *ZmSWEET14b*, the most frequent types of mutation were a 1 bp insertion at position -1 (20%), a 5 bp deletion at position -2 to +3 (20%) and a 90 bp deletion (20%) not located between the two targets. In the case of *ZmSWEET15a* only one plant was retrieved after stable genetic transformation, and this plant carried a 23 bp deletion at the sgRNA1 target site (Supplementary Table S6). These numbers obtained in stable maize transformation of immature embryos are not statistically significant due to small sample size but fit the overall trends observed in the leaf protoplast system.

Similar efficiency of three different sgRNA scaffolds

One of the major changes in adapting the naturally occurring type II CRISPR/Cas9 bacterial defense system to a biotechnology tool was the fusion of the crRNA and a normally trans-encoded tracrRNA into a single sgRNA molecule capable to form a complex with the Cas9 protein and to sequence-specifically cleave target DNA (Jinek et al., 2012; Cong et al., 2013). Several

designs of sgRNA scaffolds have been proposed mainly differing in the length and structure of the hairpin linking the two initial molecules (Supplementary Figure S3). To compare the most frequently used scaffold in plants (Shan et al., 2013) with two alternative designs (Miao et al., 2013; Dang et al., 2015), the same 20 nucleotides complementary to the target sequence in Zm00001e008508 was linked to the three different scaffolds called hereafter Shan, Miao and Dang (Figure 4A and Supplementary Table S3). All three scaffolds were transformed in parallel into aliquots of a single batch of maize protoplasts (data set 1: Shan1, Miao1 and Dang1) and the experiment was repeated for the Shan and Miao scaffolds several months later (data set 2: Shan2 and Miao2).

In a first instance, the type of scaffold may influence the rate limiting step of double stranded breaks which is the formation of a ternary complex between Cas9/sgRNA and DNA (Raper et al., 2018). Using the ratio of mutations within over outside the target range as an indicator of CRISPR/Cas9 efficiency, all three scaffolds resulted in efficient targeted mutagenesis (Supplementary Table S5, Supplementary Figure S3). In the first experiment (single protoplast batch for three constructs), the Dang scaffold showed a lower deletion efficiency (31-fold increase within the target range) than the Shan (99-fold) and Miao scaffolds (128-fold). For insertions, the efficiency was quite similar between the Dang (42-fold), Shan (31-fold) and Miao scaffolds (35-fold) There were no tangible differences between scaffolds for mismatch mutations (0.35, 0.37 and 0.37-fold increase respectively, Supplementary Table S5).

In addition, the nature of the Cas9/sgRNA complex can have an influence on the type of double strand break (blunt versus staggered), which in turn influences the repair mechanisms involved and finally the type of mutations (Molla and Yang, 2020). A closer look at the type and position of the deletions and insertions revealed a remarkable difference of the Dang scaffold for single base deletion at the +1 position (13%) compared to the Shan (2%) and Miao (1%) scaffolds (Figure 4B). The frequency remained nevertheless lower than at the usual -1 position (36%). Despite some minor quantitative differences, the overall pattern for other deletions as well as for insertions was quite similar between repetitions and between scaffolds (Figures 4B, C).

Finally, the fully independent repetition of the experiment for the Shan and Miao scaffolds showed that the mutation rates within and outside the target range were more different between experiments than between scaffolds (Supplementary Table S5) suggesting that (semi)-quantitative comparisons need to be carried out in a single experiment with parallel plasmid DNA isolation, the same batch of protoplasts, parallel NGS library construction and the same Illumina flow cell.

Cas9 variants with relaxed PAM sites work in maize

The recent development of engineered Cas9 proteins with relaxed PAM sequences has alleviated the limitation of the strict NGG PAM sequence of the original SpCas9 system and given access to larger portions of genomes for genome editing. To assess the relative efficiencies of the xCas9 (Hu et al., 2018) and Cas9-NG (Nishimasu et al., 2018) variants, we took advantage of the high sequence similarity between the two paralog genes *ZmGASSHOa* (*ZmGSOa*, Zm00001e035023) and *ZmGASSHOb* (*ZmGSOb*, Zm00001e010407) to design two sgRNAs, each of them targeting the same string of 20 nt in both *ZmGSO* genes followed by either the canonical NGG PAM in one of the *ZmGSO* genes or an alternative NG PAM (CGC or CGA) in the other *ZmGSO* gene (Figure 5A). Protoplast transformation was performed with individual constructs for each Cas9 alternative and resulted in typical small insertions and deletions around the Cas9 cleavage site for both systems (Figure 5 and Supplementary Figure S4).

Both xCas9 and Cas9-NG actually provoked deletions at the non-canonical NGC and NGA PAM sites. However, the number of deletions for 5 selected intervals (Figures 5B, C) was on average 5 times (Cas9-NG) and 101 times (xCas9) lower than for the canonical NGG PAM at the sgRNA1 target site and on average 10 times (Cas9-NG) and 2980 times (xCas9) lower at the sgRNA2 target site. Similarly, the number of insertions at positions -3, -2, -1 and +1 (Figures 5D, E) was on average 35 times (Cas9-NG) and 87 times (xCas9) lower than for the canonical NGG PAM at the sgRNA1 target site and on average 11 times (Cas9-NG) and 2017 times (xCas9) lower at the sgRNA2 target site. Taken together these results indicate that the capacity to induce indels at NG PAM sites as compared to NGG PAM sites is one order of magnitude lower for Cas9-NG and two to three orders of magnitude lower for xCas9.

The relative frequencies of selected deletions were very similar for the NGG/NGC context for both xCas9 (at the most 1.68-fold) and Cas9-NG (at the most 1.91-fold, Supplementary Figure S4A), whereas more substantial differences existed for the NGG/NGA context for xCas9 (maximum 41-fold at positions –5 to -2) and Cas9-NG (maximum 25-fold at positions -2 to -1) Supplementary Figure S4B). Insertions were most frequent at the -1 position followed by the -2 and either the -3 or +1 position for the NGG/NGC context and by the +1 position for the NGG/NGA context. Differences affecting only one Cas9 variant in a given NGG/NG context may reflect differences in Cas9 positioning at the target site due to sub-optimal engineering.

10.3389/fpls.2022.1010030

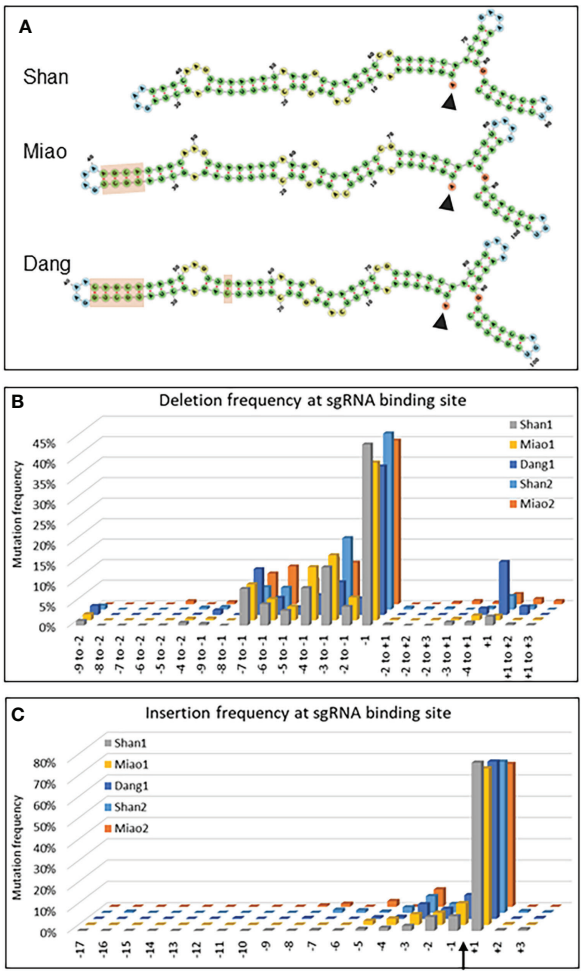

FIGURE 4
Evaluation of sgRNA scaffolds. **(A)** Secondary structures of the sgRNAs composed of the 20 nucleotides complementary to the target sequence in Zm00001e008508 (start indicated by arrowhead) and the three different scaffolds indicated. The light brown rectangles highlight the differences between the scaffolds. **(B, C)** Graphs indicating the deletion **(B)** and insertion **(C)** frequency of mutations for selected deletions **(B)** and insertions at all positions **(C)** of the 20 nt target sequence of Zm00001e008508. The Cas9 cleavage site is indicated by an arrow. Shan1 and Shan2, as well as Miao1 and Miao2, are biological replicates, i.e. represent data from two independent experiments carried out at several months' interval with different protoplast batches and independent DNA extraction, amplification and NGS analysis.

APOBEC1 C-deaminase permits efficient base editing in maize

Base editing has emerged as an efficient albeit more limited alternative to gene editing by homologous recombination (Mishra et al., 2020). For C to T editing, two main sources for cytidine deaminases have been successfully used in plants, APOBEC1 from rat (Zong et al., 2017) and CDA1 from sea lamprey (Shimatani et al., 2017). In this study the nCas9-PBE (plant base editor) was used, in which the APOBEC1 domain is fused to a Cas9-D10A nickase and an uracil glycosylase inhibitor (UGI). The presence of UGI avoids an abasic site and error-prone repair and favors mismatch repair of the nicked strand (Komor et al., 2016). The target sites were chosen in Zm00001e018755 (*ZmICEa*) and Zm00001e008118 (*ZmZOU/O11*), two transcription factors of the bHLH family (Grimault et al., 2015; Feng and Song, 2018). The goals were to create a STOP codon (Q274/, target 1) and to mutate the only serine predicted *in silico* to be phosphorylated (Walley et al., 2016) (S283L, target 2) in ZmICEa, as well as to create a STOP codon (Q355/) in ZmZOU.

Protoplast transformation with individual constructs for each of the three targets (Supplementary Table S3) resulted in efficient base editing for the two targets in Zm00001e018755 (*ZmICEa*) and moderate base editing for Zm00001e008118 (*ZmZOU/O11*, Figure 6). C to T transitions were by far the most frequently observed mismatches in the sgRNA binding site of 20 nt with 84% for target 1 of *ZmICEa*, 94% for target 2 of *ZmICEa* and 47% for *ZmZOU/O11* (Supplementary Figure S5). The frequency of other nCas9 induced mismatches was very low, since the considerable background level of mismatches likely caused by errors introduced during PCR and Illumina NGS reactions (Schirmer et al., 2015) was quite similar within and outside of the sgRNA binding range, with a ratio of 0.62, 1.04 and 1.28 for the three targets (Supplementary Figure S5). Deletions and insertion were respectively one and two orders of magnitude less frequent than mismatches and there was no notable difference between their frequency in the sgRNA binding range and neighboring regions, indicating that the D10A mutation of the Cas9 efficiently reduced or aborted Cas9-mediated double strand break and subsequent NHEJ. Deletions were most frequent in homopolymer stretches, likely reflecting Illumina NGS errors.

The frequency of C to T transitions strongly varied with distance from the nCas9 nick site. For example, in the case of Zm00001e018755 (*ZmICEa*, target 2) C to T base editing gradually increased for positions -7, -8, -9 and -13, whereas no substantial base editing occurred at positions -1, -2, -3 and -15 (Figure 6). Similarly, editing was highest at position -14 for Zm00001e018755 (*ZmICEa*, target 1) and at positions -11 and -13 for Zm00001e008118 (*ZmZOU/O11*). No substantial C to T base editing was detected at the other side of the nick (positions +1 to +3) or outside of the sgRNA binding range. The observed editing window from -7 to -14 is in overall agreement with previous work (Zong et al., 2017) despite slightly different boundaries (-9 to -15).

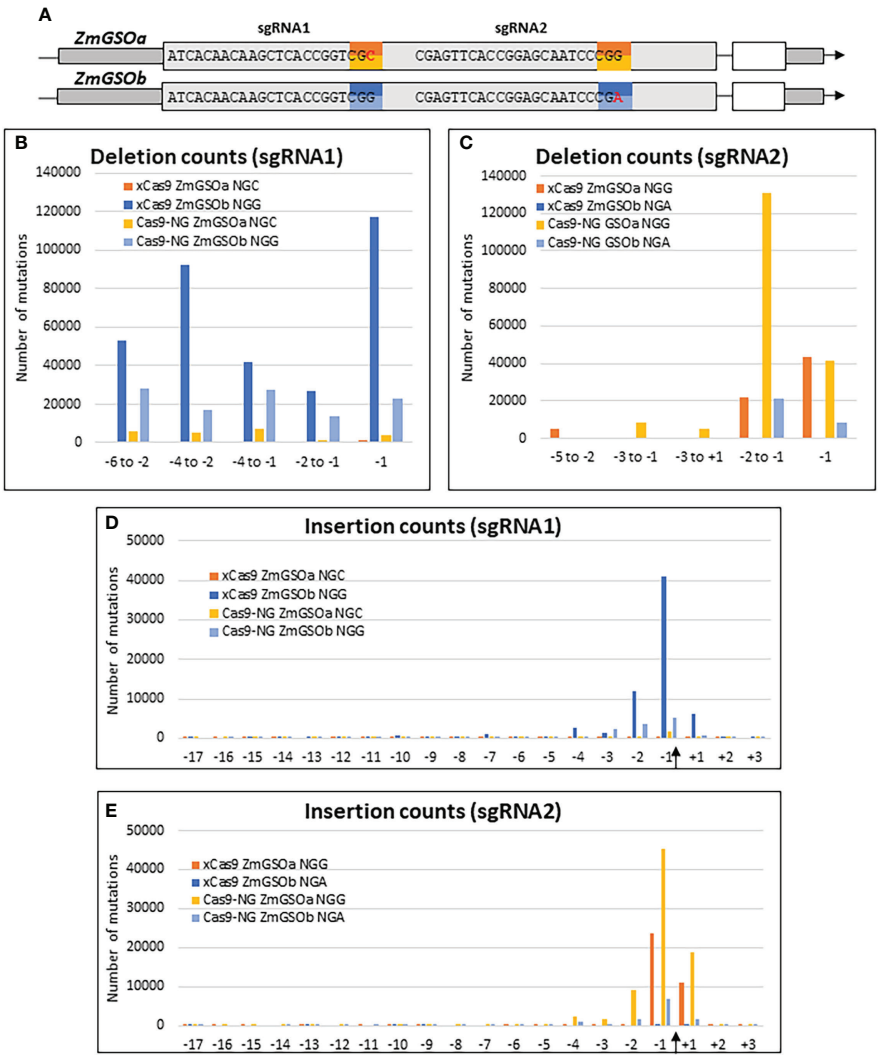

FIGURE 5
Efficiency of Cas9 variants. **(A)** Gene models of *ZmGSOa* and *ZmGSOb* indicating the target sequences and PAM sites for sgRNA1 and sgRNA2. **(B-E)** Graphs indicating the number of mutations for selected deletions **(B, C)** and insertions at all positions of the 20 nt targets **(D, E)** at the binding sites of sgRNA1 and sgRNA2 in *ZmGSOa* (NGC and NGG PAM) and *ZmGSOb* (NGG and NGA PAM) generated by xCas9 and Cas9-NG. The Cas9 cleavage site is indicated by an arrow.

Base editing of *ZmICEa* impacts stomata and plant growth

Stable transformation of the construct aiming at target 2 in *ZmICEa* (Zm00001e018755) demonstrated the predictive value of protoplast work. All 5 transformation events carried the C to T change at position -13 at target 2, which was the most frequently observed change in protoplasts (Figure 6). One of the 5 events contained in addition a double C to T mutation in positions -8 and -9 at target 2, which corresponded to the next most frequent modifications in protoplasts. More unexpectedly, another of the 5 events also carried a C to G mutation changing the triplet TCA (serine) to a TGA (stop codon), a modification also found in protoplasts but with a much lower frequency.

To assess the phenotypic impact of the loss of the single predicted phosphorylation site in ZmICEa, the corresponding *ZmiceaS283L* mutant together with the *ZmiceaS283/* mutant carrying a stop codon in the same position, and an insertional mutant *Zmicea::Mu* were propagated in parallel (Figure 7). In the T1 generation, heterozygous plants carrying the respective mutations but lacking the Cas9/sgRNA transgene were selected and self-pollinated. Phenotypic characterization was carried out on homozygous T2 plantlets. At 25 days after sowing (DAS), no notable difference in plant growth was observed for the *ZmiceaS283L* mutant, whereas the *ZmiceaS283/* and *Zmicea::*

10.3389/fpls.2022.1010030

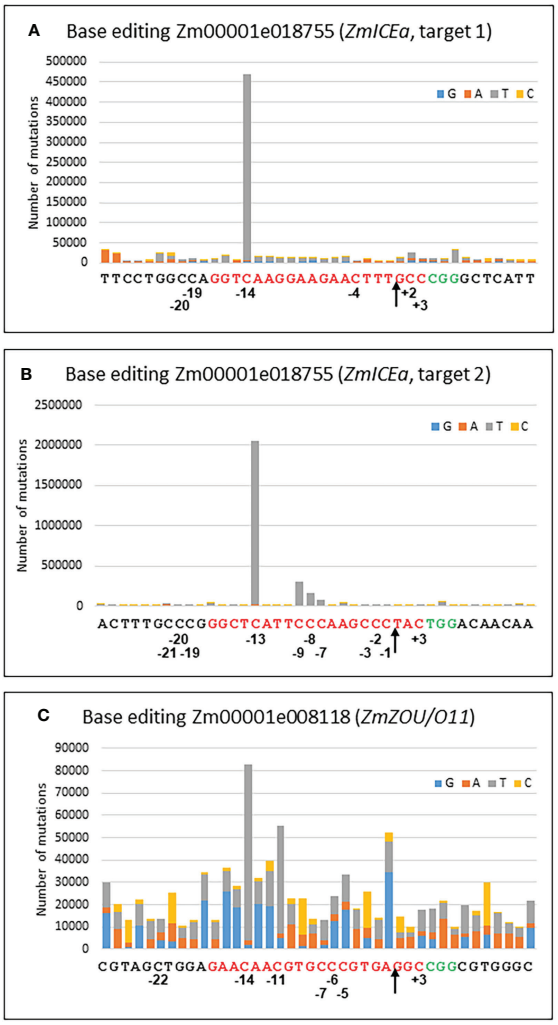

FIGURE 6
Base editing. Cumulative graph indicating the number and type of mutations for every position of the 20 nt target sequence (red) and the 10 nt upstream and downstream for target 1 **(A)** and target 2 **(B)** of Zm00001e018755 and for Zm00001e008118 **(C)**. The PAM site is in green. Positions of selected bases refer to the nCas9 nick site (arrow).

Mu mutants were smaller and had less developed root systems than wildtype siblings (Figures 7A-C). At 38 DAS (Figures 7D-F) and 66 DAS (Figures 7G-I and Supplementary Figure S6), the *ZmiceaS283L* mutant continued to grow similarly to wildtype siblings, while mutants *ZmiceaS283/* and *Zmicea::Mu* stopped growth and eventually died. Observation of leaves on a trans-illuminator revealed that mutants *ZmiceaS283/* and *Zmicea::Mu* had more transparent, paler leaves compared to wildtype and mutant *ZmiceaS283L* and presented dark green spots in the pale zones (Figures 7J-L). Leaf imprints indicated more frequent aberrations from the regularly spaced stomata pattern in mutants *ZmiceaS283/* and *Zmicea::Mu* than in wiltype and mutant *ZmiceaS283L* (Figures 7M-O). A more detailed analysis of stomata of the *Zmicea::Mu* mutant showed that they appeared small and abnormally shaped (Supplementary Figure S7). In many cases, even when the stomata looked relatively normal, the aperture of the pore which is formed by separation of the two guard cells, was not fully formed in the mutant (Supplementary Figure S7). To quantify this stomatal phenotype, indexes of normally shaped stomata, abnormally shaped stomata and meristemoids (epidermis cell number per stomata or meristemoid) on the adaxial face of the third leaf were calculated (Supplementary Figure S7J). *Zmicea::Mu* plants had 5.5-fold more abnormally shaped stomata, 5.5-fold fewer normally shaped stomata and 1.3-fold more meristemoids than wildtype.

Discussion

We present here an optimized maize protoplast system and a specifically developed bioinformatics pipeline to evaluate rapidly the efficiency of CRISPR/Cas9 constructs or of novel Cas9 variants before engaging in time- and resource-consuming stable transformation.

Protoplasts allow rapid evaluation of genome editing tools

A revisited and streamlined protocol for the preparation and transformation of maize leaf protoplasts was used to characterize the type and frequency of the modifications triggered by the CRISPR/Cas9 genome editing tool. The system showed a good repeatability between samples analyzed in two independent experiments and the comparison with the type and frequency of the modifications observed after stable transformation with some of the constructs suggested that the results of transient transformation in protoplasts were a good indicator to predict ulterior maize transformation.

As expected, the most frequently observed modifications were small indels at the cleavage site of the Cas9 enzyme 3 bp upstream of the PAM site (Chen et al., 2019; Doll et al., 2019). If most of the time the frequency of the deletions decreased both with their size and the distance of the deletion starting point from the cleavage site, in several cases specific deletions of several bases deviated from this overall pattern, for example, deletions between positions -9 and -2 in the target sequence used to compare different scaffolds (Figure 4B).

There are obvious limits to the analysis of genome editing events by PCR followed by NGS. PCR will only amplify events where both primer sequences remain present in the genome and even in paired-end mode, only PCR products smaller than 300 bp can be fully analyzed on an Illumina NextSeq500 platform, restricting the analysis to the vicinity of the target

site and excluding the detection of deletions or insertions larger than 300 bp as well as chromosome rearrangements. Large deletions of dozens of kb (Ordon et al., 2017) and recombination between chromosomes (Schmidt et al., 2020) have been reported in Arabidopsis, although they remain considerably less frequent than small indels.

For user-friendly analysis of the NGS data, a 7-step bioinformatics pipeline combining existing programs and custom-made Python scripts was developed. A first key point was the choice of the Needleman & Wunsch algorithm with a custom scoring matrix for pairwise alignments with the reference sequence to guarantee a systematic alignment over the entire length of the reference sequence and satisfactorily handle the often important size differences between the mutated and reference sequence. The other major asset was the development of an original graphical output that resumes in an intuitive logo the nature, frequency and position of the genome modifications (Figure 2).

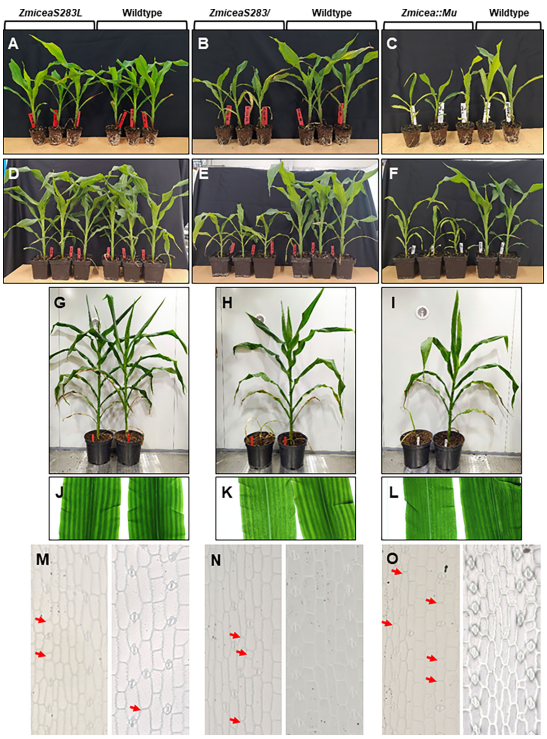

FIGURE 7
Base editing of *ZmICEa* impacts plant growth. **(A–I)** The *ZmiceaS283L* **(A, D, G, J, M)**, *ZmiceaS283/* **(B, E, H, K, N)** and *Zmicea::Mu* **(C, F, I, L, O)** mutants (T2 generation without the Cas9/sgRNA transgene, left half of the panel) and wildtype siblings (right half of the panel) were photographed 25 days after sowing (DAS, **A-C**), at 38 DAS **(D-F)** and at 66 DAS **(G-I)**. At 25 DAS the plants were removed from their pots to visually evaluate root development at the surface. **(J-L)** Observation of mutant (left) and wildtype (right) leaves on a trans-illuminator. **(M-O)** Light microscopy of leaf imprints of mutant (left) and wildtype (right) leaves. Red arrows indicate positions where stomata were expected.

Longer stems in certain plant sgRNA scaffolds do not improve genome editing

Cas9 is an inherently efficient nuclease leaving little room for improvements. On the other hand, the sgRNA is a biotechnological engineering product raising the question, whether the initial fusion of the crRNA and a normally trans-encoded tracrRNA into a single sgRNA molecule (Jinek et al., 2012; Cong et al., 2013) was the optimal solution to form a complex with the Cas9 and to be active in plants. For example, the two initial designs of Jinek et al. (2012), (Supplementary Figure S3) had quite different activity *in vitro* and underlined the importance of a minimum length of the sgRNA. The comparison of the most frequently used scaffold in plants (Shan et al., 2013) with two alternative designs with longer stems (Miao et al., 2013; Dang et al., 2015) in the maize protoplast system did not reveal any tangible differences in the efficiency of the three designs. Keeping in mind that more profound changes in the sgRNA scaffold, such as the addition of MS2 hairpins attracting transcriptional activator complexes (Chavez et al., 2016), also do not seem to notably reduce the efficiency of the system, one may conclude that the sgRNA-Cas9 interaction is rather robust to change, as long as minimum length requirements are fulfilled.

To increase the overall efficiency of genome editing in maize, other approaches may be more promising, for example the use of the *Babyboom/Wuschel* system to overcome genotype dependency (Lowe et al., 2016) and to shorten the duration of *in vitro* culture steps by the use of somatic embryogenesis (Masters et al., 2020). For genome editing of recalcitrant elite lines, trans editing also called HI editing (Kelliher et al., 2019) based on in planta transfer of the editing tool from easily transformable lab varieties also holds considerable promise (Jacquier et al., 2020). Another important consideration frequently neglected is the vectorization of Cas9. Recent studies underline the importance of optimized promoter-Cas9 and Cas9-terminator junctions for efficient genome editing (Castel et al., 2019) and report a substantial improvement by the introduction of introns in the *Cas9* coding sequence (Grutzner et al., 2021).

Relaxed PAM increases the choice of target sites for genome editing

For the first time, the activity of two Cas9 variants, xCas9 and Cas9-NG, has been assessed in maize. The efficiency of the two enzymes recognizing relaxed PAM sites differed in maize protoplasts depending on the type of the PAM sequence. In the case of the canonical NGG PAM, the lower activity of Cas9-NG compared to xCas9 observed here, has been reported before in rice protoplasts (Zhong et al., 2019) and mammalian cells

(Nishimasu et al., 2018). On the other hand, other studies report higher efficiency of Cas9-NG compared to xCas9 on NGG PAM targets in stable Arabidopsis (Ge et al., 2019) and rice transformants (Ren et al., 2019). Consequently, the relative efficiency of xCas9 and Cas9-NG in an NGG PAM context seems to vary, possibly depending on the protospacer context, the species, the vectorization (promoter, terminator) of the Cas9, and/or the method of transformation. Our study did not include a wildtype Cas9 for the same target sites, but several studies have shown that it systematically displays higher efficiencies than xCas9 and Cas9-NG on targets with NGG PAM sequence (Nishimasu et al., 2018; Ge et al., 2019; Ren et al., 2019; Zhong et al., 2019). Therefore, native Cas9 remains the system of choice for a targeted mutagenesis aiming at a single 20 nt target followed by NGG.

In the context of the non-canonical NGC PAM, the efficiencies observed here for indel induction at the target site were considerably higher for Cas9-NG than for xCas9. This observation is in agreement with other studies which consistently report higher efficiency of Cas9-NG compared to xCas9 in rice (Ren et al., 2019; Zhong et al., 2019), Arabidopsis (Ge et al., 2019) and tomato (Niu et al., 2020) with non-NGG PAMs. The efficiency observed in maize protoplasts for xCas9, at least at the tested alternative CGC PAM site, seems incompatible with routine use in stable maize transformation, despite the fact that a C in the last position of the PAM site is less favorable than a T or A (Nishimasu et al., 2018). In contrast, the frequency for Cas9-NG was more encouraging and it would be interesting to test the system to see if stable maize transformants can be generated at a reasonable rate. In conclusion, Cas9-NG but not xCas9 has the potential to expand the scope of putative targets in the maize genome not only for targeted mutagenesis but also for base or prime editing using a nickase version of the Cas9-NG backbone.

Efficient base editing in maize

C to T base editing with the nCas9-PBE (Zong et al., 2017) in maize protoplasts gave rise to contrasting results for three target sites in *ZmICEa* (Zm00001e018755) and *ZmZOU/O11* (Zm00001e008118), two transcription factors of the bHLH family (Grimault et al., 2015; Feng and Song, 2018). In *ZmICEa*, target 1 and target 2 were edited with a high efficiency comparable to targeted mutagenesis. The edits were almost exclusively of the C to T type and limited to a window from positions -7 to -14 counting from the nicking site, which is in agreement with the -9 to -15 window reported previously (Zong et al., 2017). Furthermore, the relative frequencies of edits observed during transient expression in protoplasts had predictive value for the edits actually found in stable transformants. Stable transformation also demonstrated that rare events in protoplasts may occasionally be found in transgenic maize plants, such as a C to G mutation creating a stop codon in ZmICEa.

Unexpectedly, base editing using the same base editor and identical criteria for sgRNA design was 25 times less efficient for *ZmZOU/O11*. There is no obvious explanation for this difference, but the situation is reminiscent of targeted mutagenesis of ZmZOU/O11 with an active Cas9, which has so far proven impossible to achieve in our hands, although another study managed to obtain mutant alleles (Feng et al., 2018). One may hypothesize differences in the accessibility of ZmICEa and ZmZOU/O11 for the CRISPR/Cas9 tools, for example related to different degrees of chromatin condensation. It has been shown that chromatin de-condensation by Trichostatin A (TSA) can increase the efficiency of CRISPR/Cas9-mediated indel formation in lettuce and tobacco protoplasts (Choi et al., 2021).

The results also highlighted some current limitations of base editing, which remains limited to C and A base editors that act in a narrow window. T and G base editors are needed to complete the tool kit, while variations in the length of the linker between the nCas9 and the base editor domain can give access to other editing windows (Tan et al., 2019). Optimized prime editing fusing nCas9 to a reverse transcriptase rather than a base editor is another promising alternative to overcome present limitations (Lin et al., 2021; Xu et al., 2022).

ZmICEa is necessary for stomatal development and plant growth

In Arabidopsis, AtICE1, the founding member of the ICE family, is a bHLH transcription factor involved in three different pathways: cold-tolerance (Chinnusamy et al., 2003), stomatal development (Kanaoka et al., 2008) and seed development (Xing et al., 2013; Denay et al., 2014). In leaves, AtICE1 and AtCRM2 form heterodimers with AtSPEECHLESS, AtMUTE and AtFAMA, three bHLH transcription factors, to regulate stomatal development (Kanaoka et al., 2008). This regulation is conserved in grasses such as Brachypodium (Raissig et al., 2016) and rice (Wu et al., 2019), although the wiring is somewhat modified (Nunes et al., 2020). These data, together with the stomatal phenotype reported in ZmZOU/O11 ectopic expression lines (Grimault et al., 2015), and the fact that *ZmiceaS283/* and *Zmicea::Mu* mutants showed reduced growth and chlorosis, led us to test whether ZmICEa (Zm00001e018755) plays a role in stomatal development. We found that in *Zmicea::Mu* mutants, even when the stomata looked relatively normal, the aperture of the pore was not fully formed, a phenotype which is likely to restrict gas exchange potentially leading to the chlorotic leaf phenotype. We also

found abnormally shaped stomata similar to those observed in the *Osfama-1* mutant (Liu et al., 2009). Our data suggest that, contrary to AtICE1 which, redundantly with AtSCRM2, is necessary throughout stomatal development, ZmICEa could be specifically and non-redundantly be required during the last steps of stomatal differentiation. It would be interesting to test the physical interactions of ZmFAMA with ZmICEa in order to see whether this apparently specific late role reflects a specific protein binding affinity.

The absence of a strong stomatal phenotype in the *ZmiceaS283L* mutant, where base editing prevents the predicted phosphorylation of the serine residue, may be explained either by the fact that this phosphorylation is not indispensable for ZmICEa to fulfill its role in stomatal development, or by a stabilization of ZmICEa in the absence of phosphorylation, leading to a gain-of-function rather than loss-of-function phenotype similarly to what has been reported for the semi-dominant *Atice1-1/AtScrm-D* allele (Chinnusamy et al., 2003).

Data availability statement

The data for this study have been deposited in the European Nucleotide Archive (ENA) at EMBL-EBI under accession number PRJEB56234 (https://www.ebi.ac.uk/ena/browser/view/PRJEB56234).

Author contributions

ND-F, AG, TW, and PR designed the research; YF, NMAJ, EM, CR, and JL-M performed research; LG and JJ contributed new computational tools; YF, NMAJ, LG, JJ, JL-M, TW, and PR analyzed data; and YF and PR wrote the paper. All authors contributed to the article and approved the submitted version.

Funding

The work was financed in part by the Investissement d'Avenir program of the French National Agency of Research for the project GENIUS (ANR-11-BTBR-0001_GENIUS). YF was supported by a CIFRE fellowship of the ANRT (grant N° 2018/0480).

Acknowledgments

We thank Justin Berger, Alexis Lacroix and Patrice Bolland for maize culture, Hervé Leyral and Isabelle Desbouchages for media preparation, Claire Lionnet for assistance with epifluorescent microscopy, Ghislaine Gendrot and Kathy Gallay for maize transformation, and Antoine Heurtel, Marie Martelat and Hadrien Guichard for initial developments of the bioinformatics pipeline. Benjamin Gillet and Sandrine Hughes (ENS de Lyon) of the IGFL sequencing platform (PSI) are acknowledged for expert advice, library preparation and Illumina runs, and Stefan Scholten (University Göttingen) for tricks in maize protoplast isolation. Credits are attributed to Bakunetsu Kaito, Yohann Berger, Julie Ko, Smalllike, N.Style and IYIKON for their vectorial images under CC BY 3.0 license, (https://thenounproject.com/) used and modified in Figure 1A.

Conflict of interest

YF and AG were employed by MAS Seeds, NMAJ is presently employed by Limagrain Europe, TW has currently a collaborative research project with Limagrain Europe, and PR is a member of the operational directorate of the PlantAlliance consortium.

The remaining authors declare that the research was conducted in the absence of any commercial or financial relationships that could be construed as a potential conflict of interest.

Publisher's note

Supplementary material

The Supplementary Material for this article can be found online at: https://www.frontiersin.org/articles/10.3389/fpls.2022.1010030/full#supplementary-material

References

Adli, M. (2018). The CRISPR tool kit for genome editing and beyond. *Nat. Commun.* 9, 1911. doi: 10.1038/s41467-018-04252-2

Andrews, S. (2010). *FastQC: a quality control tool for high throughput sequence data* (Cambridge, United Kingdom: Babraham Bioinformatics, Babraham Institute).

Aronesty, E. (2013).). comparison of sequencing utility programs. *Open Bioinf. J.* 7, 1–8. doi: 10.2174/1875036201307010001

Banks, M. S., and Evans, P. K. (1976). A comparison of the isolation and culture of mesophyll protoplasts from several nicotiana species and their hybrids. *Plant Sci. Lett.* 7, 409–416. doi: 10.1016/0304-4211(76)90162-0

Boel, A., Steyaert, W., De Rocker, N., Menten, B., Callewaert, B., De Paepe, A., et al. (2016).). BATCH-GE: Batch analysis of next-generation sequencing data for genome editing assessment. *Sci. Rep.* 6, 30330. doi: 10.1038/srep30330

Castel, B., Tomlinson, L., Locci, F., Yang, Y., and Jones, J. D. G. (2019). Optimization of T-DNA architecture for Cas9-mediated mutagenesis in arabidopsis. *PloS One* 14, e0204778. doi: 10.1371/journal.pone.0204778

Chavez, A., Tuttle, M., Pruitt, B. W., Ewen-Campen, B., Chari, R., Ter-Ovanesyan, D., et al. (2016). Comparison of Cas9 activators in multiple species. *Nat. Methods* 13, 563–567. doi: 10.1038/nmeth.3871

Chen, K., Wang, Y., Zhang, R., Zhang, H., and Gao, C. (2019). CRISPR/Cas genome editing and precision plant breeding in agriculture. *Annu. Rev. Plant Biol.* 70, 667–697. doi: 10.1146/annurev-arplant-050718-100049

Chinnusamy, V., Ohta, M., Kanrar, S., Lee, B. H., Hong, X., Agarwal, M., et al. (2003). *ICE1: regulator cold-induced transcriptome freezing tolerance Arabidopsis. Genes Dev.* 17, 1043–1054. doi: 10.1101/gad.1077503

Choi, S. H., Lee, M. H., Jin, D. M., Ju, S. J., Ahn, W. S., Jie, E. Y., et al. (2021). TSA promotes CRISPR/Cas9 editing efficiency and expression of cell division-related genes from plant protoplasts. *Int. J. Mol. Sci.* 22. doi: 10.3390/ijms22157817

Cong, L., Ran, F. A., Cox, D., Lin, S., Barretto, R., Habib, N., et al. (2013). Multiplex genome engineering using CRISPR/Cas systems. *Science* 339, 819–823. doi: 10.1126/science.1231143

Dang, Y., Jia, G., Choi, J., Ma, H., Anaya, E., Ye, C., et al. (2015). Optimizing sgRNA structure to improve CRISPR-Cas9 knockout efficiency. *Genome Biol.* 16, 280. doi: 10.1186/s13059-015-0846-3

Denay, G., Creff, A., Moussu, S., Wagnon, P., Thevenin, J., Gerentes, M. F., et al. (2014). Endosperm breakdown in arabidopsis requires heterodimers of the basic helix-loop-helix proteins ZHOUPI and INDUCER OF CBP EXPRESSION 1. *Development* 141, 1222–1227. doi: 10.1242/dev.103531

Doll, N. M., Gilles, L. M., Gerentes, M. F., Richard, C., Just, J., Fierlej, Y., et al. (2019). Single and multiple gene knockouts by CRISPR-Cas9 in maize. *Plant Cell Rep.* 38, 487–501. doi: 10.1007/s00299-019-02378-1

Doll, N. M., Just, J., Brunaud, V., Caius, J., Grimault, A., Depege-Fargeix, N., et al. (2020). Transcriptomics at maize Embryo/Endosperm interfaces identifies a transcriptionally distinct endosperm subdomain adjacent to the embryo scutellum. *Plant Cell* 32, 833–852. doi: 10.1105/tpc.19.00756

Feng, F., Qi, W., Lv, Y., Yan, S., Xu, L., Yang, W., et al. (2018). OPAQUE11 is a central hub of the regulatory network for maize endosperm development and nutrient metabolism. *Plant Cell* 30, 375–396. doi: 10.1105/tpc.17.00616

Feng, F., and Song, R. (2018). O11 is multi-functional regulator in maize endosperm. *Plant Signal Behav.* 13, e1451709. doi: 10.1080/15592324.2018.1451709

Feng, C., Yuan, J., Wang, R., Liu, Y., Birchler, J. A., and Han, F. (2016). Efficient targeted genome modification in maize using CRISPR/Cas9 system. *J. Genet. Genomics* 43, 37–43. doi: 10.1016/j.jgg.2015.10.002

Gentzel, I. N., Park, C. H., Bellizzi, M., Xiao, G., Gadhave, K. R., Murphree, C., et al. (2020). A CRISPR/dCas9 toolkit for functional analysis of maize genes. *Plant Methods* 16, 133. doi: 10.1186/s13007-020-00675-5

Gerdes, J. T., and Tracy, W. F. (1993). Pedigree diversity within the Lancaster surecrop heterotic group of maize. *Crop Sci.* 33, 334–337. doi: 10.2135/cropsci1993.0011183X003300020025x

Ge, Z., Zheng, L., Zhao, Y., Jiang, J., Zhang, E. J., Liu, T., et al. (2019). Engineered xCas9 and SpCas9-NG variants broaden PAM recognition sites to generate mutations in arabidopsis plants. *Plant Biotechnol. J.* 17, 1865–1867. doi: 10.1111/pbi.13148

Gilles, L. M., Calhau, A. R. M., La Padula, V., Jacquier, N. M. A., Lionnet, C., Martinant, J. P., et al. (2021). Lipid anchoring and electrostatic interactions target NOT-LIKE-DAD to pollen endo-plasma membrane. *J. Cell Biol.* 220. doi: 10.1083/jcb.202010077

Gilles, L. M., Khaled, A., Laffaire, J. B., Chaignon, S., Gendrot, G., Laplaige, J., et al. (2017). Loss of pollen-specific phospholipase NOT LIKE DAD triggers gynogenesis in maize. *EMBO J.* 36, 707–717. doi: 10.15252/embj.201796603

Grimault, A., Gendrot, G., Chamot, S., Widiez, T., Rabille, H., Gerentes, M. F., et al. (2015). ZmZHOUPI, an endosperm-specific basic helix-loop-helix transcription factor involved in maize seed development. *Plant J.* 84, 574–586. doi: 10.1111/tpj.13024

Grutzner, R., Martin, P., Horn, C., Mortensen, S., Cram, E. J., Lee-Parsons, C. W. T., et al. (2021). High-efficiency genome editing in plants mediated by a Cas9 gene containing multiple introns. *Plant Commun.* 2, 100135. doi: 10.1016/j.xplc.2020.100135

Guell, M., Yang, L., and Church, G. M. (2014). Genome editing assessment using CRISPR genome analyzer (CRISPR-GA). *Bioinformatics* 30, 2968–2970. doi: 10.1093/bioinformatics/btu427

Hua, K., Jiang, Y., Tao, X., and Zhu, J. K. (2020). Precision genome engineering in rice using prime editing system. *Plant Biotechnol. J.* 18, 2167–2169. doi: 10.1111/pbi.13395

Huang, T. K., and Puchta, H. (2019). CRISPR/Cas-mediated gene targeting in plants: finally a turn for the better for homologous recombination. *Plant Cell Rep.* 38, 443–453. doi: 10.1007/s00299-019-02379-0

Hu, J. H., Miller, S. M., Geurts, M. H., Tang, W., Chen, L., Sun, N., et al. (2018). Evolved Cas9 variants with broad PAM compatibility and high DNA specificity. *Nat.* 556, 57–63. doi: 10.1038/nature26155

Ishida, Y., Hiei, Y., and Komari, T. (2007). Agrobacterium-mediated transformation of maize. *Nat. Protoc.* 2, 1614–1621. doi: 10.1038/nprot.2007.241

Jacquier, N. M. A., Gilles, L. M., Pyott, D. E., Martinant, J. P., Rogowsky, P. M., and Widiez, T. (2020). Puzzling out plant reproduction by haploid induction for innovations in plant breeding. *Nat. Plants* 6, 610–619. doi: 10.1038/s41477-020-0664-9

Jinek, M., Chylinski, K., Fonfara, I., Hauer, M., Doudna, J. A., and Charpentier, E. (2012). A programmable dual-RNA-guided DNA endonuclease in adaptive bacterial immunity. *Sci.* 337, 816–821. doi: 10.1126/science.1225829

Kanaoka, M. M., Pillitteri, L. J., Fujii, H., Yoshida, Y., Bogenschutz, N. L., Takabayashi, J., et al. (2008). SCREAM/ICE1 and SCREAM2 specify three cell-state transitional steps leading to arabidopsis stomatal differentiation. *Plant Cell* 20, 1775–1785. doi: 10.1105/tpc.108.060848

Kelliher, T., Starr, D., Su, X., Tang, G., Chen, Z., Carter, J., et al. (2019). One-step genome editing of elite crop germplasm during haploid induction. *Nat. Biotechnol.* 37, 287–292. doi: 10.1038/s41587-019-0038-x

Komor, A. C., Kim, Y. B., Packer, M. S., Zuris, J. A., and Liu, D. R. (2016). Programmable editing of a target base in genomic DNA without double-stranded DNA cleavage. *Nature* 533, 420–424. doi: 10.1038/nature17946

Lin, C. S., Hsu, C. T., Yang, L. H., Lee, L. Y., Fu, J. Y., Cheng, Q. W., et al. (2018). Application of protoplast technology to CRISPR/Cas9 mutagenesis: from single-cell mutation detection to mutant plant regeneration. *Plant Biotechnol. J.* 16, 1295–1310. doi: 10.1111/pbi.12870

Lin, Q., Jin, S., Zong, Y., Yu, H., Zhu, Z., Liu, G., et al. (2021). High-efficiency prime editing with optimized, paired pegRNAs in plants. *Nat. Biotechnol.* 39, 923–927. doi: 10.1038/s41587-021-00868-w

Lin, Q., Zong, Y., Xue, C., Wang, S., Jin, S., Zhu, Z., et al. (2020). Prime genome editing in rice and wheat. *Nat. Biotechnol.* 38, 582–585. doi: 10.1038/s41587-020-0455-x

Liu, T., Ohashi-Ito, K., and Bergmann, D. C. (2009). Orthologs of arabidopsis thaliana stomatal bHLH genes and regulation of stomatal development in grasses. *Development* 136, 2265–2276. doi: 10.1242/dev.032938

Liu, Q., Wang, C., Jiao, X., Zhang, H., Song, L., Li, Y., et al. (2019). Hi-TOM: a platform for high-throughput tracking of mutations induced by CRISPR/Cas systems. *Sci. China Life Sci.* 62, 1–7. doi: 10.1007/s11427-018-9402-9

Li, C., Zhang, R., Meng, X., Chen, S., Zong, Y., Lu, C., et al. (2020). Targeted, random mutagenesis of plant genes with dual cytosine and adenine base editors. *Nat. Biotechnol.* 38, 875–882. doi: 10.1038/s41587-019-0393-7

Lowe, K., Wu, E., Wang, N., Hoerster, G., Hastings, C., Cho, M. J., et al. (2016). Morphogenic regulators baby boom and wuschel improve monocot transformation. *Plant Cell* 28, 1998–2015. doi: 10.1105/tpc.16.00124

Mali, P., Yang, L., Esvelt, K. M., Aach, J., Guell, M., DiCarlo, J. E., et al. (2013). RNA-Guided human genome engineering *via* Cas9. *Science* 339, 823–826. doi: 10.1126/science.1232033

Masters, A., Kang, M., McCaw, M., Zobrist, J. D., Gordon-Kamm, W., Jones, T., et al. (2020). Agrobacterium-mediated immature embryo transformation of recalcitrant maize inbred lines using morphogenic genes. *J. Vis. Exp.* doi: 10.3791/60782

Miao, J., Guo, D., Zhang, J., Huang, Q., Qin, G., Zhang, X., et al. (2013). Targeted mutagenesis in rice using CRISPR-cas system. *Cell Res.* 23, 1233–1236. doi: 10.1038/cr.2013.123

Mishra, R., Joshi, R. K., and Zhao, K. (2020). Base editing in crops: current advances, limitations and future implications. *Plant Biotechnol. J.* 18, 20–31. doi: 10.1111/pbi.13225

Modrzejewski, D., Hartung, F., Sprink, T., Krause, D., Kohl, C., and Wilhelm, R. (2019). What is the available evidence for the range of applications of genome-editing as a new tool for plant trait modifcation and the potential occurrence of associated of-target efects: a systematic map. *Environ. Evid* 8, 27–59. doi: 10.1186/s13750-019-0171-5

Molla, K. A., and Yang, Y. (2020). Predicting CRISPR/Cas9-induced mutations for precise genome editing. *Trends Biotechnol.* 38, 136–141. doi: 10.1016/j.tibtech.2019.08.002

Needleman, S. B., and Wunsch, C. D. (1970). A general method applicable to the search for similarities in the amino acid sequence of two proteins. *J. Mol. Biol.* 48, 443–453. doi: 10.1016/0022-2836(70)90057-4

Nishimasu, H., Shi, X., Ishiguro, S., Gao, L., Hirano, S., Okazaki, S., et al. (2018). Engineered CRISPR-Cas9 nuclease with expanded targeting space. *Science* 361, 1259–1262. doi: 10.1126/science.aas9129

Niu, Q., Wu, S., Li, Y., Yang, X., Liu, P., Xu, Y., et al. (2020). Expanding the scope of CRISPR/Cas9-mediated genome editing in plants using an xCas9 and Cas9-NG hybrid. *J. Integr. Plant Biol.* 62, 398–402. doi: 10.1111/jipb.12886

Nunes, T. D. G., Zhang, D., and Raissig, M. T. (2020). Form, development and function of grass stomata. *Plant J.* 101, 780–799. doi: 10.1111/tpj.14552

Ordon, J., Gantner, J., Kemna, J., Schwalgun, L., Reschke, M., Streubel, J., et al. (2017). Generation of chromosomal deletions in dicotyledonous plants employing a user-friendly genome editing toolkit. *Plant J.* 89, 155–168. doi: 10.1111/tpj.13319

Park, J., Lim, K., Kim, J.-S., and Bae, S. (2016). Cas-analyzer: an online tool for assessing genome editing results using NGS data. *Bioinformatics* 33, 286–288. doi: 10.1093/bioinformatics/btw561

Pinello, L., Canver, M. C., Hoban, M. D., Orkin, S. H., Kohn, D. B., Bauer, D. E., et al. (2016). Analyzing CRISPR genome-editing experiments with CRISPResso. *Nat. Biotechnol.* 34, 695–697. doi: 10.1038/nbt.3583

Raissig, M. T., Abrash, E., Bettadapur, A., Vogel, J. P., and Bergmann, D. C. (2016). Grasses use an alternatively wired bHLH transcription factor network to establish stomatal identity. *Proc. Natl. Acad. Sci. U.S.A.* 113, 8326–8331. doi: 10.1073/pnas.1606728113

Raper, A. T., Stephenson, A. A., and Suo, Z. (2018). Functional insights revealed by the kinetic mechanism of CRISPR/Cas9. *J. Am. Chem. Soc.* 140, 2971–2984. doi: 10.1021/jacs.7b13047

Ren, B., Liu, L., Li, S., Kuang, Y., Wang, J., Zhang, D., et al. (2019). Cas9-NG greatly expands the targeting scope of the genome-editing toolkit by recognizing NG and other atypical PAMs in rice. *Mol. Plant* 12, 1015–1026. doi: 10.1016/j.molp.2019.03.010

Ren, Q., Sretenovic, S., Liu, S., Tang, X., Huang, L., He, Y., et al. (2021). PAM-less plant genome editing using a CRISPR-SpRY toolbox. *Nat. Plants* 7, 25–33. doi: 10.1038/s41477-020-00827-4

Rice, P., Longden, I., and Bleasby, A. (2000). EMBOSS: the European molecular biology open software suite. *Trends Genet.* 16, 276–277. doi: 10.1016/s0168-9525(00)02024-2

Sant'Ana, R. R. A., Caprestano, C. A., Nodari, R. O., and Agapito-Tenfen, S. Z. (2020). PEG-delivered CRISPR-Cas9 ribonucleoproteins system for gene-editing screening of maize protoplasts 158(9):1029. doi: 10.3390/genes11091029

Schindele, A., Dorn, A., and Puchta, H. (2020). CRISPR/Cas brings plant biology and breeding into the fast lane. *Curr. Opin. Biotechnol.* 61, 7–14. doi: 10.1016/j.copbio.2019.08.006

Schirmer, M., Ijaz, U. Z., D'Amore, R., Hall, N., Sloan, W. T., and Quince, C. (2015). Insight into biases and sequencing errors for amplicon sequencing with the illumina MiSeq platform. *Nucleic Acids Res.* 43, e37. doi: 10.1093/nar/gku1341

Schmidt, C., Fransz, P., Ronspies, M., Dreissig, S., Fuchs, J., Heckmann, S., et al. (2020). Changing local recombination patterns in arabidopsis by CRISPR/Cas mediated chromosome engineering. *Nat. Commun.* 11, 4418. doi: 10.1038/s41467-020-18277-z

Schnable, P. S., Ware, D., Fulton, R. S., Stein, J. C., Wei, F., Pasternak, S., et al. (2009). The B73 maize genome: complexity, diversity, and dynamics. *Sci.* 326, 1112–1115. doi: 10.1126/science.1178534

Settles, A. M., Holding, D. R., Tan, B. C., Latshaw, S. P., Liu, J., Suzuki, M., et al. (2007). Sequence-indexed mutations in maize using the UniformMu transposon-tagging population. *BMC Genomics* 8, 116. doi: 10.1186/1471-2164-8-116

Shan, Q., Wang, Y., Li, J., Zhang, Y., Chen, K., Liang, Z., et al. (2013). Targeted genome modification of crop plants using a CRISPR-cas system. *Nat. Biotechnol.* 31, 686–688. doi: 10.1038/nbt.2650

Shimatani, Z., Kashojiya, S., Takayama, M., Terada, R., Arazoe, T., Ishii, H., et al. (2017). Targeted base editing in rice and tomato using a CRISPR-Cas9 cytidine deaminase fusion. *Nat. Biotechnol.* 35, 441–443. doi: 10.1038/nbt.3833

Tan, J., Zhang, F., Karcher, D., and Bock, R. (2019). Engineering of high-precision base editors for site-specific single nucleotide replacement. *Nat. Commun.* 10, 439. doi: 10.1038/s41467-018-08034-8

Walley, J. W., Sartor, R. C., Shen, Z., Schmitz, R. J., Wu, K. J., Urich, M. A., et al. (2016). Integration of omic networks in a developmental atlas of maize. *Sci.* 353, 814–818. doi: 10.1126/science.aag1125

Wang, X., Tilford, C., Neuhaus, I., Mintier, G., Guo, Q., Feder, J. N., et al. (2017). CRISPR-DAV: CRISPR NGS data analysis and visualization pipeline. *Bioinf.* 33, 3811–3812. doi: 10.1093/bioinformatics/btx518

Wolter, F., Edelmann, S., Kadri, A., and Scholten, S. (2017). Characterization of paired Cas9 nickases induced mutations in maize mesophyll protoplasts. *Maydica* 62, 1–11. doi: not available

Wu, Z., Chen, L., Yu, Q., Zhou, W., Gou, X., Li, J., et al. (2019). Multiple transcriptional factors control stomata development in rice. *New Phytol.* 223, 220–232. doi: 10.1111/nph.15766

Xing, Q., Creff, A., Waters, A., Tanaka, H., Goodrich, J., and Ingram, G. C. (2013). ZHOUPI controls embryonic cuticle formation *via* a signalling pathway involving the subtilisin protease ABNORMAL LEAF-SHAPE1 and the receptor kinases GASSHO1 and GASSHO2. *Dev.* 140, 770–779. doi: 10.1242/dev.088898

Xing, H. L., Dong, L., Wang, Z. P., Zhang, H. Y., Han, C. Y., Liu, B., et al. (2014). A CRISPR/Cas9 toolkit for multiplex genome editing in plants. *BMC Plant Biol.* 14, 327. doi: 10.1186/s12870-014-0327-y

Xu, W., Yang, Y., Yang, B., Krueger, C. J., Xiao, Q., Zhao, S., et al. (2022). *A design optimized prime editor with expanded scope and capability in plants. Nat. Plants* 8, 45–52. doi: 10.1038/s41477-021-01043-4

Yan, F., Kuang, Y., Ren, B., Wang, J., Zhang, D., Lin, H., et al. (2018). Highly efficient A.T to G.C base editing by Cas9n-guided tRNA adenosine deaminase in rice. *Mol. Plant* 11, 631–634. doi: 10.1016/j.molp.2018.02.008

Zetsche, B., Gootenberg, J. S., Abudayyeh, O. O., Slaymaker, I. M., Makarova, K. S., Essletzbichler, P., et al. (2015). Cpf1 is a single RNA-guided endonuclease of a class 2 CRISPR-cas system. *Cell* 163, 759–771. doi: 10.1016/j.cell.2015.09.038

Zhang, J., Kobert, K., Flouri, T., and Stamatakis, A. (2014). PEAR: a fast and accurate illumina paired-end reAd mergeR. *Bioinformatics* 30, 614–620. doi: 10.1093/bioinformatics/btt593

Zhong, Z., Sretenovic, S., Ren, Q., Yang, L., Bao, Y., Qi, C., et al. (2019). Improving plant genome editing with high-fidelity xCas9 and non-canonical PAM-targeting Cas9-NG. *Mol. Plant* 12, 1027–1036. doi: 10.1016/j.molp.2019.03.011

Zhu, J., Song, N., Sun, S., Yang, W., Zhao, H., Song, W., et al. (2016). Efficiency and inheritance of targeted mutagenesis in maize using CRISPR-Cas9. *J. Genet. Genomics* 43, 25–36. doi: 10.1016/j.jgg.2015.10.006

Zong, Y., Wang, Y., Li, C., Zhang, R., Chen, K., Ran, Y., et al. (2017). Precise base editing in rice, wheat and maize with a Cas9-cytidine deaminase fusion. *Nat. Biotechnol.* 35, 438–440. doi: 10.1038/nbt.3811

frontiers | Frontiers in Plant Science

TYPE Original Research
PUBLISHED 10 January 2023
DOI 10.3389/fpls.2022.1017983

OPEN ACCESS

EDITED BY
Rogelio Santiago Carabelos,
Spanish National Research Council (CSIC), Spain

REVIEWED BY
Pedro Revilla,
Biological Mission of Galicia, Spanish National Research Council (CSIC), Spain
Ana Nikolić,
Maize research Institute Zemun Polje, Serbia

*CORRESPONDENCE
Silvio Salvi
silvio.salvi@unibo.it

SPECIALTY SECTION
This article was submitted to Plant Breeding, a section of the journal Frontiers in Plant Science

RECEIVED 12 August 2022
ACCEPTED 14 December 2022
PUBLISHED 10 January 2023

CITATION
Li K, Tassinari A, Giuliani S, Rosignoli S, Urbany C, Tuberosa R and Salvi S (2023) QTL mapping identifies novel major loci for kernel row number-associated ear fasciation, ear prolificacy and tillering in maize (*Zea mays* L.). *Front. Plant Sci.* 13:1017983. doi: 10.3389/fpls.2022.1017983

QTL mapping identifies novel major loci for kernel row number-associated ear fasciation, ear prolificacy and tillering in maize (*Zea mays* L.)

Kai Li[1], Alberto Tassinari[1], Silvia Giuliani[1], Serena Rosignoli[1], Claude Urbany[2], Roberto Tuberosa[1] and Silvio Salvi[1]*

[1]Department of Agricultural and Food Sciences (DISTAL), University of Bologna, Bologna, Italy, [2]KWS SAAT SE & Co. KGaA, Einbeck, Germany

Maize ear fasciation originates from excessive or abnormal proliferation of the ear meristem and usually manifests as flattened multiple-tipped ear and/or disordered kernel arrangement. Ear prolificacy expresses as multiple ears per plant or per node. Both ear fasciation and prolificacy can affect grain yield. The genetic control of the two traits was studied using two recombinant inbred line populations (B73 × Lo1016 and Lo964 × Lo1016) with Lo1016 and Lo964 as donors of ear fasciation and prolificacy, respectively. Ear fasciation-related traits, number of kernel rows (KRN), ear prolificacy and number of tillers were phenotyped in multi-year field experiments. Ear fasciation traits and KRN showed relatively high heritability ($h^2 > 0.5$) except ratio of ear diameters. For all ear fasciation-related traits, fasciation level positively correlated with KRN ($0.30 \leq r \leq 0.68$). Prolificacy and tillering were not correlated and their h^2 ranged from 0.41 to 0.78. QTL mapping identified four QTLs for ear fasciation, on chromosomes 1 (two QTLs), 5 and 7, the latter two overlapping with QTLs for number of kernel rows. Notably, at these QTLs, the Lo1016 alleles increased both ear fasciation and KRN across populations, thus showing potential breeding applicability. Four and five non-overlapping QTLs were mapped for ear prolificacy and tillering, respectively. Two ear fasciation QTLs, *qFas1.2* and *qFas7*, overlapped with fasciation QTLs mapped in other studies and spanned *compact plant2* and *ramosa1* candidate genes. Our study identified novel ear fasciation loci and alleles positively affecting grain yield components, and ear prolificacy and tillering loci which are unexpectedly still segregating in elite maize materials, contributing useful information for genomics-assisted breeding programs.

KEYWORDS

ear fasciation, ear prolificacy, maize, QTL mapping, tillering, yield components

1 Introduction

Fasciation is a deviational proliferation of cells and tissues eventually manifesting as widened and flattened organs (most commonly stems or inflorescences) that has been reported in more than a hundred plant families, including trees, shrubs and grasses (White, 1948; Iliev and Kitin, 2011). Ontogenetically, fasciation has been interpreted as (i) an excrescence or fusion of organs due to deviations from normal meristematic processes or crowding of buds, or (ii) a transformation of a single growing meristematic point into a line, this sometime called 'true fasciation' (Clark et al., 1993; Iliev and Kitin, 2011). Either way, mutations at genes involved in the maintenance and functions of the shoot apical meristem (SAM) and the early generative inflorescence meristem play a major role in fasciation, along with environmental factors (Somssich et al., 2016; Wu et al., 2018; Ortez et al., 2022).

Based on studies first carried out in *Arabidopsis*, SAM homeostasis was shown to be controlled by the *CLAVATA3* (*CLV3*) - *WUSCHEL* (*WUS*) feedback signaling pathway (Brand et al., 2000; Schoof et al., 2000; Somssich et al., 2016). WUS is a stem cell-promoting homeodomain transcription factor, whereas CLV3 is a differentiation-promoting peptide that belongs to the CLAVATA3/EMBRYOSURROUNDING REGION (ESR) CLE peptide family (Opsahl-Ferstad et al., 1997; Trotochaud et al., 1999). While WUS activates the expression of *CLV3*, *WUS* expression is repressed by CLV3 through its binding to a number of leucine-rich repeat receptor-like proteins (including CLV1 and CLV2), causing the decline of stem cell proliferation, and a corresponding decrease of CLV3 production (Brand et al., 2000; Schoof et al., 2000). This feedback mechanism keeps meristem size under control and appears to be largely conserved in maize. For instance, maize *CLV3/EMBRYO-SURROUNDING REGION7* (*ZmCLE7*) is a *CLV3* ortholog; *THICK TASSEL DWARF1* (*TD1*) and *FASCIATED EAR2* (*FEA2*) encode receptor-like proteins related with CLV1 and CLV2, and regulates the size of the ear IM and SAM growth; *ZmWUS1* seems to be a direct *WUS* ortholog and is expressed in the late vegetative SAM (Wu et al., 2018; Kitagawa and Jackson, 2019; Kim et al., 2022). Genes affecting meristem size and involved in ear fasciation and acting outside the CLV3-WUS loop have also been described. For instance, *ZmFEA4* encodes a basic leucine zipper domain (bZIP) transcription factor that is expressed in the shoot meristem peripheral zone and is likely involved in cell transiting from SAM to organ primordium (Kitagawa and Jackson, 2019); the SQUAMOSA PROMOTER BINDING (SBP)-box transcription factors *unbranched2* (*UB2*) and *unbranched3* (*UB3*) are expressed in the initiating leaf primordia and the base of the SAM and control lateral organs initiation (Chuck et al., 2014). Finally, ear shape is also under the control of genes expressed later in development, at the inflorescence or even floret meristem levels, including *ramosa1* (*ra1*), *ra2* and *ra3* (Vollbrecht et al., 2005; Kellogg, 2022), or *growth regulating factor-interacting factor1* (*gif1*. Zhang et al., 2018), which were shown to control inflorescence (tassel and ear) branching and, when mutated, to produce multiple-tip or branched ears.

Fasciated mutants can be of interest in plant breeding programs for their ornamental characteristics or because their abnormal development may favorably affect yield components such as fruit and/or seed size and number. Indeed, fasciated tomato mutants showed increased number of flowers, fruits, fruit locules and fruit size (Tanksley, 2004; Iliev and Kitin, 2011; Xu et al., 2015). Similarly, mutations in *CLV* genes in *Brassica* resulted in higher number of locules in fruits, leading to higher yield (Fan et al., 2014; Xiao et al., 2018). In maize, ear fasciation has been suggested as a potential target for increasing ear size and/or number of kernels per ear under the expectation that a larger SAM should lead to a wider ear meristem eventually harboring more spikelet pair meristems and thus kernel rows (Otegui and Bonhomme, 1998; Somssich et al., 2016; Kim et al., 2022; Li et al., 2022). However, accumulating evidences indicate that strong ear fasciation alleles do not improve productivity because they usually induce a shorter, stunted ear; instead, weaker fasciation alleles show more potential (Bommert et al., 2013b; Je et al., 2016; Kim et al., 2022; Ortez et al., 2022). In line with this evidence, quantitative genetic variation for ear fasciation was analyzed using QTL mapping (Mendes-Moreira et al., 2015) and, in a different study, a QTL for kernel row number (KRN) was shown to correspond to *ZmFEA2* (Bommert et al., 2013b). A different QTL on the same chromosome explained 12% of KRN variance, was cloned and shown to correspond to a cis-regulatory element of *UB3* (Chuck et al., 2014; Du et al., 2020).

In maize, prolificacy is a general term indicating the presence of multiple ears in a plant (Ortez et al., 2022). Prolificacy can be classified as three types: multi-node prolificacy (i.e., multiple ears growing at different nodes), multi-tiller prolificacy (i.e., multiple stems growing from basal nodes) and single-node prolificacy [i.e., multiple ears growing at the same nodes, also known as 'multi-ears', 'bouquet ears' or 'shank ears' (Ortez et al., 2022)]. In single-node prolificacy, the presence of multiple ears is the result of multiple axillary meristems located on the same ear shank, giving rise to additional ear inflorescences alongside the central one. The presence of a single major ear per plant *vs*. multiple ears is one the major contrasting difference between currently cultivated maize and its progenitor teosinte (Stitzer and Ross-Ibarra, 2018). Because of this, domesticated maize was referred as 'not prolific', while its progenitor teosinte as 'prolific' (Doebley et al., 1995; Prakash et al., 2019; Yang et al., 2019). Although most of the modern maize hybrid cultivars cultivated in the high-dense stands in temperate environment develop only one ear, the potential presence of multiple ears per plant has physiological and breeding implications. For instance, maize hybrid cultivars with some level of plasticity to develop tillers

and multiple ears per plant may turn out advantageous in semi-arid regions with high inter-annual variation of summer rainfall, where they are cultivated at low plant population densities (i.e., less than 4 plants m^{-2}. Rotili et al., 2022). Additionally, ear prolificacy is considered a positive feature in 'baby corn' specialty maize cultivars whose unfertilized ears are consumed in salads, soups, fried snacks and other ways (Prakash et al., 2019). The genetic control of multiple ears per plant is complex and received little attention so far. A major QTL for single-node prolificacy, *prol1.1*, was mapped on chr. 1 in a maize-teosinte BC_2S_3 population, at a chromosomal location that had previously been shown to influence domestication traits and shown to correspond to the expression regulatory region of *grassy tillers1* (*gt1*), encoding a homeodomain leucine zipper transcription factor (Wills et al., 2013). More recently, major multi-node prolificacy QTLs were mapped in different crosses (Prakash et al., 2021; Wang et al., 2021).

Ears and tillers both originate from axillary buds developing into shorter or longer shoots, therefore they are expected to share developmental mechanisms. This was indeed confirmed by the identification and cloning of genes such as *barren stalk1* (*ba1*), encoding a bHLH transcription factor orthologous to rice *LAX PANICLE1* (*LAX1*. Gallavotti et al., 2004) . Additionally, *ba1* mutants fail to initiate all vegetative and reproductive axillary meristems. BA1 levels are under the control of BARREN STALK FASTIGIATE1 (BAF1), a transcriptional regulator with an AT-hook DNA binding motif (Gallavotti et al., 2011). Mutant *baf1* plants fail to initiate axillary buds that are fated to become lateral ear shoots; as a result, *baf1* mutants are earless (Gallavotti et al., 2011).

This study investigated the genetic control of ear fasciation and ear prolificacy and their links with KRN and tillering, respectively, using QTL mapping. Mapping was carried out in two connected (ie. sharing one parental line) RIL populations, B73 × Lo1016 and Lo964 × Lo1016 analyzed as a joint population. Line Lo1016 was the genetic source of mild ear fasciation while Lo964 was the source of ear prolificacy.

2 Materials and methods

2.1 Plant materials and marker genotyping

Two recombinant inbred line (RIL) populations were developed as follows. The line Lo1016 was crossed with B73 and with Lo964 to create two F_1s. Both Lo964 and Lo1016 are typical dent lines originally bred at the Bergamo breeding station (Italy), shown to be genetically related based on molecular marker analysis and classified as BSSS = Iowa Stiff Stalk Synthetic heterotic group (Losa et al., 2011). B73 is the maize reference inbred line (Schnable et al., 2009). Single seed descent method was utilized to reach F_7 generation, after which each line was multiplied following standard procedures. The B73 × Lo1016 (B×L) and Lo964 × Lo1016 (L×L) populations eventually included 97 and 68 RILs, respectively. We will refer to the Joint Population (JP) as the assembly of the whole set of 165 (97 + 68) RILs.

2.2 Field experiment and phenotypic data collection

Field trials were carried out in Cadriano, near Bologna, Italy (44°33'02.5"N, 11°24'43.9"E) in 2017 and in Monselice, near Padova, Italy (45°12'42.4"N, 11°45'14.8"E) in 2018 and 2019. Field experiments were organized as a randomized complete block design with two replicates (one rep = one plot with 10 plants per RIL). Plots for each of the three parental lines were included in the experiment. Plot length was 2.5 m, distance between rows was 0.8 m and between plants was 0.25 m. Plots were overplanted by hand and thinned at the V7 growth stage to one plant per hill equivalent to 11 plants per plot, and with an overall investment of 5.5 plants per square meter. The field was managed following standard agronomic practices of the area.

Phenotyping for ear fasciation was carried out by collecting four traits, namely 'ear ovality' (OVA, defined after visual inspection of elliptic/ovality degree of cob cross-section, from 0 to 10, corresponding from perfect circle to extremely elliptic/flat cob cross sections, respectively; higher values indicated strong fasciation); 'kernel row disorder' (DIS, defined as a visual score from 0 = perfectly linearly arranged kernels on ears, to 10 = highly disordered arrangement; higher values indicated strong fasciation); 'ear diameters ratio' (DIA, defined as ratio of minimum diameter divided by maximum diameter, where the two diameters were measured mutually perpendicularly by a caliper at the middle of the ear; lower values corresponded to strong fasciation); 'ear fasciation index' (FAS, a visual score for ear fasciation scaled from 0 to 3, where 3 indicated a strongly fasciated ear). Visual scores per ear were given by three persons independently, and mean values were utilized as entries for subsequent analysis. Number of kernel rows (KRN) was collected by counting the number of kernel rows at mid-ear position, on the same ears subjected to phenotyping for fasciation. Plant architecture traits collected were number of tillers per plants (TIL) and proportion of plants per plot showing prolificacy (PROL), i.e., proportion of plants showing >1 ear at the top ear node. For all traits, three central contiguous plants per plot were considered.

Raw phenotypic data for all traits were modified by using the model Best Linear Unbiased Estimator (BLUES) in the R package "tidyverse" (Wickham et al., 2019). BLUES values were utilized for biometric, correlation and QTL analyses. Correlation analysis was carried out by the Spearman method which is little sensitive to deviation from normal distributions (Wickham et al., 2019). We utilized the common letter '*r*' instead

of the more appropriated '*rho*' for clarity in text. Trait distributions were normal or reached normality after square root transformation (Sokal and Rohlf, 2012), except for ear diameters rate, prolificacy and tillering (Supplementary Table 1). We used original data for visualization (Figure 1 and Supplementary Figures 1, 2).

Analysis of variance (ANOVA) was run for six out of seven traits and for two (2018 and 2019, corresponding to experiments in Monselice, near Padua) out of three years. Specifically, ANOVA was not run for ear fasciation index since this phenotypic dataset was only available as mean value of two repetitions. Similarly, phenotypic data for year 2017 were not included in ANOVA because mean values (as mean of two repetitions) were available only. ANOVA output tables for six traits are provided in Supplementary Table 2. For each trait, ANOVA had three sources of variation, namely Year (2018 and 2019), Population (B×L, and L×L) and RIL (97 RILs for B×L and 68 RILs for L×L). RILs were treated as 'Nested' in Population. The final linear model utilized (in R) was Trait ~ Year * Population/RIL. Year was considered as random while Population and RIL factors were considered as fixed effect.

2.3 SNP genotyping, construction of linkage map and QTL mapping

B×L and L×L were genotyped using a high density 15-K SNP array (Rousselle et al., 2015) using a commercial service. Genomic DNA was prepared following standard protocols by a DNA extraction kit (NucleoSpin Plant II, Macherey Nagel, Duren, Germany) based on the manufacturer's protocol. Marker alleles from Lo1016 were coded as 0 while alleles from Lo964 and B73 were coded as 2 and missing values as -1. Linkage map construction was obtained using QTL Icimapping (Meng et al., 2015) by first removing redundant markers using the procedure "BIN", and then building linkage maps using "MAP". Three linkage maps were constructed, one for each biparental cross RIL population, and one as joint population. For "BIN" function, markers whose missing rate was higher than 50% and distortion rate higher than 0.01 were deleted. For "MAP" function, the algorithm nnTwoOpt and SARF (sum of adjacent recombination fractions) for rippling were applied, and the window size was specified as 9. QTL mapping was carried out by QTL Icimapping using the Nested Association Mapping (NAM) functionality, treating the two subpopulations (B×L and L×L) as a single population (ie. Joint Population, JP). This was possible because the two subpopulations share on common parent (Lo1016), making it equivalent to a NAM design (Li et al., 2011). Under NAM functionality, QTL Icimapping applies 'joint inclusive composite interval mapping' (JICIM. Li et al., 2011). The JICM-based QTL analysis was proved to provide higher QTL detection power and mapping precision as compared to the analysis of the single biparental populations (Li et al., 2011). In parallel, we carried out QTL analysis on single subpopulations (using the options BIP and composite interval mapping in QTL Icimapping) for checking purposes. The scanning step was set as 0.1 cM in NAM and 1 cM in biparental populations, respectively. Probability of stepwise regression was set to 0.0001. The LOD threshold for declaring QTL significance was set as 3.3, 3.6 and 4.6, for B×L, L×L and JP, respectively, after permutation test ($P \leq 0.05$ with 1,000 permutation). QTL additive effects were always computed by the formula 2a = (mean homozygous B73 – mean homozygous Lo1016) or 2a = (mean homozygous Lo964 – mean homozygous Lo1016), for the two RIL populations, respectively.

Additionally, QTL mapping for ear diameters rate, ear prolificacy and tillering (ie. traits showing deviation from normal distribution) was also carried out by Kruskal-Wallis (KW) test, known to be robust to deviation from distribution normality, as implemented in MapQTL6 (Van Ooijen, 2009). For these traits, QTL results obtained both with JICIM and KW tests are provided and compared in Supplementary Table 3. Since the two methods basically provided the same results, results from KW test will be no further discussed, with the exception of QTLs *qProl1* and *qProl4*, for which we provided footnotes in Table 2.

2.4 Screening candidate genes and variant calling

QTL confidence intervals from this study were projected on B73 reference genome (B73v5. Hufford et al., 2021) and included gene models that were considered for further investigations. Whole genome sequencing of the two lines Lo964 and Lo1016 was carried out with Illumina HiSeq PE150 at 20× of coverage. Reads were aligned to the B73v5 using BWA v.7.17 (Li and Durbin, 2009). Variants were called with BCFtools v. 1.10.2 (Li, 2011) and were filtered for a minimum reads depth of 10×, PHRED quality > 40 and a minimum DV/AD ratio of 0.8, where DP is the coverage depth at the variant position and AD is the allelic depth of the alternate allele. Variant effects were predicted with SNPEff v.3.0.7 (Cingolani et al., 2012) and among variants in the gene space, only high or moderate effects were considered. Additionally, alleles sequences of candidate genes were extracted for Lo964 and Lo1016 from their whole variant call format (vcf) files and the FASTA sequences were obtained with the command bcftools consensus. The 25 NAM founder sequences were downloaded from MaizeGDB (Portwood et al., 2019). The FASTA sequences were aligned using MUSCLE (Edgar, 2004) from MEGAX (Kumar et al., 2018). The coding sequences were obtained starting from the genomic sequence and the B73v5_Zm00001eb.1.gff3 annotation file downloaded from MaizeGDB, using GFFRead (Pertea and Pertea, 2020). The alignment images were elaborated with Jalview (Waterhouse

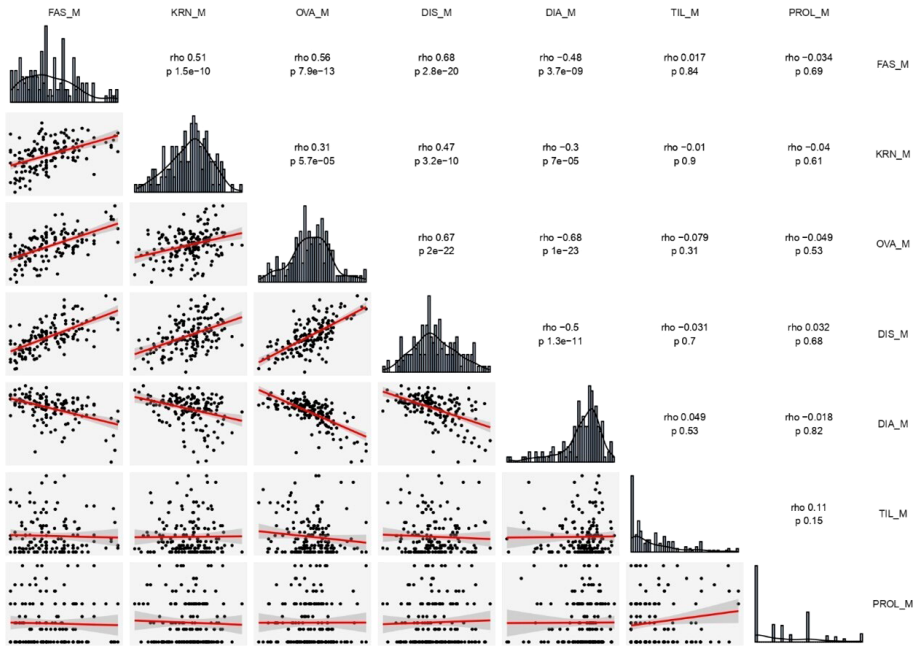

FIGURE 1
Distribution frequency histograms of, and correlation among all traits estimated on the two RILs (B×L and L×L) combined. The upper right part reports all correlation indexes (*rho*) and corresponding significant levels (*p*). The lower left part presents scatter plots and fitter curve (the red line inside) between two traits. The diagonal shows histogram charts of each trait. DIA (ear diameters rate), DIS (kernel row disorder), OVA (ear ovality), FAS (ear fasciation index), KRN (kernel row number), PROL (prolificacy), TIL (number of tillers), M, mean value.

et al., 2009). Finally, a review of published QTLs and genes in maize was carried out by searching major bibliographic databases using 'ear fasciation', 'prolificacy' or 'tillering' terms as keywords, and information on QTL and genes physical position, bin and type of mapping population was collected. Gene name formats and symbols followed the indications given at www.maizegdb.org/nomenclature.

3 Results

3.1 Trait biometrics, heritability and phenotypic correlations

This study confirmed that Lo1016 and Lo964 are characterized by ear fasciation and ear prolificacy, respectively (Figure 2, Supplementary Figure 1, Table 1). Specifically, Lo1016 showed the highest fasciation values when compared to Lo964 and B73 except kernel row disorder (Tab. 1. $P < 0.01$ for all comparisons for ear diameters rate, ear fasciation index and ear ovality/flatness, Tukey's test). Alongside, Lo1016 also showed the highest KRN (19.75 *vs* 16.33 or 14.54, for B73 or Lo964, respectively, $P < 0.01$). Lo964 showed the highest ear prolificacy among the three parental lines (2.75 *vs* 0.0 or 0.25, for B73 or Lo1016, respectively, $P < 0.01$). In addition, Lo1016 was the only parental line developing tillers (ca. 1.5 tillers per plant). Values for additional plant architecture traits recorded in this study are reported in Table 1. ANOVA showed that ear diameters rate, kernel row disorder, KRN and prolificacy were strongly affected by 'Year' ($P < 0.01$) while ear ovality and number of tillers were only mildly affected ($0.01 < P < 0.05$) (Supplementary Table 2). 'Population' significantly affected all traits ($P < 0.01$) except number of tillers. No 'Population-Year' interactions were observed for any traits with the exception of prolificacy. For any trait, RIL (ie. lines) was a major source of variation, in line with the presence of segregating QTLs. Broad sense heritability (h^2) for ear-fasciation traits ranged from 0.13 for ear diameters rate in L×L to 0.95 for ear fasciation index in B×L. Ear prolificacy and TIL h^2 were relatively high (ranged between 0.41 and 0.78, Table 1).

Positive transgressive segregation was observed for TIL only, with some RIL lines belonging to both populations that showed > 5 tillers per plant as compared to 1.5 tillers per plant on average in the high-tillering parent Lo1016. Negative transgressive segregation was observed for KRN, with RIL lines from L×L showing as few as 12.7 kernel rows as compared to 14.5 or 19.7 kernel rows recorded for Lo964 or Lo1016. Negative transgressive segregation was also observed for DIS in both RIL populations.

TABLE 1 Descriptive statistics for ear and plant architecture traits in the two RIL populations B73 × Lo1016 (B×L) and Lo964 × Lo1016 (L×L).

	B73	Lo964	Lo1016	RIL population B×L		RIL population L×L	
Traits†	Mean ± sd	Mean ± sd	Mean ± sd	Min - Mean - Max	h^2	Min - Mean - Max	h^2
DIA	0.95 ± 0.04 (a)	0.95 ± 0.04 (a)	0.85 ± 0.11 (a)	0.86 - 0.94 - 0.98	0.45	0.88 - 0.95 - 0.98	0.13
DIS	7.17 ± 1.18 (a)	6.33 ± 1.89 (a)	7.18 ± 0.94 (a)	2.75 - 6.02 - 8.89	0.58	3 - 5.25 - 8.61	0.63
FAS	0.18 ± 0.39 (a)	0.50 ± 0.50 (a)	2.20 ± 0.75 (b)	0 - 1.38 - 3	0.95	0 - 0.79 - 2.92	0.94
KRN	16.33 ± 1.20 (a)	14.54 ± 1.03 (a)	19.75 ± 1.71 (b)	14.58 - 17.40 - 20.90	0.59	12.67 - 15.97 - 20.13	0.85
OVA	5.85 ± 1.03 (a)	4.92 ± 1.82 (a)	7.13 ± 1.17 (b)	4.1 - 6.02 - 8.11	0.50	3.69 - 5.60 - 8.11	0.55
PROL	0 ± 0 (a)	2.75 ± 2.36 (b)	0.25 ± 0.5 (a)	0 - 0.40 - 1	0.41	0 - 0.59 - 1	0.78
TIL	0 ± 0 (a)	0 ± 0 (a)	1.5 ± 2.38 (b)	0 - 1.22 - 5.75	0.62	0 - 1.24 - 5.25	0.68

Different letters (a and b) indicate statistical significance, Tukey's test ($P < 0.05$).
†) DIA (ear diameters rate), DIS (kernel row disorder), OVA (ear ovality), FAS (ear fasciation index), KRN (kernel row number), PROL (prolificacy), TIL (number of tillers).

The four ear-fasciation-related traits (ear diameters rate, ear fasciation index, ear ovality, kernel disorder) resulted significantly correlated, with r ranging from |0.48| to |0.68| ($P < 0.001$, Figure 1, Supplementary Figures 2, 3), with ear diameters rate negatively correlated as expected (i.e., the smaller the rate, the stronger ear fasciation). Additionally, the same traits correlated with KRN. Among ear fasciation-related traits, ear fasciation index showed the highest correlation ($r = 0.51$) with KRN and ear diameters rate the lowest ($r = -0.30$, $P < 0.001$. Figure 1), again with ear diameters rate as the only trait negatively correlated with KRN. Overall, the correlation results suggested that variation for KRN and ear fasciation could partially be due to the same loci. Ear fasciation traits did not show correlation with ear prolificacy or tillering (Figure 1).

3.2 Linkage maps

The three linkage maps, namely B×L, L×L and JP included 1,186, 984 and 1,303 markers, and covered 1,819.52 cM, 2,504.5 cM and 1,661.0 cM, respectively (Table 2 and Supplementary Figure 4). The different linkage maps covered well the maize genome with the unavoidable exception of those regions characterized by lack of markers polymorphism due to identity-by-descent between lines. In B×L, those regions were identified as the middle part of chr. 1 between PZE-101130395 (168,493,734) and PZE-101137700 (180,295,042), accounting for 3.8% of the chromosome, and the upper and lower parts of chr. 3, for a total of 88.7 Mb (37.6% of chr. 3). In L×L, almost the whole chr. 3 resulted monomorphic and thus uninformative for QTL mapping. Additionally, deficits of polymorphic markers resulted in long intervals between markers on the upper parts of chr. 4 and 7, accounting for 4.9 and 7.0% for each corresponding chromosome, respectively. Overall, 87.7 and 75.7% of the maize map was sufficiently covered by molecular markers in B×L and L×L, respectively.

3.3 QTL results

3.3.1 Four ear-fasciation QTLs were identified and ear fasciation alleles were always contributed by Lo1016

In the following, QTLs for different ear fasciation-related traits (ear diameters rate, ear fasciation index, ear ovality, kernel disorder) will be considered as the same QTL whenever their supporting intervals overlap, considering QTL results from B×L, L×L and JP (Figure 3 and Supplementary Figures 5, 6). Four QTL for ear fasciation traits were mapped (*qFas1.1* and *qFas1.2* on chr. 1; *qFas5* and *qFas7* on chr. 5 and 7, respectively. Table 2). *qFas1.1* and *qFas1.2* were detected for ear diameters rate and fasciation index, respectively, and mapped nearby on chr. 1 (bins 1.01/1.02) within two narrow supporting intervals of < 2 Mb, and both segregated within B×L only. *qFas5* was mapped on bin 5.07 for fasciation index and ear ovality and appeared to segregate mainly in L×L. *qFas7* was mapped on bin 7.02 and shown to affect ear fasciation index, ear ovality and kernel disorder in both B×L and L×L. Notably, for all *qFas* QTLs, the fasciation-increasing allele was provided by Lo1016, the parental line showing ear fasciation (Figure 2), as indicated by the direction of QTL effects (Table 2).

3.3.2 KRN QTLs partially overlapped to ear fasciation QTLs

Five KRN QTLs were mapped. The QTL with the strongest effect, *qKRN2*, was mapped on bin 2.02 in a < 2 Mb-supporting interval and explained 13 or 23% (JP or L×L, respectively) of phenotypic variation with a genetic effect 2a = 0.69 or 0.87 kernel rows, in JP or L×L, respectively ('+' allele from Lo964). The QTL *qKRN5* on bin 5.07 controlled 10% of phenotypic variance and showed an effect of 2a = − 0.57 kernel rows ('+' allele contributed by Lo1016). Two KRN QTLs, *qKRN7.1* and *qKRN7.2*, mapped on bin 7.02 and 7.03, respectively, and had similar genetic effect (2a = −0.62 and −0.65 kernel rows, '+' allele by Lo1016). The

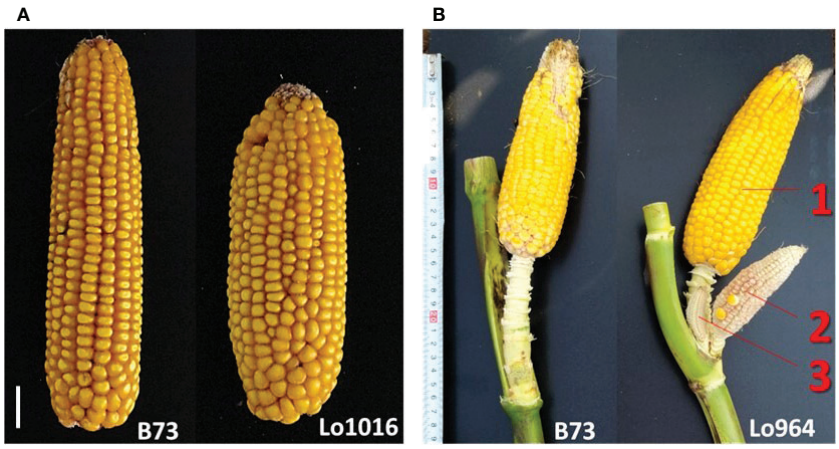

FIGURE 2
Target ear traits analyzed in this study. **(A)** Representative images of the ear-fasciation phenotype observed in Lo1016 (B73 is shown as comparison). White line, 1 cm. **(B)** Representative images of the ear prolificacy phenotype at top ear-bearing node as observed in Lo964 (B73 is shown as comparison). Numbers (1-3) indicate different ears at the same node.

QTL *qKRN8* mapped on bin 8.02, with a genetic effect of 2a = −0.79 in L×L ('+' allele by Lo1016). Notably, all KRN QTLs segregated in L×L while none in B×L. Overall, *qKRN2* was the only KRN QTL with the '+' allele contributed by Lo964, while Lo1016 contributed the '+' allele at the other four KRN QTLs (Table 2). Notably, two out of five KRN QTLs overlapped with ear fasciation QTLs. Specifically, *qKRN5* overlapped with *qFas5* on bin 5.05 and *qKRN7.1* with *qFas7* on bin 7.02. At both chromosome regions, the ear fasciation-increasing allele (provided by Lo1016) also increased kernel row number, supporting the hypothesis of a functional association due to the presence of causative gene(s) affecting both ear fasciation and number of kernel rows, and in line with the observed positive correlation between the two traits (Figure 2).

TABLE 2 QTL results for ear-fasciation (and related traits), kernel row number, ear prolificacy and tillering as obtained by composite interval mapping using BLUES-modified phenotypic values, on single RIL populations (B×L and L×L) and by analysis of joint population (JP).

Trait type	QTL	Trait	Source[a]	Genetic[b]	Bin	Physical B73v4Gramene	LOD[c]	PVE[d]	LOD B×L[e]	LOD L×L[f]	Add B×L[g]	Add L×L[h]
Ear fasciation and KRN	*qFas1.1*	Ear diameter rate	B×L	chr1:18	1.01	1:4,727,090.5,522,697	3.97	13.35			0.01	
	qFas1.2	Fasciation	B×L	chr. 1:40	1.02	1:16,049,788.18,019,336	4.23	17.53			-0.33	
	qKRN2	Kernel row number	JP	chr. 2:18.8	2.02	2:4,139,916.4,808,238	5.77	13.23		5.45		0.69
		Kernel row number	L×L	chr2:27	2.02	2:4,335,580.5,766,846	7.76	22.99				0.87
	qFas5	Fasciation	L×L	chr5:114	5.07	5:210,666,787.211,006,289	4.09	21.70				-0.24
		Ovality	JP	chr5	5.07	5:216,124,262.218,020,826	4.51	11.41	1.88	2.64	-0.21	-0.34
	qKRN5	Kernel row number	L×L	chr5:154	5.07	5:217,164,610.218,092,335	3.83	10.01				-0.57

(Continued)

TABLE 2 Continued

Trait type	QTL	Trait	Source[a]	Genetic[b]	Bin	Physical B73v4Gramene	LOD[c]	PVE[d]	LOD B×L[e]	LOD L×L[f]	Add B×L[g]	Add L×L[h]
	qKRN7.1	Kernel row number	L×L	chr7:131	7.02	7:110,164,470.123,888,193	4.33	11.80				-0.62
	qFas7	Fasciation	JP	chr7:32.8	7.02	7:114,986,412.118,589,566	6.95	10.92	3.20	3.75	-0.23	-0.24
		Fasciation	B×L	chr7:44	7.02	7:114,986,412.118,512,477	4.58	19.41			-0.35	
		Disorder	JP	chr7:34.2	7.02	7:115,485,353.123,389,126	5.18	10.51	3.11	2.08	-0.43	-0.41
		Ovality	JP	chr7:39.4	7.02	7:125,598,407.125,842,182	4.65	11.48	*1.79*	2.85	*-0.19*	-0.36
	qKRN7.2	Kernel row number	JP	chr7:93.7	7.03	7:149,411,478.150,243,845	5.27	8.77		4.94		-0.65
	qKRN8	Kernel row number	L×L	chr8:34	8.02	8:18,827,357.20,248,512	6.29	17.88				-0.79
		Kernel row number	JP	chr8:23.5	8.02	8:19,522,583.20,248,512	4.71	8.30		4.53		-0.63
Tillering	*qTil1*	Tillering	JP	chr1:110.0	1.05	1:85,069,032.94,479,235	7.59	12.15	3.06	4.53	-0.40	-0.57
		Tillering	L×L	chr1:118.0	1.05	1:96,638,867.164,032,566	4.45	22.25				-0.85
	qTil2	Tillering	JP	chr2:7.3	2.01	2:2,067,198.3,242,152	7.05	13.08	6.42		0.58	
		Tillering	B×L	chr2:9	2.01	2:2,802,567.4,139,916	6.93	18.38			0.70	
	qTil4	Tillering	JP	chr4:115.9	4.04/05	4:30,890,749.37,691,500	6.70	10.66	3.19	3.51	-0.41	-0.51
	qTil9	Tillering	JP	chr9:67.5	9.03	9:92,749,841.97,243,143	6.19	9.50	3.40	2.79	-0.42	-0.45
Prolificacy	*qProl1* [i]	Prolificacy	L×L	chr1:2.0	1.01	1:6,272,408.7,074,707	6.07	5.58				0.34
	qProl2	Prolificacy	JP	chr2:139.2	2.06/7	2:187,831,696.191,179,806	6.34	13.97	4.52	*1.82*	0.13	*0.11*
	qProl4 [j]	Prolificacy	L×L	chr4:371.1	4.05/4.08	4:148,677,638.181,859,161	6.22	5.74				0.34
	qProl9	Prolificacy	B×L	chr9:62	9.03	9:28,670,077.74,515,763	3.64	16.72			-0.21	

[a]) Actual population (B×L, L×L or JP, with JP indicating the two populations jointly analyzed for QTL using the command 'NAM' in QTL Icimapping.
[b]) QTL peak position in cM in the specific linkage map (B×L, L×L or JP, from this study).
[c]) Peak LOD value from Composite Interval Mapping.
[d]) PVE = Proportion of phenotypic variance explained.
[e]) Peak LOD value of the single population B×L when analysed as JP. Sub-significant relevant LOD score are in Italics.
[f]) Peak LOD value of the single population L×L when analysed as JP. Sub-significant relevant LOD score are in Italics.
[g]) QTL additive effect express as 2a = (mean homozygous B73 – mean homozygous Lo1016). Additive values related with sub-significant LOD scores are in Italics.
[h]) QTL additive effect express as 2a = (mean homozygous Lo964 – mean homozygous Lo1016). Additive values related with sub-significant LOD scores are in Italics.
[i]) The position of *qProl1* was shifted to approx. 29 Mb based on Kruskal-Wallis test for ear prolificacy QTL (Supplementary Table 3).
[j]) qProl4 was not detected based on Kruskal-Wallis test for ear prolificacy QTL (Supplementary Table 3).

3.3.3 Ear prolificacy is under polygenic control in B×L and L×L populations independently from tillering

Four QTLs were mapped for ear prolificacy (*qProl1, qProl2*, *qProl4* and *qProl9*. Table 2). *qProl1* and *qProl4* were detected in L×L only, *qProl2* was mapped in JP and *qProl9* in B×L only. The highest PVE values were recorded for *qProl2* (14.0%) and *qProl9* (16.7%). At *qProl1*, *qProl2* and *qProl4*, the high ear prolificacy parent Lo964 contributed the '+' QTL allele. Both *qProl1* and *qProl2* showed narrow physical supporting intervals (0.8 Mb and 3.3 Mb, respectively). Tillering variation was also shown to be under polygenic control with four QTLs. The two strongest

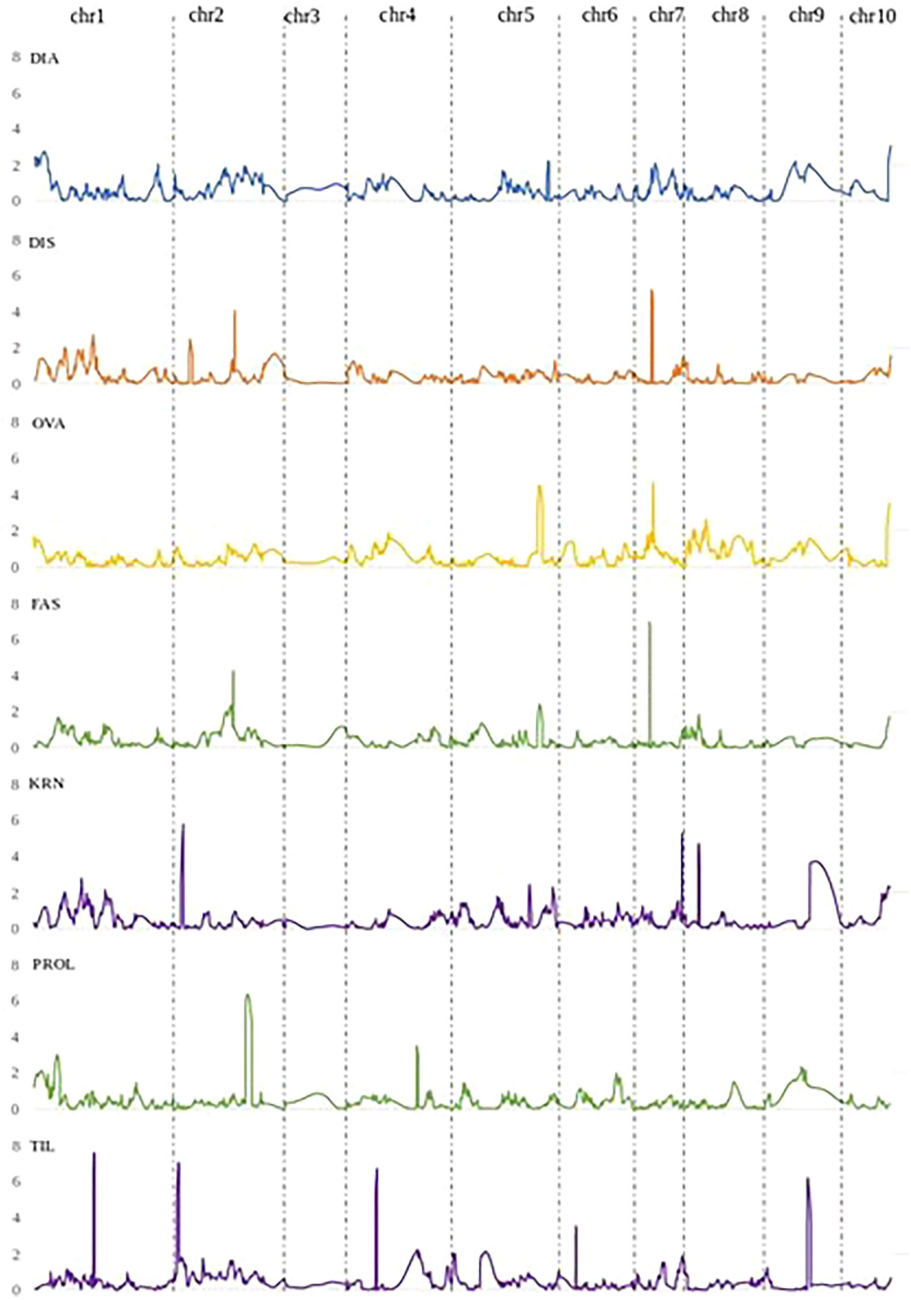

FIGURE 3
QTL LOD profiles obtained by the joint analysis of the two RIL populations B×L and L×L, for DIA (ear diameters rate), DIS (kernel row disorder), OVA (ear ovality), FAS (ear fasciation index), KRN (kernel row number), PROL (prolificacy), TIL (number of tillers).

QTLs in terms of genetic effect, *qTil1* and *qTil2*, mapped on bin 1.05 and 2.01, controlled 12-13% of phenotypic variance in JP with a genetic effect of 2a = 0.6 tillers per plant. Although the '+' allele was contributed by Lo1016 for *qTil1*, *qTil4* and *qTil9*, in both B×L and L×L B73 contributed a positive tillering allele at *qTil2*. No overlap was found between prolificacy and tillering QTLs.

3.3.4 Meristem genes *compact plant2* (*ct2*) and *ramosa1* (*ra1*) co-map with QTLs for ear fasciation *qFas1.2* and *qFas7*, and *barren inflorescence1* (*bif1*) co-maps with *qKRN8*

In order to search for candidate genes of ear fasciation QTLs identified in this study, we extracted all gene models included in the QTL supporting intervals present in B73 v4 (www.maizegdb.org)

along with gene expression information in meristem and ear primordium. Alongside, a list of 42 genes involved in development and/or proliferation of ear meristem was collected by screening the scientific literature (Supplementary Table 5); a sublist of genes comapping with QTLs in our study is provided in Supplementary Table 6. For instance, at *qFas1.2* (chr. 1, 16.0-18.0 Mb), *compact plant2* (*ct2*. Bommert et al., 2013a), and *big grain1 homolog1* (*bgh1*. Simmons et al., 2020) at chr. 1, 16.7 Mb, were identified as candidate genes. The well-known *ra1* (Vollbrecht et al., 2005; Dempewolf, 2010) on chr. 7, 113.6 Mb, is included in the supporting interval of *qFas7*/*qKRN7.1* (chr. 7, 110.2-123.9 Mb). Additionally, at *qKRN8* (chr. 8, 18.8–20.2 Mb), *barren inflorescence1* (*bif1*. Barazesh and McSteen, 2008), chr. 8, 18.9 Mb was identified as candidate gene for KRN. As far as tillering is concerned, two candidate genes, namely *crr1* (*cytokinin response regulator1*, gene model Zm00001d001865) and *arftf3* (*ARF-transcription factor 3*, gene model Zm00001d001879) were identified within the supporting interval of *qTil2*, on chr. 2.

3.3.4 Investigation of nucleotide and amino acid sequence variation at candidate genes for ear fasciation, number of kernel rows QTLs and tillering

The nucleotide sequences of candidate genes listed in Supplementary Table 6 were recovered for the three parental lines based on the reference genome sequence (B73 v4 from www.maizegdb.org) or based on the *de novo* whole genome shotgun sequences obtained in this work (Lo964 and Lo1016), and compared in order to identify functional variants. Specifically, variants were searched for *ra1* (candidate at *qKRN7.1*/*qFas7*), *ct2* and *bgh1* (candidates at *qFas1.2*) and *crr1* (candidate for *qTil2*. Supplementary Figures 7-11). However, in all these cases, no nucleotide difference was observed between the parental alleles. This result does not rule out *ra1*, *ct2*/*bgh1* and *crr1* as possible candidate genes for their QTLs, instead, it suggests that the candidate genes could act on ear fasciation by gene expression changes.

4 Discussion

We phenotyped ear fasciation using four approaches, namely collecting the rate between the minor and the major cob diameters, ear ovality or flatness, kernel row disorder index and an ear fasciation index. Thus, our phenotyping approaches covered well the different ways ear fasciation manifests, namely cob flatness and kernel disorder as shown previously (Mendes-Moreira et al., 2015; Kim et al., 2022). Confirming other authors' observations, cob ovality/flatness and kernel row disorder correlated, and correlated also with ear fasciation index. Additionally, cob ovality, kernel disorder and ear fasciation index QTLs showed a sizeable level of overlap. At the same time, both the imperfect correlation between such traits (e.g., r = 0.67 between ear ovality/flatness and kernel row disorder) and the presence of QTLs affecting only one out of four ear-fasciation-related traits (e.g., *qFas1.1*, controlling ear diameters rate) confirmed that ear fasciation is a genetically and physiologically complex polygenic trait and that at least some genes can possibly affect kernel disorder without affecting cob ovality/flatness, or vice versa. The presence of QTLs specific for single components of ear fasciation was already reported (Mendes-Moreira et al., 2015).

Confirming earlier observations, phenotypic variation for ear fasciation and KRN were found associated in our study, both in terms of positive correlation and QTLs overlap. Specifically, two out of four ear fasciation QTLs overlapped with two out of five KRN QTLs. Furthermore, at the overlapping loci, namely *qFas5-qKRN5* and *qFas7-qKRN7.1*, the direction of genetic effects agreed (i.e., '+' alleles increased both ear fasciation index and the number of kernel rows), as previously hypothesized or shown. Notably, at both *qFas5-qKRN5* and *qFas7-qKRN7.1* the fasciation/KRN-increasing allele was provided by Lo1016, and the effect of the Lo1016 alleles at the two QTLs was detected in both B×L and L×L. In other words, at both *qFas5-qKRN5* and *qFas7-qKRN7.1*, Lo1016 carries alleles increasing both ear fasciation index and kernel row number, and their positive effect on ear fasciation were detected across genetic backgrounds. However, the KRN effect was detected in the L×L background only, likely because the KRN mean value in the L×L genetic background was lower than that in B×L (16.0 and 17.4 kernel rows per ear, respectively; Table 1). Indeed, in a high KRN-context such as the B×L genetic background, any KRN-increasing allele such as the ones from Lo1016 would likely contribute marginally to KRN. In L×L, the genetic effect at both *qFas5-qKRN5* and *qFas7-qKRN7.1* QTLs was estimated to be 2a = approx. 0.6 rows per locus (|0.57| at *qKRN5* and |0.62| at *qKRN7.1*. Table 2), equivalent to approx. 4% (0.6/16.5 rows per ear) of the average trait value in these populations. Homozygous Lo1016 allele substitutions at both loci are therefore expected to add approximately one row per ear, therefore contributing approximately 6% (1/16.5 rows) of grain yield. Although this estimate should be considered with caution, the combined effect of the two QTLs on kernel per ear seems important and worthy to consider in plant breeding programs when based on marker- or genomics-assisted selection.

Our QTL consensus map (Figure 4A, Supplementary Table 7) supported the pleiotropic connection between ear fasciation and KRN. For example, QTLs for cob ovality and KRN (*qCF1* and *qKRN1a*, respectively) by Mei et al. (2021) on chr. 1 overlapped with *qFas1.2* mapped in our study. Liu et al. (2015) found a QTL (*qKRN5-4*) between *umc1971* and *umc1071*

10.3389/fpls.2022.1017983

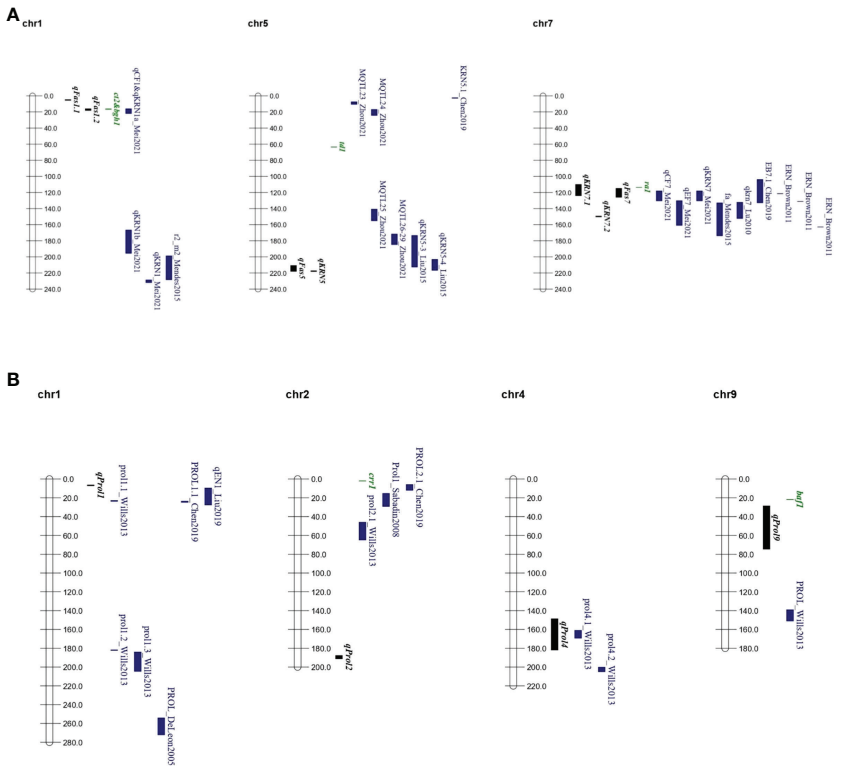

FIGURE 4
QTL and main candidate genes consensus maps. **(A)** QTL consensus map for ear fasciation including QTL from literature and this study. **(B)** QTL consensus map for ear prolificacy, including QTL from literature and from this study. Chromosome bars and numbers represent physical distances in Mb. QTL positions are represented following physical positions reported in Supplementary Tables 7, 8. In black, QTL from this study; in green, tentative candidate genes; in blue, QTL from other studies. Full QTL information from other studies is provided in Supplementary Table 7.

on chr. 5 affecting kernel row number, and mapping nearby our *qFAS5*. Finally, the chr. 7 region corresponding to our *qFas7-qKRN7.1* appears as an ear fasciation/KRN QTL hot spot. QTLs mapped in this region included cob and ear flatness *qCF7* and *qEF7* by Mei et al. (2021), ear fasciation *fa_c1* by Mendes-Moreira et al. (2015), several ear row number QTLs within the B73 NAM population by Brown et al. (2011), *qkrn7* by Lu et al. (2011), *KRN7.1* by Chen et al. (2019), *qKRN7* by Mei et al. (2021).

We also detected QTLs affecting the number of kernel rows independently from ear fasciation on chr. 2 and chr. 8 (*qKRN2* and *qKRN8*, respectively. Table 2) with (+) alleles dispersed between parental lines (from Lo964 and Lo1016, respectively). Many independent QTL mapping studies for number of kernel rows have already been carried out and a comprehensive review is beyond the scope of this study. However, it should be noted that a major KRN QTL mapping on chr. 2, just 10 Mb away from *qKRN2* was cloned and shown to encode for a member of the highly duplicated *WD40* gene and protein family (Chen et al., 2022), which affects diverse cellular functions like signal transduction, cell cycle control, intracellular transport, chromatin remodelling, cytoskeletal organization and others. The authors reported that the *WD40* allele increasing the number of kernel rows enhanced the inflorescence meristem size, likely providing additional space for initiation of spikelet pair meristems and hence a higher number of kernel rows (Chen et al., 2022). Given the close proximity (ca. 10 Mb) between *WD40* and the QTL *qKRN2* reported herein in the subtelomeric region of chr. 2, it will certainly be worth checking the actual identity between the two loci.

By comparing QTL supporting intervals from our and other studies with the genomic positions of inflorescence-related genes we shortlisted candidate genes possibly involved in controlling ear fasciation QTLs (Figure 4A, Supplementary Tables 5, 6). The maize historical tassel and ear mutant *ra1*, encoding a zinc-finger transcriptional factor and producing ear and tassel with increased branches (Vollbrecht et al., 2005; Kim et al., 2022) maps only 0.5 Mb away from the QTL cluster region including *qFas7*, and within the QTL supporting interval of *qKRN7.1*. Comparison of genomic sequences between our three parental

lines showed lack of nucleotide sequence variation at *ra1* (Supplementary Figure 8), in line with former observations which showed *ra1* as very poor of sequence diversity in maize (Sigmon and Vollbrecht, 2010). However, as shown in other studies (Salvi et al., 2007; Li et al., 2012; Salvi and Tuberosa, 2015), QTLs are often due to gene expression level variation rather than variation of coding sequences, therefore quantification of the expression of *ra1* in the ear primordium of Lo1016 and Lo964 will enable to test *ra1* involvement in ear fasciation driven by *qFas7*. The genes *ct2* and *bgh1* were identified as candidate genes for *qFas1.2* (Supplementary Table 6) based on former observations that maize lines carrying mutations at *ct2* produced fasciated ears (Bommert et al., 2013a), and that the overexpression of *bgh1* resulted in increased ear kernel row number (Zhang et al., 2022). Five common native *bgh1* alleles exhibited little structural and expression variation compared to the large increased expression conferred by these ectopic alleles (Simmons et al., 2020). In line with this observation, genomic sequence comparison between B73 and Lo1016 (*qFas1.2* was detected in B×L only; Table 2) showed no difference in coding sequences.

Our study addressed single-node ear prolificacy (Wang et al., 2021), a trait hardly investigated across maize genetics and we identified four major QTLs. An overlap was observed between our *qProl4* and *prol4.1* by Wills et al. (2013) in a maize × teosinte cross (Figure 4B, Supplementary Table 8), although no association with known genes inside this interval was established. Additionally, *qProl1* mapped in the proximity of three ear prolificacy QTLs reported in other studies (Wills et al., 2013; Chen et al., 2019; Liu et al., 2019; Figure 4B, Supplementary Table 8), The gene *grassy tillers1* (*gt1*) known to be involved in ear prolificacy (Wills et al., 2013) maps just ~16 Mb away from *qProl1* (Table 2; Supplementary Table 5). Finally, *barren stalk fastigiate1* (*baf1*), a known gene that when mutated produces barred shoots with no ear (Zhou et al., 2021) maps very close (~7 Mb) to the north border of *qProl9* (Figure 4B). Thus, given the vagaries of QTL mapping, both *gt1* and *baf1* cannot be excluded as possible causative genes for their corresponding QTLs.

Among the four QTLs controlling the number of tillers per plant, three (*qTil1*, *-4* and *-9*) had the tillers-increasing allele provided by Lo1016, in line with the phenotype of parental lines (Lo1016 is the only parent showing tillering when grown in the field in standard conditions). However, *qTil2* had the tiller-increasing allele contributed by B73 that develops hardly no tillers in our field conditions (Table 1), which suggests that at least some level of epistasis occurs between tillering loci in our genetic materials, in line with former observations of epistasis for domestication traits, including tillering (Stitzer and Ross-Ibarra, 2018). Finally, it should be noted that while shoot branching producing ears and tillering share obvious developmental similarities (e.g., both branching types originate from axillary buds at stem nodes), ear prolificacy and tillering did not correlate and did not show QTL overlap. The most likely explanation lies in the genetic architecture of the two traits in the lines tested in this study, i.e., no strong pleiotropic gene segregated. Another factor, partially connected with this, is that the parental line contributing ear prolificacy (Lo964) showed virtually no tillering, and the parental line contributing high tillering (Lo1016) showed no ear prolificacy, suggesting that each parental line possibly contributed relatively strong alleles at genes acting only on one of the two traits.

5 Conclusions

This study identified solid positive correlation between ear fasciation and KRN in an elite genetic background, and provided evidence that the correlation was at least partially due to pleiotropic genes at ear fasciation QTLs on chr. 5 and chr. 7 and affecting KRN. The fasciation effects and the correlated effect on KRN were confirmed across genetic backgrounds, making these QTLs an interesting source of yield-positive alleles. While candidate genes were identified at major QTLs, including the correspondence between *qFas7-qKRN7.1* and *ra1* on chr. 7, further work is required for candidate genes validation.

Analysis for ear prolificacy at a single node enabled us to identify four QTLs, of which one (on chr. 4) perfectly overlapped with an ear prolificacy QTL formerly identified in a maize × teosinte cross. Quite unexpectedly, we did not find correlation or QTL overlaps between ear prolificacy and tillering, although the two traits share obvious developmental basis.

Overall, our study provides clear entry points for the molecular dissection of important yield component traits, which should help both developing molecular markers for marker-assisted selection to be deployed in breeding programs and starting the procedures leading to cloning the genes underpinning the QTLs described and eventually their manipulation by engineering or editing.

Data availability statement

The raw data supporting the conclusions of this article will be made available by the authors, without undue reservation.

Author contributions

SS and RT conceived the project and acquired funding; KL, AT, SG, SR, CU and SS designed and curated field trials, collected phenotypic and genotypic data and analyzed the data; KL, RT and

SS wrote the first manuscript draft. All authors contributed to the article and approved the submitted version.

Funding

This work was supported by KWS SAAT SE & Co. KGaA, Germany. KL has received research support from China Scholarship Council.

Acknowledgments

We gratefully acknowledge the technical contribution of Simona Corneti, Sandra Stefanelli and Stefano Vecchi. This work was supported by KWS SAAT SE & Co. KGaA, Germany.

Conflict of interest

Author CU was employed by the KWS SAAT SE & Co. KGaA.

The remaining authors declare that the research was conducted in the absence of any commercial or financial relationships that could be construed as a potential conflict of interest.

The authors declare that this study received funding from KWS SAAT SE & Co. KGaA. The funders had no role in data collection and analysis.

Publisher's note

Supplementary material

The Supplementary Material for this article can be found online at: https://www.frontiersin.org/articles/10.3389/fpls.2022.1017983/full#supplementary-material

References

Barazesh, S., and McSteen, P. (2008). Barren inflorescence1 functions in organogenesis during vegetative and inflorescence development in maize. *Genetics* 179, 389–401. doi: 10.1534/genetics.107.084079

Bommert, P., Je, B. I., Goldshmidt, A., and Jackson, D. (2013a). The maize gα gene COMPACT PLANT2 functions in CLAVATA signalling to control shoot meristem size. *Nature* 502, 555–558. doi: 10.1038/nature12583

Bommert, P., Nagasawa, N. S., and Jackson, D. (2013b). Quantitative variation in maize kernel row number is controlled by the FASCIATED EAR2 locus. *Nat. Genet.* 45, 334–337. doi: 10.1038/ng.2534

Brand, U., Fletcher, J. C., Hobe, M., Meyerowitz, E. M., and Simon, R. (2000). Dependence of stem cell fate in arabidopsis on a feedback loop regulated by CLV3 activity. *Science* 289, 617–619. doi: 10.1126/science.289.5479.617

Brown, P. J., Upadyayula, N., Mahone, G. S., Tian, F., Bradbury, P. J., Myles, S., et al. (2011). Distinct genetic architectures for male and female inflorescence traits of maize. *PloS Genet.* 7, e1002383. doi: 10.1371/journal.pgen.1002383

Chen, W., Chen, L., Zhang, X., Yang, N., Guo, J., Wang, M., et al. (2022). Convergent selection of a WD40 protein that enhances grain yield in maize and rice. *Science* 375, eabg7985. doi: 10.1126/science.abg7985

Chen, Q., Yang, C. J., York, A. M., Xue, W., Daskalska, L. L., DeValk, C. A., et al. (2019). TeoNAM: A nested association mapping population for domestication and agronomic trait analysis in maize. *Genetics* 213, 1065–1078. doi: 10.1534/genetics.119.302594

Chuck, G. S., Brown, P. J., Meeley, R., and Hake, S. (2014). Maize SBP-box transcription factors unbranched2 and unbranched3 affect yield traits by regulating the rate of lateral primordia initiation. *Proc. Natl. Acad. Sci. U. S. A.* 111, 18775–18780. doi: 10.1073/pnas.1407401112

Cingolani, P., Platts, A., Wang, L. L., Coon, M., Nguyen, T., Wang, L., et al. (2012). A program for annotating and predicting the effects of single nucleotide polymorphisms, SnpEff: SNPs in the genome of drosophila melanogaster strain w1118; iso-2; iso-3. *Fly (Austin)* 6, 80–92. doi: 10.4161/fly.19695

Clark, S. E., Running, M. P., and Meyerowitz, E. M. (1993). CLAVATA1, a regulator of meristem and flower development in arabidopsis. *Development* 119, 397–418. doi: 10.1242/dev.119.2.397

Dempewolf, H. (2010). Getting domestication straight: Ramosa1 in maize. *Mol. Ecol.* 19, 1267–1269. doi: 10.1111/j.1365-294X.2010.04563.x

Doebley, J., Stec, A., and Gustus, C. (1995). Teosinte branched1 and the origin of maize: Evidence for epistasis and the evolution of dominance. *Genetics* 141, 333–346. doi: 10.1093/genetics/141.1.333

Du, Y., Liu, L., Peng, Y., Li, M., Li, Y., Liu, D., et al. (2020). UNBRANCHED3 expression and inflorescence development is mediated by UNBRANCHED2 and the distal enhancer, KRN4, in maize. *PLoS Genet.* 16, e1008764. doi: 10.1371/journal.pgen.1008764

Edgar, R. C. (2004). MUSCLE: A multiple sequence alignment method with reduced time and space complexity. *BMC Bioinf.* 5, 113. doi: 10.1186/1471-2105-5-113

Fan, C., Wu, Y., Yang, Q., Yang, Y., Meng, Q., Zhang, K., et al. (2014). A novel single-nucleotide mutation in a CLAVATA3 gene homolog controls a multilocular silique trait in brassica rapa l. *Mol. Plant* 7, 1788–1792. doi: 10.1093/mp/ssu090

Gallavotti, A., Malcomber, S., Gaines, C., Stanfield, S., Whipple, C., Kellogg, E., et al. (2011). BARREN STALK FASTIGIATE1 is an AT-hook protein required for the formation of maize ears. *Plant Cell* 23, 1756–1771. doi: 10.1105/tpc.111.084590

Gallavotti, A., Zhao, Q., Kyozuka, J., Meeley, R. B., Ritter, M. K., Doebley, J. F., et al. (2004). The role of barren stalk1 in the architecture of maize. *Nature* 432, 630–635. doi: 10.1038/nature03148

Hufford, M. B., Seetharam, A. S., Woodhouse, M. R., Chougule, K. M., Ou, S., Liu, J., et al. (2021). *De novo* assembly, annotation, and comparative analysis of 26 diverse maize genomes. *Science* 373, 655–662. doi: 10.1126/science.abg5289

Iliev, I., and Kitin, P. (2011). Origin, morphology, and anatomy of fasciation in plants cultured *in vivo* and *in vitro*. *Plant Growth Regul.* 63, 115–129. doi: 10.1007/s10725-010-9540-3

Je, B. I., Gruel, J., Lee, Y. K., Bommert, P., Arevalo, E. D., Eveland, A. L., et al. (2016). Signaling from maize organ primordia *via* FASCIATED EAR3 regulates stem cell proliferation and yield traits. *Nat. Genet.* 48, 785–791. doi: 10.1038/ng.3567

Kellogg, E. A. (2022). Genetic control of branching patterns in grass inflorescences. *Plant Cell* 34, 2518–2533. doi: 10.1093/plcell/koac080

Kim, D. E., Jeong, J.-H., Kang, Y. M., Park, Y.-H., Lee, Y.-J., Kang, J.-S., et al. (2022). The impact of fasciation on maize inflorescence architecture. *J. Plant Biol.* 65, 87–98. doi: 10.1007/s12374-021-09342-1

Kitagawa, M., and Jackson, D. (2019). Control of meristem size. *Annu. Rev. Plant Biol.* 70, 269–291. doi: 10.1146/annurev-arplant-042817-040549

Kumar, S., Stecher, G., Li, M., Knyaz, C., and Tamura, K. (2018). MEGA X: Molecular evolutionary genetics analysis across computing platforms. *Mol. Biol. Evol.* 35, 1547–1549. doi: 10.1093/molbev/msy096

Li, H. (2011). A statistical framework for SNP calling, mutation discovery, association mapping and population genetical parameter estimation from sequencing data. *Bioinformatics* 27, 2987–2993. doi: 10.1093/bioinformatics/btr509

Li, H., Bradbury, P., Ersoz, E., Buckler, E. S., and Wang, J. (2011). Joint QTL linkage mapping for multiple-cross mating design sharing one common parent. *PLoS One* 6, e17573. doi: 10.1371/journal.pone.0017573

Li, H., and Durbin, R. (2009). Fast and accurate short read alignment with burrows-wheeler transform. *Bioinformatics* 25, 1754–1760. doi: 10.1093/bioinformatics/btp324

Li, S., Meng, S., Weng, J., and Wu, Q. (2022). Fine-tuning shoot meristem size to feed the world. *Trends Plant Sci.* 27, 355–363. doi: 10.1016/j.tplants.2021.10.004

Liu, L., Du, Y., Huo, D., Wang, M., Shen, X., Yue, B., et al. (2015). Genetic architecture of maize kernel row number and whole genome prediction. *Züchter Genet. Breed. Res.* 128, 2243–2254. doi: 10.1007/s00122-015-2581-2

Liu, X., Galli, M., Camehl, I., and Gallavotti, A. (2019). RAMOSA1 ENHANCER LOCUS2-mediated transcriptional repression regulates vegetative and reproductive architecture. *Plant Physiol.* 179, 348–363. doi: 10.1104/pp.18.00913

Li, X., Zhu, C., Yeh, C.-T., Wu, W., Takacs, E. M., Petsch, K. A., et al. (2012). Genic and nongenic contributions to natural variation of quantitative traits in maize. *Genome Res.* 22, 2436–2444. doi: 10.1101/gr.140277.112

Losa, A., Hartings, H., Verderio, A., and Motto, M. (2011). Assesment of genetic diversity and relationships among maize inbred lines developed in Italy. *Maydica* 56, 95-104.

Lu, M., Xie, C.-X., Li, X.-H., Hao, Z.-F., Li, M.-S., Weng, J.-F., et al. (2011). Mapping of quantitative trait loci for kernel row number in maize across seven environments. *Mol. Breed.* 28, 143–152. doi: 10.1007/s11032-010-9468-3

Mei, X., Dong, E., Liang, Q., Bai, Y., Nan, J., Yang, Y., et al. (2021). Identification of QTL for fasciated ear related traits in maize. *Crop Sci.* 61, 1184–1193. doi: 10.1002/csc2.20435

Mendes-Moreira, P., Alves, M. L., Satovic, Z., Dos Santos, J. P., Santos, J. N., Souza, J. C., et al. (2015). Genetic architecture of ear fasciation in maize (Zea mays) under QTL scrutiny. *PLoS One* 10, e0124543. doi: 10.1371/journal.pone.0124543

Meng, L., Li, H., Zhang, L., and Wang, J. (2015). QTL IciMapping: Integrated software for genetic linkage map construction and quantitative trait locus mapping in biparental populations. *Crop J.* 3, 269–283. doi: 10.1016/j.cj.2015.01.001

Opsahl-Ferstad, H. G., Le Deunff, E., Dumas, C., and Rogowsky, P. M. (1997). ZmEsr, a novel endosperm-specific gene expressed in a restricted region around the maize embryo. *Plant J.* 12, 235–246. doi: 10.1046/j.1365-313X.1997.12010235.x

Ortez, O. A., McMechan, A. J., Hoegemeyer, T., Ciampitti, I. A., Nielsen, R., Thomison, P. R., et al. (2022). Abnormal ear development in corn: A review. *Agron. J.* 114, 1168–1183. doi: 10.1002/agj2.20986

Otegui, M. E., and Bonhomme, R. (1998). Grain yield components in maize. *Field Crops Res.* 56, 247–256. doi: 10.1016/S0378-4290(97)00093-2

Pertea, G., and Pertea, M. (2020). GFF utilities: GffRead and GffCompare. *F1000Res* 9, 304. doi: 10.12688/f1000research.23297.1

Portwood, J. L.2nd, Woodhouse, M. R., Cannon, E. K., Gardiner, J. M., Harper, L. C., Schaeffer, M. L., et al. (2019). MaizeGDB 2018: The maize multi-genome genetics and genomics database. *Nucleic Acids Res.* 47, D1146–D1154. doi: 10.1093/nar/gky1046

Prakash, N. R., Zunjare, R. U., Muthusamy, V., Chand, G., Kamboj, M. C., Bhat, J. S., et al. (2019). Genetic analysis of prolificacy in "Sikkim primitive"–a prolific maize (Zea mays) landrace of north-Eastern himalaya. *Plant Breed.* 138, 781–789. doi: 10.1111/pbr.12736

Prakash, N. R., Zunjare, R. U., Muthusamy, V., Rai, M., Kumar, A., Guleria, S. K., et al. (2021). A novel quantitative trait loci governs prolificacy in 'Sikkim primitive' – a unique maize (zea mays) landrace of north-Eastern himalaya. *Plant Breed.* 140, 400–408. doi: 10.1111/pbr.12924

Rotili, D. H., Abeledo, L. G., Martínez Larrea, S., and Maddonni, G. Á. (2022). Grain yield and kernel setting of multiple-shoot and/or multiple-ear maize hybrids. *Field Crops Res.* 279, 108471. doi: 10.1016/j.fcr.2022.108471

Rousselle, Y., Jones, E., Charcosset, A., Moreau, P., Robbins, K., Stich, B., et al. (2015). Study on essential derivation in maize: III. Selection and evaluation of a panel of single nucleotide polymorphism loci for use in European and north American germplasm. *Crop Sci.* 55, 1170–1180.
doi: 10.2135/cropsci2014.09.0627

Salvi, S., Sponza, G., Morgante, M., Tomes, D., Niu, X., Fengler, K. A., et al. (2007). Conserved noncoding genomic sequences associated with a flowering-time quantitative trait locus in maize. *Proc. Natl. Acad. Sci. U. S. A.* 104, 11376–11381. doi: 10.1073/pnas.0704145104

Salvi, S., and Tuberosa, R. (2015). The crop QTLome comes of age. *Curr. Opin. Biotechnol.* 32, 179–185. doi: 10.1016/j.copbio.2015.01.001

Schnable, P. S., Ware, D., Fulton, R. S., Stein, J. C., Wei, F., Pasternak, S., et al. (2009). The B73 maize genome: Complexity, diversity, and dynamics. *Science* 326, 1112–1115. doi: 10.1126/science.1178534

Schoof, H., Lenhard, M., Haecker, A., Mayer, K. F. X., Jürgens, G., and Laux, T. (2000). The stem cell population of arabidopsis shoot meristems is maintained by a regulatory loop between the CLAVATA and WUSCHEL genes. *Cell* 100, 635–644. doi: 10.1016/S0092-8674(00)80700-X

Sigmon, B., and Vollbrecht, E. (2010). Evidence of selection at the ramosa1 locus during maize domestication. *Mol. Ecol.* 19, 1296–1311. doi: 10.1111/j.1365-294X.2010.04562.x

Simmons, C. R., Weers, B. P., Reimann, K. S., Abbitt, S. E., Frank, M. J., Wang, W., et al. (2020). Maize BIG GRAIN1 homolog overexpression increases maize grain yield. *Plant Biotechnol. J.* 18, 2304–2315. doi: 10.1111/pbi.13392

Sokal, R. R., and Rohlf, F. J. (2012). *Biometry. 4th ed* (New York, NY: W.H. Freeman).

Somssich, M., Je, B. I., Simon, R., and Jackson, D. (2016). CLAVATA-WUSCHEL signaling in the shoot meristem. *Development* 143, 3238–3248. doi: 10.1242/dev.133645

Stitzer, M. C., and Ross-Ibarra, J. (2018). Maize domestication and gene interaction. *New Phytol.* 220, 395–408. doi: 10.1111/nph.15350

Tanksley, S. D. (2004). The genetic, developmental, and molecular bases of fruit size and shape variation in tomato. *Plant Cell* 16 Suppl, S181–S189. doi: 10.1105/tpc.018119

Trotochaud, A. E., Hao, T., Wu, G., Yang, Z., and Clark, S. E. (1999). The CLAVATA1 receptor-like kinase requires CLAVATA3 for its assembly into a signaling complex that includes KAPP and a rho-related protein. *Plant Cell* 11, 393–406. doi: 10.1105/tpc.11.3.393

Van Ooijen, J. W. (2009). *MapQTL 6, software for the mapping of quantitative trait loci in experimental populations of diploid species*. Ed. B. V. Kyazma (Wageningen, Netherlands: Kyazma).

Vollbrecht, E., Springer, P. S., Goh, L., Buckler, E.S., IV, and Martienssen, R. (2005). Architecture of floral branch systems in maize and related grasses. *Nature* 436, 1119–1126. doi: 10.1038/nature03892

Wang, Z., Gao, J., Li, Y., Razia sultana, J., Luan, Y., Mu, C., et al. (2021). Combined linkage analysis and genome-wide association study reveal QTLs and candidate genes conferring genetic control of prolificacy trait in maize. *Preprints*. doi: 10.20944/preprints202101.0185.v1

Waterhouse, A. M., Procter, J. B., Martin, D. M. A., Clamp, M., and Barton, G. J. (2009). Jalview version 2–a multiple sequence alignment editor and analysis workbench. *Bioinformatics* 25, 1189–1191. doi: 10.1093/bioinformatics/btp033

White, O. E. (1948). Fasciation. *Bot. Rev.* 14, 319–358. doi: 10.1007/BF02861723

Wickham, H., Averick, M., Bryan, J., Chang, W., McGowan, L., François, R., et al. (2019). Welcome to the tidyverse. *J. Open Source Software* 4, 1686. doi: 10.21105/joss.01686

Wills, D. M., Whipple, C. J., Takuno, S., Kursel, L. E., Shannon, L. M., Ross-Ibarra, J., et al. (2013). From many, one: Genetic control of prolificacy during maize domestication. *PLoS Genet.* 9, e1003604. doi: 10.1371/journal.pgen.1003604

Wu, Q., Xu, F., and Jackson, D. (2018). All together now, a magical mystery tour of the maize shoot meristem. *Curr. Opin. Plant Biol.* 45, 26–35. doi: 10.1016/j.pbi.2018.04.010

Xiao, L., Li, X., Liu, F., Zhao, Z., Xu, L., Chen, C., et al. (2018). Mutations in the CDS and promoter of BjuA07.CLV1 cause a multilocular trait in brassica juncea. *Sci. Rep.* 8. doi: 10.1038/s41598-018-23636-4

Xu, C., Liberatore, K. L., MacAlister, C. A., Huang, Z., Chu, Y.-H., Jiang, K., et al. (2015). A cascade of arabinosyltransferases controls shoot meristem size in tomato. *Nat. Genet.* 47, 784–792. doi: 10.1038/ng.3309

Yang, C. J., Samayoa, L. F., Bradbury, P. J., Olukolu, B. A., Xue, W., York, A. M., et al. (2019). The genetic architecture of teosinte catalyzed and constrained maize domestication. *Proc. Natl. Acad. Sci. U. S. A.* 116, 5643–5652. doi: 10.1073/pnas.1820997116

Zhang, Y., Jiao, F., Li, J., Pei, Y., Zhao, M., Song, X., et al. (2022). Transcriptomic analysis of the maize inbred line Chang7-2 and a large-grain mutant tc19. *BMC Genomics* 23, 4. doi: 10.1186/s12864-021-08230-9

Zhang, D., Sun, W., Singh, R., Zheng, Y., Cao, Z., Li, M., et al. (2018). GRF-interacting factor1 regulates shoot architecture and meristem determinacy in maize. *Plant Cell* 30, 360–374. doi: 10.1105/tpc.17.00791

Zhou, Y., Kusmec, A., Mirnezami, S. V., Attigala, L., Srinivasan, S., Jubery, T. Z., et al. (2021). Identification and utilization of genetic determinants of trait measurement errors in image-based, high-throughput phenotyping. *Plant Cell* 33, 2562–2582. doi: 10.1093/plcell/koab134

Frontiers in
Plant Science

Cultivates the science of plant biology and its applications

The most cited plant science journal, which advances our understanding of plant biology for sustainable food security, functional ecosystems and human health.

Discover the latest Research Topics

See more →

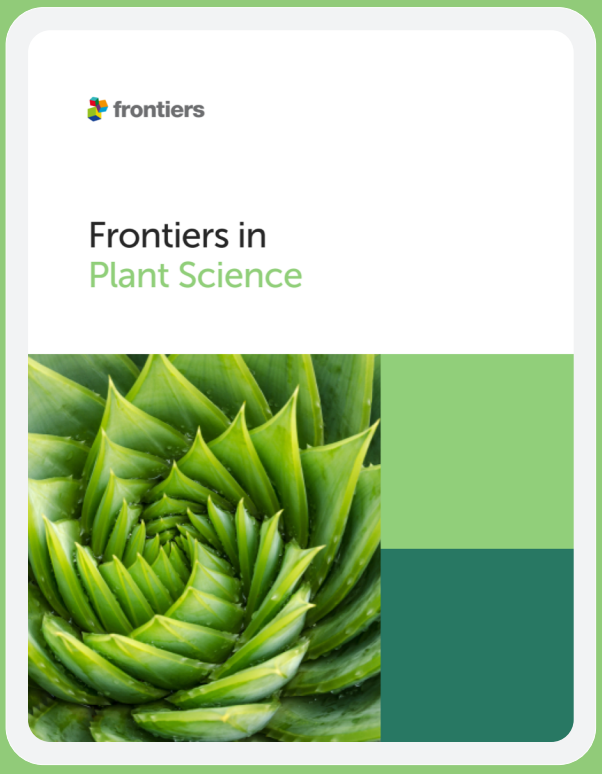

Frontiers

Avenue du Tribunal-Fédéral 34
1005 Lausanne, Switzerland
frontiersin.org

Contact us

+41 (0)21 510 17 00
frontiersin.org/about/contact